DRAFT FINAL REPORT

Load Distribution on Highway Bridges Based On Field Test Data : Phase II

Principal investigator
M. AROCKIASAMY, Ph.D., P.E.
Professor and Director

Ahmed Amer, Ph.D.
Research Associate

Submitted to:
Florida Department of Transportation

under:
WPI No. 0510668, State Job No. 99700-3512-119
Contract No. B-9944

Monitored by:
Structural Research Center
Florida Department of Transportation
2007 E. Paul Dirac Drive
Tallahassee, FL 32304

Center for Infrastructure and Constructed Facilities
Department of Ocean Engineering
FLORIDA ATLANTIC UNIVERSITY
Boca Raton, Florida-33431
USA

FEBRUARY 1997

TECHNICAL REPORT STANDARD TITLE PAGE

1. Report No.	2. Government Accession No.	3. Recipient's Catalog No.

4. Title and Subtitle	5. Report Date
Load Distribution on Highway Bridges Based on Field Test Data : Phase II	February 1997
	6. Performing Organization Code
7. Authors	8. Performing Organization Report No.
M. Arockiasamy and Ahmed Amer	
9. Performing Organization Name and Address	10. Work Unit No.
Florida Atlantic University Center for Infrastructure and Constructed Facilities Department of Ocean Engineering Boca Ration, Florida 33731	11. Contract or Grant No. WPI 0510668
12. Sponsoring Agency Name and Address	13. Type of Report and Period Covered
Florida Department of Transportation 605 Suwannee Street Tallahassee, Florida 32399-0466	Draft Final Report
	14. Sponsoring Agency Code 99700-3512-119, B-9944

15. Supplementary Notes

Prepared in cooperation with the Federal Highway Administration

16. Abstract

The primary aim of the study was to investigate the wheel load distribution of different bridge types -solid slab bridges and slab-on-girder bridges with varying skew angles and multiple continuous spans. The study reviewed the existing analytical and field load distribution methods for different bridge types. Finite element method was used to carry out the detailed analyses to study the various parameters affecting wheel load distribution. The data from field tests were collected and analyzed to evaluate the LRFD specifications and the results from the finite element method.

The influence of the parameters such as skew angle, girder spacing, span length, slab thickness, and number of traffic lanes were studied in the load distribution of the skew solid slab and skew slab-on-girder bridges. In addition to the parametric study, data from field tests performed by the Structures Research Center, FDOT, are compared with those based on FEM analysis, AASHTO and LRFD codes. Simplified formulae for the effective width of skew solid slab bridges are proposed in this study.

The response of continuous bridges was studied by modeling several continuous bridge types (skew and straight slab-on-girder) using finite element method. Several parameters such as span length, number of spans, ratio between spans and skew angle were considered in the parametric studies. The wheel-load distribution factors from the analyses were compared with the field test data. The study indicated that the analyses based on finite element method are close to the field test results.

17. Key Words	18. Distribution Statement
wheel load distribution; effective width; skew bridges; continuous bridges; slab-on-girder; solid slab; slab-on-bulb-tee; finite element method; field test; LRFD codes	No restrictions. This document is available to the public through the National Technical Information Service, Springfield, Virginia 22161

19. Security Classif. (of this report)	20. Security Classif. (of this page)	21. No. of Pages	22. Price
Unclassified	Unclassified	218	

Form DOT F 1700.7 (8-89)

UNIT CONVERSION TABLE

To convert from	To	Multiply by
inch	centimeter	2.54
square inch	square centimeter	6.4516
kip	kiloNewton (kN)	4.44747
kip/sq. in. (ksi)	kN/sq. m (kPa)	6,894.28
-T	kN-meter	1.3556

DISCLAIMER

The opinions, findings and conclusions expressed in this publication are those of the authors who are responsible for the facts and accuracy of the data presented herein. The contents do not necessarily reflect the views or the policies of the Florida Department of Transportation or the Federal Highway Administration. This report does not constitute a standard, specification or regulation.

The report is prepared in cooperation with the Florida Department of Transportation and the Federal Highway Administration.

ACKNOWLEDGMENTS

The authors wish to express their sincere thanks to Dr. Mohsen A. Shahawy, Chief Structures Analyst, and Mr. Adman, Research Engineer, Florida Department of Transportation, for their excellent suggestions, discussions and constructive criticisms throughout the project. They wish to express their appreciation to Dr. S. E. Dunn, Professor and Chairman, Department of Ocean Engineering, and Dr. J. Juvenwicz, Acting Dean, College of Engineering, Florida Atlantic University for their continued interest and encouragement.

The valuable assistance in the preparation of the report from Mr. Nathaniel Bell and Mrs. Tian Xang, Graduate Students, Florida Atlantic University, is gratefully acknowledged.

SUMMARY

The primary aim of the study was to investigate the wheel load distribution of different bridge types - solid slab bridges and slab-on-girder bridges with varying skew angles and multiple continuous spans. The study reviewed the existing analytical and field load distribution methods for different bridge types. Finite element method was used to carry out the detailed analyses to study the various parameters affecting wheel load distribution. The data from field tests were collected and analyzed to evaluate the LRFD specifications and the results from the finite element method.

The influence of the parameters such as skew angle, girder spacing, span length, slab thickness, and number of traffic lanes was studied in the load distribution of the skew solid slab and skew slab-on-girder bridges. In addition to the parametric study, data from field tests performed by the Structures Research Center, FDOT, are compared with those based on FEM analysis, AASHTO and LRFD codes. Simplified formulae for the effective width of skew solid slab bridges are proposed in this study.

The response of continuous bridges were studied by modeling several continuous bridge types (skew and straight slab-on-girder) using finite element method. Several parameters such as span length, number of spans, ratio between spans and skew angle were considered in the parametric studies. The wheel-load distribution factors from the analyses were compared with the field test data. The study indicated that the analytical results based on finite element method are close to the field test data.

TABLE OF CONTENTS

CHAPTER 7 SUMMARY AND CONCLUSIONS

LIST OF FIGURES

LIST OF TABLES

CHAPTER I

INTRODUCTION

1.1 INTRODUCTION

Wheel load distribution on highway bridges is an important response parameter in determining structural member size and consequently the strength and serviceability of bridge members. It is, therefore, of critical importance in the design of new bridges and the evaluation of the load carrying capacity of existing bridges.

The American Association of State Highways and Transportation Officials (AASHTO) method of load distribution reduces the complex analysis of a bridge subjected to one or more vehicles to simple analysis of a beam. According to the AASHTO method, the maximum load effects in a girder can be obtained by treating a girder as a one-dimensional beam subject to loading, which is obtained by multiplying one line of wheels of the design vehicle by a load fraction (Wheel-Load Distribution Factor). This concept was first introduced by Newmark (1948).

Recent research resulted in a substantial amount of information on various bridge types indicating a need for revisions of the AASHTO bridge specifications (1992). These conservative load distribution factors may be acceptable for the design of new bridges, but are unacceptable for evaluating

existing bridges. NCHRP project 12-26 (1992) was initiated in the mid-1980s in order to develop comprehensive specification provisions for distribution of wheel loads in highway bridges.

Within a time span of more than thirty years, the science of bridge analysis and design has undergone major changes. Following the advent of digital computers, the bridge engineers have available today a number of powerful analytical tools for refined methods of analysis including (i) the grillage analogy method, (ii) the orthotropic plate method, (iii) the articulated plate method, and (iv) the finite element method including finite strip formulation. The results from the above refined methods of analysis should be used to improve the existing simplified approaches. These approaches would aid the designer to compute the distribution factors more efficiently without the need for performing complicated analysis in the design office.

Field load testing of highway bridges has increased significantly in recent years. The increased interest has resulted in part from the large number of older bridges with posted load limits that are below the normal legal truck weights. Field load testing in determining the safe load capacity of a bridge, which should be greater than the capacity determined from standard rating calculations based on the AASHTO method. One method for use of bridge test results in rating calculations is to determine wheel-load distribution factors for the girders based on test data. These measured wheel-load distribution factors can be used in bridge rating calculations in the place of those factors defined by AASHTO code.

The studies carried out by the Principal Investigator (Arockiasamy, 1994) on "Load Distribution on Highway Bridges Based on Field Test Data - Phase I" present the load distribution on certain bridge types in Florida viz., slab-on-girder, solid slab, voided slab and double-tee bridges. The existing analytical

and field load distribution methods for different bridge types are reviewed in this study. Grillage analogy is used as an analytical tool to study the various parameters affecting wheel-load distribution. The results from the analytical study is compared with those based on the field test data.

1.2 METHODOLOGY AND APPROACH

The finite element method was used to carry out the detailed analyses of different bridge types - solid slab bridges and slab-on-girder bridges with varying skew angles and multiple continuous spans. The actual loads used in the bridge tests were modeled in the analysis. The field test results were compared with the analytical values.

Important parameters such as beam spacing, span length, slab thickness, number of spans, skew angle, etc. were identified for every bridge type. The average properties were used in the parametric studies of different bridge types. The data from field tests were collected and analyzed to evaluate the current LRFD specifications and the results from the finite element method. The structural analysis program ANSYS was used in the modeling and detailed analysis of different bridge types.

1.2.1 SKEW BRIDGES

The AASHTO specifications (1992) do not include approximate formulae for moments to account for the effect of skewed supports. It is frequently considered safe to ignore the skew angle, if it is less than 20 degrees and analyze the bridge as a right bridge with a span equal to the skew span, since

leads to a conservative safe estimate of longitudinal moments and shears in the skew bridge. The use of this approximate procedure may lead to significant differences between the skew bridge responses and those of the equivalent right bridge with larger skew angles.

The influence of the parameters such as girder spacing, span length, slab thickness, flexural rigidities of longitudinal and transverse girders, number of traffic lanes and total curb-to-curb deck width were studied in the load distribution of the skew bridges for varying skew angles. The available field test data for different skew bridge types viz., solid slab and slab-on-AASHTO girder, etc. were analyzed and compared with the analytical results.

1.2.2 CONTINUOUS BRIDGES

The response of continuous bridges were studied by modeling several continuous bridge types (slab bridges, beam-and-slab bridges, etc.) using finite element method. The wheel-load distribution factors from the analyses were compared with the field test data.

1.3 OBJECTIVES AND SCOPE

The objective of the research in Phase II is to determine the load distribution factors for the following specific bridge types:

(I) Slab-on-bulb-Tee girder bridges

(iii) Continuous bridges

The load distribution parametric studies were carried out using finite element method. The measured field test data available with the Florida Department of Transportation were used in evaluating the analytical values based on i) AASHTO specifications, ii) LRFD bridge specifications and iii) finite element method. Based on the analyses and field tests, simple design formulae were drived for distribution factors, if needed, that would provide a more accurate and realistic alternative to the current design codes.

Chapter 2 reviews the available literature regarding the different analytical and field load distribution methods for different bridge types. Chapter 3 discusses the finite element method concepts, the idealization of different bridge types, field test procedures and methodologies.
Chapter 4 summarizes the results of the finite element method and field test studies of skew slab-onAASHTO girder bridges. Chapter 5 presents the analytical studies and analysis of field test data for solid slab skewed bridges. Chapter 6 presents the analysis of continuous bridges and a comparison with the field test results. The summary and conclusions are presented in Chapter 7.

CHAPTER 2

LITERATURE REVIEW

2.1 INTRODUCTION

The AASHTO specifications (1992) do not include formulae for moments that account for the effect of skewed supports. However, the LRFD specifications (1994) recommend modification factors that account for the skew effects in wheel load distribution. The LRFD factors for skew angle effect are based on analytical studies and need to be verified using field tests. Besides published information on shear effects due to skewed supports is limited. It is frequently considered safe to ignore the skew angle, if it is less than 20 degrees and analyze the bridge as a right bridge with a span equal to the skew span, since it leads to a conservative estimate of longitudinal moments and shears in the skew bridge. The use of this approximate procedure may lead to significant differences between the skew bridge responses and those of the equivalent right bridge with larger skew angles.

The studies carried out by the Principal Investigator (Arockiasamy, 1995) on "Load Distribution on Highway Bridges Based on Field Test Data - Phase I" present the load distribution on certain bridge types in Florida viz., slab-on-girder, solid slab, voided slab and double-tee bridges. The existing analytical methods for different straight bridge types are reviewed in this section. Grillage analogy was used as an analytical tool to study the various parameters affecting

wheel-load distribution. The results from the analytical study are compared with those based on the field test data.

The following sections summarize the literature review of the load distribution factors of the following specific bridge types: (i) Skew bridges and (ii) Continuous bridges.

2.2 LOAD DISTRIBUTION ANALYSES OF SKEW BRIDGES

Limited research has been conducted in the study of load distribution of skew bridges. Newmark et al (1948) tested five quarter-scale, simply supported, skew slab-on-girder bridge models and the AASHTO specifications were based on these test results. Chen et al (1954) used the finite difference method to analyze simply supported skew slab on noncomposite multisteel girder bridges. Several parameters have been considered such as spacing between girders, span length, skew angle, and girder-to-slab stiffness ratio. Moment coefficients for skew bridges were determined and used in establishing design relationships.

Hendry and Jaeger (1957) applied grid frame analysis to determine the load distribution in skew bridges. In the grid frame analysis method, the deck and girders are idealized as a grillage of beam elements. Gustafson (1966) developed a finite element method for the analysis of skew-stiffened plates. Two skew slab-and-girder bridges were analyzed using this method. Gustafson and Wright (1968) presented a finite element method that employed parallelogram plates and eccentric beam elements. Two typical composite skew bridges with steel I-beams were analyzed, and the behavior due to the effects of skew and midspan diaphragms were illustrated in the study. The parallelogram plate elements do not satisfy the slope compatibility requirements at the element

boundaries and the study did not include the analysis of the load distribution of skewed slab-girder structures.

Mehrain (1967) developed and tested finite element computer programs for analysis of various skew composite slab-and-girder bridges and studied the convergence assuming different finite elements. Decastro et al (1979) developed load distribution equations for simply supported prestressed concrete beam-slab bridges. A finite element approach was used to analyze 120 1beam superstructures, varying in length from 10.4 to 39.0 m (34 to 128 ft.) and width from 7.3 to 21.9 m (24 to 72 ft.). They discretized the superstructure into plate and eccentric beam elements. Skew effects were correlated for bridges of different span lengths, widths, and number of beams. They concluded that the skew correction factors reduced the distribution factor for interior girders, and increased the distribution factor for exterior girders. Kostem and DeCastro (1979) studied the effects of diaphragms on lateral load distribution and found the effects to be insignificant.

Marx, Khachaturion and Gamble (1986) developed design criteria for wheel-load distribution in simply supported skew slab-on prestressed-girder bridges. In this study, slab-and precast-prestressed I-girder bridges were analyzed by three-dimensional finite element method in which slab was modeled by nine-noded Lagrangian-type isoparametric thin shell elements and girders modeled using eccentric isoparametric beam elements. The shell and beam elements were joined together by rigid links connecting their centroids.

Nutt et al (1988) analyzed multigirder composite steel bridge using equivalent orthotropic plate and ribbed plate models. El-Ali (1986) used SAP-IV finite element program to analyze the distribution of wheel loads in skew multistringer steel composite bridges. In this study, an I-beam girder was divided into two T-shaped beam elements and the elastic properties of these elements

lumped at the centroids of the flanges. The two beam elements were further connected by another truss system to the deck slab plate elements. This procedure is very lengthy, especially in skew bridges. Only four bridges were analyzed in the study. It was concluded that live load bending moments decrease when the skew angle increases, and the live-load shear forces do not vary with the skew angle.

Bishara, Liu and El-Ali (1993) present distribution factors for wheel-load distributions for interior and exterior girders on multisteel beam composite bridges. The expressions were derived from finite element analyses of 36 bridges. The analysis recognizes the three-dimensional interaction of all bridge members, places the bearing at their actual location, and considers the effects of the restraining forces at the bearings. The distribution factors are generally lower than those specified by the AASHTO.

Bishara and Soegiarso (1993) studied the load distribution in multibeam precast pretopped prestressed bridges. Three 50 -ft. **two-lane simply supported prestressed precast pretopped doubleT bridges with and without end diaphragms are analyzed using three-dimensional finite element algorithm. The computed maximum live load moments in the interior beams were of the same order of magnitude as the AASHTO values. However, for exterior beams the computed values were only 80-85% of the AASHTO values.**

Chen (1995) proposed a refined and simplified analysis method for predicting the lateral distribution of vehicular live loads on unequally spaced I-shaped bridge girders. Finite element method was used to model the bridge. The shell elements coupling bending with membrane action were used to model the bridge slabs. Two options were considered in modeling the I-girders: beam model and plate model.

Kankam and Dagher (1995) presented a nonlinear finite element program for the analysis of reinforced concrete skewed slab bridges. The program is based on a layering formulation in which the cross section is divided into steel and concrete layers, with nonlinear material properties. They concluded that a skewed slab bridge with more reinforcement near the obtuse corner than near the acute corner has a higher ultimate strength than a corresponding bridge designed with uniform reinforcement.

2.3 LOAD DISTRIBUTION ANALYSES OF CONTINUOUS BRIDGES

Limited publications discussed the analysis and testing of continuous concrete bridges. Khaleel and Itani (1990) presented a method for determining moments in continuous normal and skew slab-and-girder bridges due to live loads. Using finite element method, 112 continuous bridges are analyzed to identify the design parameters. For a skew angle of 60° , maximum moment in the interior girder is approximately 71% of that in a normal bridge and reduction in maximum bending moment is 20% in the exterior girders, which controls the design for a bridge with long span, small girder spacing, and small relative stiffness of girder to slab. They concluded that the AASHTO distribution of wheel loads for exterior girders in normal bridges underestimates the bending moments by as much as 28%.

Zuraski (1991) presented closed-form expressions for end moments in continuous beams with three or four spans followed by a presentation of the general formulation for any number of

spans, which provides an efficient algorithm suitable for interactive microcomputer usage. Practical applications of the method were illustrated by providing expressions for bending moments caused by dead, lane and live loads

Tiedeman, Albrecht and Cayes (1993) tested a 0.4-scale model of two-span continuous composite-steel girder bridge. The reactions, moments, displacements, and rotations due to axle loading were analyzed and compared with those calculated by finite element and AASHTO methods. The results showed that finite element analysis most accurately predicted the bridge behavior under the truck axle loading.

Warren and Malvar (1993) carried out finite element analysis and in-service pier tests to study the design of flat-slab continuous navy pier decks. From these analyses and test results, a one-third scale laboratory model was designed, constructed and tested. Analyses and tests results confirmed that effective width values for reinforced concrete slabs can often be doubled over those based on AASHTO.

CHAPTER 3

METHODS OF ANALYSIS

3.1 INTRODUCTION

Recent developments in the finite element method make it possible to model a bridge in a more realistic manner. Chapter 3 presents the basic assumptions and concepts of the finite element method in calculating the wheel-load distribution factors. The different models for the slab deck and girders and the appropriate boundary conditions of different bridge structural elements are summarized in this chapter. The AASHTO and LRFD load distribution factor equations will be presented in the following chapters for each bridge type. The basic procedure for field load testing and the methodology for computing the load distribution based on field test data are summarized in section 3.5. Comparison between different finite element models and the field test measurement is presented in section 3.6.

3.2 FINITE ELEMENT METHOD

3.2.1 Introduction

There are three refined methods for bridge analysis recommended by the LRFD code (1994): the finite element method; the grillage analogy method; and the series or harmonic method. The harmonic method is incapable of modeling the diaphragms or orthotropic slab. When bridge piers and / or abutments are highly skewed (bridge skew > 45°), the grillage analogy method will generally result in inaccurate results. Of all the above methods of analyses, the finite element method is the most powerful, versatile and

important to realize that the correctness of the results obtained from the finite element method depends on the underlying assumptions and simplifications made in formulating the model

In this study, the bridge is modeled as a three dimensional system using a generalized discretization scheme in the ANSYS 5.2 finite element program. Several schemes were proposed and validated using the field test results. The field test data were provided by the Structural Research Center, FDOT. In the following sections, the analytical modeling is outlined for slab-on-girder bridges.

3.2.2 The Finite Element Types Used in the Modeling

In this study, the shell elements coupling bending with membrane action were used to model the bridge deck / slab. Also, beam elements were used to model the girder or the top or bottom flanges of the girder.

3.2.2.1 Elastic Shell Elements

The shell elements used in the analyses have both bending and membrane characteristics. The elements were derived based on the following assumptions: i) Lines originally normal to the midsurface of the shell remain straight after deformation, and ii) All points on a line originally normal to the midsurface have the same vertical displacement, w. Thus a normal line is inextensible during deformation.

Figs. 3.1 and 3.2 show the typical thin shell elements with 4-nodes and 8-nodes. Each node has six degrees of freedom- three displacements: u, v, w; and three rotations: 8_X , 6,. , 9_Z. The elements have no stiffness associated with the A_Z rotational degree of freedom. A small stiffness is added to prevent

numerical instability following the approach presented by Kanok-Nukulchai. Details of the development of the element can be found in ANSYS theoretical manual.

3.2.2.2 Elastic Three Dimensional Beam Element

Three dimensional uniaxial prismatic beam element with tension, compression, torsion, and bending capabilities was used in the analysis. The element has six degrees of freedom at each beam node (Fig. 3.3) and for unsymmetric beams (Fig. 3.4). These elements were used to model the girder or the girder flanges in the bridge.

3.3 FINITE ELEMENT DISCRETIZATION FOR SKEWED SLAB-ON-GIRDER BRIDGES

Linear elastic material properties are used in the modeling. The slab elements may have either isotropic or orthotropic properties. In the first discretization, 4 or 8-node shell elements were used to model the reinforced concrete slab. These shell elements couple the bending with the membrane action. The girders were modeled using three dimensional beam elements. The shell elements are connected to the beam elements by rigid links. Fig. 3.5 gives a schematic view of this model. Rigid links connect the nodal degrees of freedom of the beam to those of the shell element. Thus the displacements in the beam element are dictated by those in the shell. There is one incompatibility in this model which is unavoidable. Marx et al (1986) claimed that this incompatibility is not important in a slab-on-girder bridge. However, this was not the case as shown in section 3.6.

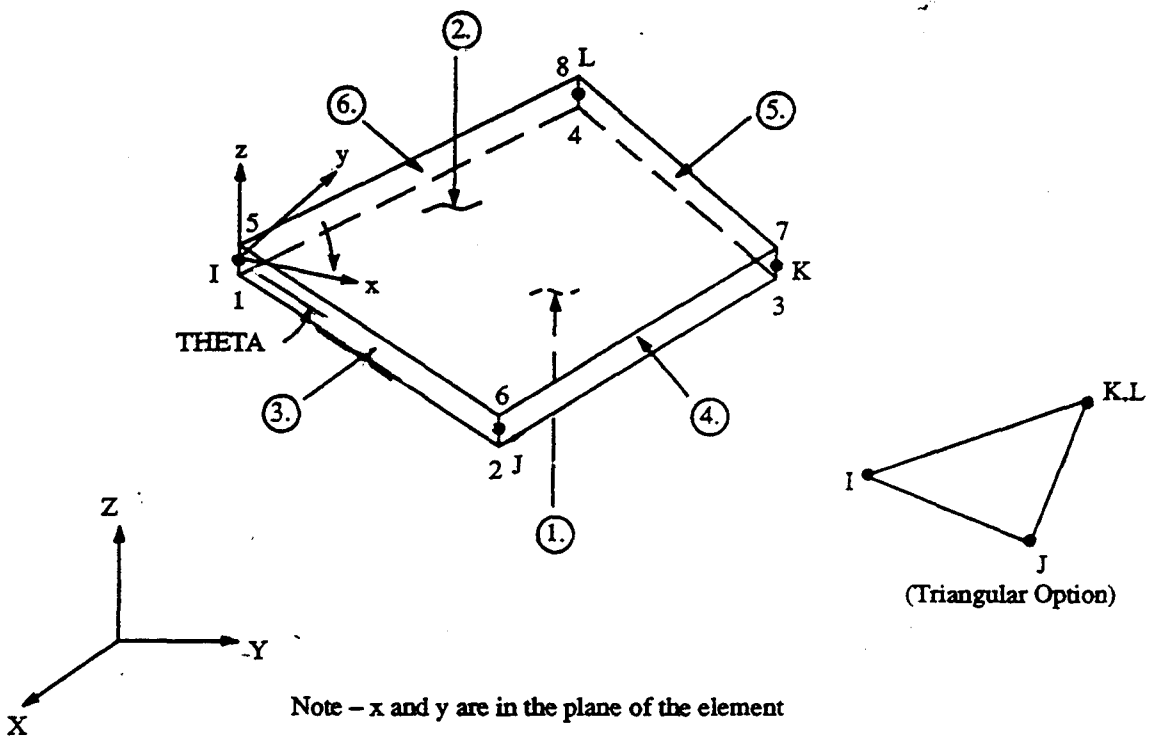

Fig. 3.1 Four-node shell element details

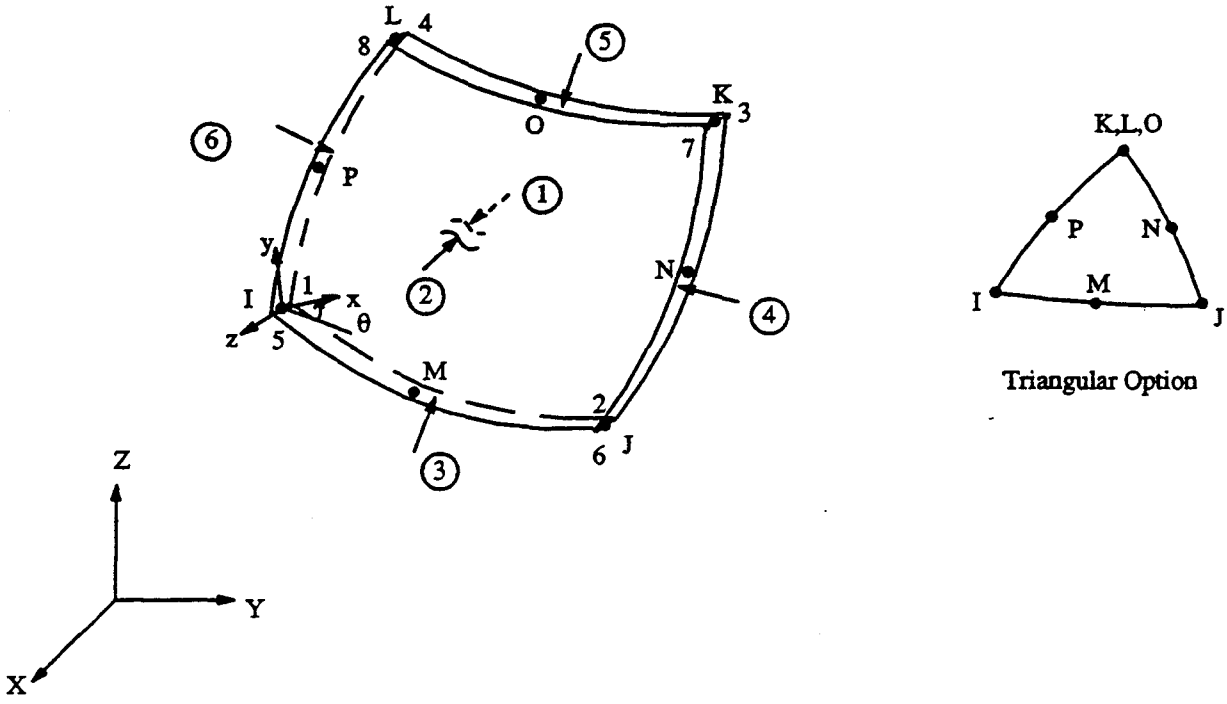

Fig. 3.2 Eight-node shell element details

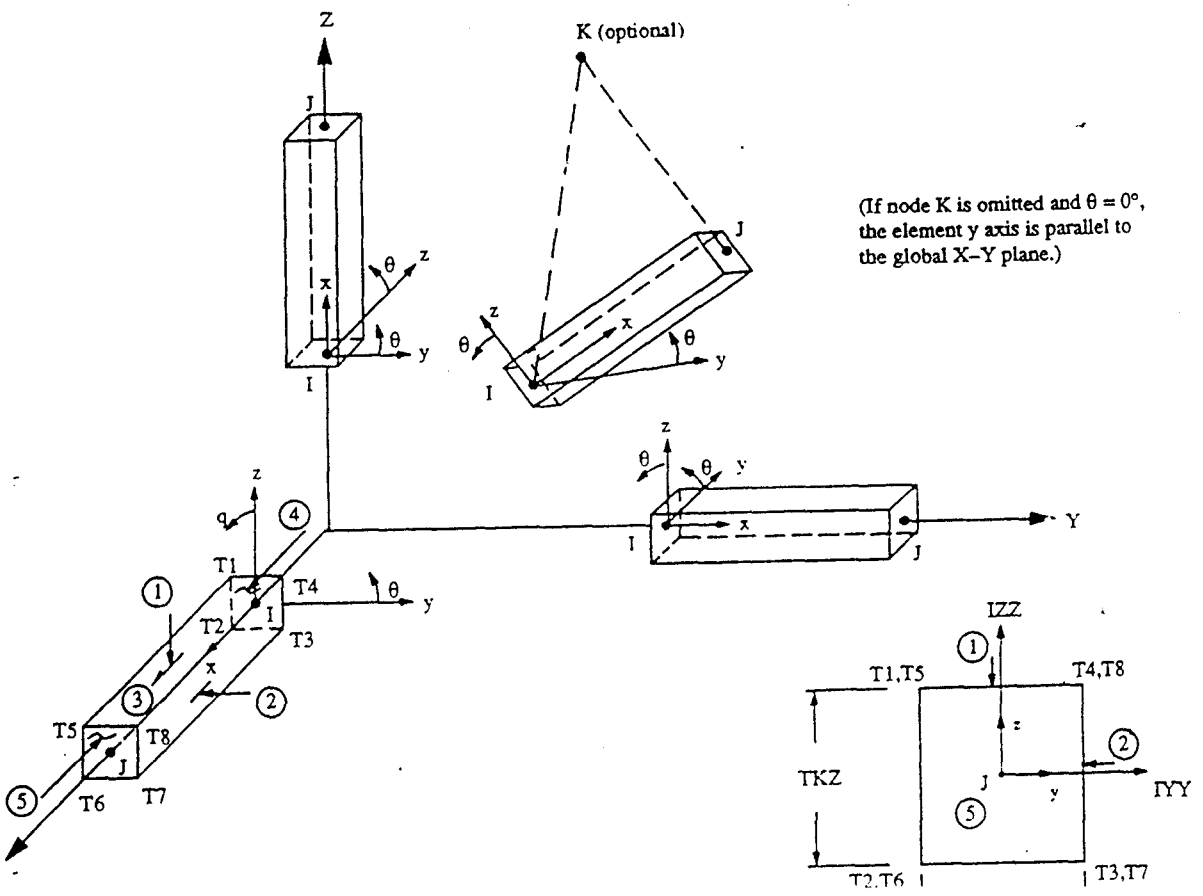

Fig. 3.3 Three-dimensional prismatic beam element details

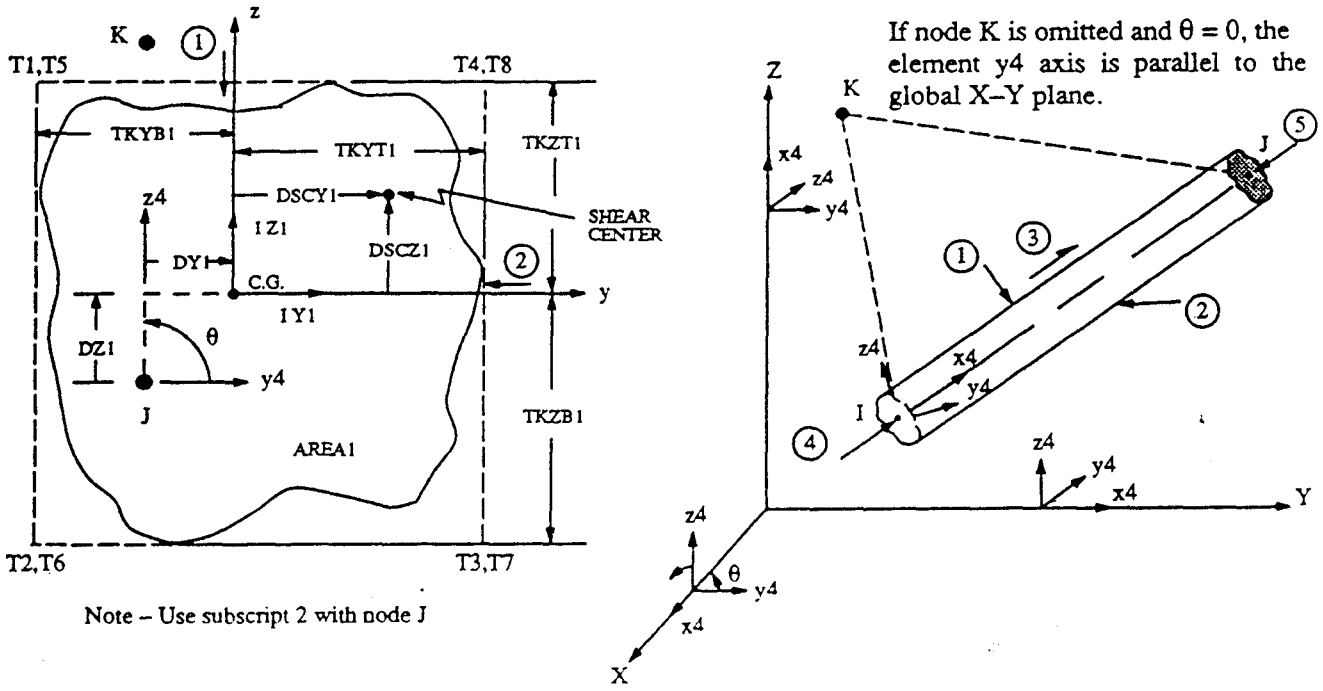

Fig. 3.4 Three-dimensional unsymmetric beam element details

Fig. 3.6 shows the second modeling in which the reinforced concrete slab was discretized using an 8 or 4 node shell elements. Each 1-girder was divided into three parts: the two flanges and the web. Each flange was modeled by a beam element with its properties lumped at the centroid of the flange. The web was modeled by shell elements with four or eight midsurface nodes. Each mid surface node has six degrees of freedom. To satisfy the compatibility of composite behavior, the coupling command specifying a highly rigid element was assumed between the top beam elements and the centroids of the top deck slab shell elements. Each bearing support was assumed to be located at the centroid of the beam element representing the bottom flange of the girder. Under linear elastic conditions, stresses are proportional to the bending moments in the girders. Hence, maximum stresses at the extreme fiber of the bottom flanges obtained from finite element results were used to compute the wheel - load distribution factors of the girders, and compare them with those of AASHTO and LRFD specifications.

The third modeling was similar to the second model in discretizing the reinforced concrete slab using shell elements with six degrees of freedom shown in Fig. 3.7. However, plate (shell) elements are used to model the 1-girders. The 1-girders were divided into web, top and bottom flanges. Each part was modeled using three dimensional shell elements. The composite action between the slab and girder is modeled by connecting the centers of gravity of the slab and girder with rigid elements.

3.4 BRIDGE TYPES

The scope of this study includes skew solid slab bridges, skew simply supported slab-on-l-girder bridges (AASHTO type) and skew and straight continuous slab-on-l-girder bridges. These are shallow superstructures in the sense that load distribution takes place mainly through bending and torsion in the longitudinal and transverse directions, and is assumed that deflections due to shear are negligible. These structures were analyzed using the finite element models summarized in section 3.3. Typical section properties and mesh design used in the analyses of skew solid slab bridge are summarized in Chapter 5. The typical section properties and meshes of skew simply supported and continuous slab-on-l-girder

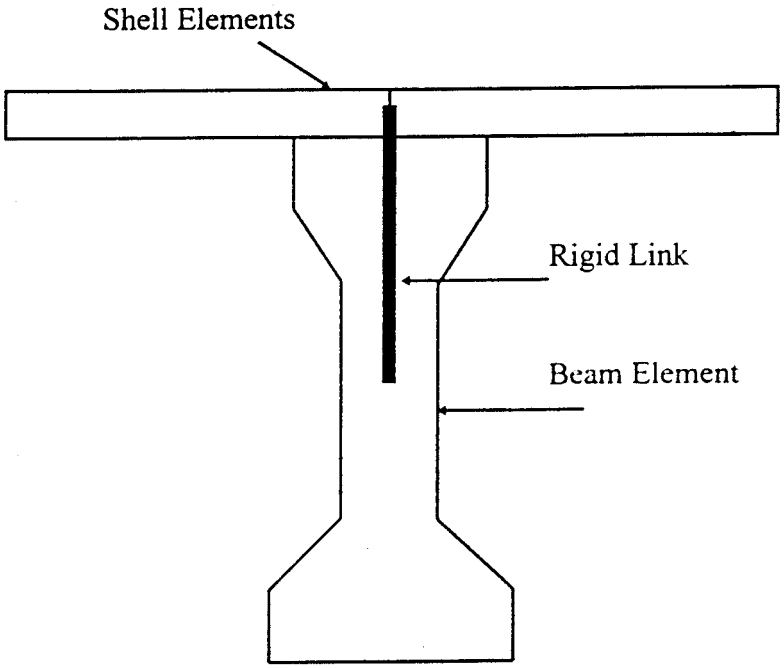

Fig. 3.5 Details of Model 1

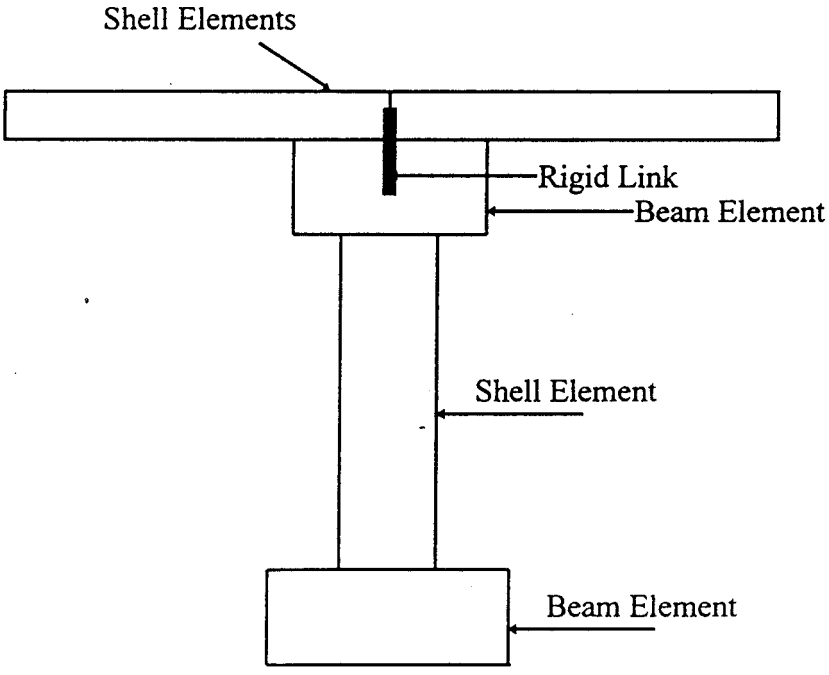

Fig. 3.6 Details of Model 2

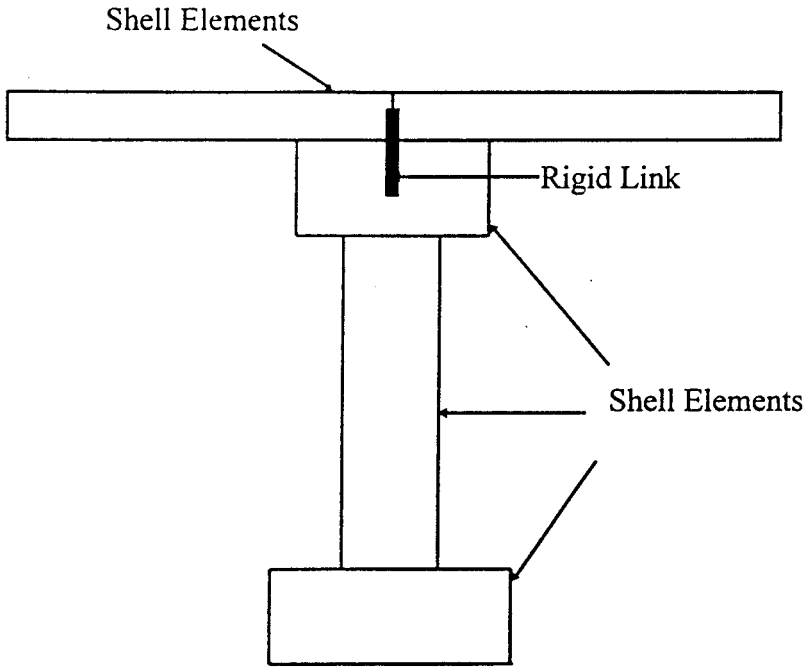

Fig. 3.7 Details of Model 3

3.5 LOAD DISTRIBUTION FACTORS BASED ON FIELD TESTS

Field load testing frequently offers a means of determining whether the load capacity of a bridge is greater than the capacity determined from standard rating calculation based on the AASHTO and LRFD methods. In some cases the field tests indicate a higher load capacity because the AASHTO wheel load distribution factors used in standard rating calculations tends to overestimate the loads carried by the individual girders. Examples of how field tests have been used to assess various aspects of bridge behavior are given by Bakht and Csagoly (1980), Bakht and Jaeger (1990) and others.

Florida Department of Transportation (FDOT) have been testing many bridges to check the strengths and establish bridge ratings. The strength of bridge elements is generally determined by first placing strain or deflection transducer gages at the bridge critical locations along the elements, and then incrementally loading them to induce maximum effects. The data collected can then be analyzed and used to establish the strength of each component as well as the load distribution factors.

The FDOT's bridge load testing system consists of two test vehicles, a mobile data acquisition system and a mobile machine shop. The two test vehicles have been designed to deliver the ultimate live loads specified by AASHTO code. Each vehicle is a specially designed tractor-trailer combination, weighing in excess of 200 kips when fully loaded with concrete blocks. Detailed dimensions of the test vehicles are shown in Figure 3.8. Each vehicle can carry maximum of 72 concrete blocks, each weighing approximately 2,150 pounds. Incremental loading is achieved by adding blocks with a self-contained hydraulic crane mounted on each truck. Figs. 3.9 and 3.10 show the wheel loads for each load increment.

Once a bridge is identified for load testing, a site survey and an analysis of existing plans and inspection reports gives further information on the feasibility of such a test. Details of instrumentation and loading locations are then established. The next step is to mobilize testing equipment and personnel to the bridge site.

The test vehicles are initially loaded with a number of concrete blocks, established from the preliminary analysis of the existing structure. The vehicles are then driven and placed on the critical locations of the bridge while the data acquisition system monitors the instrumentation during loading. The data are immediately analyzed, displayed and compared with the theoretical predictions to assure the safety of the bridge, equipment and testing personnel. After each load step, if the results compare favorably with the theoretical predictions, additional blocks are added to the vehicles and the test repeated until the ultimate AASHTO load is achieved. The data gathered can then be analyzed and a report of the findings prepared. Bridges that carry both vehicles without apparent distress are considered structurally safe.

Data from some bridge testing reports will be used for load distribution analyses. The typical report contains transverse strain distributions in the maximum bending moment section for several loading stages. The typical report also contains the applied moment vs strain curves for several loading stages.

Measured Distribution Factors

One method for use of test results in rating calculations is to use test data to calculate wheel-load distribution factors. This measured wheel-load distribution factor can be used in bridge-rating calculations in place of wheel load distribution defined by AASHTO. AASHTO (Guide specifications 1989) has also presented a refined bridge-rating methodology in which measured wheel-load distribution factors can be used.

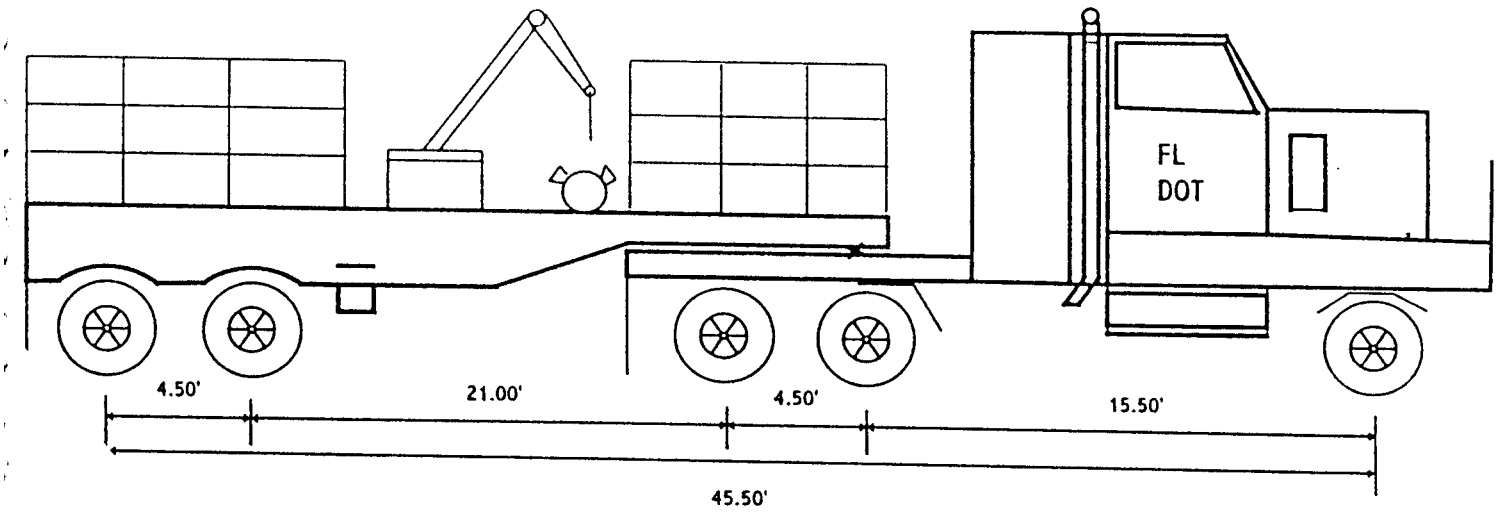

Fig 3.8 Typical FDOT test vehicle

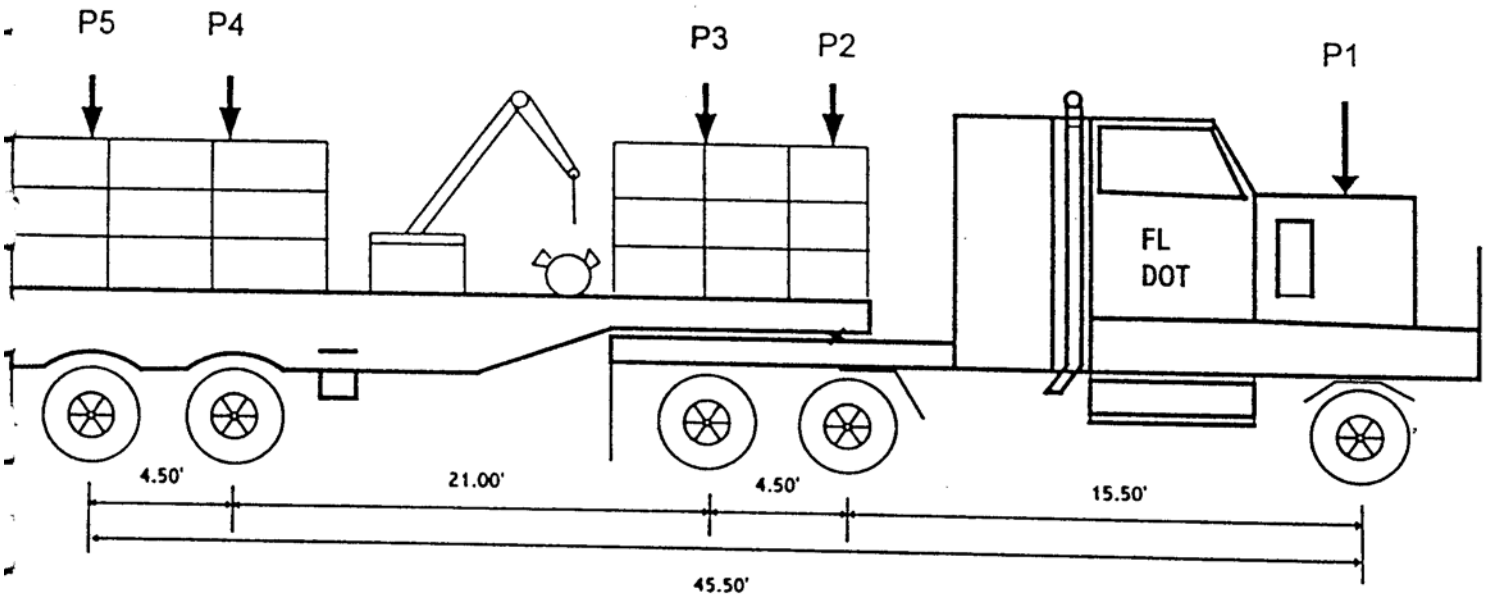

# A Block	P5	P4	P3	P2	P1
24	22.40	22.40	18.66	18.66	11.49
36	29.21	29.21	24.95	24.95	11.66
48	36.03	36.03	28.23	28.23	11.83
72	49.66	49.66	37.80	37.80	12.17

Fig. 3.9 Typical truck loads for spans larger than 55 ft.

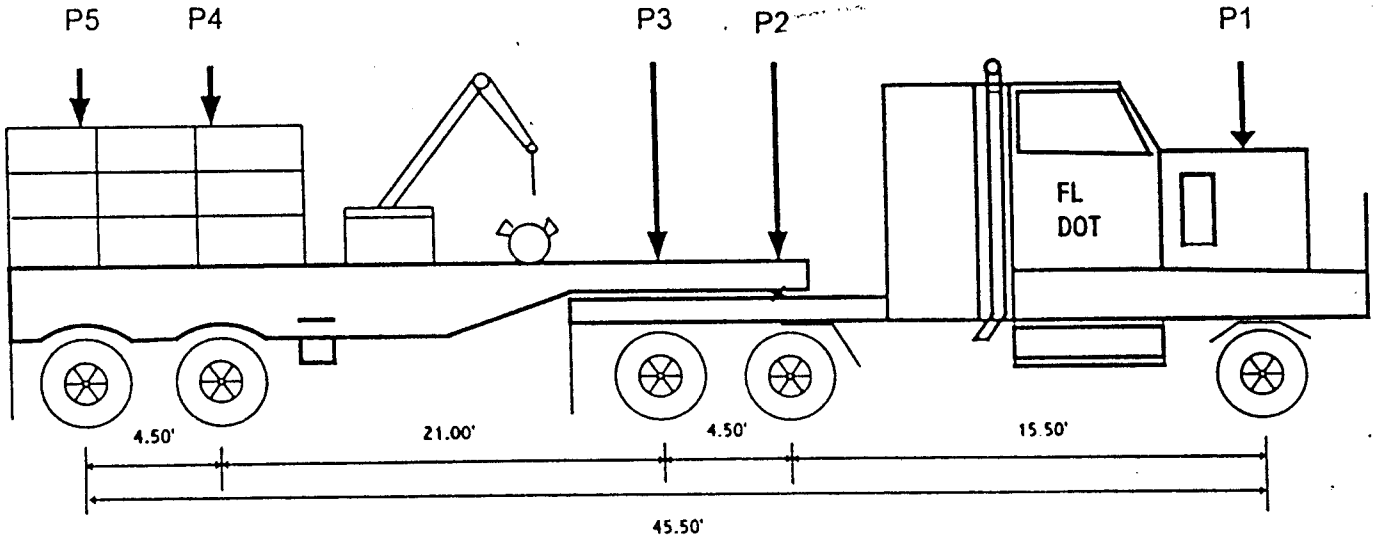

# A Block	P5	P4	P3	P2	P1
24	30.61	30.61	11.01	11.01	11.26
30	35.48	35.48	11.68	11.68	11.26
36	41.78	41.78	11.95	11.95	11.26
42	46.60	46.60	12.67	12.67	11.26

Fig. 3.10 Typical truck loads for spans less than 55 ft.

Goshen et al. (1986) assumed that the distribution factor for a girder was equal to the ratio of the strain at the girder to the sum of all the bottom-flange strains. O'Connor and Pritchard (1985) measured the total bending moment applied to a multigirder bridge by using a weighted sum of the bottom-flange strains. In the present study, the measured strains would be multiplied by the section and elastic moduli to calculate the measured moments. The ACI equation was used to calculate the elastic modulus of concrete based on f_c of 5000 psi. The measured moment distribution will be used to calculate the measured wheel-load distribution factors. The measured wheel-load distribution factors will be compared with AASHTO , LRFD and finite element analysis based wheel load distribution factors.

3.6 EXPERIMENTAL VALIDATION OF THE DIFFERENT FINITE ELEMENT DISCRETIZATION MODELS

Different finite element discretization models presented in section 3.3 were used in the analysis of a typical bridge to test the validity. The bridge is located on S.R. 17 and it consists of three simply supported spans with the longest test span of 85'-6". The test span consists of 7 Type III prestressed concrete girders, spaced at 5'-2" center to center and a slab thickness of 7.5 in. The skew angle is 45 degrees. The bridge carries two lanes of **traffic** with curb to curb width of 26 ft. as shown in Figure 3.11. Table 3.1 summarizes the material and sectional properties of the bridge.

The measured strains along the bridge width at the maximum bending moment section are presented in Table 3.2. The mesh and the finite element model for the bridge are similar to that of bridge #720408 which is presented in Chapter 4. Rigid links and simply supported boundary conditions were assumed in modeling this bridge.

Table 3.1 Material and sectional properties for bridge #720089

Material Properties	E_{deck} (ksi)	E_{girder} (ksi)	Poisson's Ratio, υ	G (ksi)
	4031	4031	0.2	1679

Section Properties	Slab	Thickness = 7.5 in.				
	Girder web	Thickness = 6 in.				
		A (in^2)	I_y (in^4)	I_z (in^4)	T_{ky} (in)	T_{kz} (in)
	Top beam	144	972	3072	16	9
	Bottom beam	242	2440	9761	22	11

Table 3.2 summarizes the results from finite element analyses and field test at a cross section corresponding to the maximum bending moment location. In this bridge, two finite element models were used to check the validity. This has been achieved by comparing the calculated strains with those based on measured strains. Figure 3.12 shows that the measured and calculated strain distributions along the transverse direction. Finite element model # 2 strains were consistent with those based on measured values. However, the calculated strains based on finite element model # 1 were higher than the measured strains. Based on the analysis of this case and other cases, finite element model # 2 were used to model slab-on-girder bridges throughout this investigation.

Table 3.2 Measured and calculated Strains

Transverse distance (in.)	Measured strains, in./in. x 10-6	Calculated strains (Model # 1) , in./in. x 10-6	Calculated strains (Model # 2) , in./in. x 10-6
41	90	305	109
103	84	269	104
165	79	205	62
227	38	127	29.4
289	29	80	13.3
351	15	44	3.55
413	5	21	-1.5

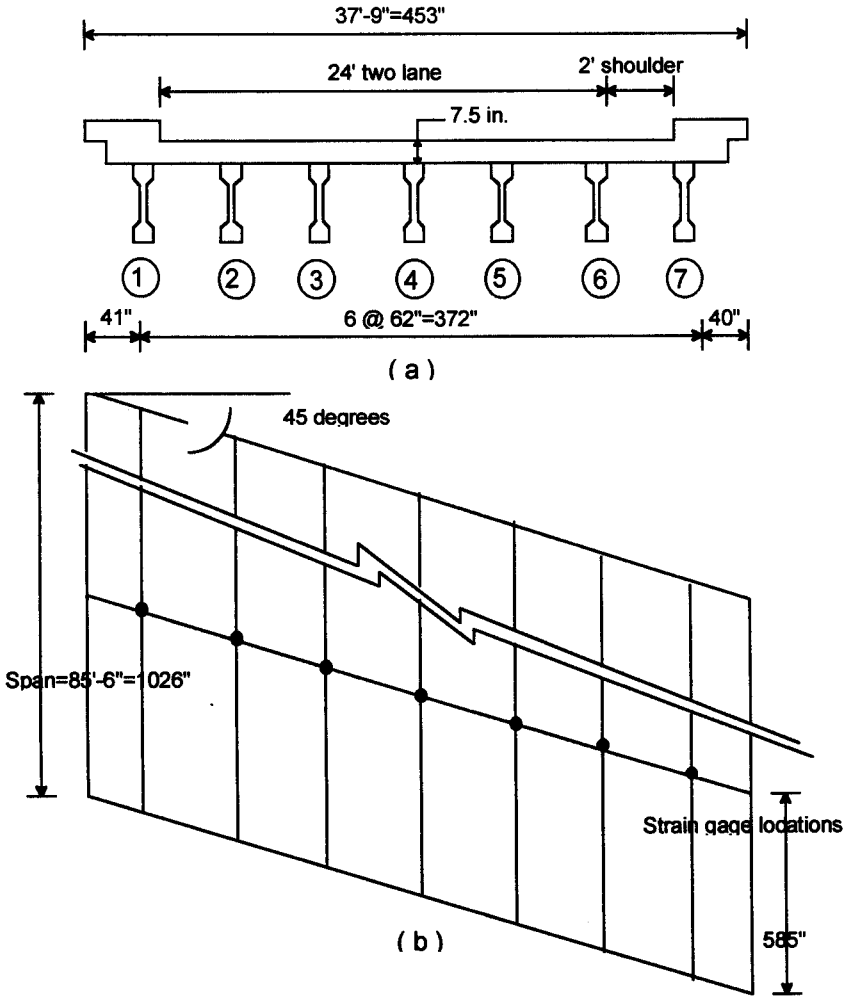

Fig. 3.11 Field test detail

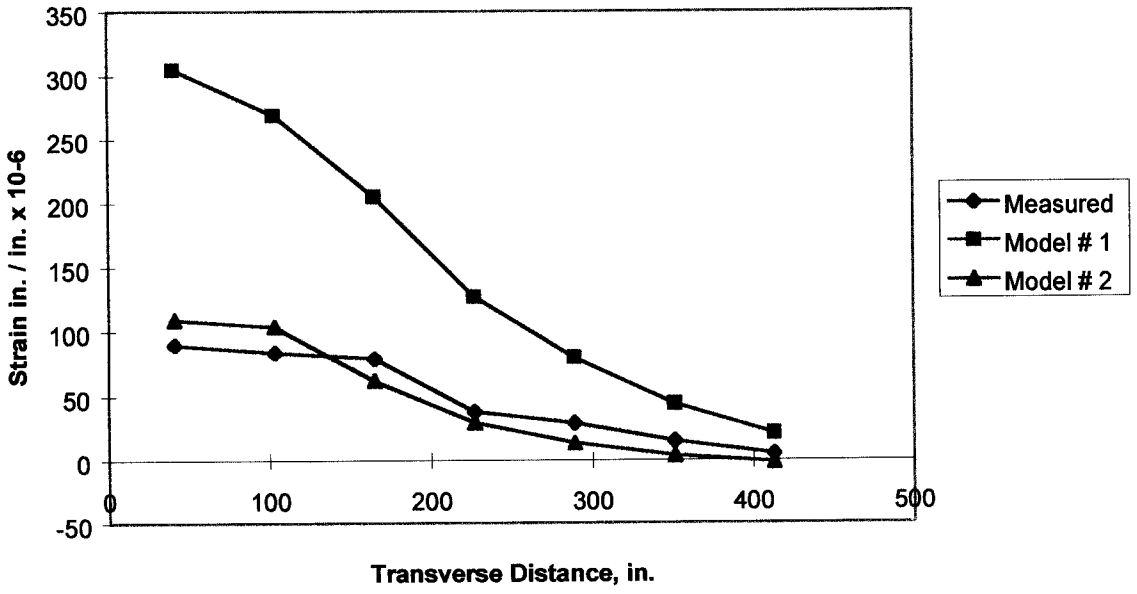

Fig. 3.12 Strain variation across the slab-on-gider bridge

CHAPTER 4

LOAD DISTRIBUTION ANALYSIS OF SKEW SLABON-GIRDER BRIDGES

4.1 INTRODUCTION

The slab-on-girder bridges are the most common type of bridges throughout the United States. The precast concrete girders such as standard precast AASHTO 1-girders are efficient and very economical. The precast concrete girders are often used with a cast-in-place deck to form the riding surface. The major restrictions to precast girder construction are the limitations in the length and weight. The slab-on-girder type bridges are practical for spans up to 120 ft. for AASHTO I-girders.

Analyses performed during design of slab-on-girder bridges are commonly based on the AASHTO wheel load distribution factors. There is a substantial amount of literature that illustrates the conservatism in using the AASHTO wheel load distribution factors (Heins and Lawrie,1984 and Warren and Malvar,1993). This led to the NCHRP to develop and propose the LRFD simplified load distribution factors. However, advances in computing technology have facilitated the use of refined analysis methods. In some cases, it is desirable to perform a more advanced structural analysis. This is especially true, when an evaluation of the load capacity of an existing bridge is being made. Finite element analysis can be used to obtain a more accurate and reliable prediction of the load distribution factors.

The studies carried out by the Principal Investigator (Acrockiasamy,1995) on "Load Distribution on Highway Bridges Based on Field Test Data - Phase I" present the load distribution on certain non-skew bridge types in Florida viz., slab-on-girder, solid slab, voided slab and double-tee bridges. Truck load distributions of skew slab-on-girder bridges based on finite element method and field tests performed by Florida Department of Transportation (FDOT) are investigated in this chapter. The objectives of this study are the following:

I) Determine the wheel load distribution using finite element method and study the effects of skew angle, span length, girder spacing and slab thickness, exterior and interior girders and other parameters.

II) Verify the AASHTO and the LRFD load distribution factors using several skew slab-on girder bridge field tests.

III) Derive simple empirical design criteria, if needed, for load distribution that would provide more accurate alternative to current designs.

4.2 METHOD OF ANALYSIS

The measured field test data provided by Florida Department of Transportation was used in conjunction with those based on the finite element models and AASHTO and LRFD bridge specifications. Also, a parametric study for skew slab-on-girder bridges is conducted to identify the main parameters. In the following sections, a summary of the AASHTO and LRFD specifications is presented.

The AASHTO procedure to calculate the flexural distribution factors is generally used for bridges and tends to be overly conservative particularly for analysis of existing bridges. The

AASHTO method of determining load distribution factors reduces the complex analysis of a bridge subjected to one or more vehicles to the simple analysis of a beam. According to this method, the maximum moment in a girder can be obtained by treating a girder as a one-dimensional beam subjected to a loading, which is obtained by multiplying one line of wheels of the design vehicle by a load fraction (S/D) where S is average beam spacing in ft. **The quantity D in the AASHTO specifications for concrete floor on prestressed concrete girders is 7 for one lane bridges and 5.5 for mufti-lane bridges. If S exceeds 10 ft. for one lane bridges and 14 ft. for multi-lane bridges, the load in each girder shall be the reaction of the wheel loads, assuming the flooring between the girders to act as a simple beam. The AASHTO equation is based substantially on the research carried out by Newmark (1948). The AASHTO equation did not include approximate formulae for moments to account for the effects of skewed supports. It is frequently considered safe to ignore the skew angle, if it is less than 20 degrees and analyze the bridge with a span equal to the skew span, since it leads to a conservative estimate of longitudinal moments and shears in the skew bridges. This approximate procedure is inappropriate for old bridges and bridges with longer skew angles.**

The LRFD approach is similar to AASHTO method, but considers more parameters such as material properties, skew angle, sectional properties of the girders, span length, slab thickness, and number of lanes. The LRFD approach is based on NCHRP project 12-26 entitled, "Distribution of Wheel Loads on Highway Bridges", which was performed in two phases by Imbsen and Associates Inc. The LRFD approach for slab-on-girder bridges gives different factors for bending and shear. The distribution of live loads on precast concrete AASHTO I-girder is categorized under the category "K" in the LRFD specifications. The LRFD distribution of live load moment in interior beams per lane is given as:

One design lane loaded

$$g = 0.5\left[0.12 + (\frac{S}{2.5})^{0.4}(\frac{S}{L})^{0.3}(\frac{K_g}{12.0Lt_s^3})^{0.1}\right] \quad \textbf{(4.1)}$$

Two or more design lanes loaded

$$g = 0.5\left[0.15 + (\frac{S}{3.0})^{0.6}(\frac{S}{L})^{0.2}(\frac{K_g}{12.0Lt_s^3})^{0.1}\right] \quad \textbf{(4.2)}$$

Where S = Spacing of supporting beams or webs ($3.5<S<16.0$), ft.

L = Span length ($20<L<240$), ft.

t_s = Depth of concrete slab ($4<t_s<12$), in.

K_g = Longitudinal stiffness parameter,

$= n(I + Ae_g^2)$

n = Modular ratio between beam and deck materials.

I = Moment of inertia of the beam, in^4

A = Area of the beam or girder, in^2

e_g = Distance between the centers of gravity of the basic beam and deck, in.

The live load moment for exterior beams may be determined by applying the lane fraction, e,

$$g_{exterior} = e\, g_{interior} \quad \textbf{(4.3)}$$

where,

$$e = \frac{7 + d_e}{9.1} \geq 1.0$$

d_e = Distance between the center of exterior beam and the interior edge of curb or traffic barrier ($-1.0 < d_e < 5.5$), ft.

When the line supports are skewed and the difference between skew angles of two adjacent lines of supports does not exceed 10 degrees, the bending moment in the beam may be reduced by:

$$r = 1 - c_1(\tan\theta)^{1.5} \quad \textbf{(4.4)}$$

where,

$$c_l = 0.25\left(\frac{K9}{L S^3}\right)^{0.25}\left(\frac{S}{L}\right)^{0.5}$$

If $\theta < 30^{\circ}$, then $c_l = 0.0$,

If $\theta > 60^{0}$, use $\theta = 60^{0}$,

The range of applicability of the Equation 5.4 is

$30^{0} \le \theta \le 60^{0}$, $3.6ft. \le S \le 16.0ft.$, $20ft. \le L \le 240ft.$

Both analytical and field studies on the truck wheel load distribution of skew slab-on-girders are presented in this chapter. Finite element method explained in Chapter 3 is used to study the various parameters affecting load distribution and suggest which parameters must be considered. In addition to the analytical study, data from field tests performed by Structures Research center, MOT are used to verify the analytical results.

4.2.1 Load Distribution Factor

A load distribution factor may be calculated from the strains of each girder determined from finite element analyses or field tests. The distribution factor, DF is equal to the ratio of maximum girder bending moment obtained from finite element method or field test to the total bending moment in the bridge idealized as a one-dimensional beam subjected to one set of wheels.

The sum of internal bending moments is equivalent to externally applied bending moments due to the wheel loads for a straight bridge. Assuming all traffic lanes are loaded with equal-weight trucks, the wheel load distribution factor for the ith girder in a straight bridge is calculated from the strains as follows (Stalling and Yoo 1993):

$$DF_i = \frac{\varepsilon_i}{\sum_{k=1}^{n} \varepsilon_k} \qquad (4.5)$$

E_i = **the bottom flange strain at the ith girder**

W; = **ratio of the section modulus of the ith girder to the section modulus of a typical interior girder**

n = **number of wheel lines of applied loading**

Equation 4.5 is based on the assumption that the sum of the internal moments or the total area under the moment distribution curve should be equal to the externally applied moment. This assumption is valid only for straight bridges. However, this assumption is not realistic to yield the actual moment distribution in skew bridges. The distribution factor, DF is equal to the ratio of maximum girder moment obtained from finite element or field tests to the maximum moment in the bridge idealized as a one-dimensional beam subjected to one set of wheels. The sum of the internal moments in a straight bridge is equal to the maximum moment in the bridge idealized as a one-dimensional beam subjected to one set of wheels. The sum of the girder strains in a straight bridge will be used to take into account the total external load effects in skew bridges. Equation 4.5 can, therefore, be modified as follows:

$$DF_{i\theta} = \frac{n\varepsilon_{i\theta}}{\left(\sum_{j=l\rightarrow k} \varepsilon_j W_j\right)_{\theta=0}} \qquad (4.6)$$

4.3 SKEW SLAB-ON-AASHTO GIRDER FLEXURAL LOAD DISTRIBUTION FACTORS: PARAMETRIC STUDIES

It is important to understand the effect of various parameters on flexural load distribution. Several parameters affect the load distribution of skew slab-on-girder bridges. Skew angle, span length, girder spacing, thickness and load positions are the main parameters which are considered in this section. Bridge parameters are varied one at a time in a typical bridge. Variation of wheel load distribution factors with each parameter shows the relative importance of the parameters. Figure 4.1 shows the typical skew slab-on-girder bridge used in the analyses. The typical skew slab-on-girder bridge has a span length equal to 70 ft. with a bridge width of 54 ft and skew angle of 30 degrees. It has prestressed AASHTO girder IV with a slab thickness of 7 in. The AASHTO girder IV is shown in Figure 4.2. The concrete strength of both the girder and slab was taken equal to 5,000 psi.

4.3.1 Finite Element Model

The typical skew slab-on-girder bridge is shown in Figure 4.1. The analysis assumes linear elastic material behavior. The properties of the slab elements may have either isotropic or orthotropic properties. Table 4.1 summarizes the material and sectional properties of the typical bridge.

Typical top view of the finite element mesh is presented in Figure 4.3. The deck slab is divided into 24 x 14 four-node shell elements and each girder divided into 24 sections. Simply supported boundary conditions are realized by restraining the appropriate translational degrees of freedom. Details of the modeling are presented in Chapter 3.

Figure 4.4 shows cross sectional view of the finite element model, in which the reinforced concrete slab was discretized using four-node shell elements. Each I-girder was divided into three parts: the top and bottom flanges and the web. Each flange was modeled by a beam element with its properties lumped at the centroid of the flange. The web was modeled by shell elements with four mid-surface nodes. Each mid-surface node has six degrees of freedom. Rigid links are assumed between the top beam elements and the centroids of the top deck slab shell elements.

Table 4.1 Material and sectional properties for the typical skew slab-on-girder bridge

Materiel properties	E_{deck} (ksi)	E_{girder} (ksi)	Poisson's ratio, υ	G (ksi)
	4031	4031	0.2	1679

Section properties	Slab	Thickness = 7 in.				
	Girder web	Thickness = 8 in.				
		A (in^2)	I_y (in^4)	I_z (in^4)	T_{ky} (in)	T_{kz} (in)
	Top beam	244	3076	8133	20	12.2
	Bottom beam	361	5794	20330	26	13.88

* E_{deck}, E_{girder} = Elastic modulus of the deck slab and girder respectively,
G = Modulus of rigidity,
A = Area of cross section of the girder,
I_y, I_z = Moment of inertia of the girder in y and z direction respectively,
T_{ky}, T_{kz} = Thickness of the girder in y and z direction respectively, as shown in Figure 4.4.

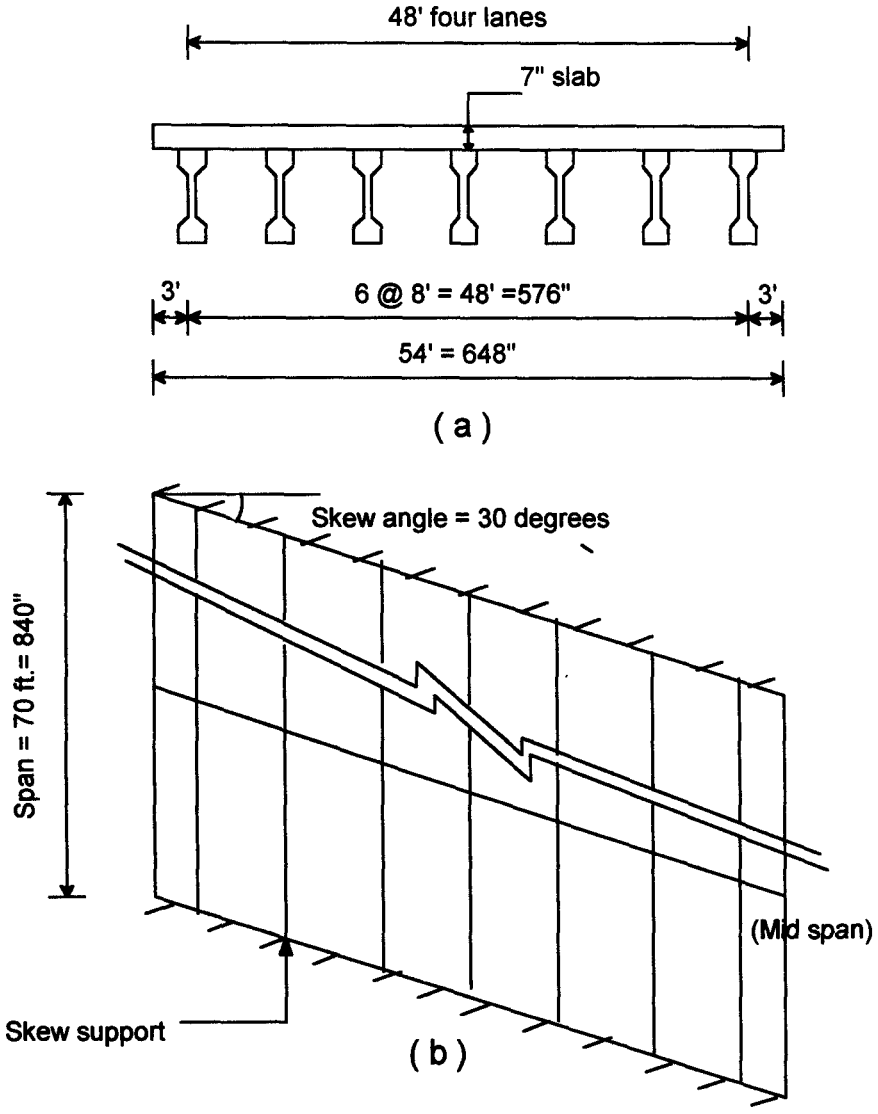

Fig 4.1 Typical skew slab-on-girder bridge details

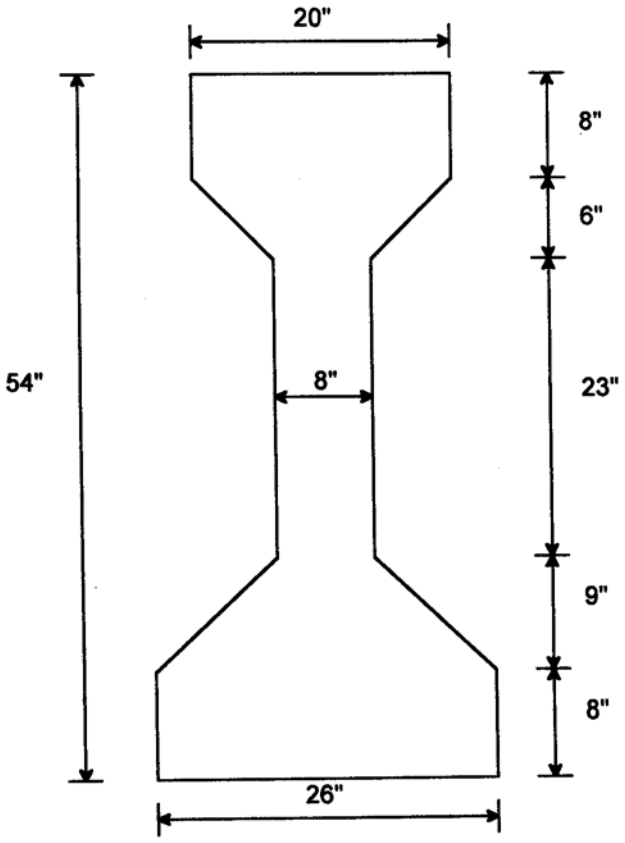

Fig.4.2 AASHTO IV girder details

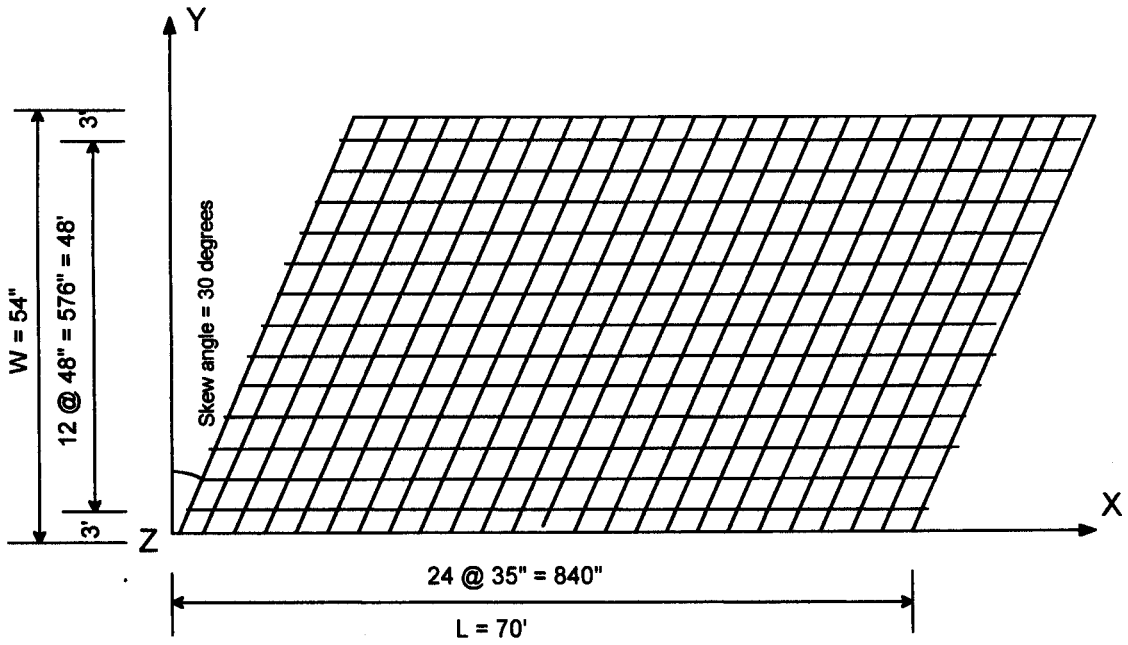

Fig.4.3 Top view of finite element mesh of typical skew slab-on-girder bridge

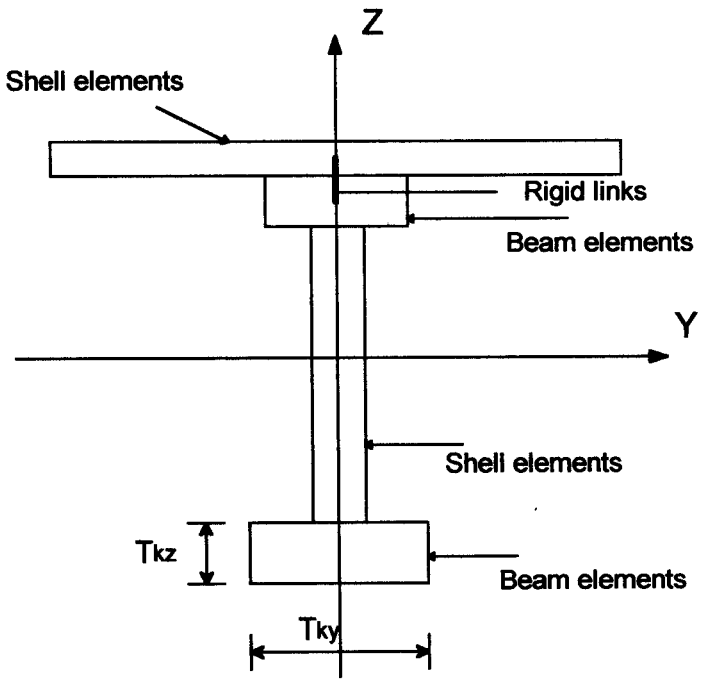

Fig.4.4 Finite element model of typical skew slab-on-girder bridge

4.3.2 Truck Load Position

The AASHTO HS-20 truck was used in this parametric study (Figure 4.5). The truck load position in the longitudinal direction (span direction) was located to produce the maximum bending moment. To get the maximum bending moments in the bridges, two, three or four trucks were positioned in the transverse direction.

Several cases were investigated to verify the critical load position. Figures 4.6 to 4.8 show the different truck positions which were used to decide the critical load position for interior beam. For exterior girders, the wheels of the first truck were at 3 ft. from the bridge edge, i.e. exactly over the exterior girder as shown in Figures 4.9 and 4.10. Three cases were investigated to decide the load position for exterior beam.

Table 4.2 summarizes the flexural load distribution factors calculated for different load positions for both interior and exterior girders. Figures 4.8a and 4.9b show the selected critical positions to calculate the load distribution factors for interior and exterior beam in this parametric study for skew slab-on-girder bridge.

Table 4.2 Load distribution factors for different load positions

Load position (Int. girders)	AASHTO code	LRFD code	F.E.M.
Fig.4.6a	1.4545	1.3896	1.2217
Fig 4.6b	1.4545	1.3896	1.2520
Fig 4.7	1.4545	1.3896	1.3581
Fig 4.8a	1.4545	1.3896	1.3697
Fig 4.8b	1.4545	1.3896	1.5422*

* This case gives higher distribution factor. However, it did not produce the maximum moments.

Load position (Ext. girders)	AASHTO code	LRFD code	F.E.M.
Fig.4.9a	1.4545	1.3896	1.2950
Fig.4.9b	1.4545	1.3896	1.4940
Fig.4.10	1.4545	1.3896	1.4810

Fig 4.5 AASHTO HS-20 truck

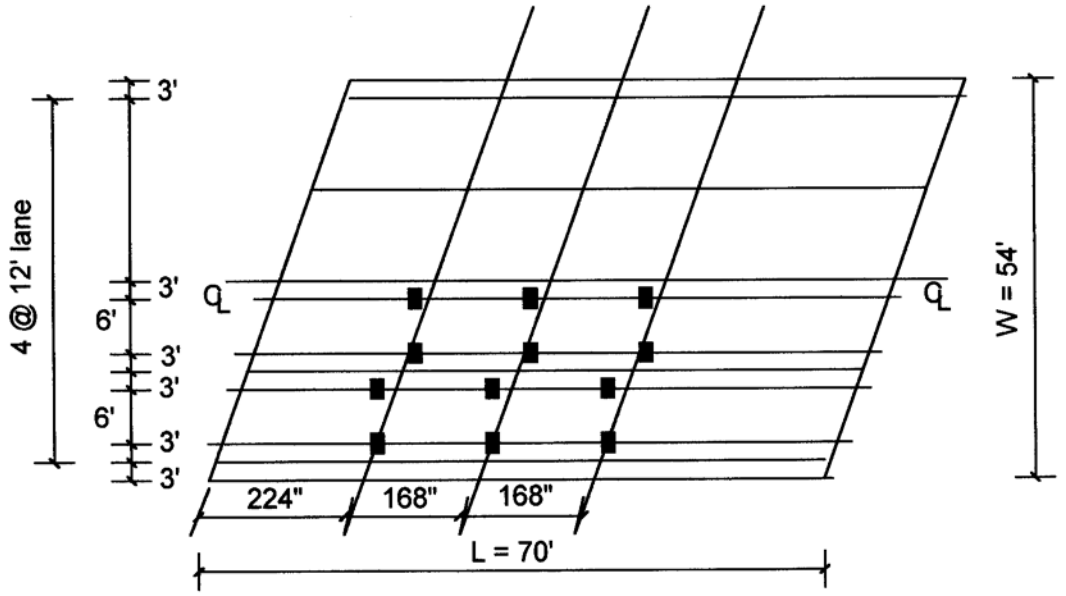

(a) Two trucks parallel to support

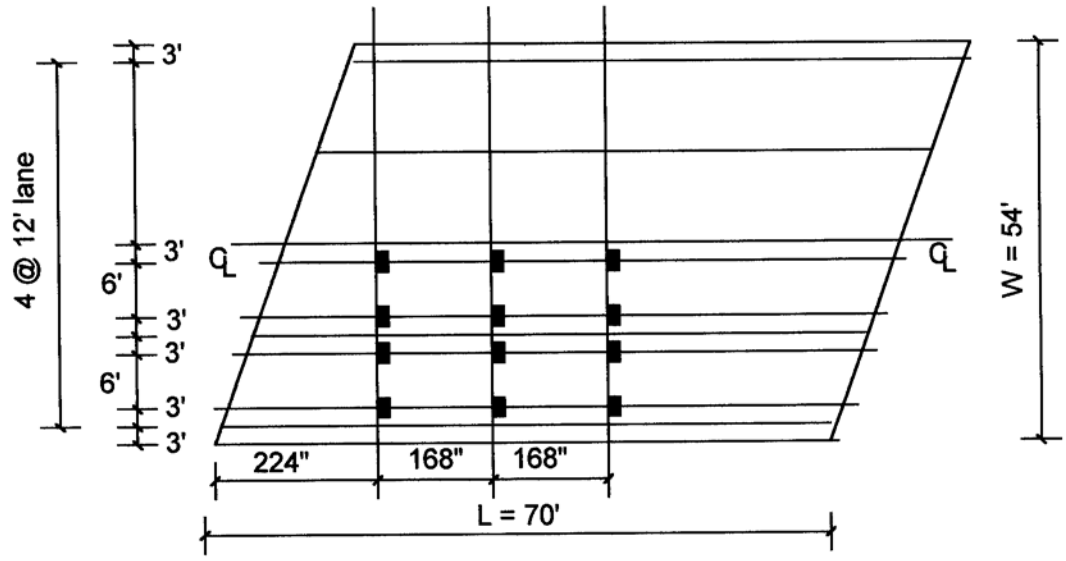

(b) Two trucks perpendicular to support

Fig 4.6 Load position for interior girders

(Two trucks)

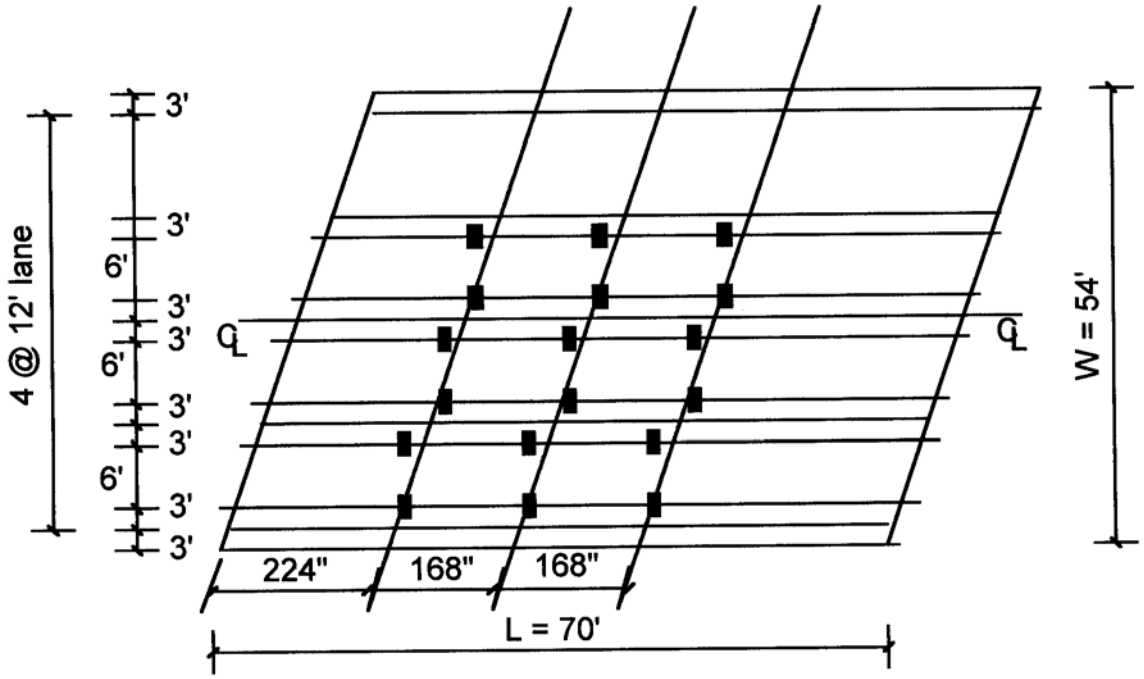

Fig 4.7 Load position for interior girders (Three trucks parallel to support)

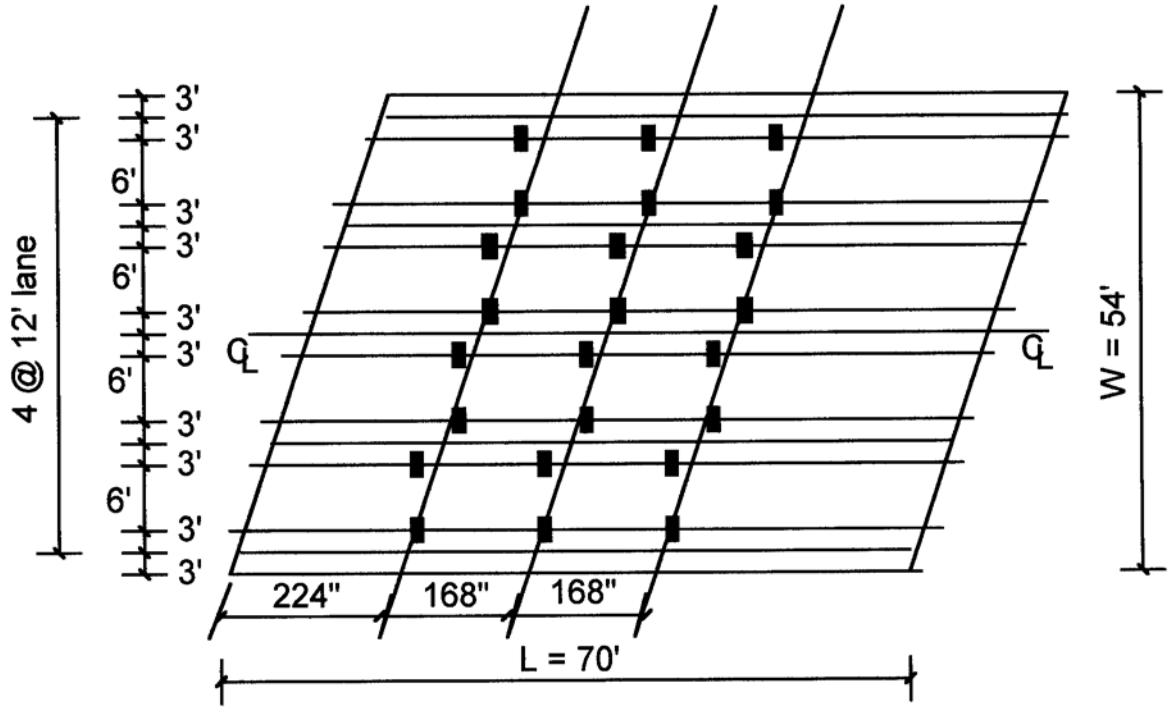

(a) Four trucks parallel to support

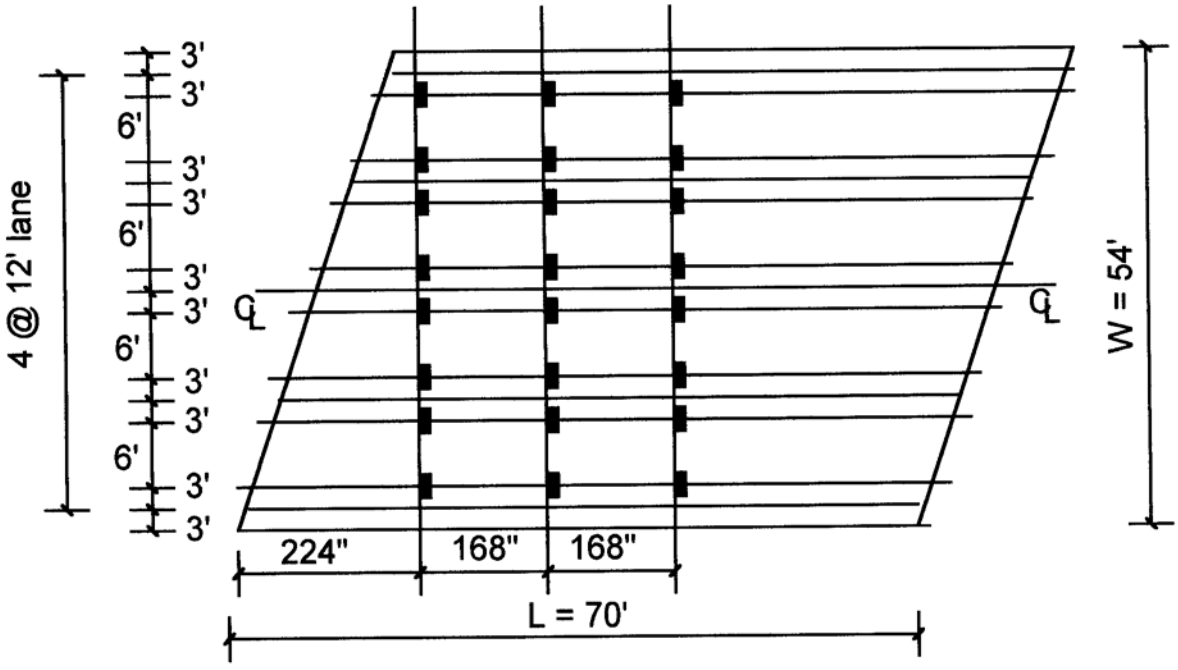

(b) Four trucks perpendicular to support

Fig 4.8 Load position for interior girders

(Four trucks)

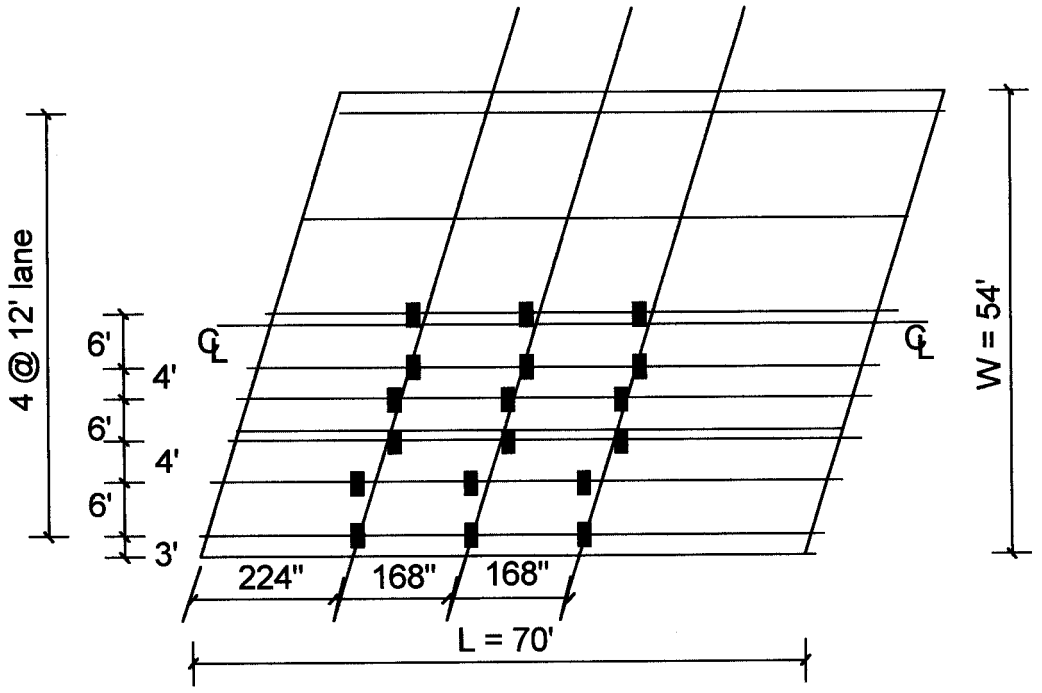

(a) Three trucks parallel to support

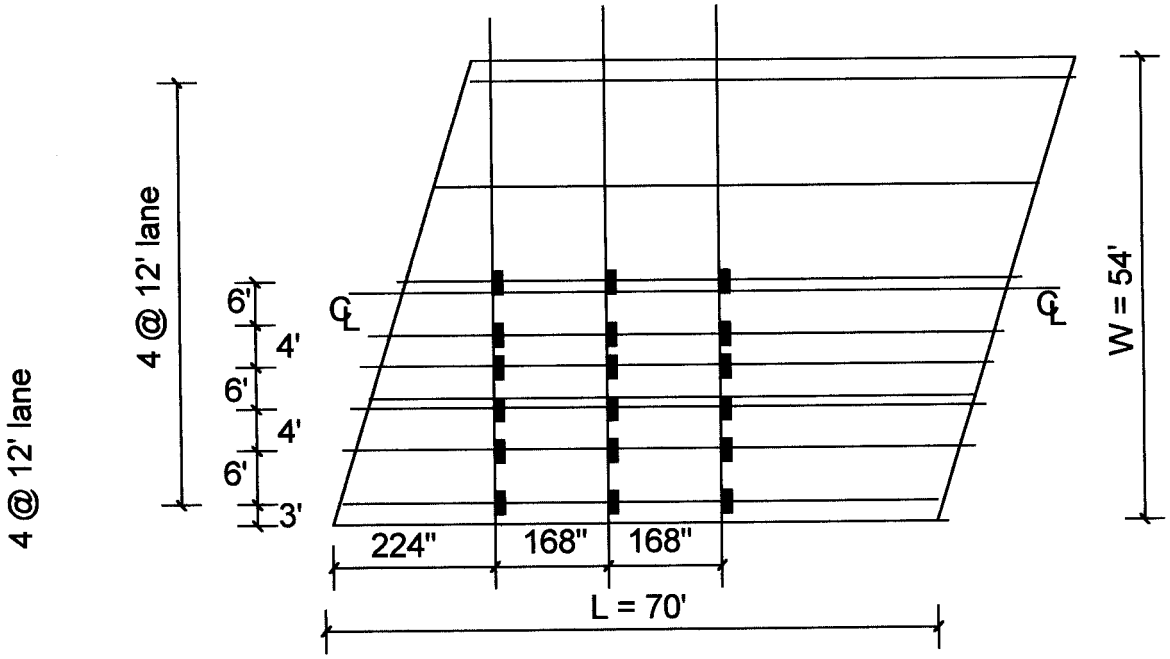

(b) Three trucks perpendicular to support

Fig.4.9 Load position for exterior girders (Three trucks)

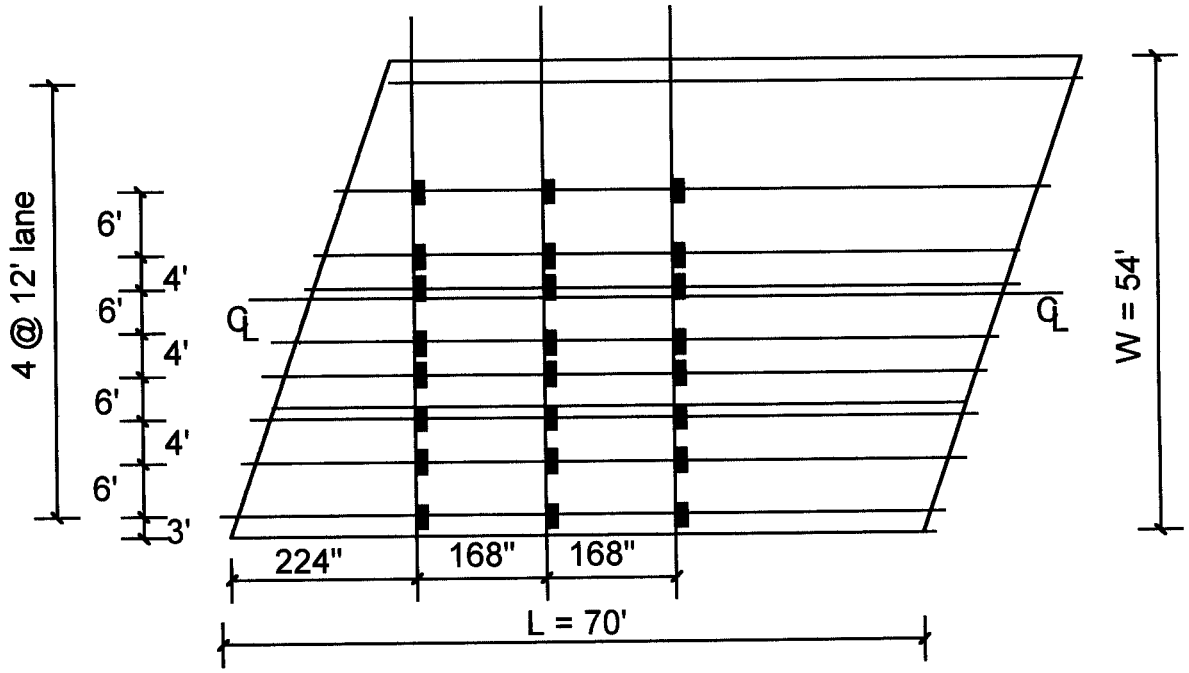

Fig 4.10 Load position for exterior girders
(Four trucks vertical to traffic direction)

4.3.3 **Parametric Studies**

Table 4.3 summarizes the cases in which several parameters such as skew angle, span length, girder spacing, slab thickness, etc., were considered to study the load distribution factors of AASHTO girders. Thirty-two cases were investigated using finite element method (Ansys Program) to establish the main parameters affecting the load distribution factors of the skew slab-on-girder bridges.

Table 4.3 Summary of parametric study cases for slab-on-bridges

Parameter	Skew angle, degree	Span Length, ft.	Girder Spacing, ft.	Thickness, in.	Width, ft.	Girder type	Comments
Skew angle (8 cases)	0 30 45 60	70 70 70 70	8 8 8 8	7 7 7 7	54 54 54 54	IV IV IV IV	4 trucks (Int. girder) 3 trucks (Ext. girder)
Span length (8 cases)	30 30 30 30	50 70 80 100	8 8 8 8	7 7 7 7	54 54 54 54	IV IV IV IV	4 trucks (Int. girder) 3 trucks (Ext. girder)
Girder spacing (8 cases)	30 30 30 30	70 70 70 70	6 8 9.6 12	7 7 7 7	54 54 54 54	IV IV IV IV	4 trucks (Int. girder) 3 trucks (Ext. girder)
Thickness* (8 cases)	30 30 30 30	70 70 70 70	8 8 8 8	7 5.55 4.40 3.85	54 54 54 54	IV IV IV IV	4 trucks (Int. girder) 3 trucks (Ext. girder)

(*Thicknesses are calculated corresponding to H=5,10,20,30)

4.3.3.1 Skew angle

Skew angle is ignored in the AASHTO code on load distribution computation, while the LRFD code considers the skew effect by multiplying the non-skew distribution factors with a reduction factor for both interior and exterior girders. The analysis based on finite element method shows that skew angle is an important factor, which should be considered in the bridge design. Slab-on-girder bridges with skew angles from 0 to 60 degrees (Table 4.3) were investigated in this section.

Four AASHTO HS-20 trucks were positioned in the transverse direction for interior girders, while three HS-20 trucks were positioned for exterior girders. Figures 4.11 and 4.13 show the strain distribution for a typical bridge with different skew angles. The strain decreases with the increase in the skew angle and the strain distribution is more uniform for larger skew angles. These strain distributions were used to calculate the distribution factors as explained in section 4.2.1.

Figures 4.12 and 4.14 show the changes in load distribution factors with increasing skew angles for interior and exterior girders respectively. It is clear that DF decreases with increasing skew angle for interior and exterior girders. For interior girders, the distribution factors calculated from the finite element method are smaller than those from the LRFD code. And the difference decreases with a corresponding increase in the skew angle. For exterior girder, the distribution factors from F.E.M. are also smaller than those from the LRFD code. The skew angle has similar effects on the load distribution factor, DF for both interior and exterior girders.

4.3.3.2 Span length

Span length is one of the main factors in load distribution of slab-on-girder bridges. The AASHTO code ignores span length effect on load distribution, while the LRFD code considers the span length as an important factor in wheel load distribution. The span length was varied between 50 ft. to 100 ft. as shown in Table 4.3.

Figures 4.15 and 4.17 show the strain distributions for typical skew bridges with different span lengths for interior and exterior girders respectively. The strains increase with the increases in the span length and strain distribution tends to be more uniform for shorter spans. The strain distributions were used to calculate the distribution factors. The D.F. calculations were based on Equation 4.5 instead of equation 4.6. The DF difference was negligible (1.5 - 5 %).

Figures 4.16 and 4.18 show the changes in load distribution factors with increasing span length for interior and exterior girders respectively. The load distribution factors of the interior girders decrease with increasing span and the load distribution factors of exterior girders increase with span increase.

AASHTO codes gives the same load distribution factors for different spans of a typical bridge. The load distribution factors calculated from the finite element method are smaller than

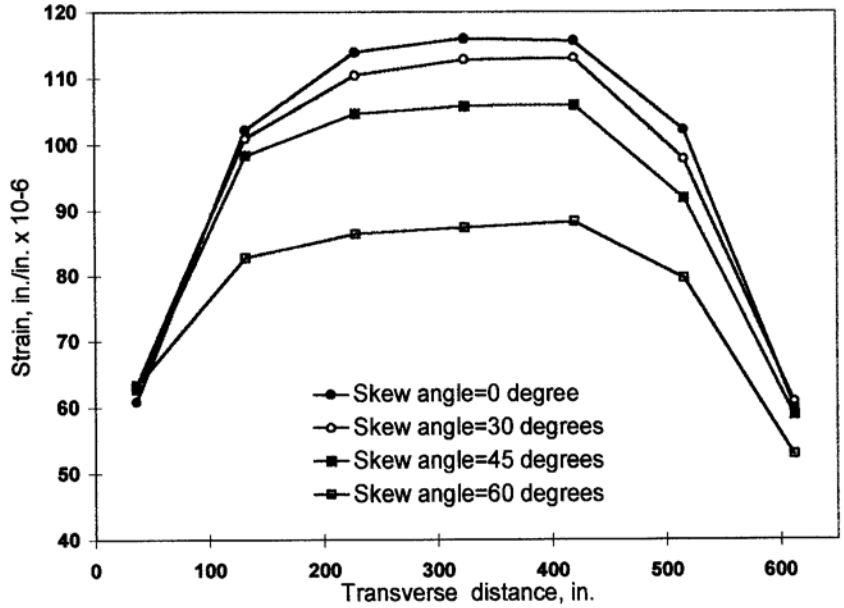

Fig.4.11 Strain distribution for different skew angles (Interior girders)

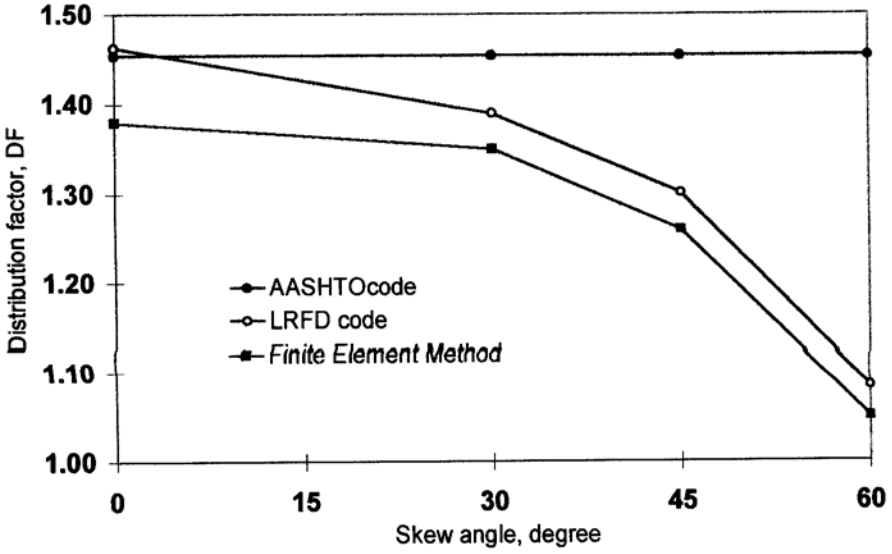

Fig.4.12 Load distribution factor variation with skew angle for slab-on-girder bridges (Interior girders)

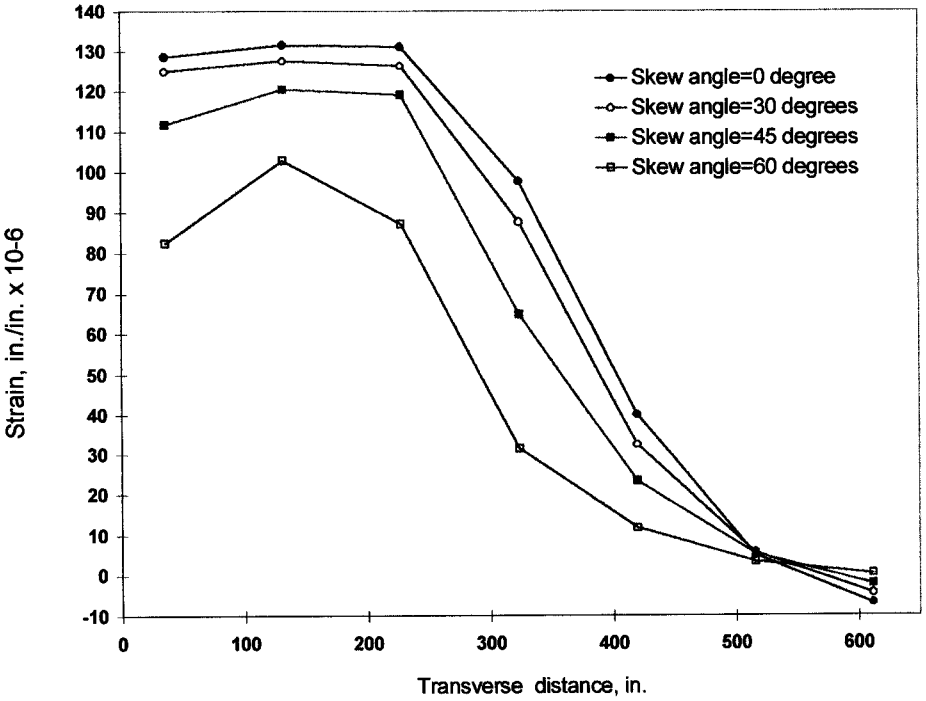

Fig.4.13 Strain distribution for different skew angles (Exterior girders)

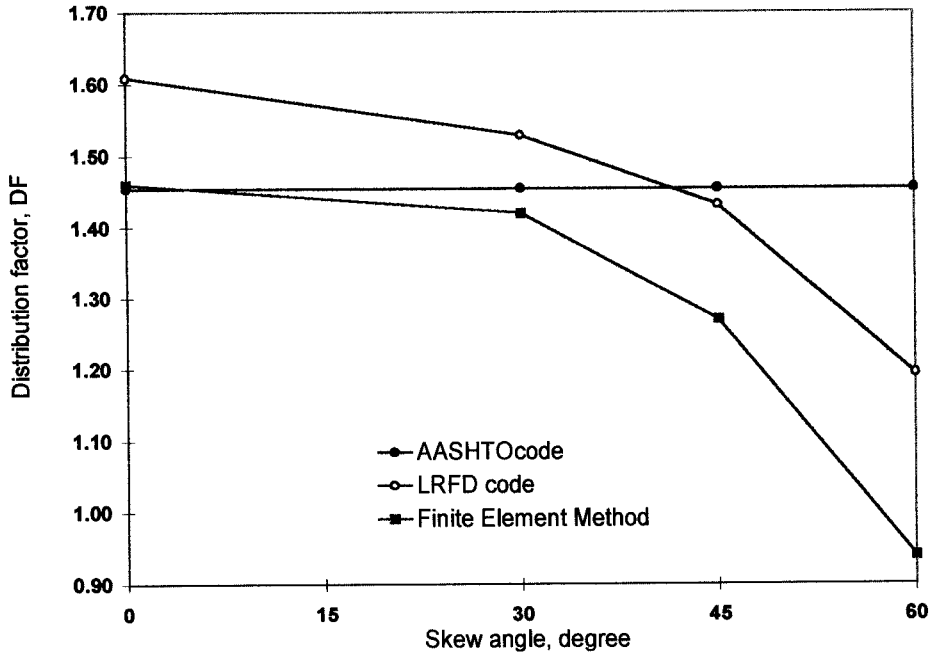

Fig.4.14 Load distribution factor variation with skew angle for slab-on-girder bridges (Exterior girders)

those from AASHTO code for interior girders. The difference only slightly increases with the corresponding increase in span length. It shows the AASHTO code gives a safe estimate of distribution factors. For exterior girders, the distribution factors based on finite element method are larger than those calculated from AASHTO code. This means that the AASHTO code gives unsafe estimate of distribution factor, DF for exterior girder.

The load distribution factors based on LRFD code show a significant decrease with the increase in span length for both interior and exterior girders. Figures 4.16 end 4.18 show that the LRFD load distribution factors are less accurate for shorter spans.

4.3.3.3 Girder spacing

Girder spacing is an important factor in load distribution of slab-on-girder bridges and it is the only parameter considered in the AASHTO code. The spacing between AASHTO girders was varied from 6 to 12 ft. as shown in Table 4.3.

Figures 4.19 and 4.21 show that the strain distribution for typical bridge with different girder spacings for interior and exterior girders respectively. The strains increase with the increase in girder spacing for both interior and exterior girders. The strain distribution is more uniform for smaller girder spacing. The load distributions were used to analyze the effect of girder spacing on load distribution factor. The D.F. calculations were based on Equation 4.5 instead of equation 4.6. Figures 4.20 and 4.22 show that the load distribution factors, DF increase with the increasing girder spacing for interior and exterior girder respectively. The DF for interior girders is more dependent on girder spacing, S than the exterior girders. In general, the girder spacing is a very important factor in determining wheel load distribution.

The load distribution factors calculated from finite element method are smaller than those based on AASHTO code for interior girders and the difference in the values is almost the same

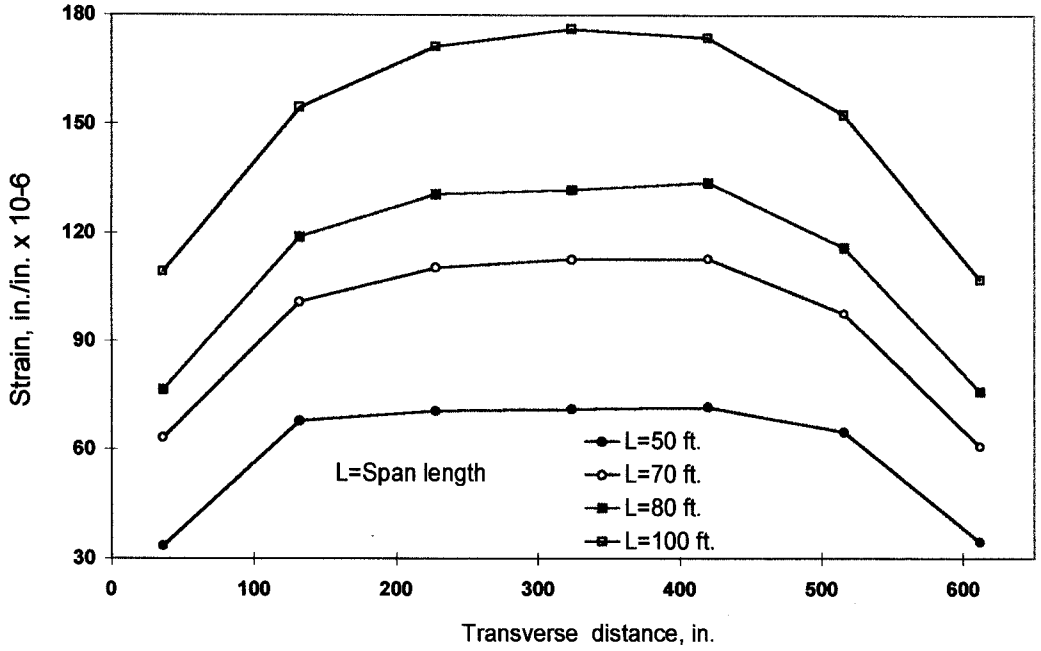

Fig.4.15 Strain distribution for different span lengths (Interior girders)

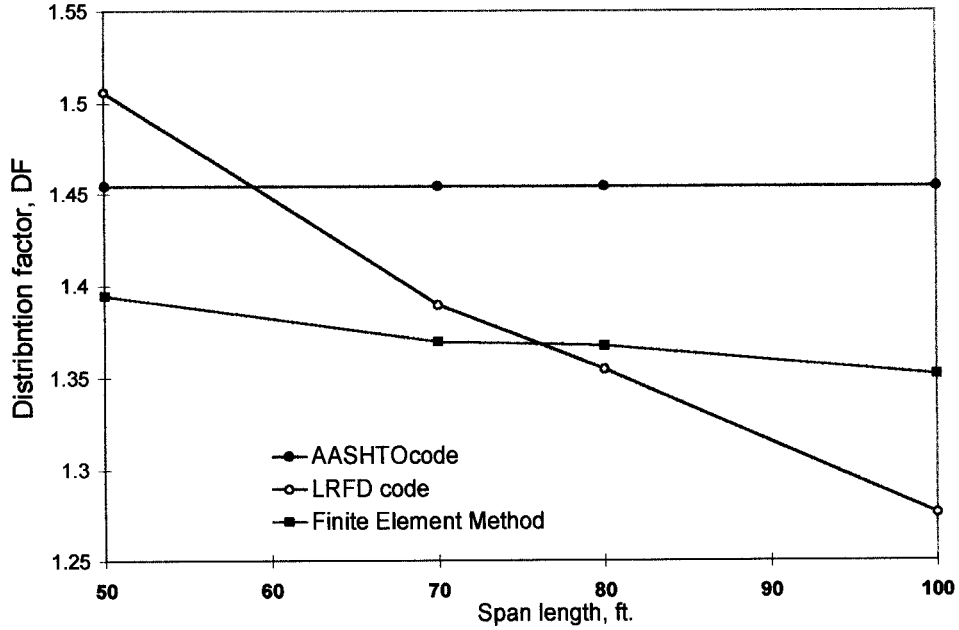

Fig.4.16 Load distribution factor variation with span length for slab-on-girder bridges (Interior girders)

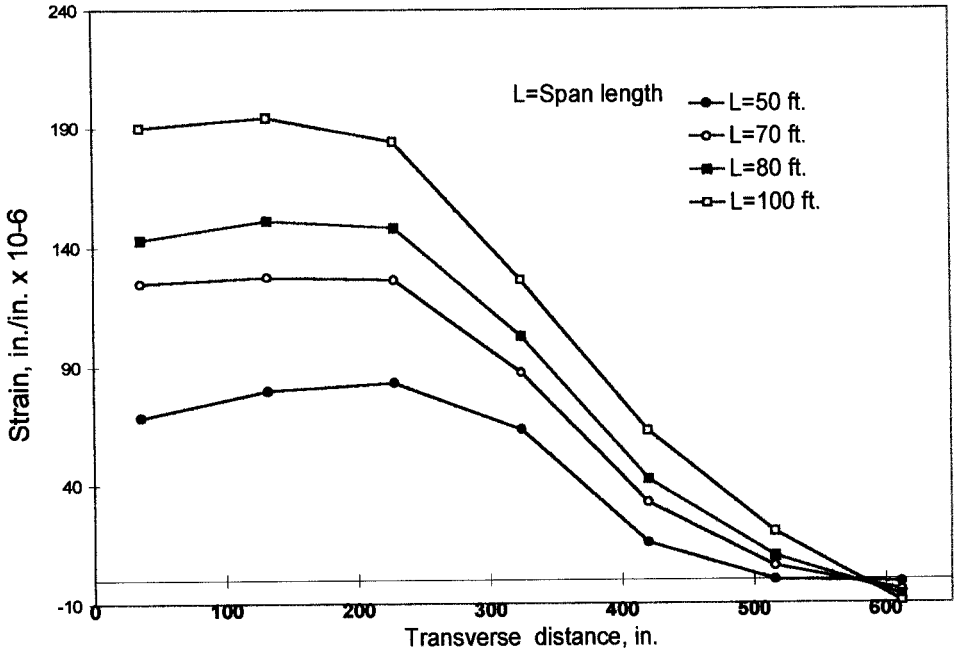

Fig.4.17 Strain distribution for different span lengths (Exterior girders)

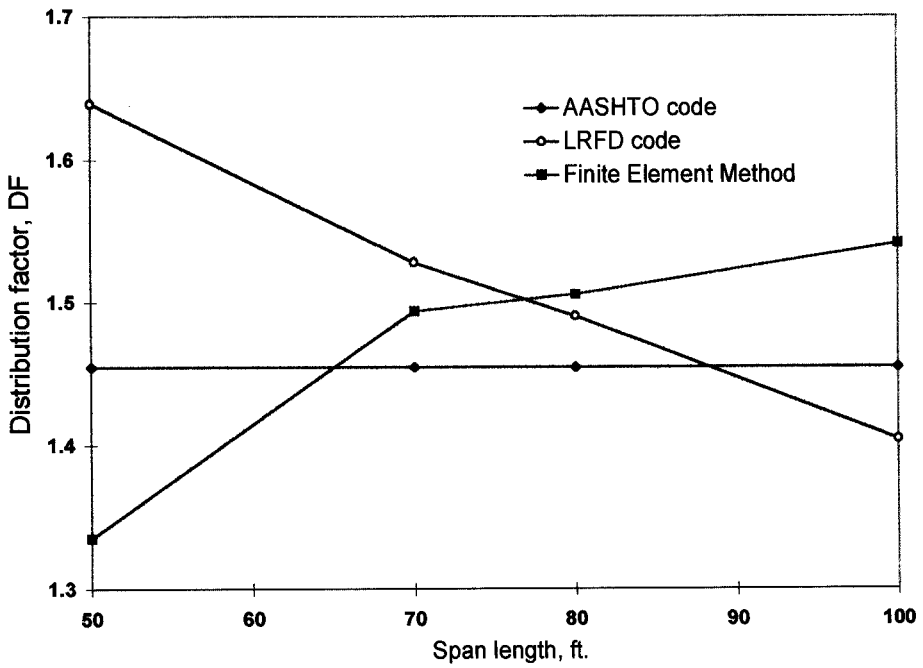

Fig.4.18 Load distribution factor variation with sapn length for slab-on-girder bridges (Exterior girders)

with the increase in girder spacing. So AASHTO code gives a conservative and reliable estimate of load distribution factor for interior girders. For exterior girders, the DF from finite element method are larger than those based on AASHTO code.

The LRFD distribution factors are smaller than those calculated from finite element method for interior girders particularly for larger spacing while they are larger for exterior girders. The wheel load distribution based on AASHTO, LRFD code and Finite Element Method are generally in good agreement when the girder spacing effect is considered.

4.3.3.4 Slab thickness

AASHTO code ignores the slab thickness as a parameter in wheel load distribution, while LRFD code considers the thickness effect on load distribution. Skew slab-on-girder bridges with slab thickness varying approximately from 4 to 7 in. are investigated in this section.

The strain distributions for different thicknesses are shown in Figures 4.23 and 4.25 for interior and exterior girders respectively. The maximum strain decreases with the increase in thickness and the strain distribution tends to be more uniform.

Figures 4.24 and 4.26 show the change in load distribution factors with the increasing slab thickness. The AASHTO load distribution factors are the same for different slab thicknesses, and for both interior and exterior girders. For interior girders, the DF calculated from finite element method are smaller than those based on AASHTO code and slightly decreases with the increasing slab thickness. For exterior girders, the DF from F.E.M. are larger than those from AASHTO code when the slab thickness becomes large. In general, AASHTO code can give a safe estimate of DF when the slab thickness is considered.

For both interior and exterior girders, the load distribution factors based on LRFD code show a significant reduction with the increase of slab thickness. The LRFD code load distribution factors are larger. than those calculated from finite element method. Both AASHTO and LRFD can

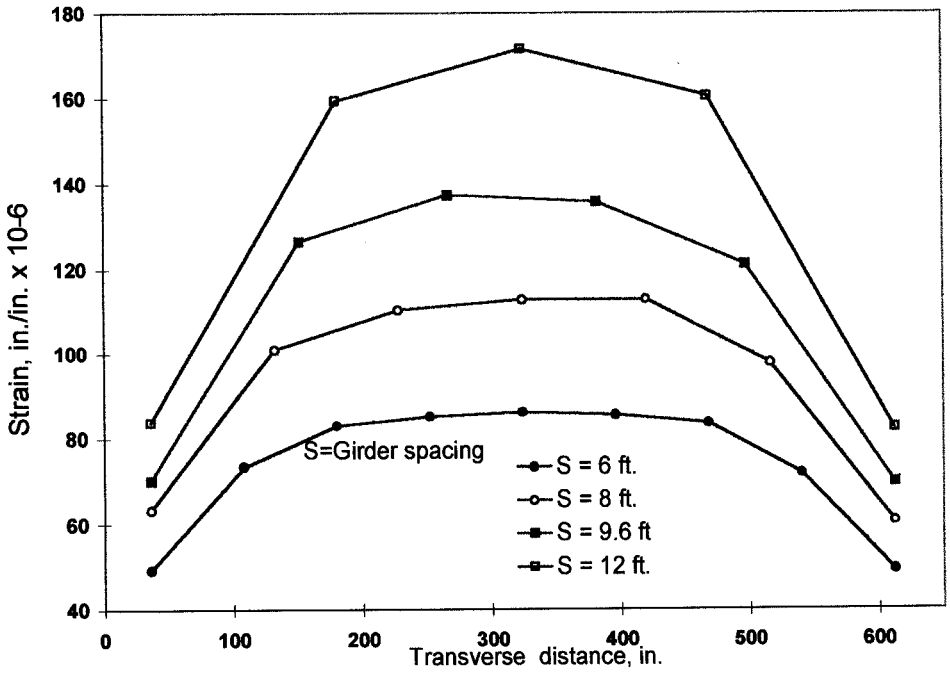

Fig.4.19 Strain distribution for different girder spacings (Interior girders)

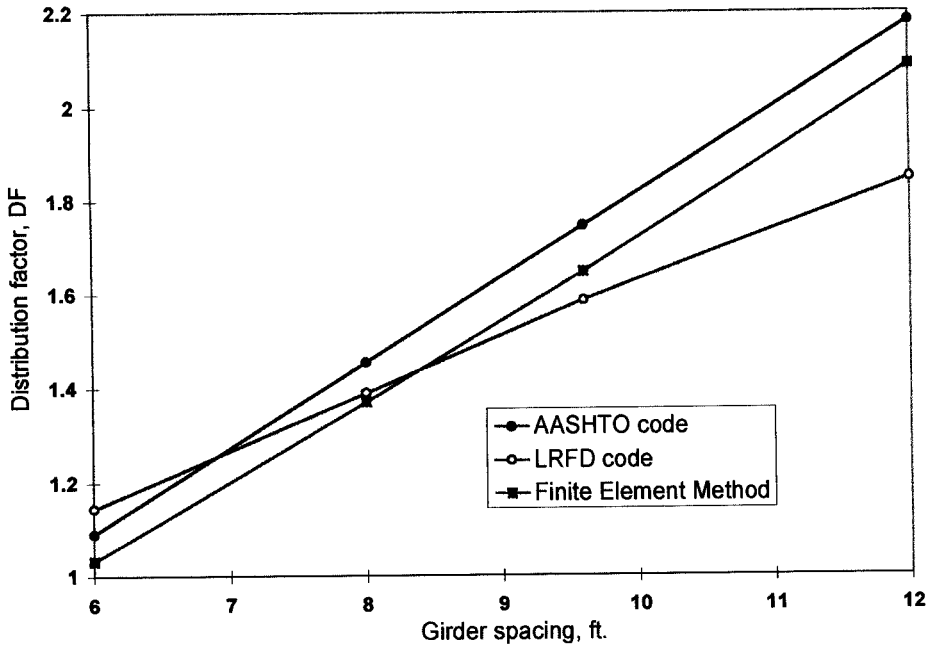

Fig.4.20 Load distribution factor variation with girder spacing for slab-on-girder bridges (Interior girders)

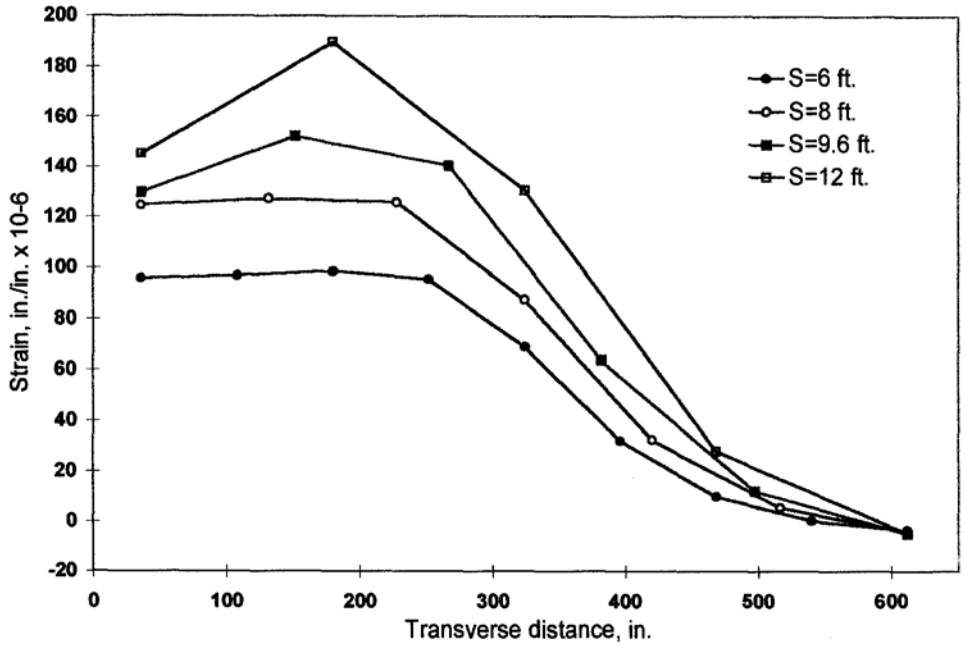

Fig.4.21 Strain distribution for different girder spacings (Exterior girders)

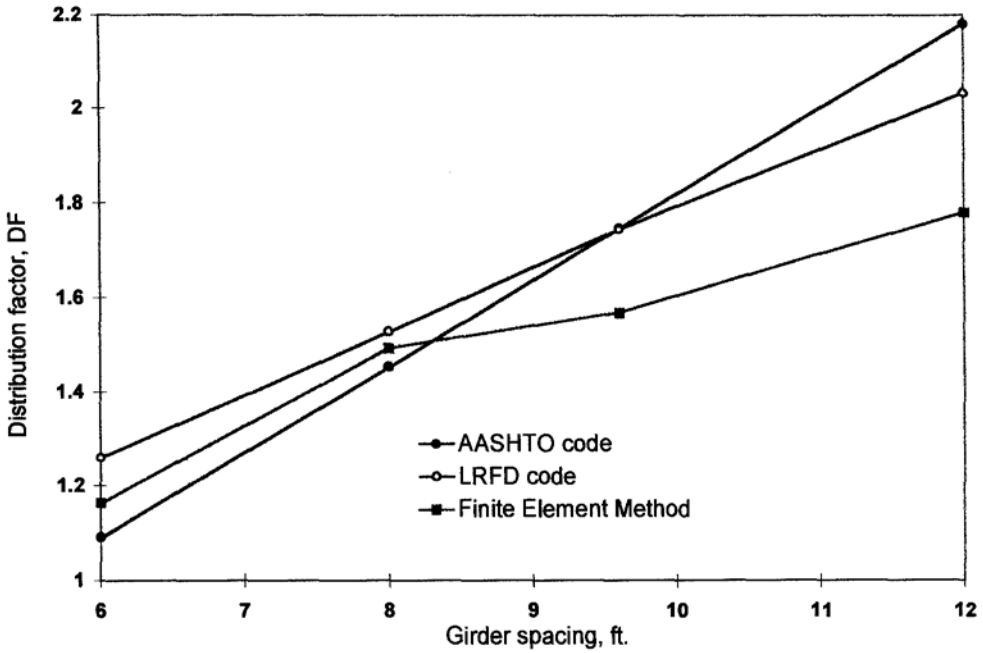

Fig.4.22 Load distribution factor variation with girder spacing for slab-0n-girder bridges (Exterior girders)

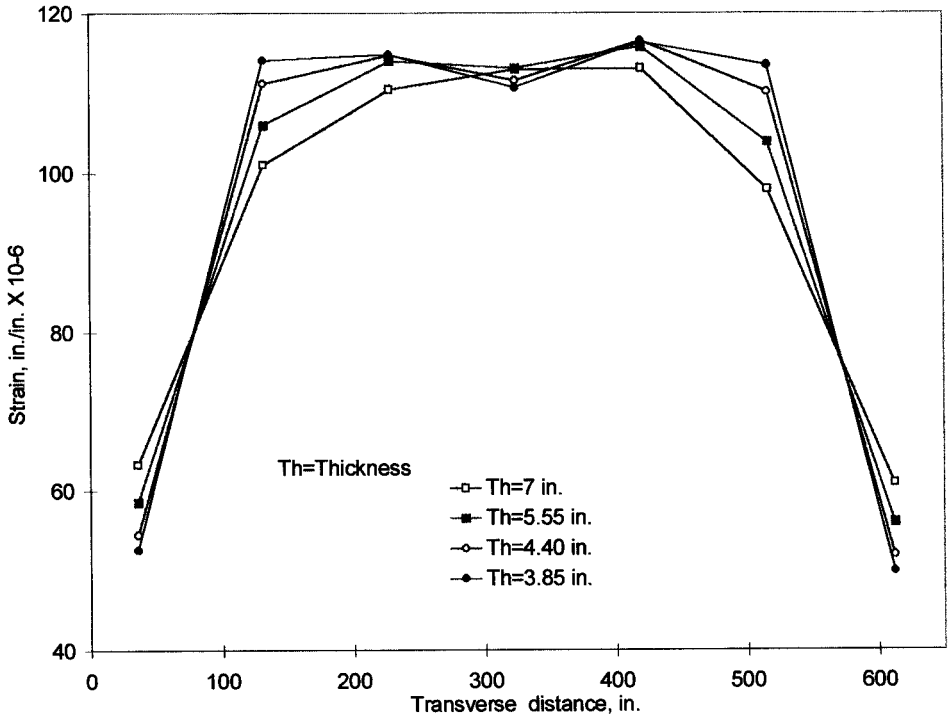

Fig.4.23 Strain distribution for different thicknesses (Interior girders)

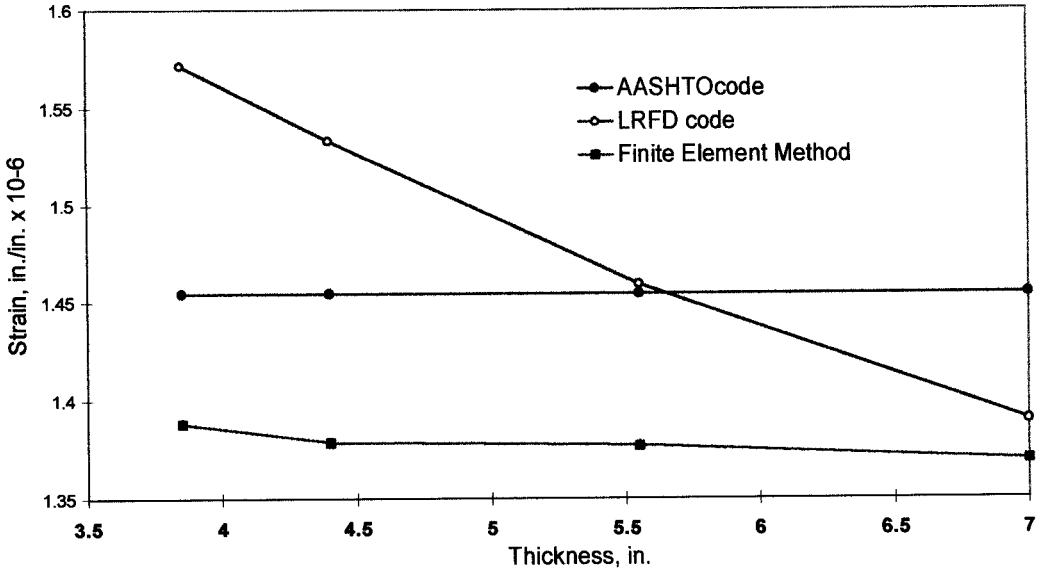

Fig.4.24 Load distribution factor variation with thickness for slab-on-girder bridges (Interior girders)

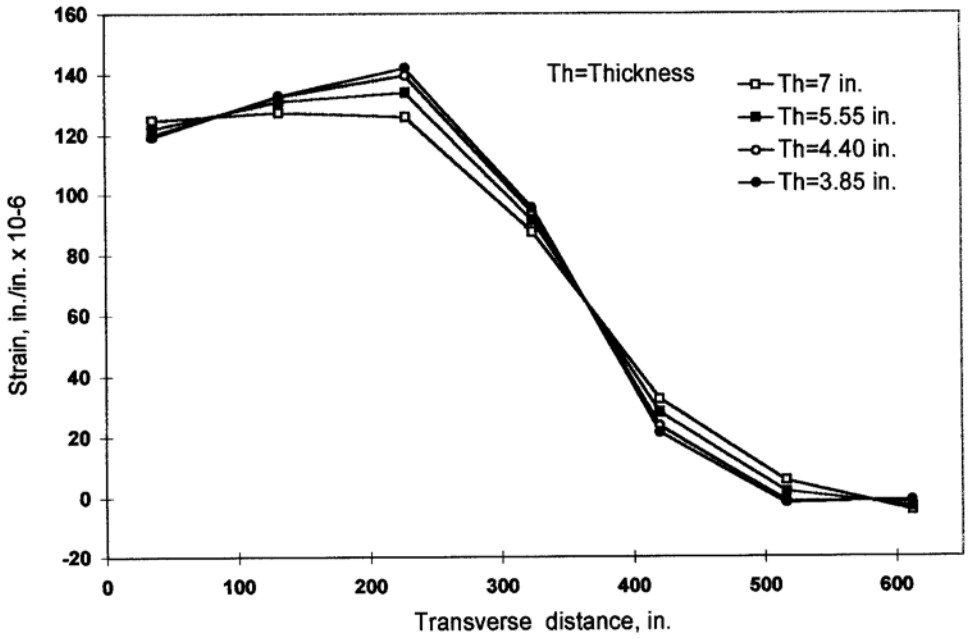

Fig.4.25 Strain distribution for different thicknesses (Exterior girders)

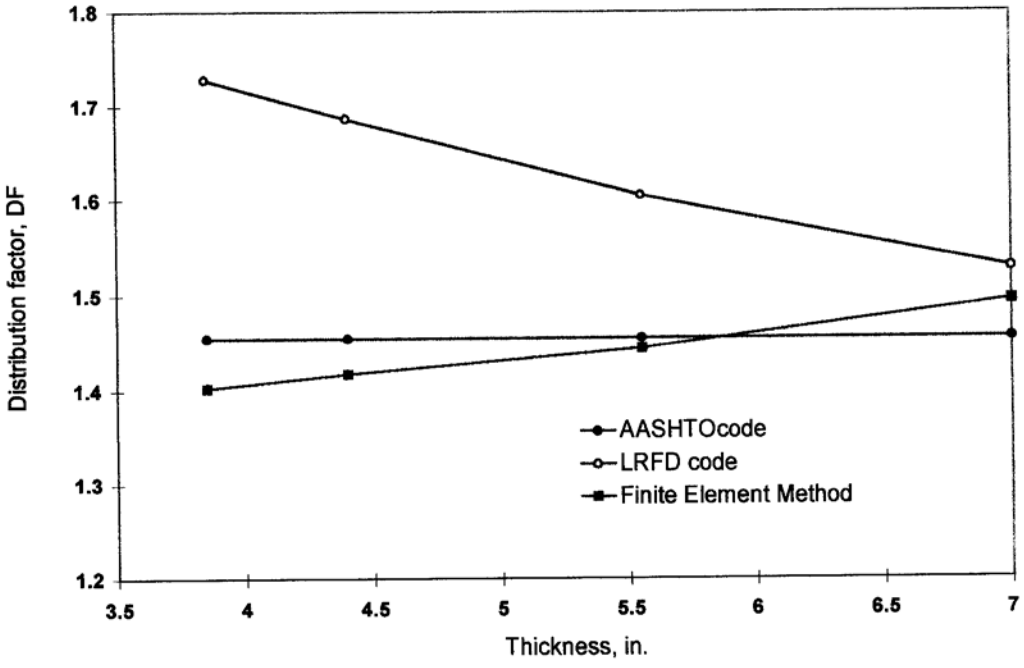

Fig.4.26 Load distribution factor variation with thickness for slab-on-girder bridges (Exterior girders)

4.4 SKEW SLAB-ON-AASHTO GIRDER BRIDGES: FIELD TESTS

Florida Department of Transportation (FDOT) have tested many bridges to check the strength. The strength of bridge elements is generally determined by first installing the strain or deflection transducer gages at the bridge critical locations along the girders, and then incrementally loading the bridge to induce maximum effects. The data collected can then be analyzed and used to establish the strength of each component as well as the load distribution.

The FDOT's bridge load testing equipment consists of two test vehicles, a mobile data acquisition system and a mobile machine shop. The two test vehicles have been designed to deliver the ultimate live loads specified by AASHTO code. Each vehicle can carry a maximum of 72 concrete blocks, each weighing approximately 2,150 pounds. Incremental loading is achieved by adding blocks with a self-contained hydraulic crane on each truck.

The test vehicles are initially loaded with a number of concrete blocks, established from the preliminary analysis of the existing structure. The vehicles are then driven and placed on the critical locations of the bridge. After each load step, the measured strain and deflections are compared with the theoretical predicted values and additional blocks are then added to the vehicles and the test repeated until the ultimate AASHTO load is achieved. The data gathered can then be analyzed and a report of the findings prepared.

Data from certain slab-on-AASHTO girder bridge test reports are used in the load distribution analyses. The typical report contains transverse strain distributions in the maximum bending moment section for several load stages. The report also contains the applied moment vs. strain curves for several load stages.

The girder bending moment can be calculated from the measured strains as follows:

$$M = E \mathbf{E} S \qquad (4.7)$$

where

E = **the strain measured at the extreme fibers of the bottom**

flange E = the modules of elasticity

S = the section modulus

The ACI equation was used to calculate the elastic modulus of concrete which is based on f,' = 5000 psi. Many bridges exhibit some degree of composite action even when they were not constructed with shear studs or other devices for transferring shear between girders and deck. The composite and non-composite section modulus were used to calculate the measured bending moments. The use of composite section modulus overestimates the measured bending moments. The use of cracked section modulus may be more realistic in the calculation of the bending moment based on the measured strains.

The skew angle for all the tests were less than 30 except for field test # 2, therefore Equation 4.5 were used instead of Equation 4.6 in the load distribution calculations for all the tests. For tests where all traffic lanes are loaded with equal-weight trucks, the measured wheel load distribution factor for the ith girder is given as [Stallings and Yoo(1993)]

DF, - $\frac{ns;}{}$ **(4.5)**

Where

8; = **the bottom flange strain at the ith girder,**

k = number of girders,

n = the number of wheel lines of applied loading

The parameter, n is required to make the measured wheel load distribution factor compatible with AASHTO definition. In this chapter, similar approach was used to calculate the measured load distribution factor based on the calculated bending moments. The measured distribution factor is compared with those based on AASHTO, LRFD and finite element analyses.

4.4.1 Duval County Bridge (#720408)

The bridge is located on I-295 over S.C.L.R.R. and U.S 90, in Duval county (Jacksonville, Florida). It consists of 7 simply supported spans with span lengths of 56', 104.15', 62.13', 64.23', 79.56' and 60.50 feet respectively. The length of tested span is 104.15 ft with a skew angle of 17.48 degrees. The span consists of 8 Type IV prestressed concrete girders, spaced at 5.30' center to center and slab thickness of 7.0 in. The bridge carries two lanes of traffic with curb to curb width of 40.0 ft. as shown in Figure 4.27. Table 4.4 summarizes the material and

Table 4.4 Material and sectional properties for bridge #720408

Material Properties	E_{deck} (ksi)	E_{girder} (ksi)	Poisson's Ratio, υ	G (ksi)
	4031	4031	0.2	1679

Section Properties	Slab	Thickness = 7 in.				
	Girder web	Thickness = 8 in.				
		A (in^2)	I_y (in^4)	I_z (in^4)	T_{ky} (in)	T_{kz} (in)
	Top beam	244	3026	8133	20	12.2
	Bot. beam	361	5794	20330	26	13.88

Instruments for measuring strains were placed at critical locations on the tested span. The bridge was loaded with two trucks incrementally with 36, 48, 60 and 72 blocks respectively. The strain readings were taken at each load increment to establish the behavior of the bridge. The load case corresponding to sixty blocks has been used in the analysis to ensure the strains are within the linear and elastic range.

Typical top view of the Finite Element Mesh is presented in Figure 4.28. Each node had six degrees of freedom and the nodes were arranged such that some nodes were located at the strain gage positions to facilitate the comparison between the measured and calculated strains The deck slab is divided into 16 x16 = 256 four node-shell elements and each girder divided into 16 sections. The I-girder section is discretized into three elements as shown in Figure 4.4. Each flange is modeled by a beam element with four midsurface nodes. The rigid links ensure coupling the vertical degrees of freedoms of the shell and top flange beam elements. Simply supported boundary conditions are realized by restraining the appropriate translafional degrees of freedom.

Table 4.5 summarizes the results from the finite element analysis and field test at a cross section corresponding to the maximum bending moment location. Figure 4.29 shows the comparison of the measured and calculated strain distribution along the bridge width. It is clear that the measured and calculated strains show good agreement. However, a better correlation may be achieved, if the actual boundary conditions and more accurate truck positions were available.

Table 4.5 Measured and calculated strains for bridge #720408

Girder Number	Measured strains, in./in. x 10-6	Calculated strains, in./in. x 10-6
1	62.5	73.5
2	107.5	113.5
3	140	147
4	150	152
5	130	135.5
6	120	102
7	77.5	63.5
8	40	22

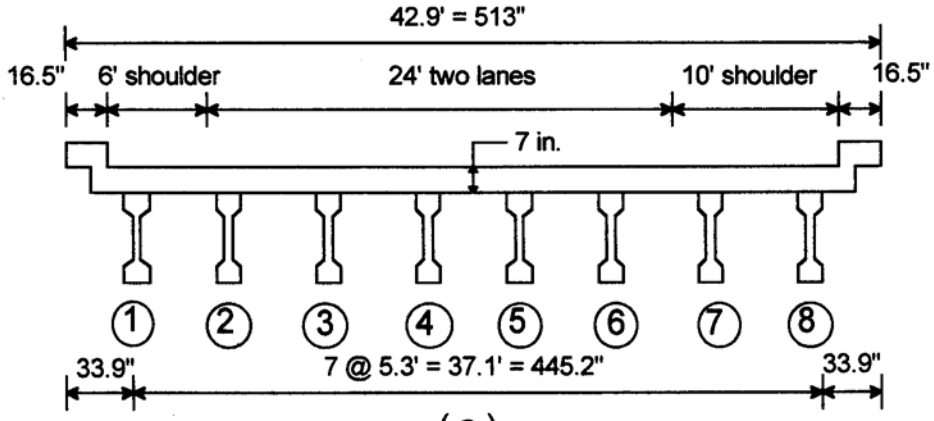

(a)

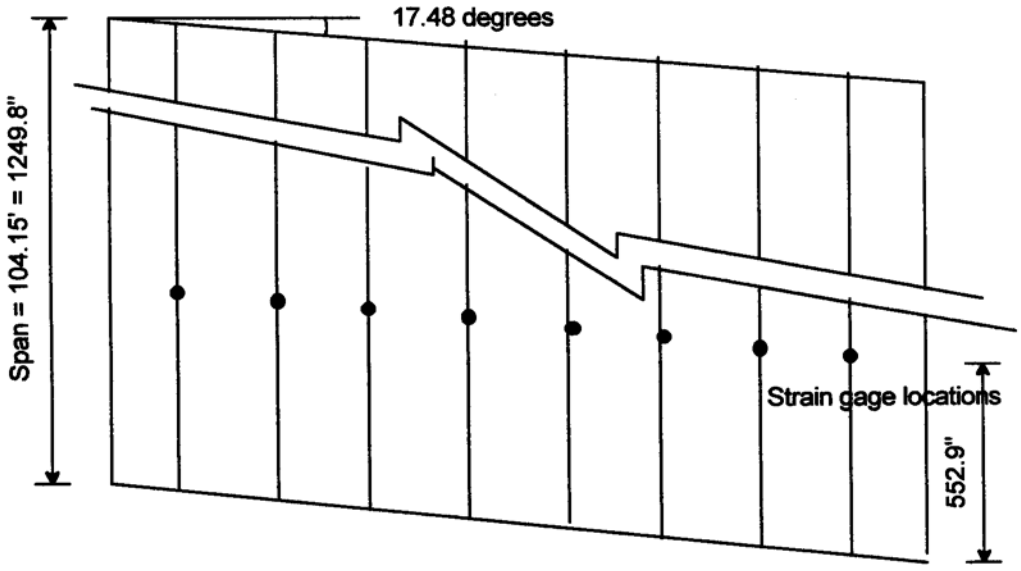

(b)

Fig.4.27 Field test detail (Bridge #720408)

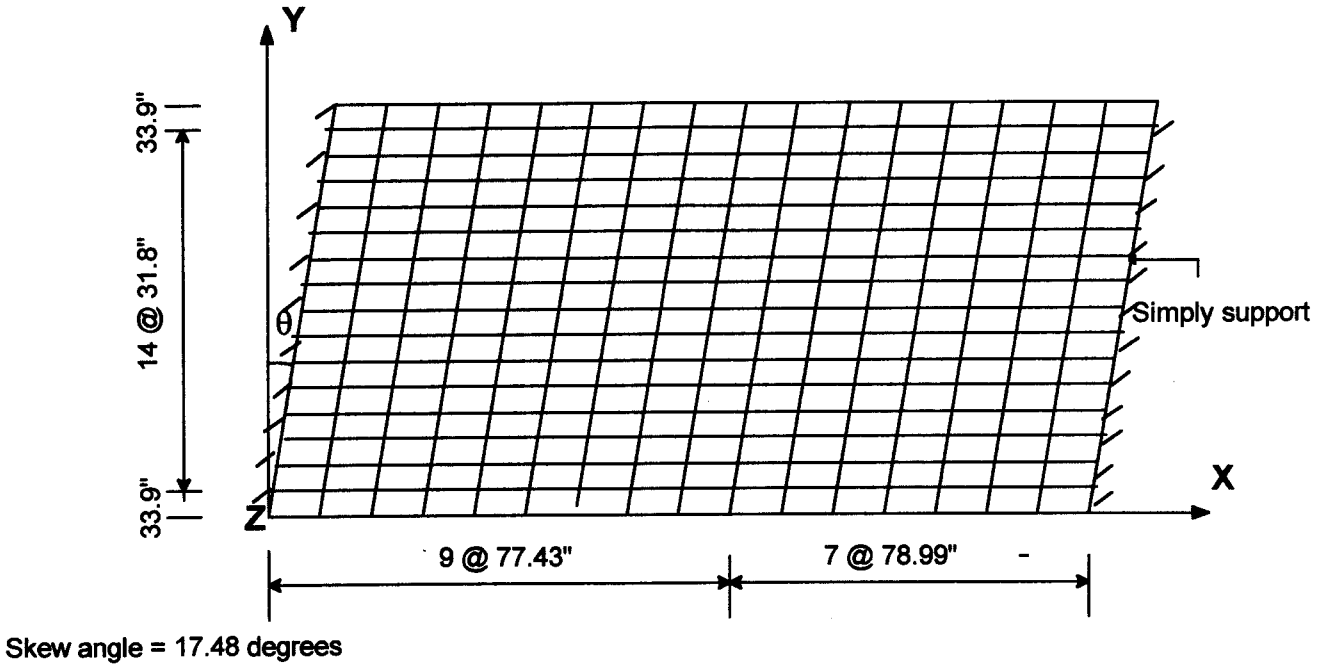

Fig.4.28 Top view of finite element mesh
(Bridge #720408)

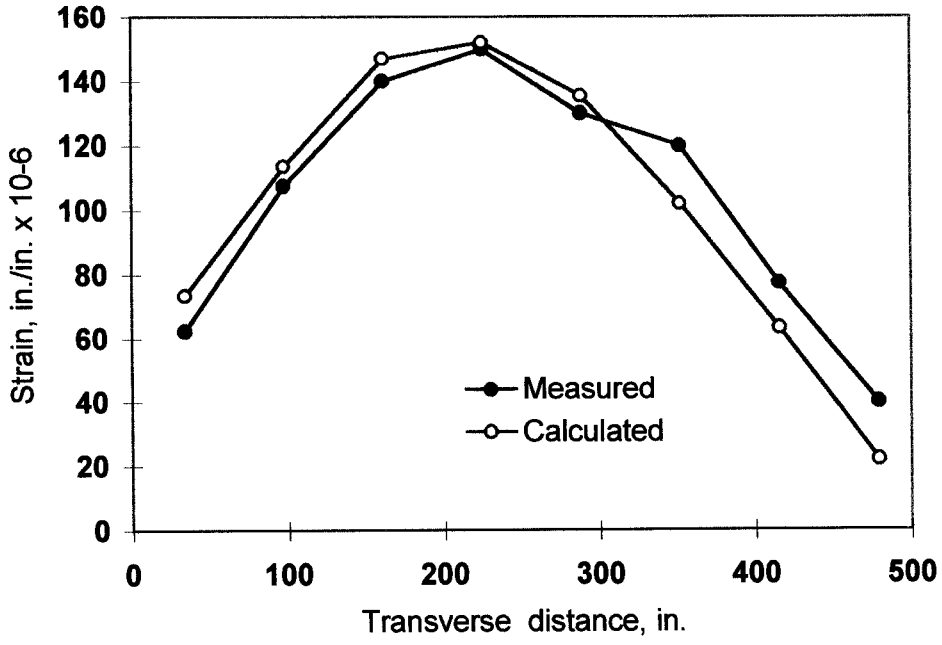

Fig 4.29 Strain variation across the slab-on-girder bridge
(Bridge #720408)

Table 4.6 **summarizes the results** of wheel load distribution factors for the bridges based on the measured strains, finite element method, AASHTO and LRFD codes. The measured wheel load distribution factor, DF compares well with calculated DF. Both DFs based on AASHTO and LRFD **were higher than the DF calculated using the measured strains and finite element method.** This confirms that AASHTO and the LRFD code give conservative values for wheel load distribution factor for skew slab-on-girder bridges.

Table 4.6 Summary of load distribution factors, DF (Interior girders)

Bridge	Measured strains	F.E.M.	AASHTO	LRFD
#720408	0.725	0.747	0.964	0.988
#720089	0.529	0.682	0.939	0.900
Turnpike bridge	0.610	0.790	1.076	1.003

4.4.2 S.R.17 Bridge #720089

The bridge is located on S.R. 17 and it consists of three simply supported spans with the longest test span of 85'-6". The length of the total structure is 181'-6". The span consists of 7 Type III prestressed concrete girders, spaced at 5'-2" center to center and a slab thickness of 7.5 in. The skew angle is 45 degrees. The bridge carries two lanes of traffic with curb to curb width of 26 ft. as shown in Figure 4.30. Table 4.7 summarizes the material and sectional properties of the bridge.

Table 4.7 Material and sectional properties for bridge #720089

Material Properties	E_{deck} (ksi)	E_{girder} (ksi)	Poisson's Ratio, υ	G (ksi)
	4031	4031	0.2	1679

Section Properties	Slab	Thickness = 7.5 in.				
	Girder web	Thickness = 6 in.				
		A (in^2)	I_y (in^4)	I_z (in^4)	T_{ky} (in)	T_{kz} (in)
	Top beam	144	972	3072	16	9
	Bottom beam	242	2440	9761	22	11

The arrangement of instruments and the location of the strain gages is similar to that of bridge #720408 (Section 4.4.1). The measured strains along the bridge width at the maximum bending moment section are presented in Table 4.8. The mesh and the finite element model for the bridge are similar to that of bridge #720408 which is shown in Fig. 4.28, while the deck slab is divided into 16 x 14 = 224 eight node-shell elements. The rigid links and simply supported boundary conditions are also applied to this bridge.

Table 4.8 summarizes the results from finite element analysis and field test at a cross section corresponding. to the maximum bending moment location. Figure 4.31 shows that the measured and calculated strain distribution along the transverse direction. In this bridge, the finite

element method strains were consistent with those based on measured strains. The DF from measured strains is smaller than the calculated strains **from finite element method.** Both DFs from calculated and measured strains are smaller than those based on AASHTO and LRFD codes as shown in Table 4.6. This again confirms that both AASHTO and LRFD codes give conservative estimate for wheel load distribution factors.

Table 4.8 Measured and calculated Strains for bridge #720089

Transverse distance (in.)	Measured strains, in./in. x 10-6	Calculated strains, in./in. x 10-6
41	90	109
103	84	104
165	79	62
227	38	29.4
289	29	13.3
351	15	3.55
413	5	-1.5

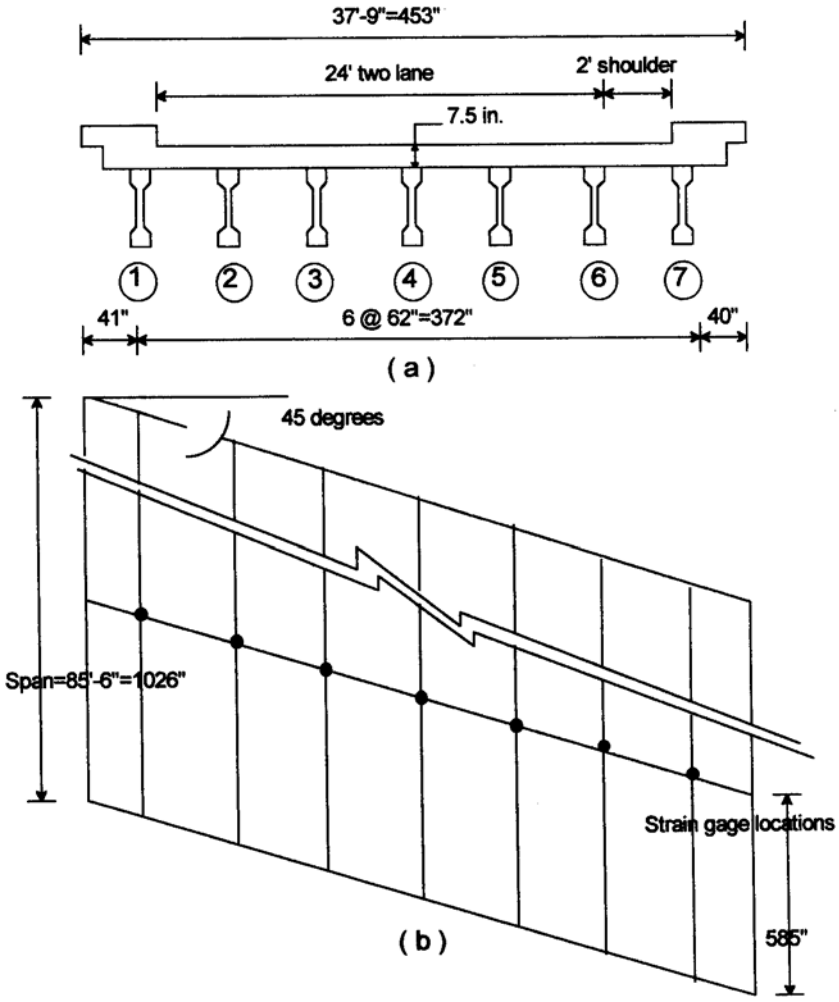

Fig.4.30 Field test detail (Bridge # 720089)

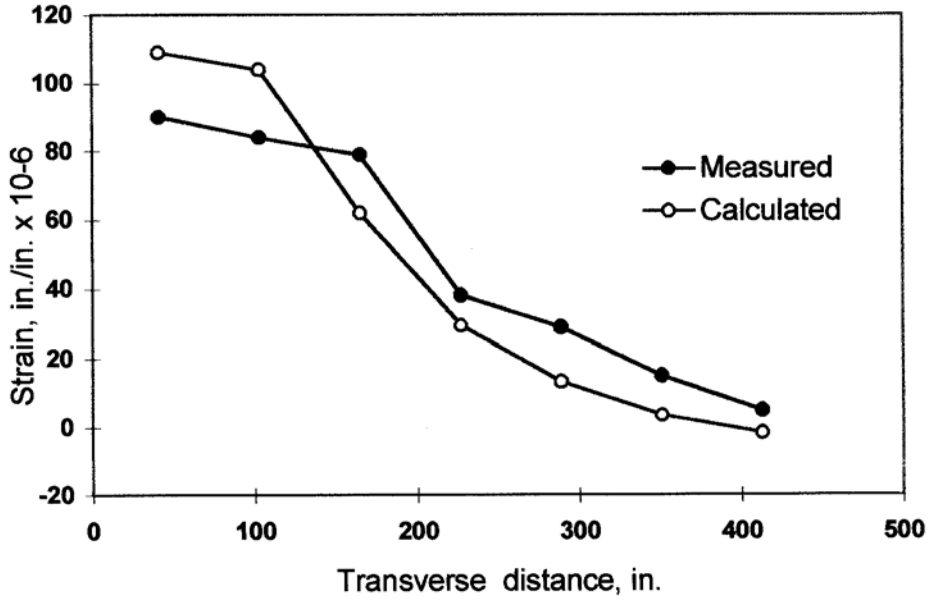

Fig.4.31 Strain variation cross the slab-on-girder bridge (Bridge #720089)

4.4.3 Turnpike Bridge over 1-595

The bridge is located on the Florida Turnpike over Interstate 595. The bridge was completed in the summer of 1989. This twin structure consists of identical northbound and southbound bridges with 5 spans of simply supported AASHTO girders 130 ft., 151 ft., 99 ft., 99 ft. and 99 ft. in **length respectively. Span 2 which was chosen as the test span consists of twelve simply supported AASHTO Type V girders and the girders are spaced at 5'-11" center to center. The bridge is 68' wide from curb to curb and carries four 12 ft. lanes and two 10 ft. shoulders with typical crash barriers on either side. The slab is 7 in. thick and the bridge is skewed 20 degrees. The bridge was constructed using an innovative shoring system which allows the section to act compositely for dead load as well as for live load. The details of the bridge are shown in Fig.4.32. Table 4.9 summarizes the material and the sectional properties of the bridge.**

Table 4.9 Material and sectional properties for turnpike bridge over I-595

Material Properties	E_{deck} (ksi)	E_{girder} (ksi)	Poisson's Ratio, υ	G (ksi)
	4031	4031	0.2	1679

Section Properties	Slab	Thickness = 7 in.				
	Girder web	Thickness = 8 in.				
		A (in^2)	I_y (in^4)	I_z (in^4)	T_{ky} (in)	T_{kz} (in)
	Top beam	385	2699	56616	42	9.17
	Bot. beam	404	7011	26397	28	14.43

The instrumentations are mounted at critical locations of the structure and connected to the data acquisition system. The bridge was loaded with two trucks and the load case corresponding to the trucks weight of 24 kips each has been used in this analysis. The measured deflection along the bridge at the maximum bending moment are presented in Table 4.10. The mesh and the finite element model for this bridge are similar to that of the bridge #720408 shown in Figures 4.28 and

4.29 except the deck slab is divided into 30 x 24 = 720 four node shell-elements, and each girder divided into 30 sections. The rigid links and the simply supported boundary conditions are applied to the bridge.

The results from the finite element method and field test at midspan section along the bridge width is shown in Table 4.10. Figure 4.33 shows the comparison of the measured and calculated strain distributions along the bridge width. It can be seen from the figure that the measured deflections are smaller than the analytical values. But it can also be seen that the finite element method predicts the behavior and load distribution of the bridge fairly well. The results show that the overall behavior of the bridge is quite adequate.

The measured wheel load distribution factor, DF was smaller than that from the finite element method as shown in Table 4.6. But both DF from finite element method and field test are smaller than those based on AASHTO and LRFD values. This shows that AASHTO and LRFD code give conservative estimate of wheel load distribution factor for skew slab-on-girder bridge.

Table 4.10 Measured and calculated deflection for turnpike bridge over I-595

Transverse distance (in.)	Measured deflection, in.	Calculated deflection, in.
34	-0.15	0.15
105	-0.30	-0.06
176	-0.45	-0.31
247	-0.65	-0.64
318	-0.85	-1.00
389	-1.05	-1.21
460	-1.00	-1.20
531	-0.80	-1.00
602	-0.63	-0.64
673	-0.43	-0.31
744	-0.28	-0.06
815	-0.15	0.15

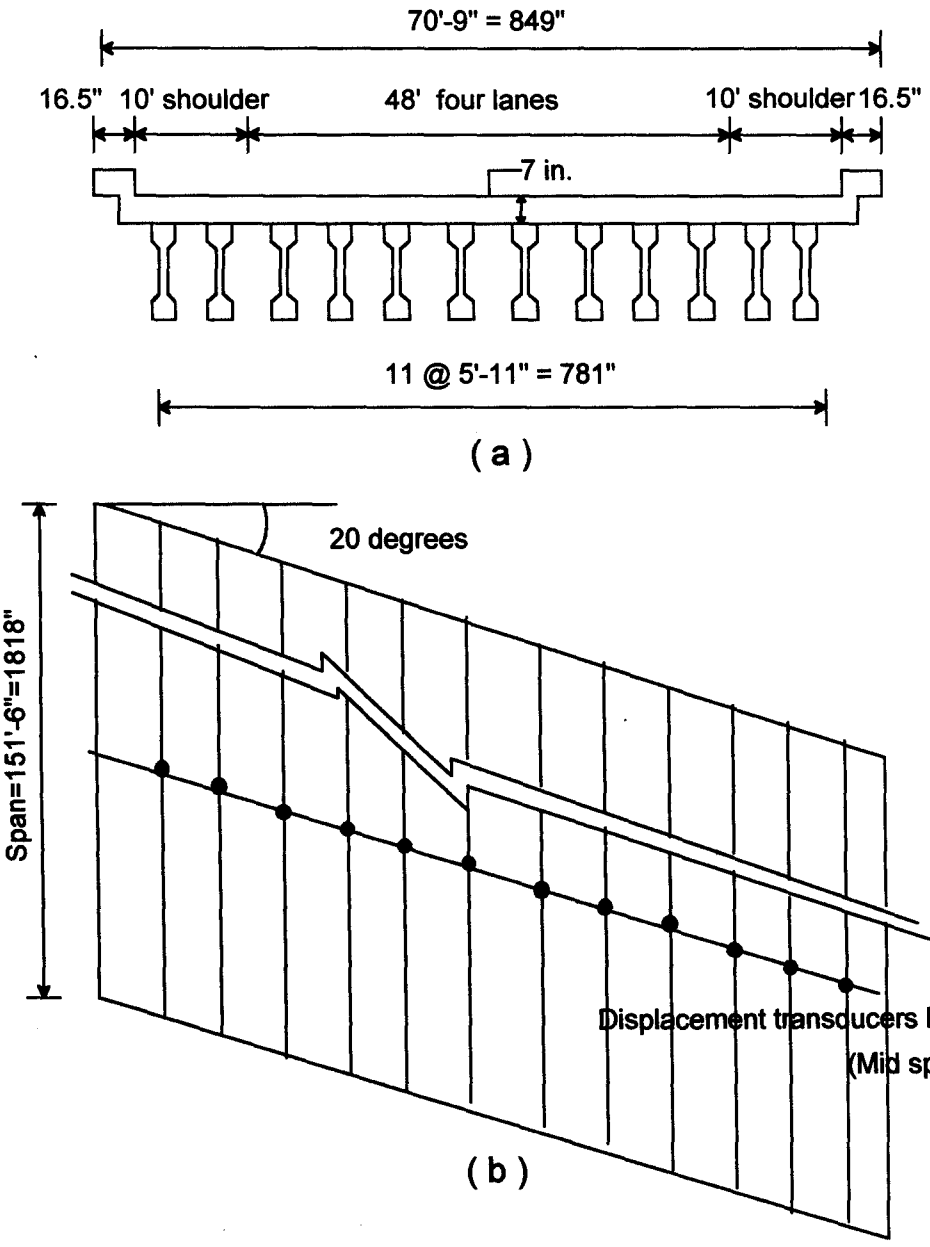

Fig.4.32 Details of Turnpike bridge

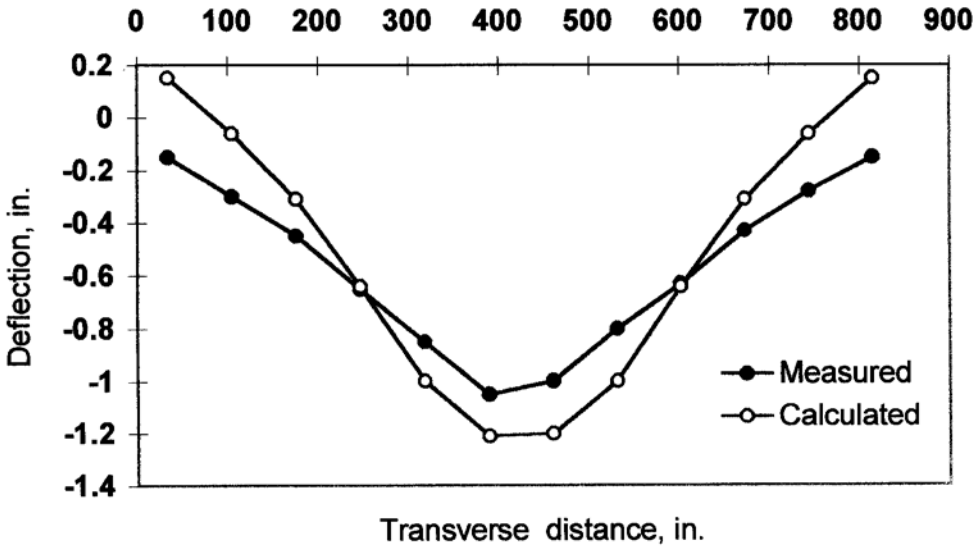

Fig.4.33 Deflection variation across the slab-on-girder bridge (Turnpike bridge over I-595)

CHAPTER 5

LOAD DISTRIBUTION ANALYSES OF SKEW SOLID SLAB BRIDGES

5.1 INTRODUCTION

Solid or voided sections are used in slab bridges, which span between supports in the longitudinal direction, i.e., traffic direction. Concrete slab bridges are economical for spans in the range of 10-26 ft. However, spans up to 50 ft. can also be feasible. These bridges are normally reinforced with reinforcing bars, but prestressing strands and I-beams have also been used in practice. They also offer a smaller structure depth where structure opening and vertical clearance are significant. In addition to the above advantages, slab bridges are commonly used due to its low construction cost.

Skew bridges have been designed for many years using approximate methods. Most of these methods do not account for high torsional moments inherent in a skewed structure. More exact methods of analysis are time consuming. In this chapter, an exact method such as finite element method is used to verify/modify the AASHTO-LRFD load distribution factor of skew slab bridges. Wheel load distribution on solid slab bridges based on both finite element method and field tests performed by Florida Department of Transportation (FDOT) is presented in this chapter. The objectives of the analyses are the following:

i) Determine the effective width using finite element method and study the effects of skew angle, span length, edge beam depth and other parameters on wheel load distribution.

ii) Verify the AASHTO and the LRFD effective widths using simply supported skew slab bridge field tests.

iii) Derive simple design criteria for effective width that would provide more accurate alternative to current designs.

5.2 METHOD OF ANALYSIS

The Finite Element Method is used to verify the effective widths based on the AASHTO and LRFD wheel load distribution methods. The AASHTO **procedure to determine the flexural distribution factors is generally used for bridge design and tends to be overly conservative particularly for analyzing and rating of existing bridges, which may cause unnecessary rerouting of vehicles in certain circumstances (Warren and Malvar,1993).** The AASHTO **approach is to calculate an effective width E, over which the concentrated wheel load (half truck load) is assumed to be uniformly distributed (AASHTO specification, 1989)**

$$E = 4.0 + 0.06S \text{ (feet)} \quad (E < 7 \text{ ft.}) \qquad (5.1)$$

Where S = span length, in feet. A larger value of E means more efficient distribution of the load. Slab thickness and flexural reinforcement are then determined from an equivalent strip of width 2E carrying the total truck load. The AASHTO **equation is based substantially on Westergaard theory for slabs (Westergaard, 1930).** The AASHTO **equation considers span length as the only parameter and neglect other important parameters such as skew angle, edge beam, etc.**

The LRFD approach is similar to AASHTO method, but considers more parameters such as skew angle, bridge width and number of lanes. The LRFD approach is based on NCHRP project 12-26 entitled, "Distribution of Wheel Load on Highway Bridges", which was performed in two phases by Imbsen & Associates, inc.(1989). The LRFD approach for slab bridges was based on limited number of analytical studies. The LRFD effective width of longitudinal strip per lane for both shear and moment with one lane, i.e., two lines of wheels, loaded may be determined as follows:

$$\mathbf{E = 10.0 + 5.0\sqrt{L_1 W_1}} \qquad \textbf{(5.2)}$$

The effective width of longitudinal strips per lane for both shear and moment more than one lane loaded, may be determined as:

$$\mathbf{E = 84.0 + 1.44\sqrt{L_1 W_1}} \leq \frac{W}{N_L} \qquad \textbf{(5.3)}$$

where

E = Effective width over which truck load is assumed to be uniformly distributed, feet (this definition of E will be used throughout this chapter),

L_1 = Modified span length taken equal to the lesser of the actual span or 60 ft.(feet units),

W_1 = Modified edge-to-edge width of bridge taken equal to the lesser of the actual width or 60.0 feet for multi-lane loading (feet. units)

W = Physical edge-to-edge width of bridge (feet.units),

N_L = Number of design lanes.

For skewed bridges, the longitudinal force effects may be reduced by the factor r:

$$r = 1.05 - 0.25 \tan\theta \leq 1.00 \qquad \textbf{(5.4)}$$

where,

9 = Skew angle (DEG)

Finite element method (ANSYS Program) presented in Chapter 3 is used as an analytical tool to study the various parameters affecting load distribution and suggest which parameters should be considered. In addition to the analytical study, data from field test performed by Structures Research Center, FDOT, are used to verify the results from the analytical study.

5.2.1 Effective Width Calculation

An effective width may be calculated from the distribution of moments determined from the finite element method and field tests. The sum of moments or the total area under the moment distribution curve is equivalent to externally applied moment due to the concentrated loads (including the edge beam moments). The effective width, E is equal to the ratio of the total area under the moment distribution curve to the maximum moment. This method of calculating E is based on the assumption that the sum of the internal moments or the total area under the moment distribution curve should be equal to the externally applied moment. This assumption is valid only for straight bridges. However, this assumption is not realistic to yield the actual effective width in skew bridges. The effective width, E is equal to the ratio of the maximum moment in the bridge idealized as a one-dimensional beam subjected to one set of wheels to the maximum moment intensity obtained from finite element or field tests. The sum of the internal moments in a straight bridge is equal to the maximum moment in the bridge idealized as a one-dimensional beam subjected to one set of wheels. The sum of the internal moments in a straight bridge will be used to take into account the total external load effects in skew bridges. Therefore, E can be obtained for a

$$E_e = \frac{(Y\text{-}\ moments)}{(5.5)\ (Moment_{m..})_B}$$

5.3 SKEW SOLID SLAB BRIDGE: PARAMETRIC STUDY

Several parameters affect the load distribution of skew solid slab bridge. Skew angle, span length, and edge beam depth are the main parameters which are considered in this section. Figure 5.1 shows the typical slab bridge cross section which is used in the analysis. The typical slab bridge has a span length of 21 ft. **with a width equal to 30 ft. and the slab thickness of 12 inch..**

5.3.1 Skew Slab Bridge Finite Element Modeling

The typical skew slab bridge cross section is shown in Figure 5.1. Linear elastic material is considered in the modeling. The slab elements are considered to be isotropic. Table 5.1 summarizes the material (Elastic modulus, E, Poisson's ratio, ν, **and modulus of rigidity, G) and sectional properties of the bridge (Area, A, and moments of inertia, I_y and I.J.**

Typical top view of the skew solid slab bridge finite element mesh is presented in Figure 5.2. Generalized shell elements coupling bending with membrane action were used to model the skew slab bridge. The shell elements were proportioned so that the maximum aspect ratio always remains at two to one or less (Chen,Y. 1995). Each node has six degrees of freedom and the nodes are arranged such that some nodes were located at the critical positions. The skew slab bridge is divided into 12 x 22 = 264 four-node shell elements. Simply supported boundary conditions are obtained by restraining the appropriate translational degrees of freedom along the edges.

Two models shown in Figure 5.3 were used in the parametric study. Only shell elements are used to model slab and the edge beams were neglected in Model 1. Beam elements are added to

model the edge beams in Model 2. The skew slab was modeled using shell element with 4 or 8 nodes. The difference in accuracy of results based on the two types of elements was small and the 4 node shell elements were used throughout the parametric study.

Table 5.1 Material and sectional properties for typical skew solid slab bridge

Material properties	E_{deck} (ksi)	E_{beam} (ksi)	Poisson's ratio, υ	G (ksi)
	4031	4031	0.2	1679

Section Properties	Slab	Thickness = 12 in.				
	Edge	A (in^2)	I_y (in^4)	I_z (in^4)	T_{ky} (in)	T_{kz} (in)
	Beam	315	11576	5906	15	21

(*T_{ky} and T_{kz} are the thicknesses of the edge beam corresponding to y and z direction which are shown in Fig.5.3)

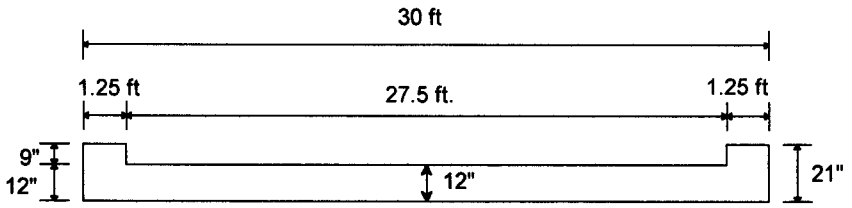

Fig 5.1 Typical solid slab bridge cross-section

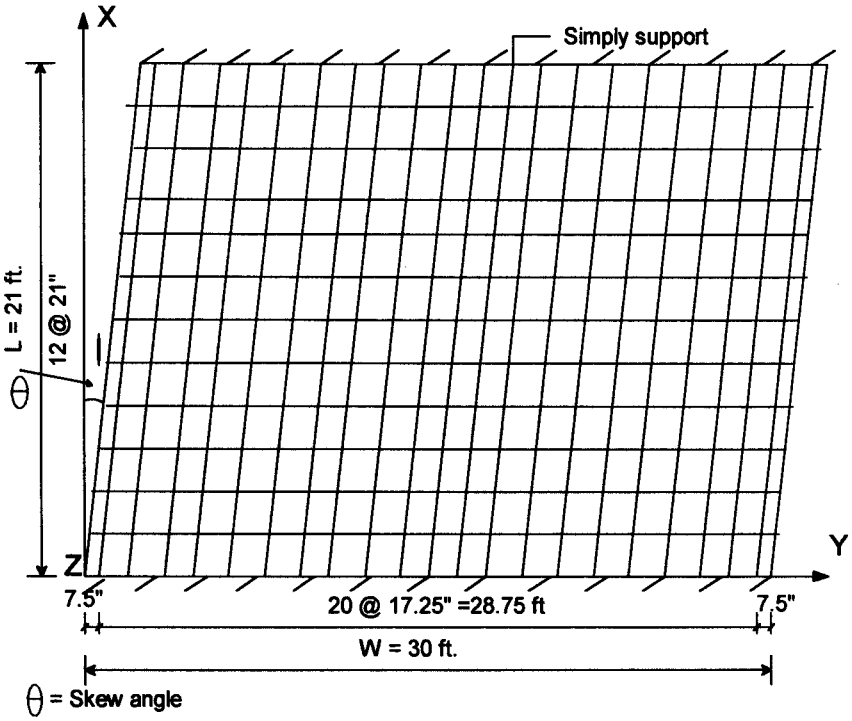

Fig. 5.2 Top view of typical skew solid slab bridge mesh

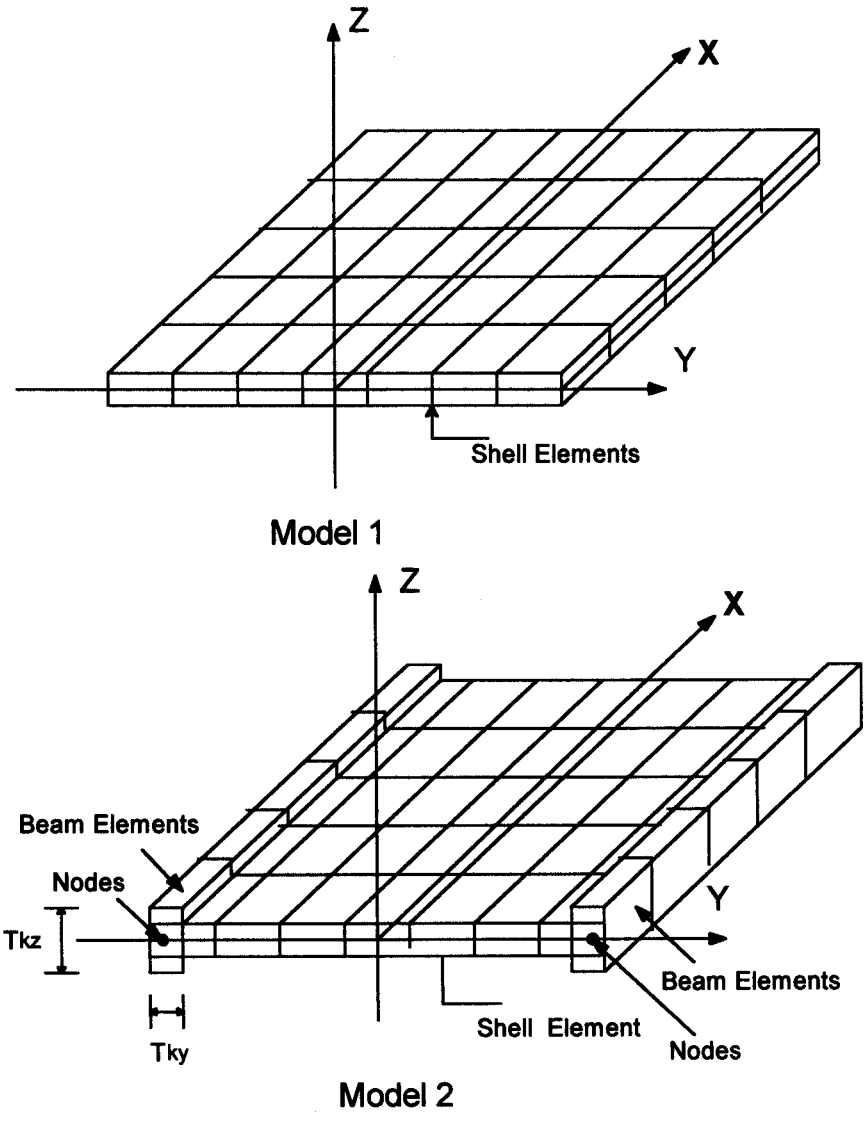

Fig. 5.3 Finite element models of typical skew solid slab bridge

5.3.2 Truck Load Position

The AASHTO HS-20 truck was used in this parametric study. The truck position in the longitudinal direction (span direction) was located so as to obtain the maximum bending moments. For skew slab bridges with relatively short spans, the maximum bending moment occurs when only one axle of the truck is at the midspan. For a two lane slab birdge, it was found that the maximum bending moment occurs when the two lanes are loaded as in Figure 5.4b. Since the locations of wheel loads will probably not coincide with nodes of the shell elements, it is necessary to calculate the equivalent nodal loads. To this end, the concept of tributary area can be used to determine the equivalent loads as explained in Chapter 3.

The exact load positions for the typical skew solid bridge are shown in Figures 5.5 and 5.6. Two different load positions were used to find out the effect of load position. The span length of the typical bridge is 21 ft which is a relatively short span, so the maximum moment will be at the midspan. But the axles of the trucks must be perpendicular to the traffic direction, hence two wheels of a truck cannot be at the midspan at the same time due to the skew angle. All the maximum moments are taken at the mid span. The comparison of the moment distribution for two different load positions is shown in Figure 5.7. The moment distribution is not a smooth curve because some of the wheels are away from the midspan. The moment distribution due to load position 2 shifts away from that due to load position l. But the trends are the same. Load position 1 is used throughout the parametric study for skew solid slab bridges.

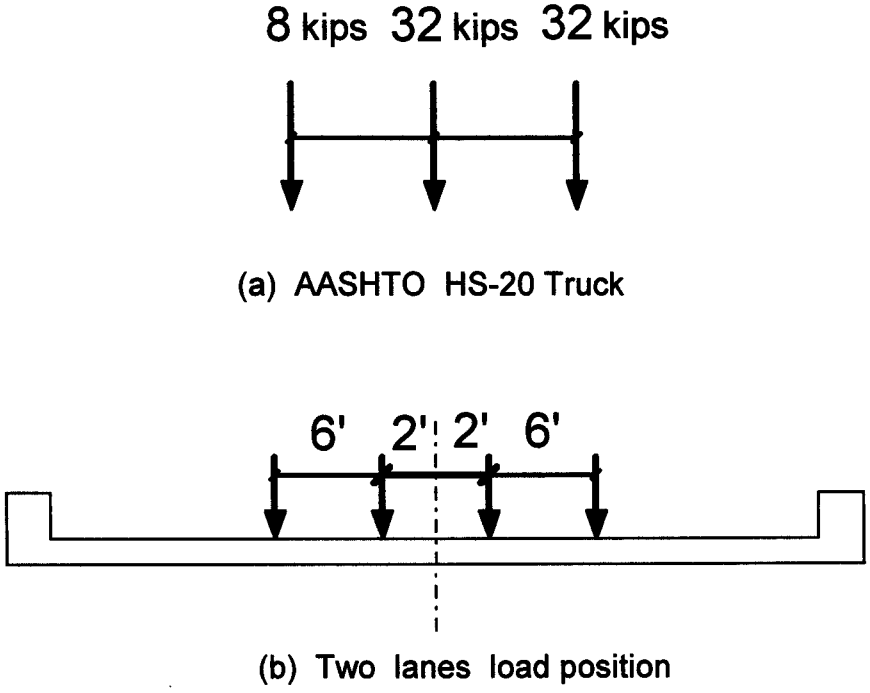

Fig.5.4 Typical truck load positions for slab bridges

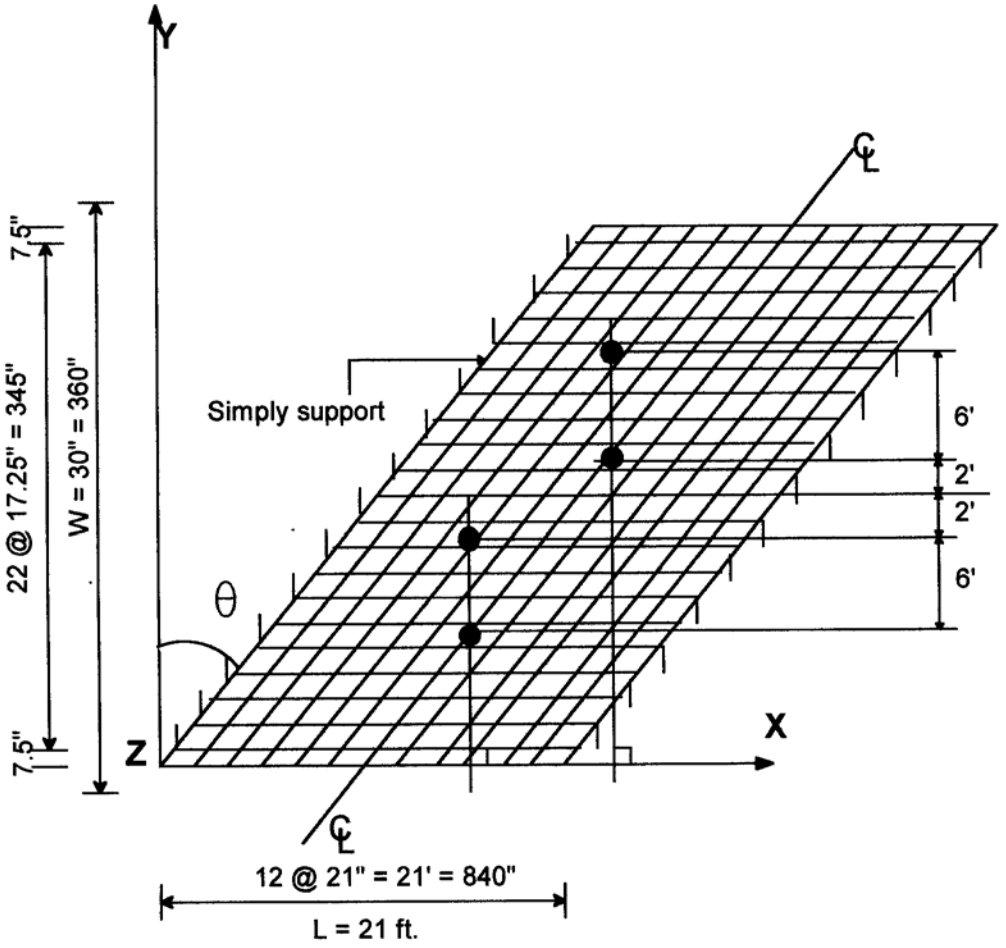

Fig.5.5 Load position 1 of typical skew slab bridge (Skew angle = 30 degrees)

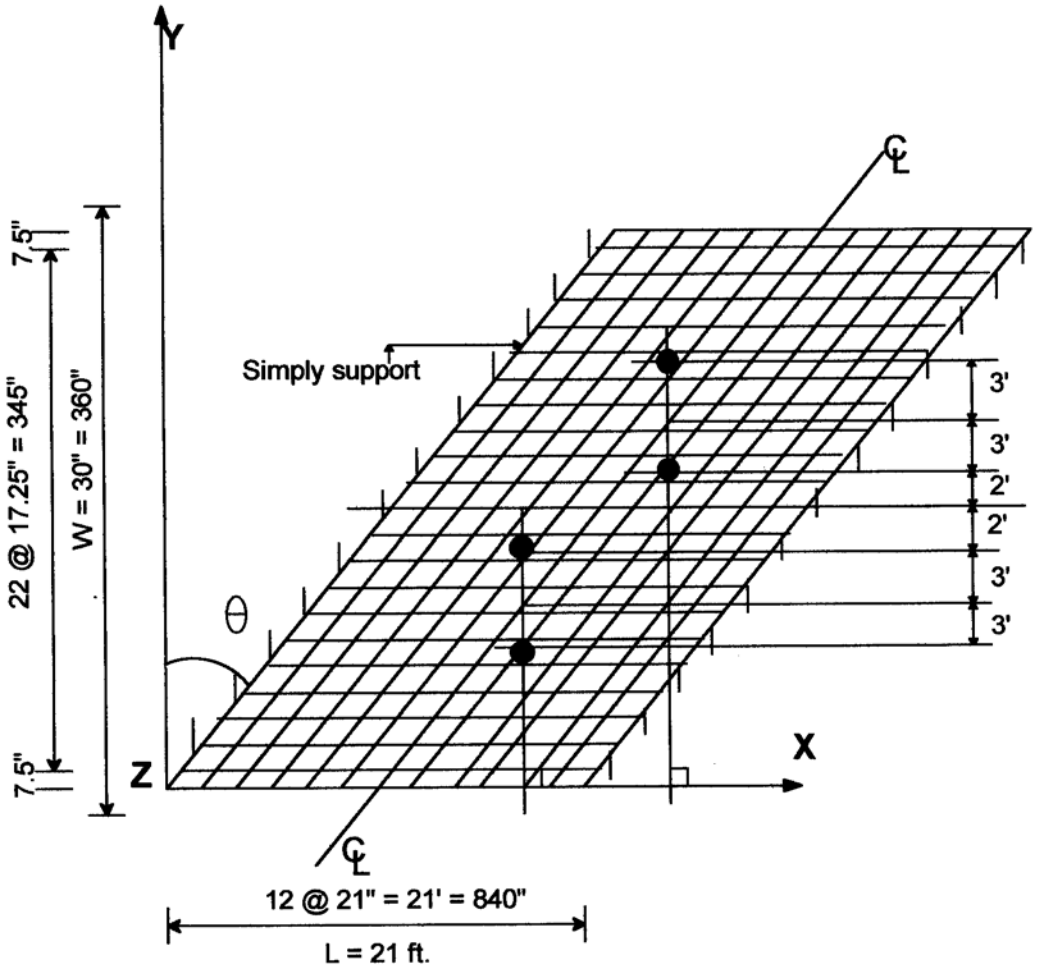

Fig.5.6 Load position 2 of typical skew slab bridge (Skew angle = 30 degrees)

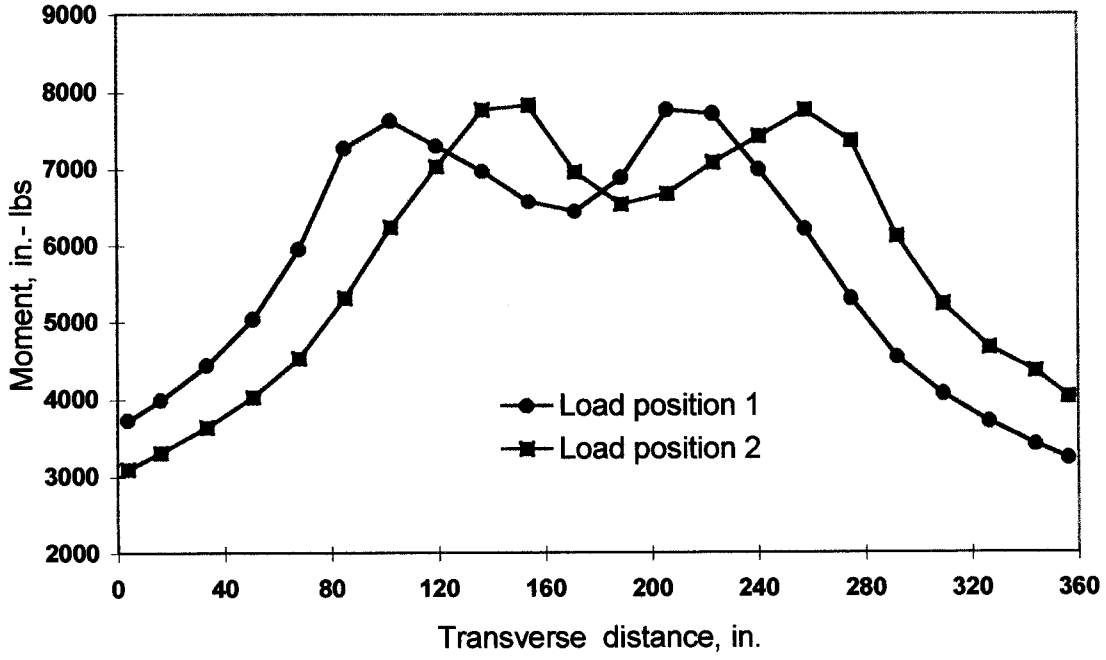

Fig.5.7 Moment distribution for different load positions of the typical bridge

5.3.2 Parametric Studies

Table 5.2 summarizes the cases and the several parameters such as skew angle, span length and edge beam depth considered in the study. Twenty-four cases were investigated using linear finite element method to establish the main parameters affecting the effective width of the skew solid slab.

5.3.2.1 Comparison of two models

Table 5.3 summarizes the results from the two models at the critical cross section for typical slab bridge. The effective widths calculated from the two models are presented in Table 5.4. The moments at the positions where edge beams were located reduce with the addition of beam elements and the maximum moment also reduces. Figure 5.8 shows the comparison of moment distributions along the width, which shows that the curve is steeper than that of model l. The effective width calculated from model 2 is smaller than that from model 1 and it seems more conservative and less significant.

Table 5.2 Summary of skew slab bridge parametric study cases

Parameter	Span length, ft.	Skew angle, (degree)	Edge beam depth, in.	Comments
Skew angle (8 cases)	21	0	9	Model 1 (without edge beam)
	21	30	9	Model 2 (with edge beam)
	21	45	9	Two lanes
	21	60	9	
Span length (8 cases)	15	30	9	Model 1 (without edge beam)
	21	30	9	Model 2 (with edge beam)
	30	30	9	Two lanes
	40	30	9	
Edge beam depth (8 cases)	21	30	6	Model 1 (without edge beam)
	21	30	9	Model 2 (with edge beam)
	21	30	12	Two lanes
	21	30	18	

(*All cases have a bridge width of 30 ft. and a slab thickness of 12 in.)

Table 5.3 Moments for typical bridge

Transverse distance, in.	Moments from model 1, in.-lbs	Moments from mode 2, in.-lbs
3.75	3735	2336
16.125	3989	2569
33.375	4440	3011
50.625	5042	3701
67.875	5950	4748
85.125	7271	6180
102.375	7632	6749
119.625	7302	6558
136.875	6966	6334
154.125	6570	6017
171.375	6445	5939
188.625	6885	6395
205.875	7770	7263
223.125	7721	7164
240.375	6996	6354
257.625	6217	5457
274.875	5304	4403
292.125	4542	3503
309.375	4062	2914
326.625	3707	2502
343.875	3413	2222
356.25	3229	2065

Table 5.4 Effective width (ft.)for typical bridge

Model	AASHTO	LRFD	F.E.M.
1	10.52	9.84	12.82
2	10.52	9.84	11.60

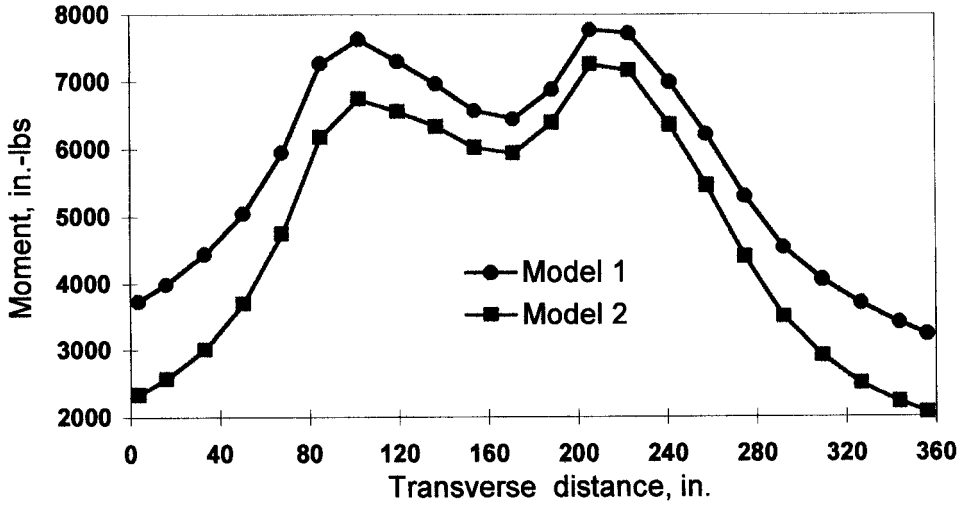

Fig.5.8 Moment distributions for typical bridge

5.3.2.2 Skew angle

Skew angle is one of the main factors affecting load distribution in slab bridge. Solid slab bridges with skew angles from 0 to 60 degrees (Table 5.2) were investigated in this study. Figures 5.9 and 5.11 show the strain distributions for typical bridges with different skew angles. The moment decreases with the increase in the skew angle and the moment distribution is more uniform for smaller skew angle. Larger effective widths are obtained with increase in the skew angle. These moment distributions were used to calculate the solid slab effective widths.

Figures 5.10 and 5.12 show the effective widths increase with the increasing skew angle for both models. In the cases where the effective width based on the finite element method exceeded the lane width, the effective width was assumed equal to the lane width of 13.75 ft. The effective widths calculated from finite element analyses are generally larger than those calculated using AASHTO and LRFD codes as shown in Figures 5.10 and 5.12. This means that AASHTO and LRFD codes give a more conservative estimate of effective width, E for solid slab bridges. It seems reasonable that the skew angle should be considered in the calculation of effective width.

Model 2 which uses slab and edge beam elements gives smaller moments than model 1 which only uses slab elements in modeling the bridge. Figure 5.13 shows the effective width calculated based on model 2 is smaller than that based on model 1 The difference in the estimated effective width value vanishes with the corresponding increase in the skew angle because all the values are higher than the lane width and taken equal to the lane width.

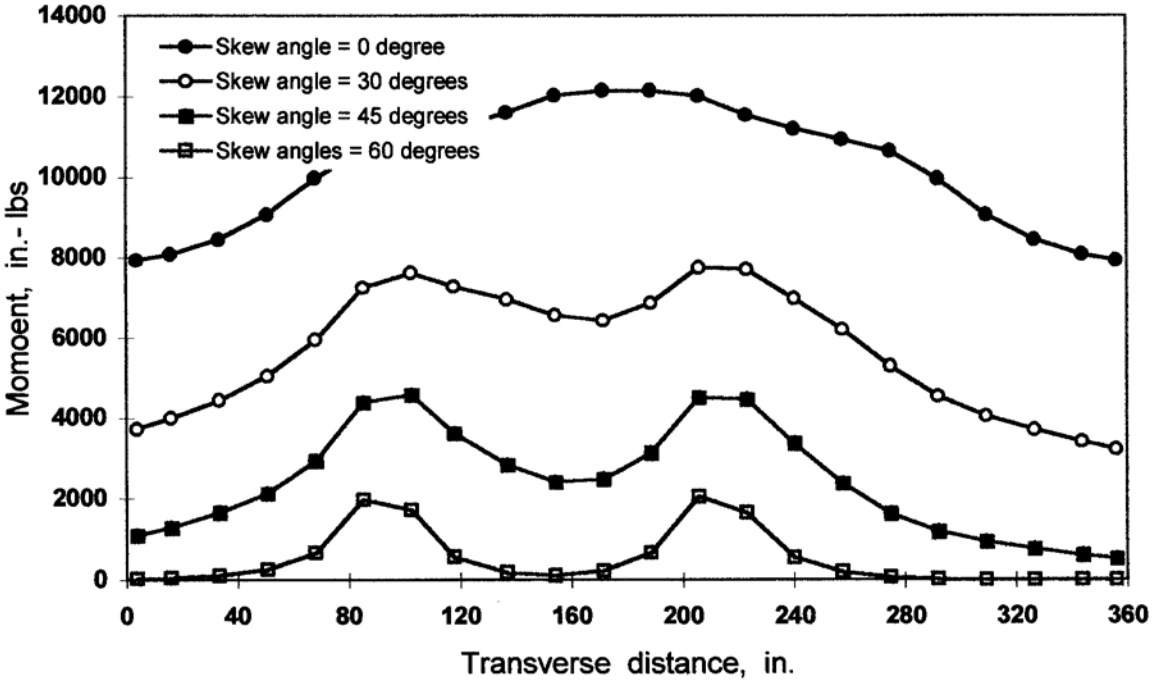

Fig.5.9 Moment distribution for different skew angles (Model 1)

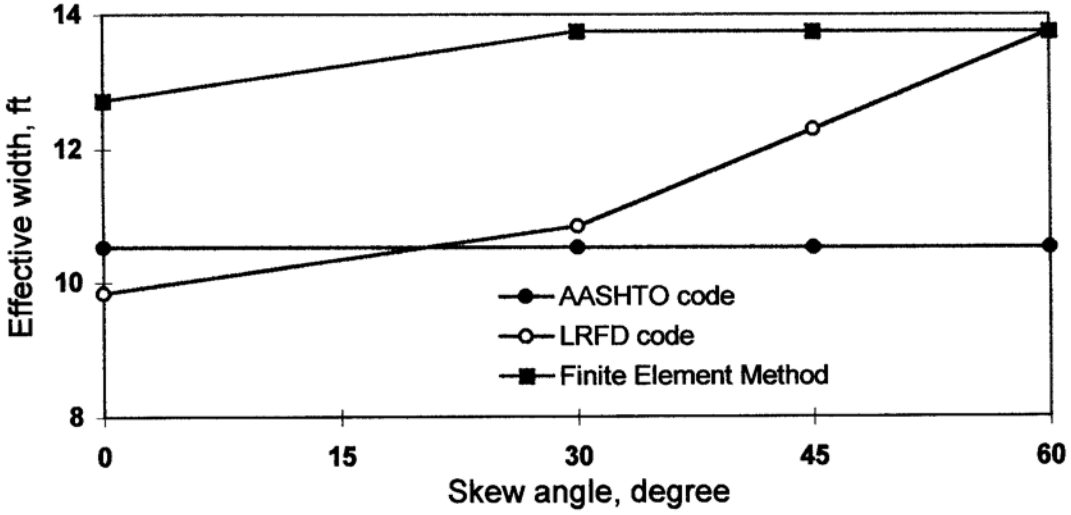

Fig.5.10 Effective width variation with skew angle for solid slab bridges (Model 1)

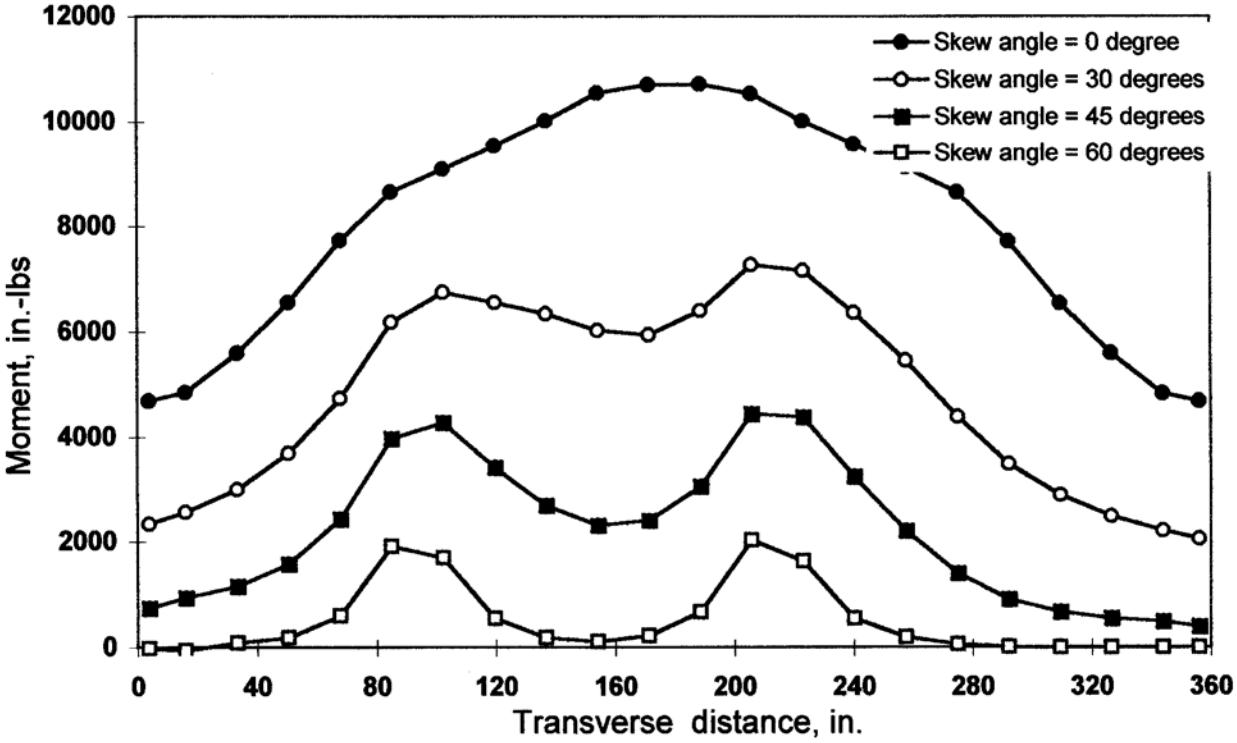

Fig.5.11 Moment distributions for different skew angles (Model 2)

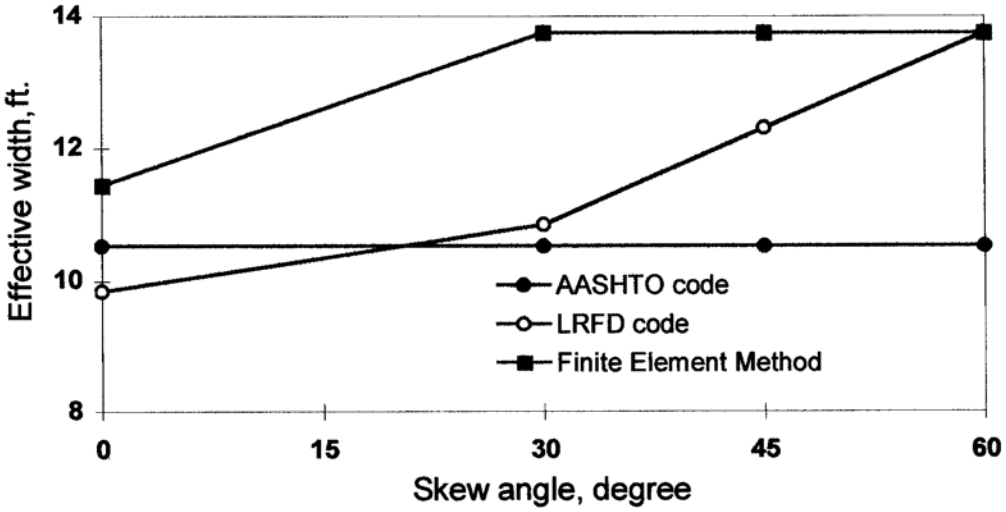

Fig.5.12 Effective width variation with skew angle for solid bridges (Model 2)

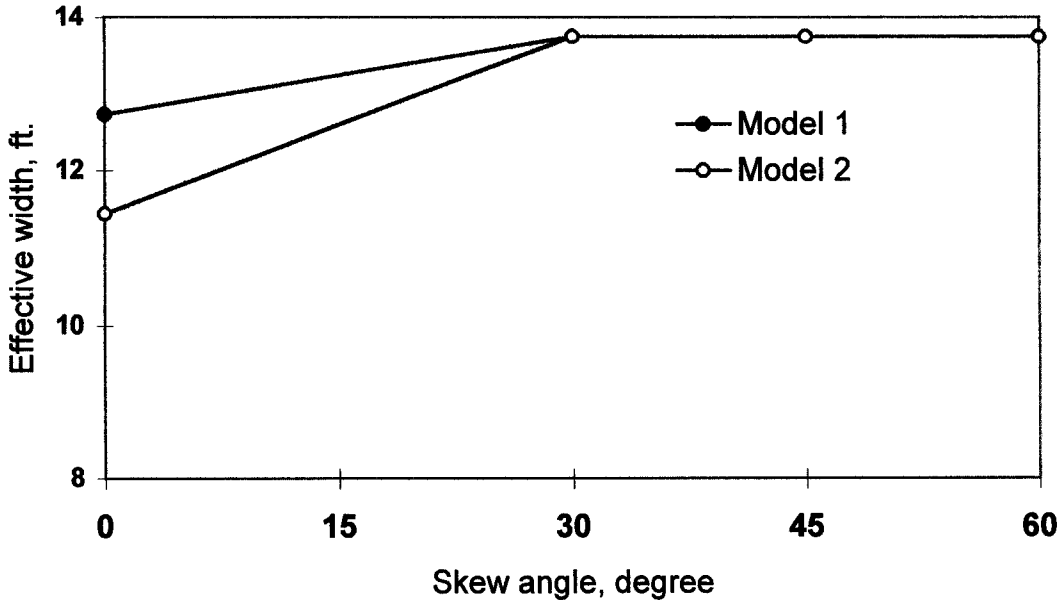

Fig.5.13 Effective width for different models

5.3.2.3 Span length

Span length is an important parameter which is considered in both AASHTO and LRFD codes. The span length for the typical bridge was varied between 15 ft. to 40 ft. as shown in Table 5.2. Figures 5.14 and 5.16 show the moment distributions for typical bridge with different span lengths. The moment increases with the increase in the span length for both models. And a larger effective width is obtained corresponding to a larger span length.

Figures 5.15 and 5.17 show that the effective width increases with increasing span length. The change in effective width is significant and hence span length cannot be neglected in the bridge design. The effective widths calculated based on the finite element method are larger than those based on AASHTO and LRFD codes. This indicates that both LRFD and AASHTO code give conservative estimates of effective width, E when span length is considered. Model 2 is a better model since it gives smaller moments and effective width than those of model 1.

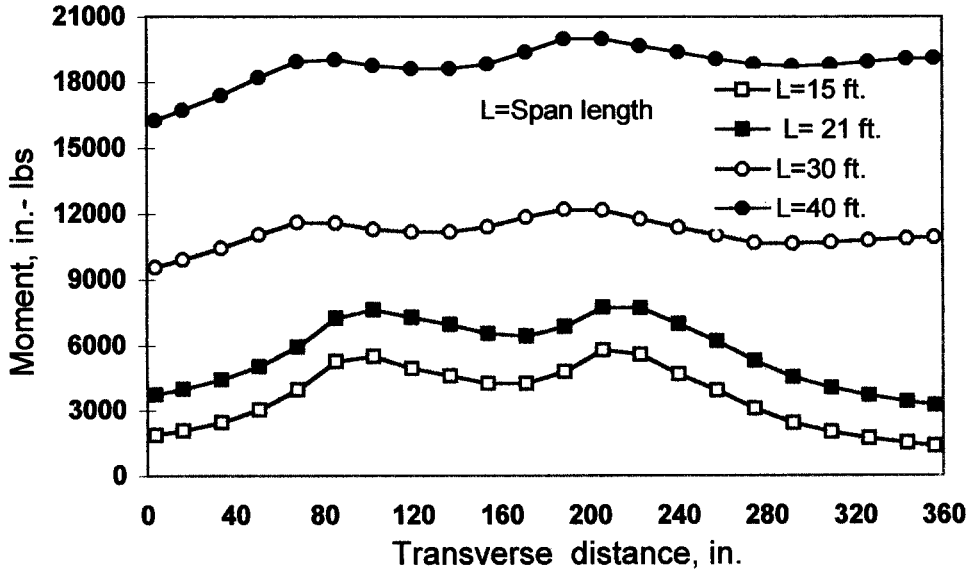

Fig.5.14 Moment distribution for different span length (Model 1)

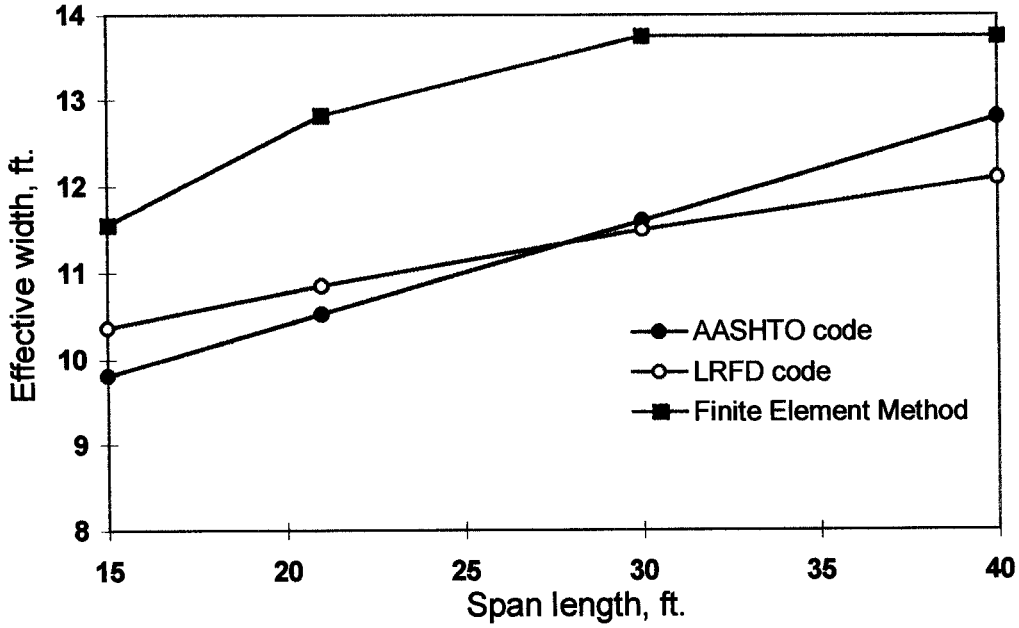

Fig.5.15 Effective width variation with span length for solid slab bridges (Model 1)

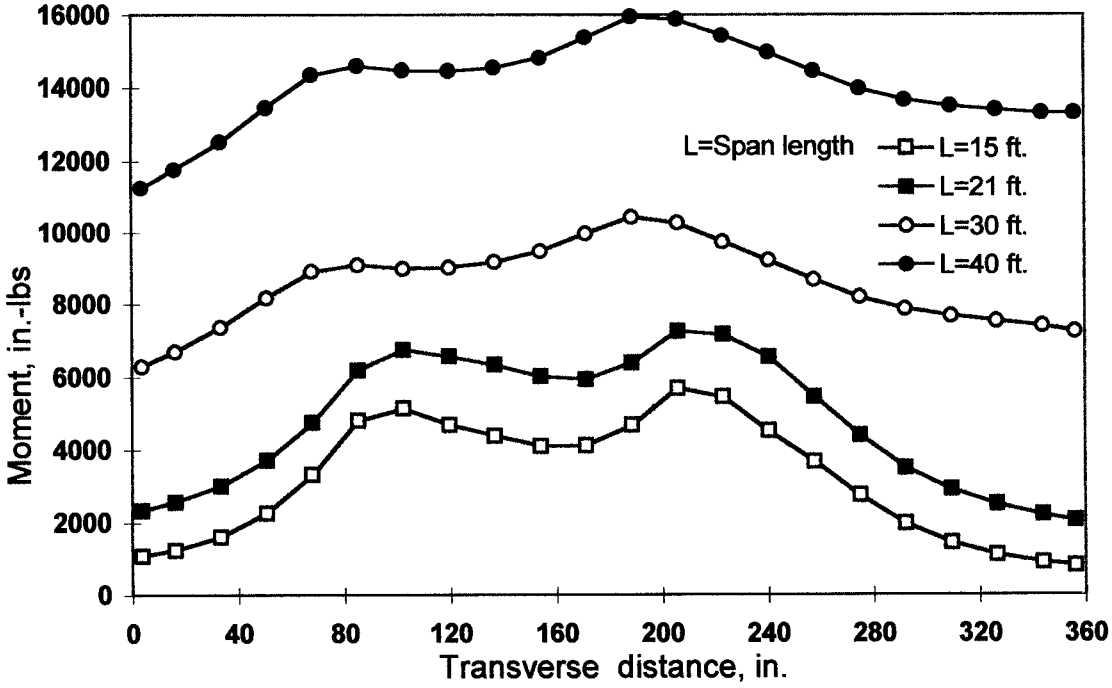

Fig.5.16 Moment distributions for different span lengths (model 2)

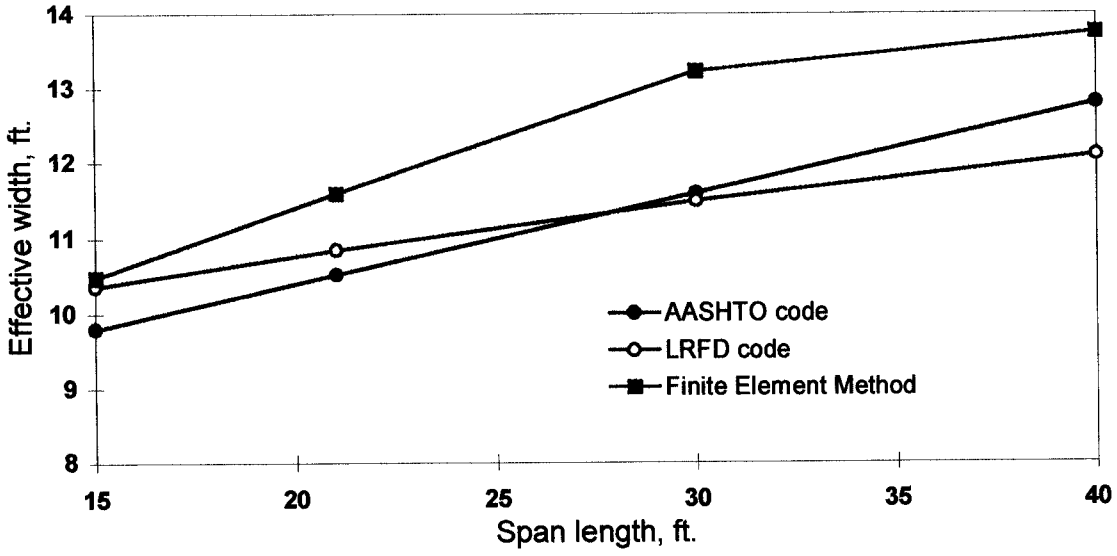

Fig.5.17 Effevtive width variation with span length for solid slab bridges (Model 2)

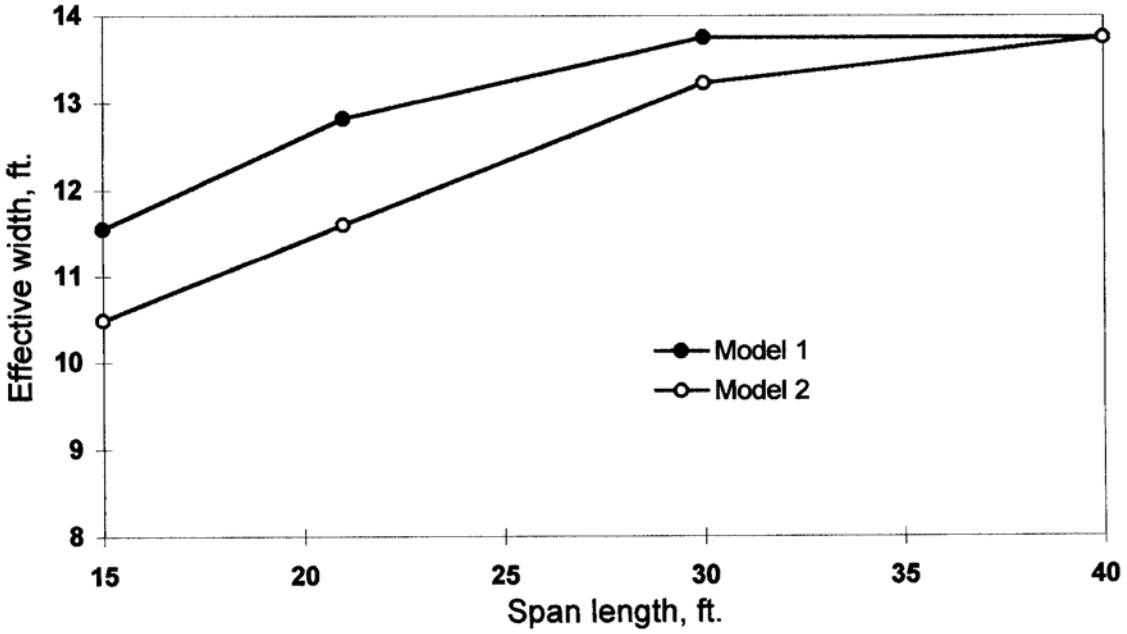

Fig.5.18 Effective width for different models

5.3.2.4 Edge beam depth

AASHTO code requires that an edge beam should be provided for longitudinally reinforced slabs (main reinforcement parallel to traffic). The edge beam of a slab bridge with simple span should be designed for a live load moment of 0.1OPS, where P = wheel load in pounds and S = span length in feet (AASHTO, 1989). One interpretation of this requirement could be that approximately 40% of the live load moment caused by one line of wheels (maximum moment for one line of wheel load in short span is approximately 0.25 PS) should be added to the other computed moment for the width selected for the edge beam. The width of edge beam as required by AASHTO specifications, should not exceed 3 feet.

The LRFD code requires that the edge beams shall be assumed to support one lane of wheels, and where appropriate, a tributary portion of the design lane load (LRFD section 4.6.2.1.4a).

Although edge beam is a very important parameter in load distribution, it is neglected in both AASHTO and LRFD effective width calculations. Figure 5.19 shows the moment distribution for different edge beam depths. Model 1 does not consider the edge beam element, therefore, Model 2 moments and effective widths are presented in Figs. 5.19 and 5.20. With the increase of edge beam depth, the maximum moment slightly decreases as shown in Figure 5.19. Consequently, the calculation shows that effective width, E decreases with the increase of edge beam depth. All the E values were larger than the lane width, therefore, E was assumed equal to the lane width of 13.75 ft as shown in Figure 5.20.

Figures 5.20 and 5.21 show the change in effective width with increase in the edge beam depth. The effective widths calculated using finite element method are larger than those calculated

using AASHTO and LRFD codes. This means AASHTO and LRFD codes give conservative estimate of effective width when the edge beam depth is considered. And these results suggest that the edge beam size should be taken into account in wheel load distribution. Neither AASHTO code nor the LRFD code considers the edge beam moment of inertia in the effective width equation.

5.3.3 Proposed Simplified Effective Width for Solid Slab Bridges

Based on the straight solid slab bridge parametric studies (Study Phase 1, Arockiasamy and Amer, 1995), the span length and the edge beam depth are the main parameters, which significantly affect the effective width calculations. For straight solid slab bridges without edge beams or with hidden edge beams, the following equation based on the least square fit of the grillage analogy results (Phase I of this study) for the effective width could be used for spans upto 40 ft. and slab thickness upto 14 in.:

$$E = 6.89 + 0.23\ L \leq W/N_L \qquad (5.8)$$

where

E = **Effective width over which truck load is assumed to be uniformly distributed,**

ft. L = **Span length,** ft.

W = **Physical edge-to-edge width of bridge ,(feet.units),**

N_L = **Number of design lanes.**

The effect of edge beam depth above the slab thickness can be taken into consideration by multiplying the above equation by a factor C_{e*} given by

where d, = Edge beam depth above the slab thickness, in.

Based on the finite element results in this study (Phase 11), it can be concluded that the effective width increases with the skew angle increases for solid slab bridges. This confirms the LRFD codes in considering the skew angle as a parameter in effective width calculation. The finite element results show the same skew angle effects as those in LRFD codes except for higher skew angle than 45 degrees where the effects are higher in finite element than in the LRFD code. Therefore, the LRFD moment reduction factor due to skewness of solid slab bridges will be used to modify the proposed simplified effective width for straight solid slab bridges.

For skewed bridges, the effective width can be enlarged by:

$$\text{Cse}_{\prime\prime} = (1/r)=1/(1.05-0.25\tan 0) \text{ where(} r<\_ \text{ 1.00)}$$

where,

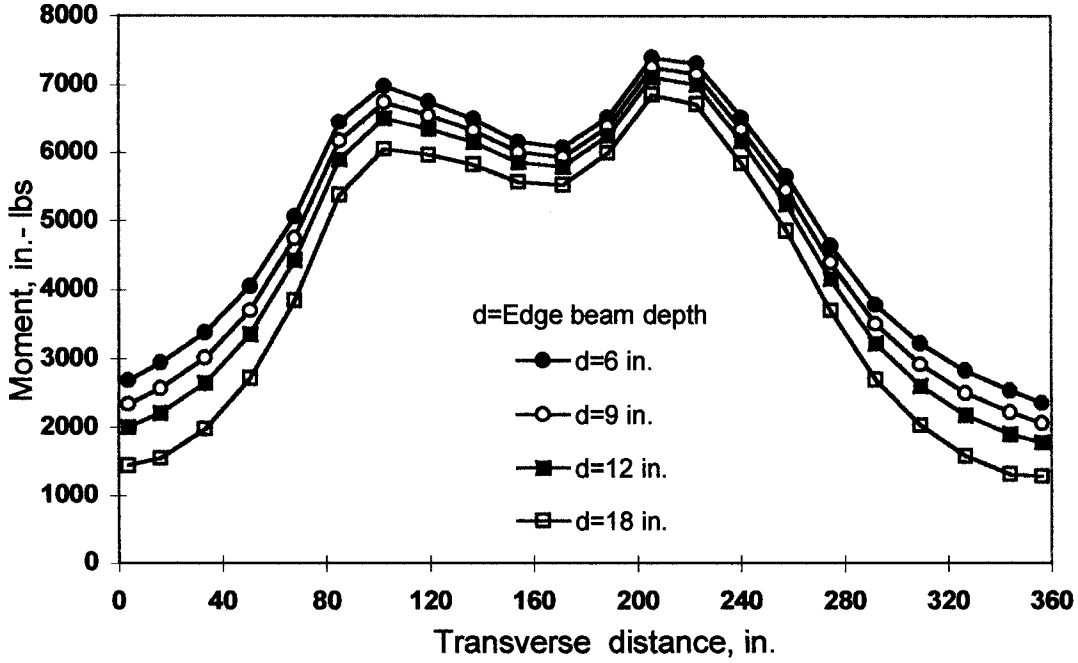

Fig.5.19 Moment distributions for different edge beam depths (Model 2)

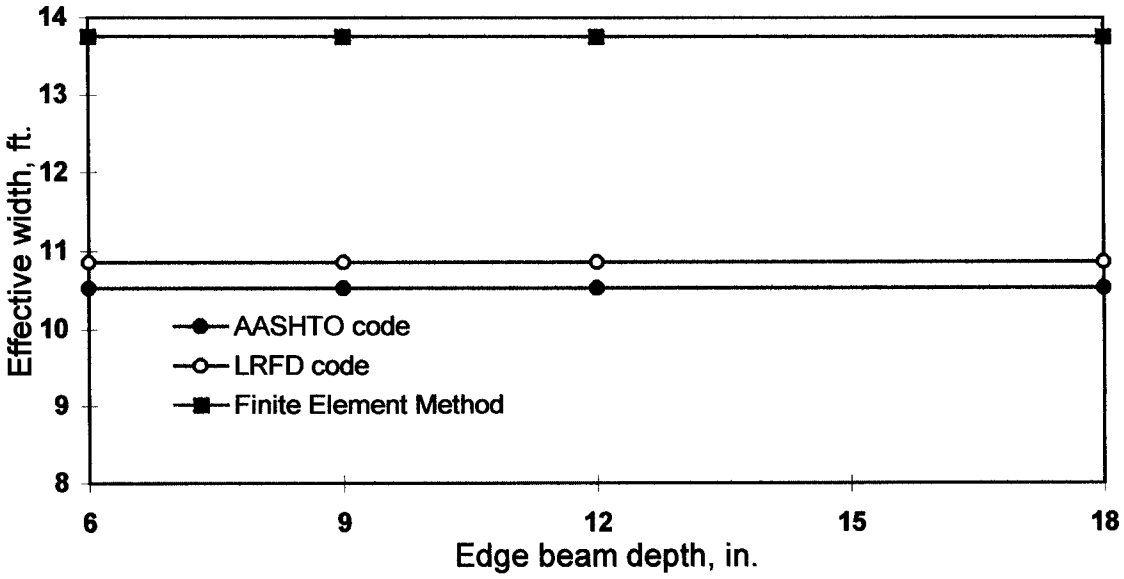

Fig.5.20 Effective width variation with edge beam depth for solid bridges (Model 2)

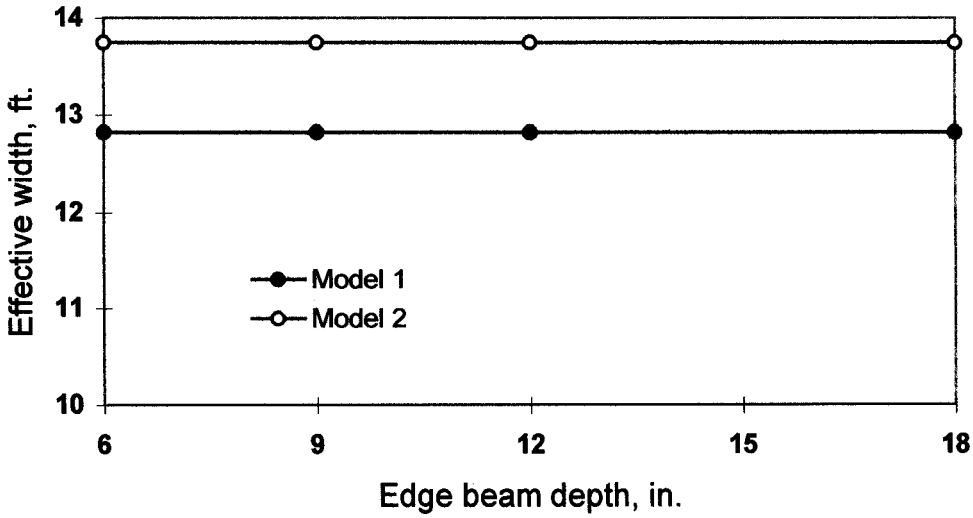

Fig.5.21 Effective width for different models

5.4 SKEW SOLID SLAB BRIDGE FIELD TEST

Florida Department of Transportation (FDOT) have tested many solid slab bridges to check their strength. The bridges are first instrumented for measuring strains and deflections at the bridge deck critical locations, and then incrementally loaded to induce maximum effects. The data collected are then analyzed and used to establish the strength of each component as well as the load distribution.

The test vehicles are initially loaded with a number of blocks of known weights, established from the preliminary analysis of the bridge. The vehicles are then driven and placed on the critical locations of the bridge, while the strains and deflections are monitored using the data acquisition system during loading. After each load step, the measured strains are compared favorably with the theoretical predictions, additional blocks are added to the vehicles and the test repeated until the ultimate AASHTO load is achieved. The data are then processed to determine the load distribution.

Test data from typical solid bridges are used for load distribution analyses. The typical test report contains transverse strain distribution in the maximum bending moment section for several loading stages. It also contains the applied moment vs. strain curves for several loading stages.

The bridge load test data are used in the determination of wheel load distribution factors, i.e. effective width, E. The measured effective width can be used in bridge-rating calculations in place of effective width defined by AASHTO.

In the present study, the measured strains will be multiplied by the slab section modulus and the elastic modulus to calculate the measured moments. The ACI equation was used to calculate the elastic modulus of concrete which is determined based on flc = 5000psi. The measured strain

distribution is used to calculate the effective width, which is compared with those based on AASHTO, LRFD and finite element method.

5.4.1 Collier County Bridge (#030144)

The bridge is built in 1963 and located on Tamiami Trail HWY41 in Collier County (Bartow, Florida). It consists of five simply supported spans with span lengths of 21 feet each. The total length and width of the bridge are 105 feet and 46'-3" respectively with curb to curb width of 44'-0". The bridge is two lane skew bridge with skew angle of 14.28 degrees as shown in Fig.5.25. The bridge is a concrete flat slab type, with 12.5 in. thick deck supported by concrete bent cap and concrete piles. An inspection of the bridge showed that the slabs, piles and pile caps along the entire length of the bridge to be good condition, except for the transverse slab cracks over each support (bent cap). Table 5.5 summarizes the material properties of the bridge.

Table 5.5 Material and sectional properties for bridge #030144

E_{deck} (ksi)	Poisson's Ratio, υ	G_{deck} (ksi)	Thickness (in.)
4031	0.2	1679	12.5

Instrumentation for measuring the strains were placed at the critical locations on the test span (northwest span). The bridge was incrementally loaded with two trucks (24, 30, 36 and 42 blocks). The strain and deflection readings were taken at each load increment to establish the behavior of the bridge. The load case corresponding to thirty blocks have been used in the analysis to ensure the behavior of the bridge was within the linear and elastic range. The measured strains along the bridge width at the maximum bending moment section are presented in Table 5.6.

Typical top view of the finite element mesh is presented in Figure 5.23. Each node had six degrees of freedom and the nodes arranged such that some nodes were located at the strain gage position to facilitate the comparison between the measured and calculated strains. The slab is divided into 24 x14 = 336 four-node shell elements. Simply supported boundary conditions are realized by restraining the appropriate translational degrees of freedom.

Table 5.6 summarizes the results from finite element analysis and field test at a cross section corresponding to the maximum bending moment location. In general, the maximum slab deflection of 0.138 in. obtained from analysis agree well with the measured value of 0.14 in.. Figure 5.24 shows the comparison of the measured and predicted strain distribution along the bridge width. It is clear that the measured and calculated strains at the bottom of the slab show a significant difference. The difference in measured strain values could be attributed to observed transverse cracks on the bottom of the slab. These cracks open under the applied loads and consequently produce higher strains in the bottom of the slab. However, the local cracking is not modeled in the finite element analysis. This observation indicates that limited local cracking of the slab does not affect the global measured response of the bridge to applied loads and computed displacements are in good agreement.

Table 5.6 Measured and calculated strains for bridge #030144

Transverse distance in.	Measured strains, in./in. x 10-6	Calculated strains, in./in. x 10-6
61.5	25	67
109.5	80	89
157.5	50	115
205.5	200	136
253.5	275	150
301.5	300	138
349.5	240	130
397.5	105	113
445.5	165	77
493.5	40	58

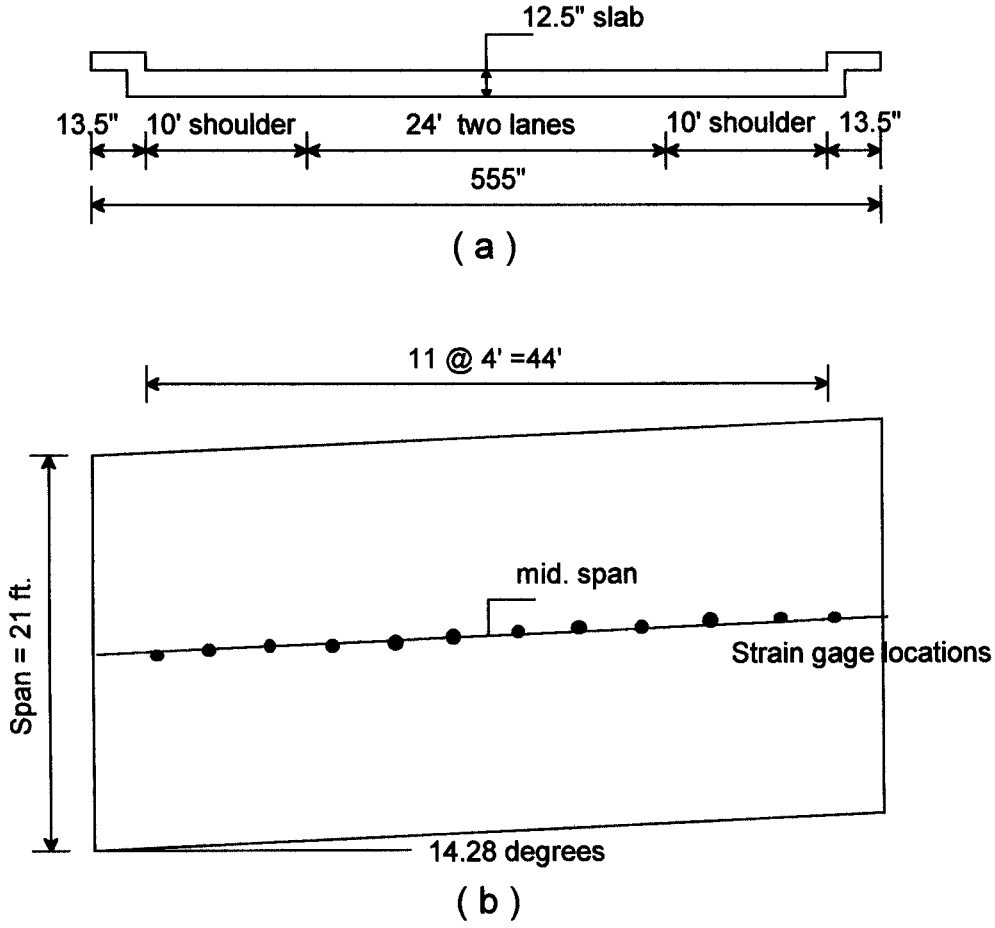

Fig.5.22 Typical cross-section of solid slab Bridge #030144

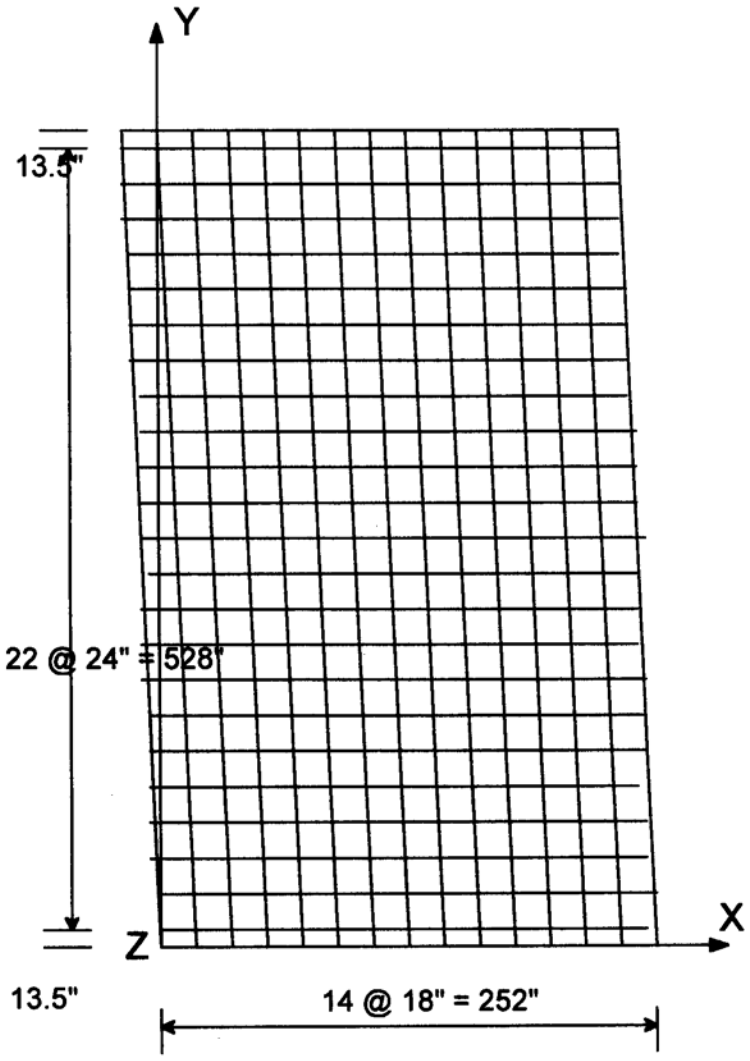

Fig.5.23 Top view of finite element mesh of Bridge #030144

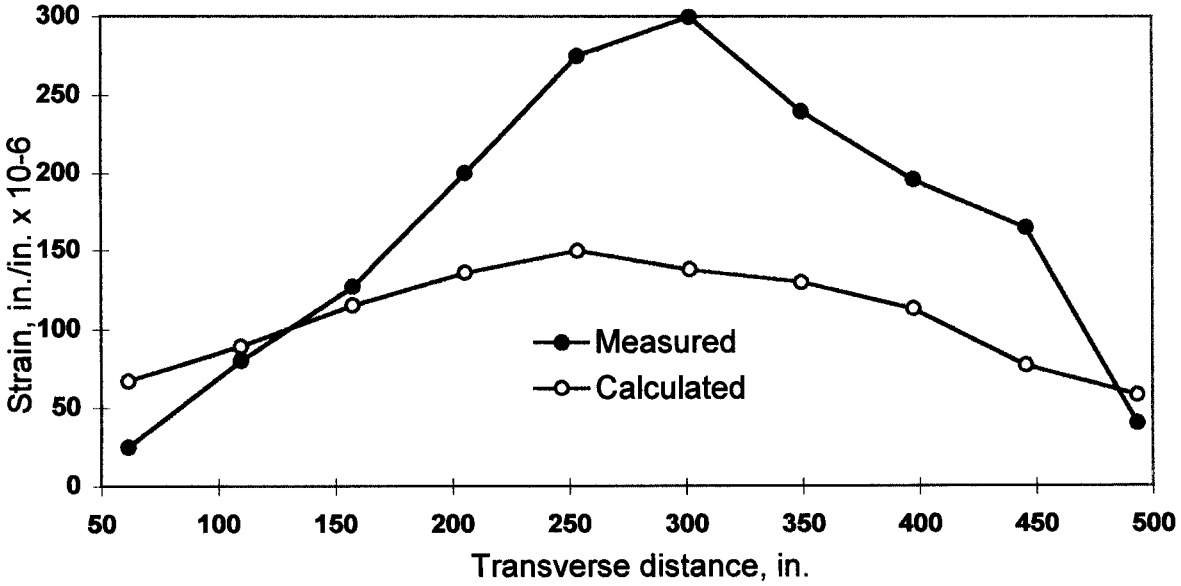

Fig.5.24 Strain variations across the slab bridge

Table 5.7 shows the effective widths calculated by different methods. The values calculated from finite element method and field test are higher than those from AASHTO and LRFD codes. The effective widths based on the AASHTO and LRFD codes are conservative.

Table 5.7 Effective width for Bridge #030144

Method	AASHTO code	LRFD code	F.E.M.	Field test
E (ft).	10.52	10.77	14.30	11.00

CHAPTER 6

LOAD DISTRIBUTION ANALYSIS OF CONTINUOUS SLAB-ON-GIRDER BRIDGES

6.1 INTRODUCTION

The design of highway bridges has followed the guidelines of the American Association of State Highways and Transportation Officials (AASHTO) or Load and Resistance Factor Design (LRFD). The AASHTO and LRFD codes do not specify any modification for computing the distribution factors for continuous bridges as they do for single span skew bridges. LRFD bridge design specifications (1994) deleted the wheel load distribution correction factors for continuity from the LRFD specifications. The code commentary gives the following reasons for deleting the correction factors: the value of the correction factors were within 5%, which is less than the level of the accuracy for the approximate distribution factor method, and the increase in the distribution coefficient for negative moments tends to cancel out when the distribution of reaction force over the bearing is considered. Other publications have recognized the need for more research to examine the importance of the correction factor for continuity (Khaleel, Itani 1990). Alternative designs for continuous bridges have taken a direction in which computer models using finite element method (FEM) accurately predict the bridge behavior for various loadings.

Research on continuous bridges has mostly been limited to the analysis of two-dimensional models to obtain the moments, shears, rotations, and deflections. AASHTO design

considers a single girder that acts compositely with a concrete deck. This composite section carries a portion of a designated wheel load that is distributed transversely to the girder (AASHTO 1992). Continuous bridges amplify the complexity of solving a two or three dimensional problem. FEM does accurately predict solutions for specific bridges. A 0.4-scale model of a two-span bridge comprised of concrete deck on steel girders, was loaded with simulated truck loads. The results of the study show that FEM predicts the reactions, moments, displacements, and rotations with a high accuracy of + 10% (Tiedman, Albrecht, Cayes 1993). The accuracy of the FEM analysis of continuous bridges is dependent on the type of the model. Each model has different elements, material properties, and boundary conditions which should be considered individually and evaluated to serve as a basis for establishing accurate predictions for continuous bridges.

The objectives of this study on continuous bridges are:

i) Study the effects of bridge skew angles, number of spans, span ratio between two spans, and other parameters on load distribution factors using FEM.

ii) Compare AASHTO, LRFD, and FEM load distribution factors with those based on field tests on continuous bridges.

iii) Recommend new methods/changes, if needed, for calculating wheel load distribution factors for continuous bridges based on correlation of field tests and FEM analysis.

6.2 METHOD OF ANALYSIS

The continuous bridge analyses using AASHTO and LRFD codes, FEM, and field test data were used to establish load distribution guidelines . The AASHTO approach is based substantially on Westergaard theory for slabs (Westergaard, 1930). The LRFD method is based on NCHRP nroiect 12-26 entitled, "Distribution of Wheel Load on Highway Bridges", which was

performed in two phases by Imbsen & Associates, inc.(1989). FEM distribution factors are calculated based on moment distribution (Stalling and Yoo 1993). The following section summarizes the method of analysis.

6.2.1 AASHTO and LRFD Distribution Factor

There are no AASHTO specifications given for multiple spans. The only parameter considered is the spacing (S) between the girders. The AASHTO Specifications (1992) for simply supported bridges will be used

	Distribution Factor	
Concrete Girders	One lane	Two or more lanes
	Sao S/5.5	(6.1
	) If S exceeds 10 feet *	If S exceeds 14 feet'

The load on the stringer shall be the reaction of the wheel loads, assuming the flooring between the stringers to act as a simple beam (AASHTO 1992).

The LRFD BRIDGE DESIGN SPECIFICATIONS (1994) is similar in the approach to the AASHTO methods. The LRFD distribution of live load moment in interior beams per lane is

$$g = 0.06 + \left(\frac{S}{4300}\right)^{0.4}\left(\frac{S}{L}\right)^{0.3}\left(\frac{K_g}{Lt_s^3}\right)^{0.1} \qquad \textbf{(6.2 SI)}$$

$$g = 0.5 * \left[0.12 + \left(\frac{S}{2.5}\right)^{0.4}\left(\frac{S}{L}\right)^{0.3}\left(\frac{K_g}{12.0Lt_s^3}\right)^{0.1}\right] \qquad \textbf{(6.2 US)}$$

Two or more lanes loaded

$$g = 0.075 + \left(\frac{S}{2900}\right)^{0.6}\left(\frac{S}{L}\right)^{0.2}\left(\frac{K_g}{Lt_s^3}\right)^{0.1} \qquad \text{(6.3 SI)}$$

$$g = 0.5 * \left[0.15 + \left(\frac{S}{3.0}\right)^{0.6}\left(\frac{S}{L}\right)^{0.2}\left(\frac{K_g}{12.0Lt_s^3}\right)^{0.1}\right] \qquad \text{(6.3 US)}$$

When the supports are skewed, the bending moments in the beams may be reduced using the following skew factor:

$$\text{skew factor} = 1 - c_1 \cdot (\tan\theta)^{1.5} \qquad \text{(6.4 SI,US)}$$

$$c_1 = 0.25\left(\frac{K_g}{Lt_s^3}\right)^{0.25}\left(\frac{S}{L}\right)^{0.5} \qquad \text{(6.5 SI)}$$

$$c_1 = 0.25\left(\frac{K_g}{12.0Lt_s^3}\right)^{0.25}\left(\frac{S}{L}\right)^{0.5} \qquad \text{(6.5 US)}$$

If $\theta < 30°$ then $c_1 = 0.0$ If $\theta > 60°$ use $\theta = 60°$
g = distribution factor
S = spacing of supporting component (mm SI)(ft US)
L = span length (mm SI)(ft US)
K_g= longitudinal stiffness parameter (mm^4 SI)(in^4 US)
t_s= depth of concrete slab (mm SI)(in US)
N_b= number of beams,stringers,girders
$K_g = n(I + Ae_g^2)$
n = modular ratio between beam and deck
I = second moment of inertia of beam (mm^4 SI)(in^4 US)
A = area of the beam (mm^2 SI)(in^2 US)
e_g= distance between centers of gravity of the basic beam and deck (mm SI)(in US)

The distribution factor for exterior beams should be determined by applying the lane fraction (g) as specified below:

8.a= e(g)

e=0.77+ de > 1.0 (6.6SI)
2800

e = 7+d ` >_ 1.0 (6.6 US)
9.1

de= distance between the center of exterior beam and the interior edge of curb or traffic barrier (mm Sn(ft US)

No specifications are given for calculating/modifying wheel load distribution factors for continuous bridges in the LRFD BRIDGE DESIGN SPECIFICATIONS 1994. The AASTHO and LRFD distribution factors for continuous bridges in this study, are calculated using the above equations which only are specified for simply supported and skew bridges.

6.2.2 Finite Element Method

Chapter 3 summarizes the principles and the details for slab-on-girder bridges. The ANSYS software (Swanson Analysis Systems, Inc. 1995) was used in the analysis and modeling of the continuous highway bridges. The three-dimensional model consists of deck slab elements and girder elements (Figure 6.2). The deck slab was modeled using a 4-node quadrilateral shell element (SHELL 63) with six degrees of freedom (u_X u_y u_Z rot rot_y rat,) at each node. The girder was modeled using a 4 -node quadrilateral shell element (SHELL 63) for the web and two elastic frame elements (BEAM 4) for the top and bottom flanges. The frame element is a 3-D 2-node element with six degrees of freedom (u, u_y u_Z rot. rot_y rot,). Composite action between the deck slab and the girder is achieved by coupling vertically the nodes in the deck which coincide with the nodes in the top flange of the girder. The coupling prescribes identical translations in vertical direction for both deck and girder. The deck slab finite element mesh was selected with an aspect ratio less than 1:2. The boundary conditions imposed on the model were selected to represent the

actual behavior of the continuous bridge field tests. All nodes at each end of the bridge were prevented from translating in u_X , u,. , and u_Z direction. The bottom flange at the interior supports for the continuous bridge were prevented from moving vertically.

The FEM strains and deflections were calculated at the girder's bottom flange at the mid-spans and supports. Distribution factors based on the finite element results are calculated from the strain distribution in the transverse direction. Assuming all traffic lanes are loaded with equal-weight trucks, the wheel load distribution factor for the tth girder in a straight bridge is calculated as follows (Stalling and Yoo 1993):

$$DF_{,.} = \frac{ns;}{}$$

E j- C.W. s,= **the bottom flange strain at the ith**

girder

W_j= **ratio of the section modulus of the ith girder to the section modulus of a typical interior girder**

n = number of wheel lines of applied loading

Equation 6.7 is based on the assumption that the sum of the internal moments or the total area under the moment distribution curve should be equal to the externally applied moment. This assumption is valid only for straight bridges. However, this assumption is not realistic to yield the actual moment distribution in skew bridges. The distribution factor is equal to the ratio of maximum girder moment obtained from finite element or field tests to the maximum moment in the bridge idealized as a one-dimensional beam subjected to one set of wheels. The sum of the internal moments in a straight bridge is equal to the maximum moment in the bridge idealized as a one-dimensional beam subjected to one set of wheels. The sum of the girder strains in a straight bridge will be used to take into account the total external load effects in skew bridges. Therefore, equation 6.7 can be modified as follows:

$$DF_{i\theta} = \frac{n\varepsilon_{i\theta}}{\left(\sum_{j=1\to k} \varepsilon_j W_j\right)_{\theta=0}} \qquad (6.8)$$

6.3 CONTINUOUS SLAB-ON-AASHTO GIRDER FLEXURAL LOAD DISTRIBUTION FACTORS: PARAMETRIC STUDY 6.3.1 Introduction

To study the parameters which affect the design of continuous bridges, a group of main parameters were chosen that frequently appear when designing continuous slab-on-AASHTO girder bridges. The chosen parameters for this study are: number of spans, skew variation, and span length ratios. Figure 6.1 shows the typical slab-on-girder bridge cross-section used in the analysis. The typical two span slab-on-girder bridge has a slab thickness of 7", span lengths of 70', and bridge widths of 54'. The bridge has nine AASHTO N girders spaced at 6' center to center. The concrete strengths of the girder and the slab are 5000 psi.

Typical continuous slab-on-girder bridge which is shown in Figure 6.3 is divided longitudinally into twenty elements for each span. The slab deck is divided in the transverse direction into two elements between each girder. The material properties used in the analysis are presented in Table 6.1 (Elastic modulus, E, Poisson's ratio, u, and modulus of,rigidity, G) along with the sectional properties of the AASHTO N girder (Area, A, and moments of inertia, I_y and 1j.

Table 6.1 Material and Sectional Properties for Typical Continuous Slab-on-Girder Bridge

Material properties	Ed~k i	E~ i	Poisson's ratio, v	G si)
	4031	4031	0.2	1679

Section Properties	Slab	Thickness = 7 in.				
	Top	A (in)	l_y (in)	1. (in^4)	Tk_y (in)	Tk_Z (in)
	Flange	220	2218	7333	20	11
AASHTO IV Girder	Web	Thickness = 8 in.				
	Bottom	A (in)	I_y (in)	I_Z (in)	T_{ky} (in)	T_k. (in)
	Flange	312	3744	17576	26	12

70' 70'

3'

T'slab

48'

9 AASHTO TYPE N @ 6'

T

Fig. 6.1 Typical Continuous Slab-on-Girder Bridge Details

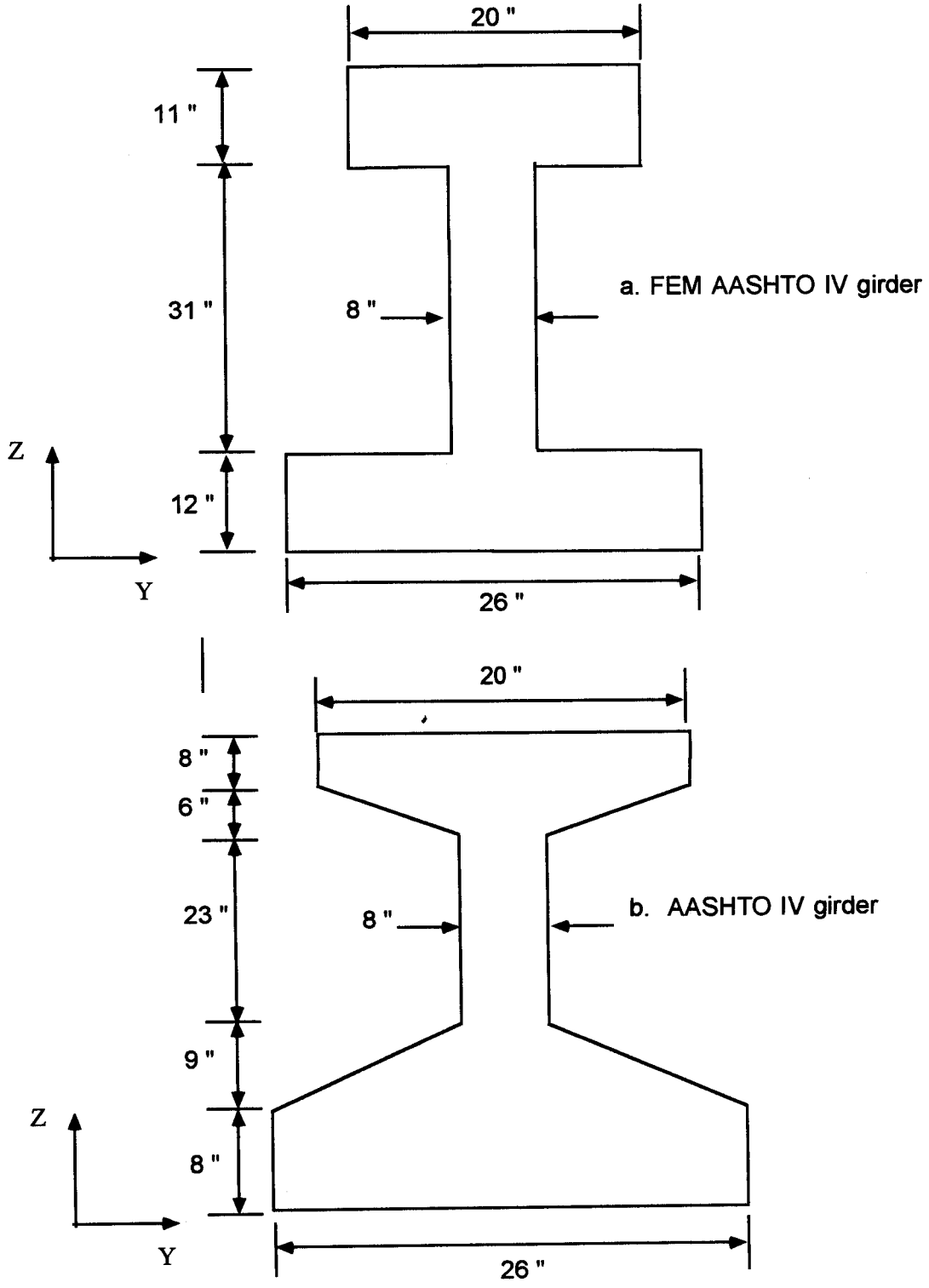

Fig. 6.2 AASHTO IV Girder Details

Figure 6.3 Finite Element Mesh of Continuous Slab-on-Girder Bridge

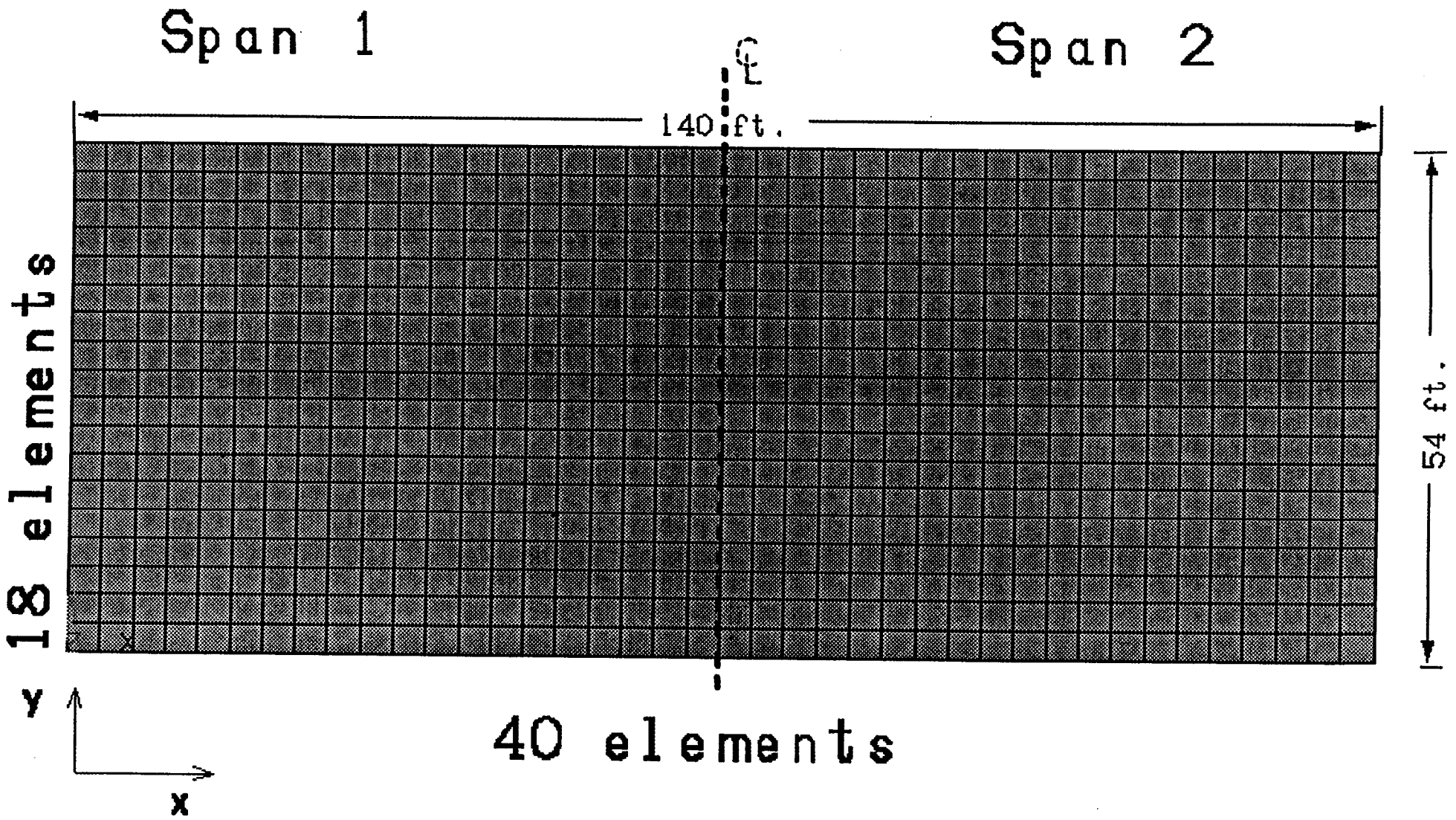

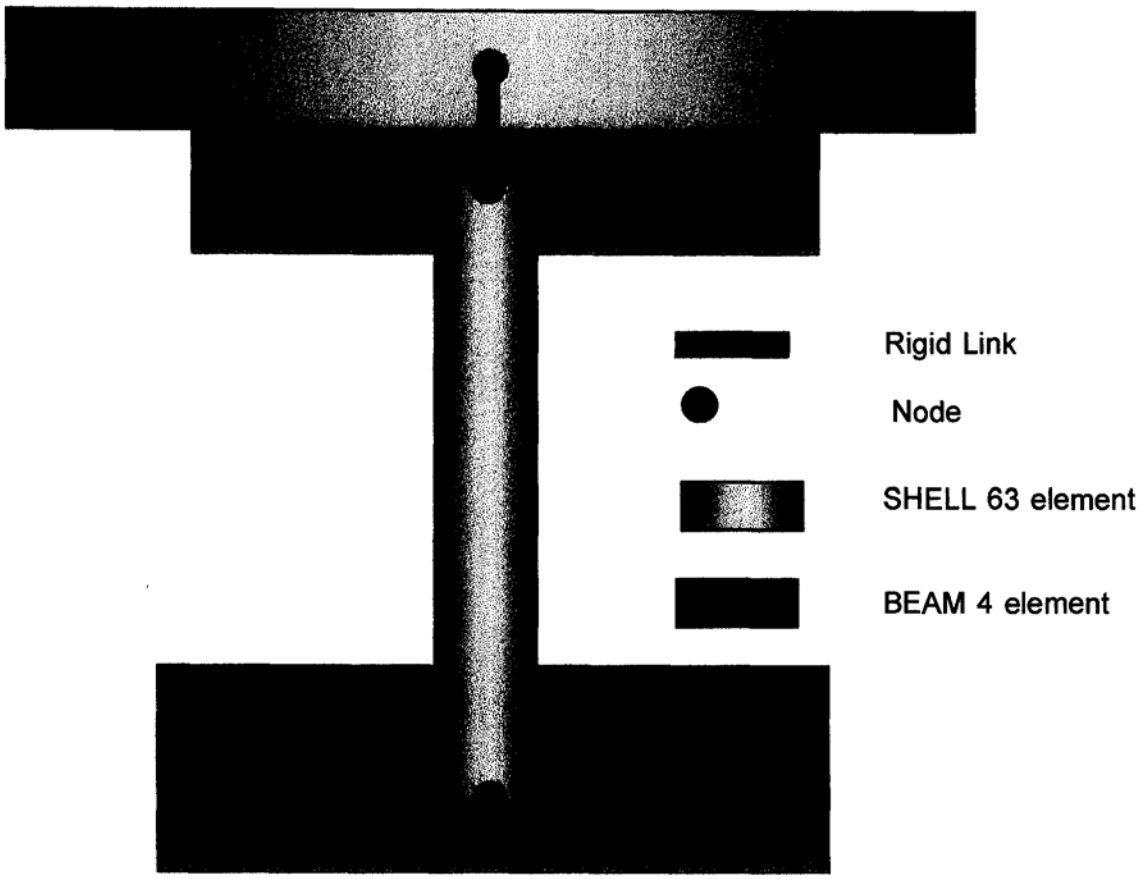

Fig. 6.4 Finite Element Model of Typical Continuous Slab-on-Girder Bridge

6.3.2 Truck Load Position

The AASHTO HS20-44 trucks are used with a minimum spacing of fourteen feet between axles to give the maximum moment. Based on the analysis in Chapter 5, three trucks loaded transversely are used for determination of load distribution factors for the exterior girders. Four trucks are used in calculating the load distribution factors of interior girders. Typical loading positions for interior and exterior girders are shown in Figure 6.5. Prior to the FEM analysis, the truck positions in the longitudinal direction were determined to obtain the maximum positive or negative moments in the continuous bridge by using PC BRIDGE (Joe Murphy, Ph.D.,P.E. 1992). A spacing of fifty feet between the rear axle of one truck and the front axle of another truck facing

the same direction is used for calculating the maximum negative moment (AASHTO 1992). Figures 6.6-6.19 show the load position for each loading case.

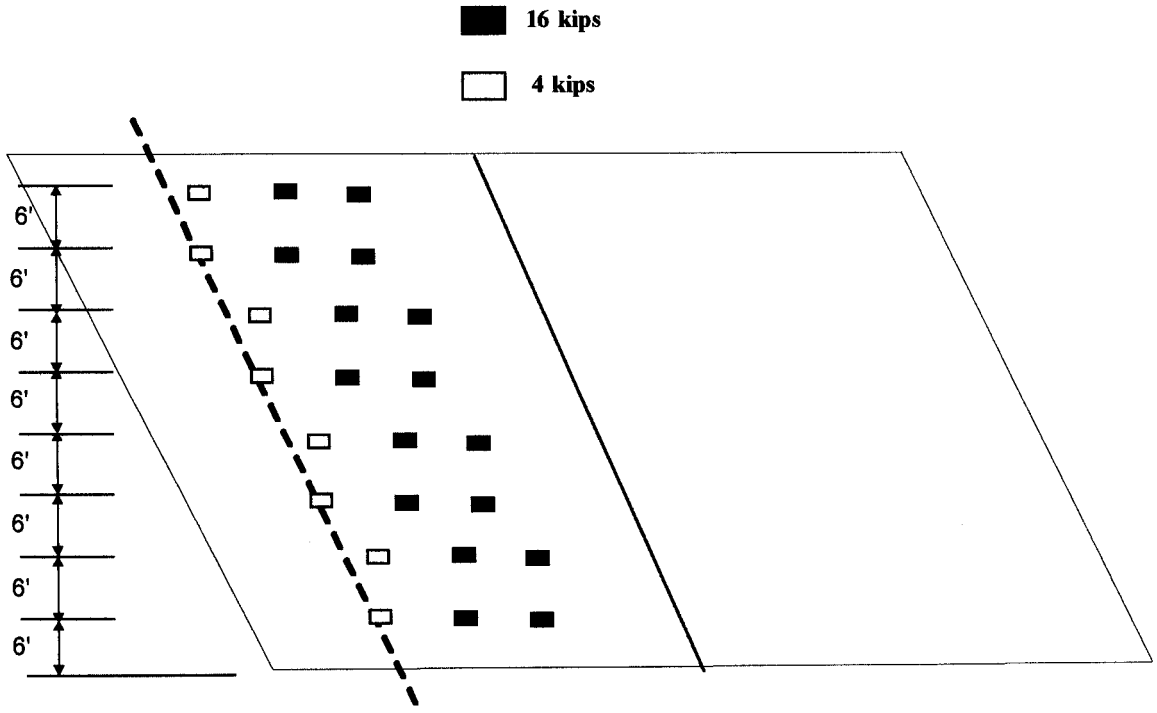

a. Interior girder load position

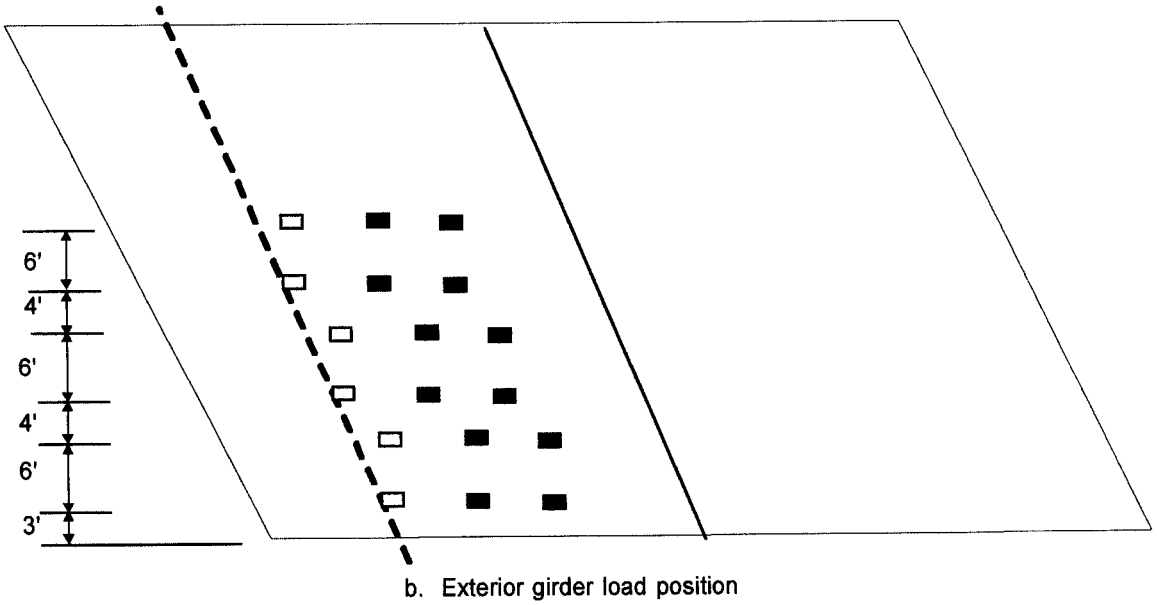

b. Exterior girder load position

Fig. 6.5 Load Positions for Interior and Exterior Girders

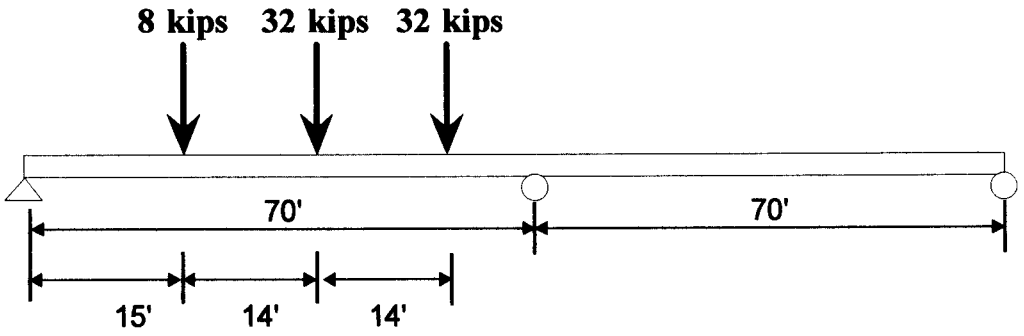

a. Positive moment load position

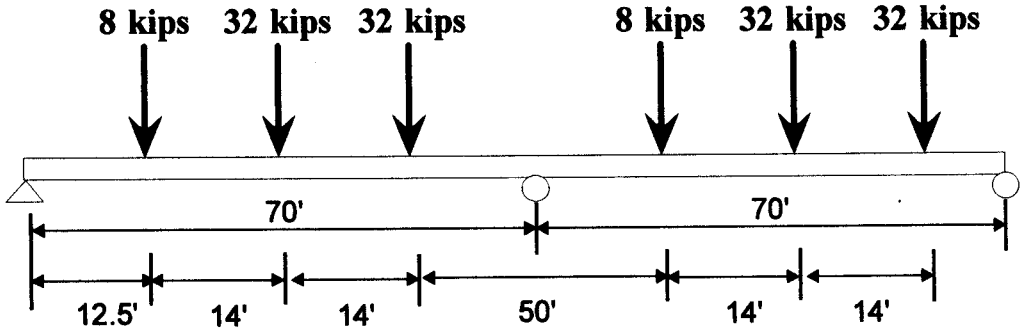

b. Negative moment load position

Fig. 6.6 Load Positions for Two Span Continuous Bridges (Skew angles= 0^0,30^0,45^0,60^0)

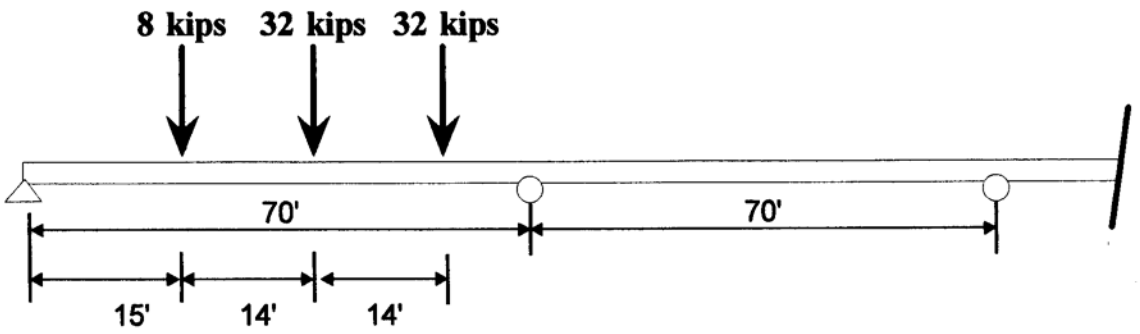

a. Positive moment load position

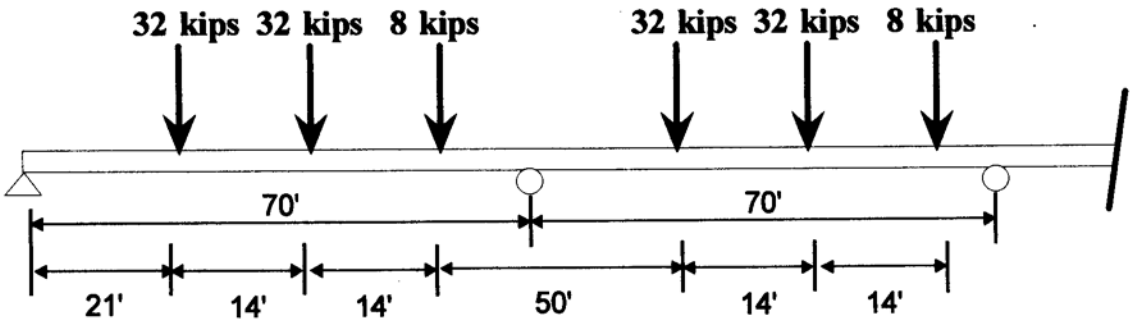

b. Negative moment load position

Fig. 6.7 Load Positions for Three Span Continuous Bridges (Skew angles= 0^0,30^0)

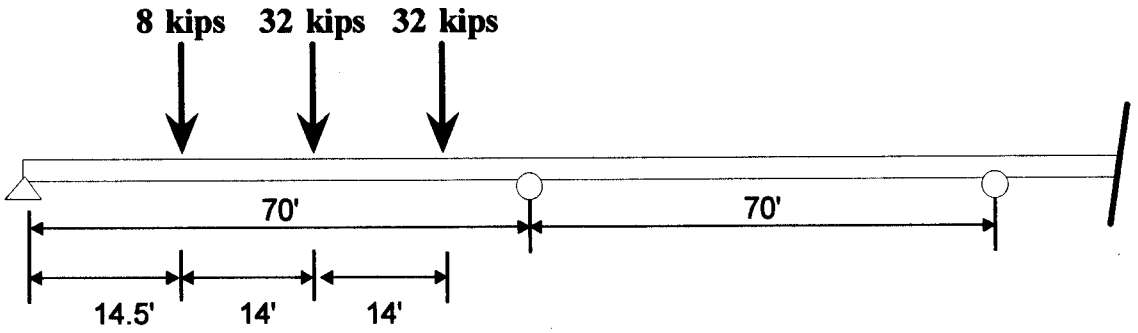

a. Positive moment load position

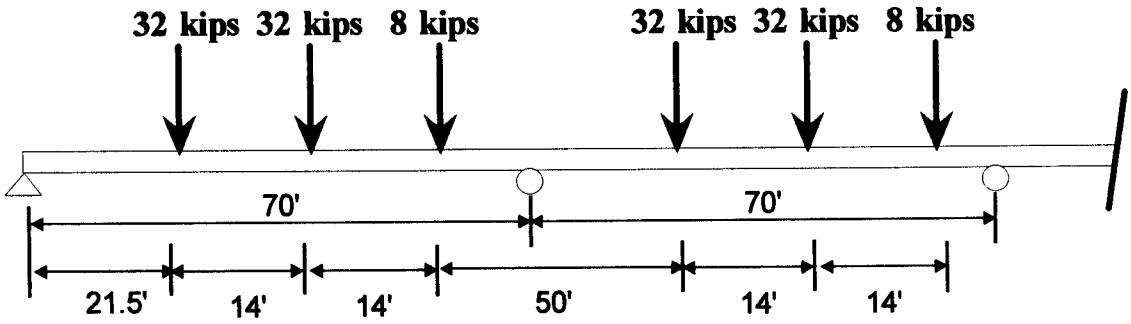

b. Negative moment load position

Fig. 6.8 Load Positions for Four Span Continuous Bridges (Skew angles= 0^0,30^0)

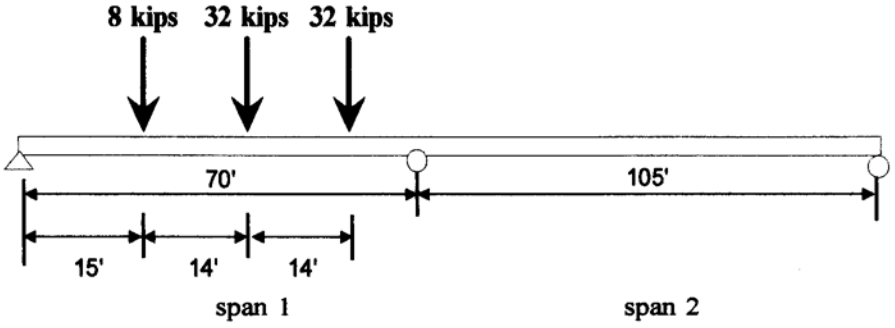

a. Positive moment load position span 1

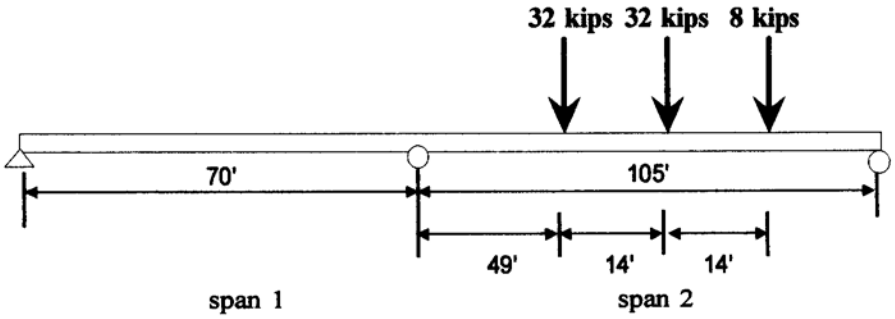

b. Positive moment load position span 2

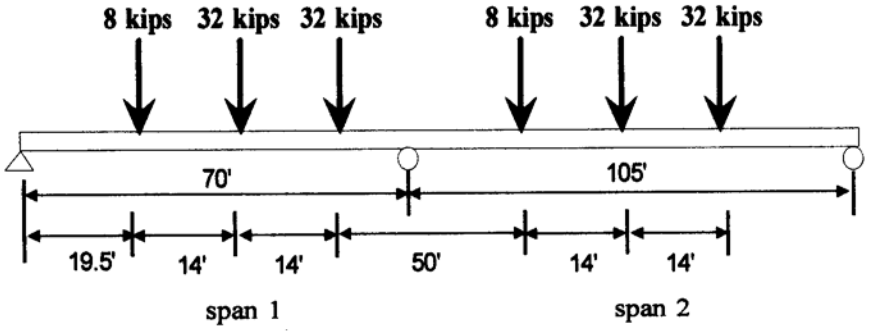

c. Negative moment load position

Fig. 6.9 Load Positions for Two Span Continuous Bridges (Ratio=1:1.5 Skew angles= 0^0,30^0)

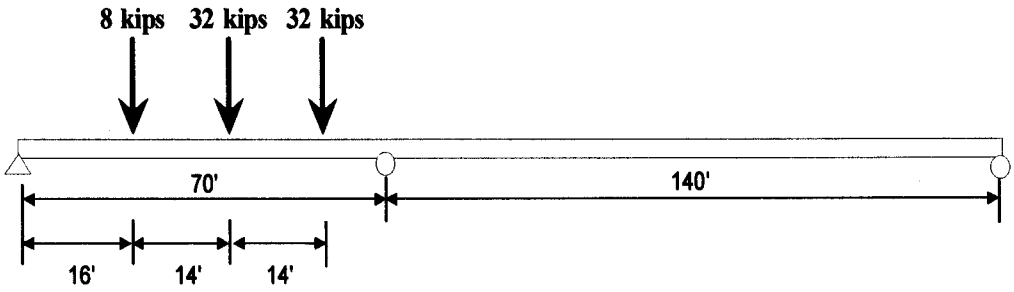

span 1 span 2

a. Positive moment load position span 1

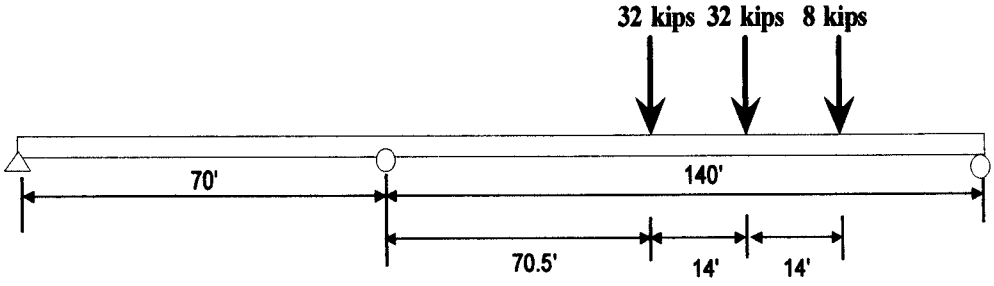

span 1 span 2

b. Positive moment load position span 2

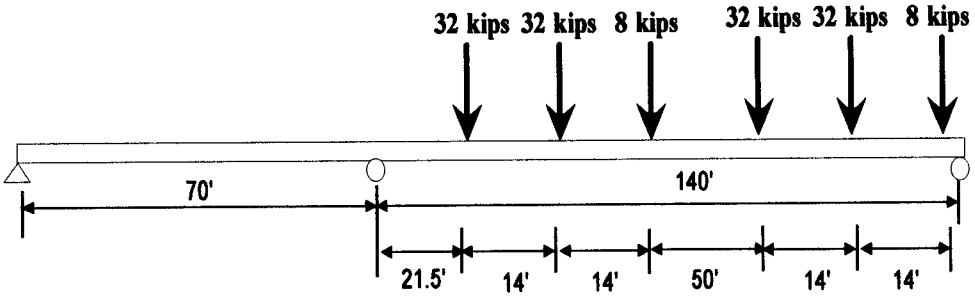

span 1 span 2

c. Negative moment load position

Fig. 6.10 Load Positions for Two Span Continuous Bridges (Ratio=1:2 Skew angles= 0^0,30^0)

6.3.3 Parametric Studies

The parametric study is focused on three main parameters: variation of skew angle, variation in the number of spans, and change in the ratio between two spans. A total of 64 cases have been investigated in this parametric study. The first section studies the effects of changing the skew angle for a two-span continuous bridge. Each of these bridges with different skew angles have four truck loading positions for obtaining the positive and negative moment distribution for interior and exterior girders.

The second section involves changing the number of equal spans with two different skew angles. Each bridge has four truck loading positions for obtaining the positive and negative moment distribution for interior and exterior girders.

The third section studies the effect of varying ratios between the spans for two different skew angles. The four truck ,load positions are also considered in each case. The summary of parametric study is presented in Table 6.2. The load distribution factors for each case are calculated and presented in Table 6.3.

Table 6.2 Summary of Parametric Studies for Continuous Slab-on-Girder Bridges

Parameter	Span lengths (ft.)	Skew angles (degrees)	Cases	Comments
Skew angle (2 spans)	70, 70	0	4	Cases:Interior Positive Mom.
	70, 70	30	4	Exterior Positive Mom.
	70, 70	45	4	Interior Negative Mom.
	70, 70	60	4	Exterior Negative Mom.
Number of Spans (2-4)	70, 70	0	4	
	70,70,70	0	4	Cases:Interior Positive Mom.
	70,70,70,70	0	4	Exterior Positive Mom.
	70, 70	30	4	Interior Negative Mom.
	70,70,70	30	4	Exterior Negative Mom.
	70,70,70,70	30	4	
Ratio between two spans	70, 105	0	6	Cases:Int. Pos. Mom. Span 1
	70, 140	0	6	Ext. Pos. Mom. Span 1
	70, 105	30	6	Int. Pos. Mom. Span 2
	70, 140	30	6	Ext. Pos. Mom Span 2
				Int. Negative Mom.
				Ext. Negative Mom.

(*All cases have a bridge width of 54 ft. and a slab thickness of 7 in. on 9 AASHTO IV girders)

Table 6.3 Distribution Factors for Continuous Slab-on-Girder Bridges

Skew Angle	AASHTO	LRFD	FEM	Number of Spans	AASHTO	LRFD	FEM	Ratio between spans	AASHTO	LRFD	FEM span 1	FEM span 2
Skew=0				Span=2 skew=0				Ratio=1:1 skew=0				
Pos. Int.	1.09	1.21	1.03		1.09	1.21	1.03		1.09	1.21	1.03	1.03
Pos. Ext.	1.09	1.33	1		1.09	1.33	1		1.09	1.33	1	1
Neg. Int.	1.09	1.21	1.04		1.09	1.21	1.04		1.09	1.21	1.04	1.04
Neg. Ext.	1.09	1.33	1.02		1.09	1.33	1.05		1.09	1.33	1.05	1.05
Skew=30				Span=3 skew=0				Ratio=1:1.5 skew=0				
Pos. Int.	1.09	1.16	1.04		1.09	1.21	1.03		1.09	1.21	1.03	1.04
Pos. Ext.	1.09	1.27	1.02		1.09	1.33	1.06		1.09	1.33	1.07	1.15
Neg. Int.	1.09	1.16	1.03		1.09	1.21	1.03		1.09	1.21	1.03	1.03
Neg. Ext.	1.09	1.27	1		1.09	1.33	1.08		1.09	1.33	1.11	1.11
Skew=45				Span=4 skew=0				Ratio=1:2 skew=0				
Pos. Int.	1.09	1.09	0.91		1.09	1.21	1.03		1.09	1.21	1.04	1.02
Pos. Ext.	1.09	1.19	1.14		1.09	1.33	1.08		1.09	1.33	1.06	1.2
Neg. Int.	1.09	1.09	1.02		1.09	1.21	1.03		1.09	1.21	1.02	1.02
Neg. Ext.	1.09	1.19	0.97		1.09	1.33	1.08		1.09	1.33	1.2	1.2
Skew=60				Span=2 skew=30				Ratio=1:1 skew=30				
Pos. Int.	1.09	0.93	0.73		1.09	1.21	1.04		1.09	1.16	1.04	1.04
Pos. Ext.	1.09	1.02	1.16		1.09	1.27	1.02		1.09	1.27	1.02	1.02
Neg. Int.	1.09	0.93	0.98		1.09	1.21	1.03		1.09	1.16	1.08	1.08
Neg. Ext.	1.09	1.19	0.95		1.09	1.27	1.11		1.09	1.27	1.08	1.08
				Span=3 skew=30				Ratio=1:1.5 skew=30				
					1.09	1.21	1		1.09	1.16	0.99	1.06
					1.09	1.27	1.11		1.09	1.27	1.07	1.09
					1.09	1.21	1.03		1.09	1.16	1.03	1.03
					1.09	1.27	1.09		1.09	1.27	1.14	1.14
				Span=4 skew=30				Ratio=1:2 skew=30				
					1.09	1.21	0.9		1.09	1.16	0.98	1.03
					1.09	1.27	1		1.09	1.27	1.03	1.14
					1.09	1.21	1.03		1.09	1.16	1.02	1.02
					1.09	1.27	1.08		1.09	1.27	1.22	1.22

6.3.3.1 Skew angle

Skew angle is an important factor in bridge design. The LRFD code provides for adjusting the load distribution factors for different skew angles. The code does not specify any recommendations for continuous bridges with different skew angles. The results from FEM analysis of the continuous bridges are compared with LRFD load distribution factors based on single span bridges.

Equation 6.8 is used to calculate the distribution factor of the internal girder. When calculating the distribution factor for exterior girders, the exterior girder strains replace the maximum strains as follows:

$$DF_{i\theta,ext} = \frac{n\varepsilon_{i\theta,ext}}{\left(\sum_{j=1\to k} \varepsilon_j W_j\right)_{\theta=0}} \qquad (6.9)$$

Figure 6.11 shows that the strains decrease with increase in skew angles for interior girders. The skew angle induces significant twisting moment in the girders and gives an uneven transverse strain distribution. The distribution factors at midspan of interior girders are shown in Figure 6.12. The distribution factors based on FEM analysis are smaller than those based on LRFD code. The difference in the distribution factors range from 15% for a straight bridge to 21% for a bridge with a skew angle of 60 degrees. The trends of the variations are, however, the same for both LRFD and FEM methods. Figure 6.13 shows the transverse strain distribution at midspan for exterior girder loading. In general, the strain decreases as the skew angle increases. Figure 6.14 shows no clear trend for the change of load distribution factor with an increase in skew angle.

There is limited information on calculating distribution factors for negative moments in continuous bridges. Figure 6.15 shows the transverse strain distribution at the interior support for a continuous two-span bridge with different skew angles. The positive and negative strains (Figs. 6.11 and 6.15) decrease with an increase in skew angles. Figure 6.16 shows the decrease in distribution factors at the interior support for different skew angles. The rate of decrease in the distribution factors based on FEM is less than that obtained using LRFD. This may be due to the FEM idealization of the interior support as a knife edge, whereas, the interior support reaction is distributed over a finite bearing width. This is also true in the case of negative moment distribution factors for the exterior girders, as observed in Figs 6.17 and 6.18.

Based on the present studies on the effect of skew angles on continuous bridges, the following observations are presented. The strains are higher at the interior supports than at midspans. The higher strains at the interior support are the result of loading both spans with a total of 8 trucks; four loaded in each span. The strains at midspan are due to only one span loaded with four trucks. The strain .distributions are similar for both positive and negative moment loading. The FEM distribution factors vary with different skew angles.

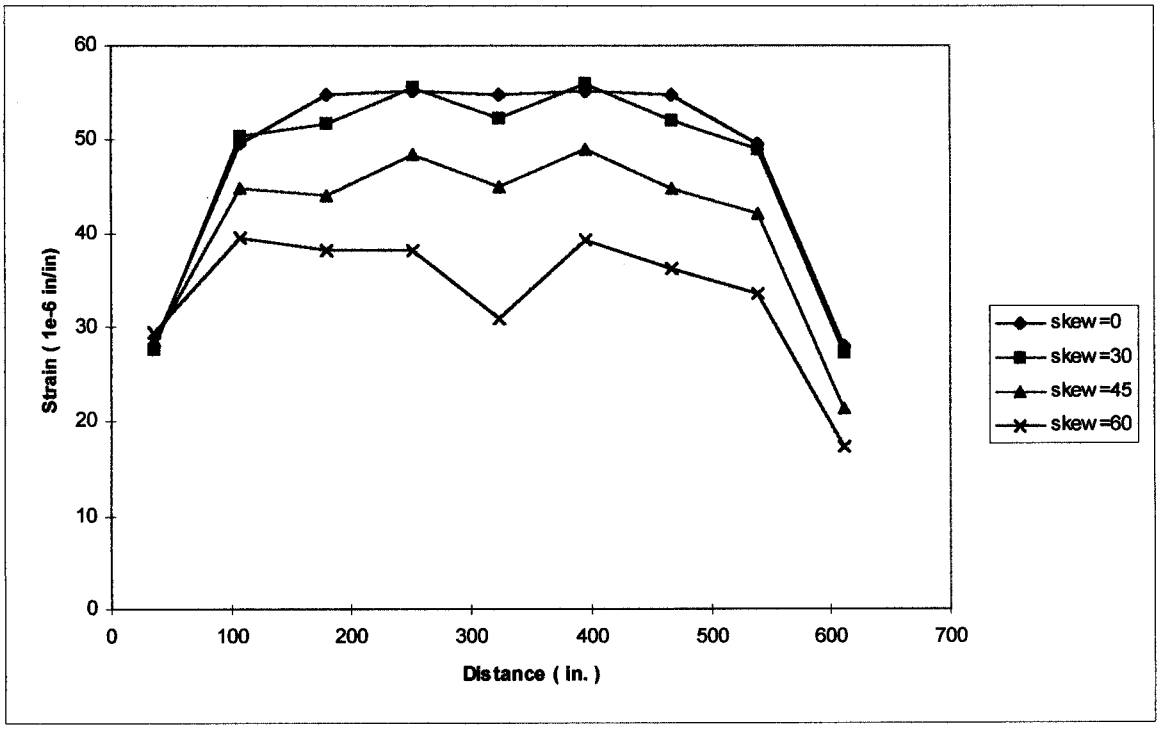

Fig. 6.11 Strain Distribution at Midspan for Two Span Bridges with Different Skew Angles (Interior Girder Loading)

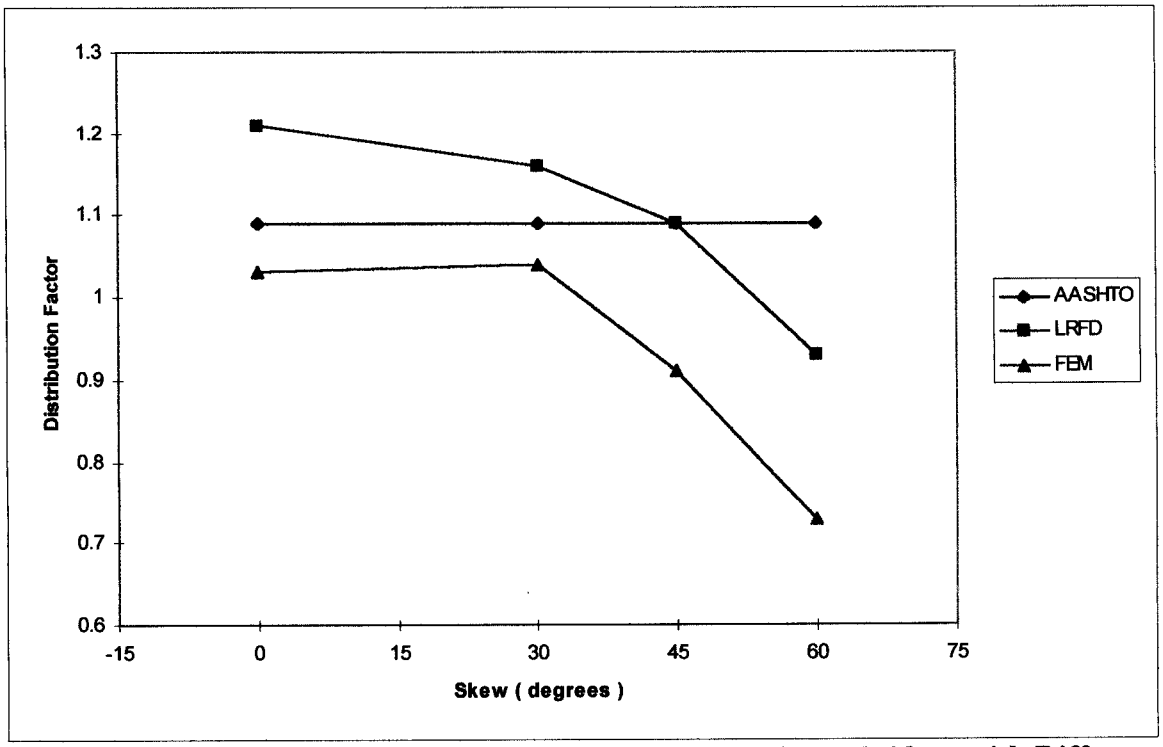

Fig. 6.12 Positive Moment Distribution Factors for Two Span Bridges with Different Skew Angles (Interior Girder)

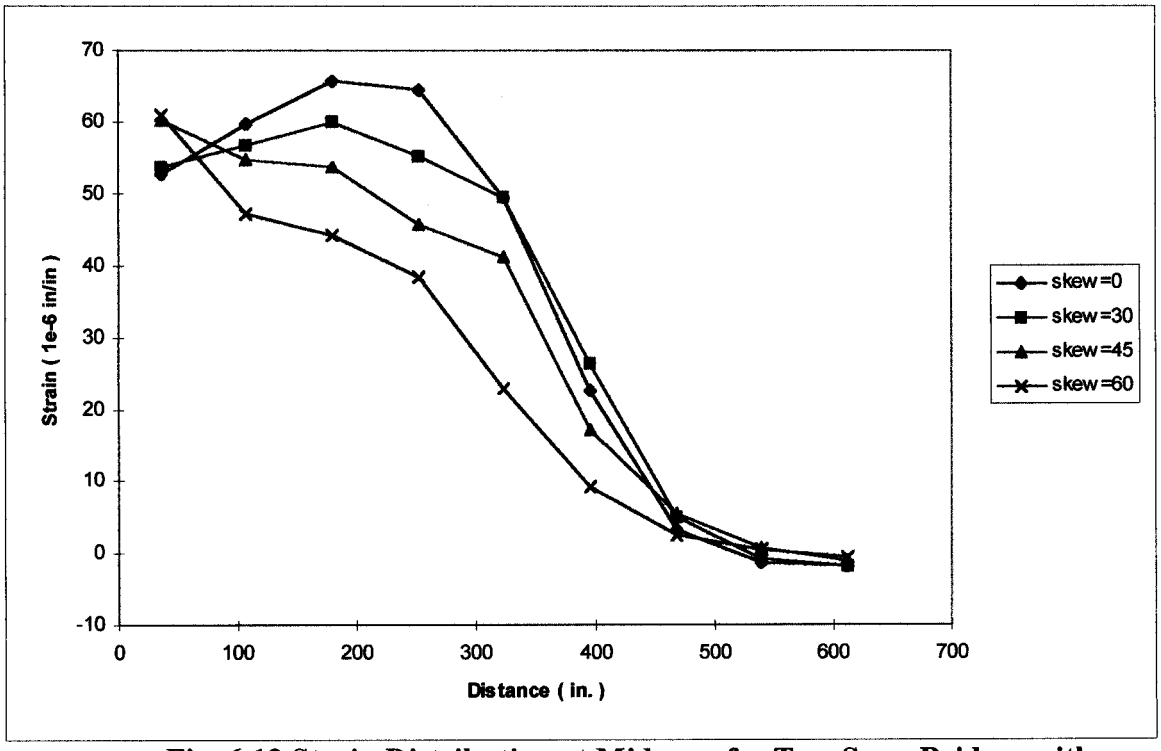

Fig. 6.13 Strain Distribution at Midspan for Two Span Bridges with Different Skew Angles (Exterior Girder Loading)

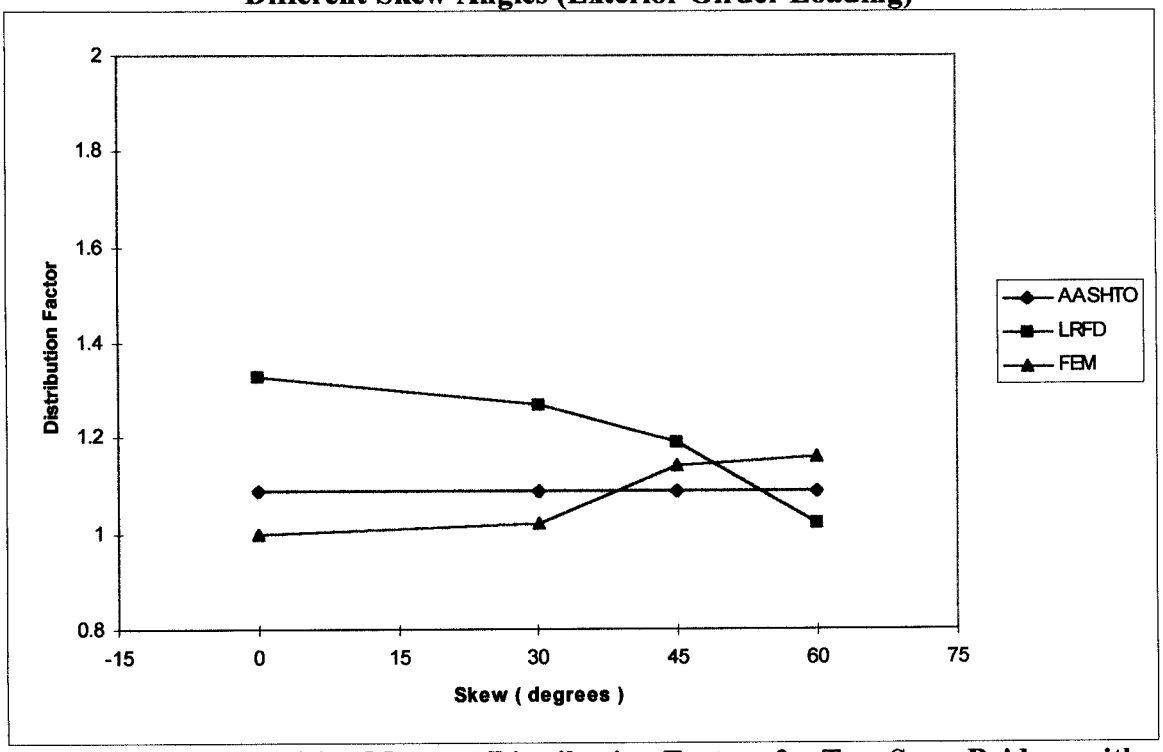

Fig. 6.14 Positive Moment Distribution Factors for Two Span Bridges with Different Skew Angles (Exterior Girder)

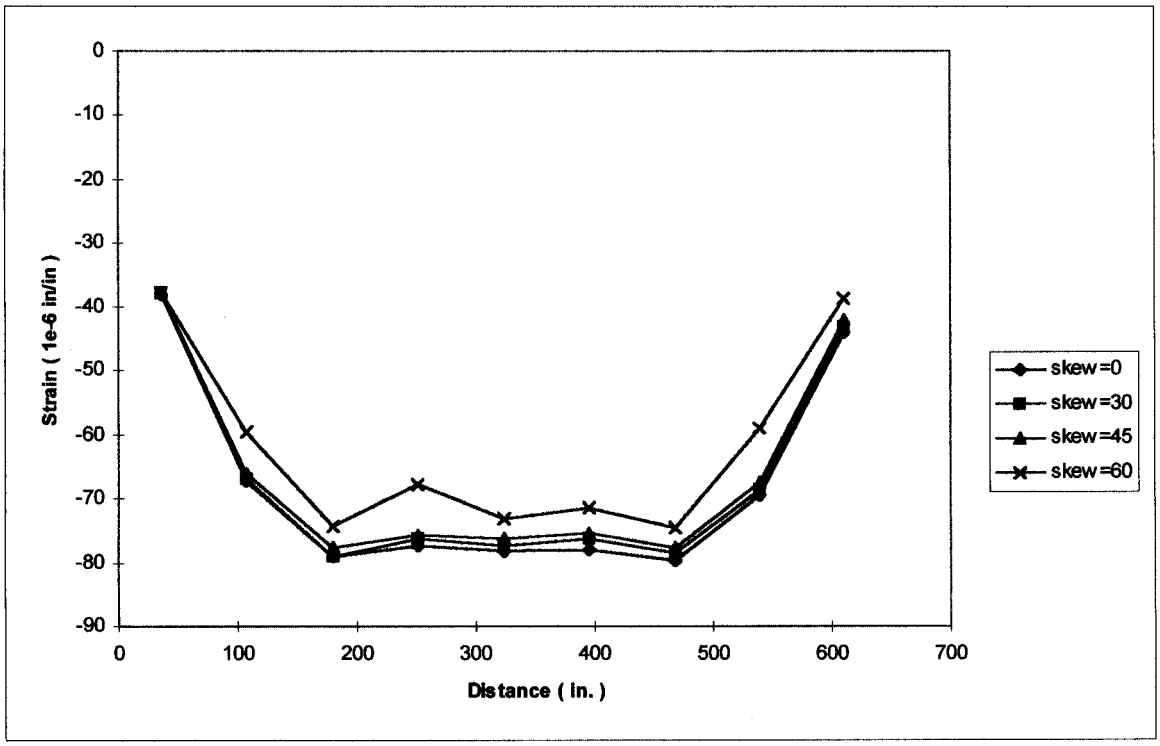

Fig. 6.15 Strain Distribution at the Interior Support for Two Span Bridges with Different Skew Angles (Interior Girder Loading)

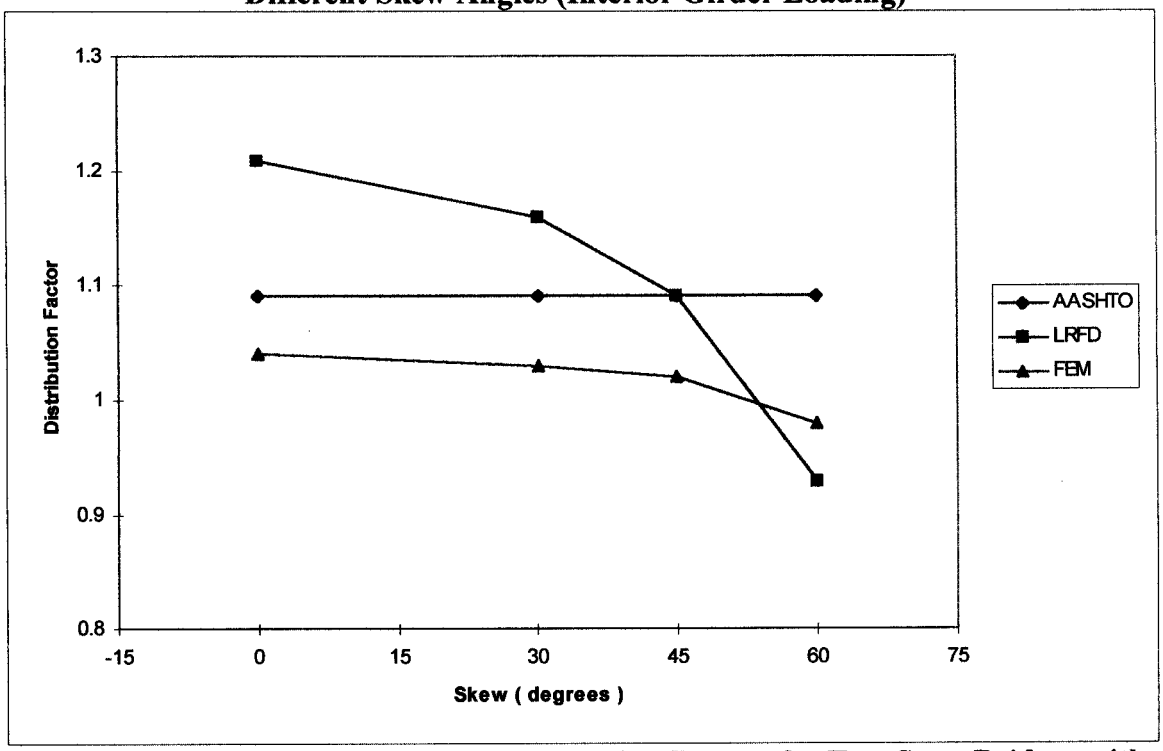

Fig. 6.16 Negative Moment Distribution Factors for Two Span Bridges with Different Skew Angles (Interior Girder)

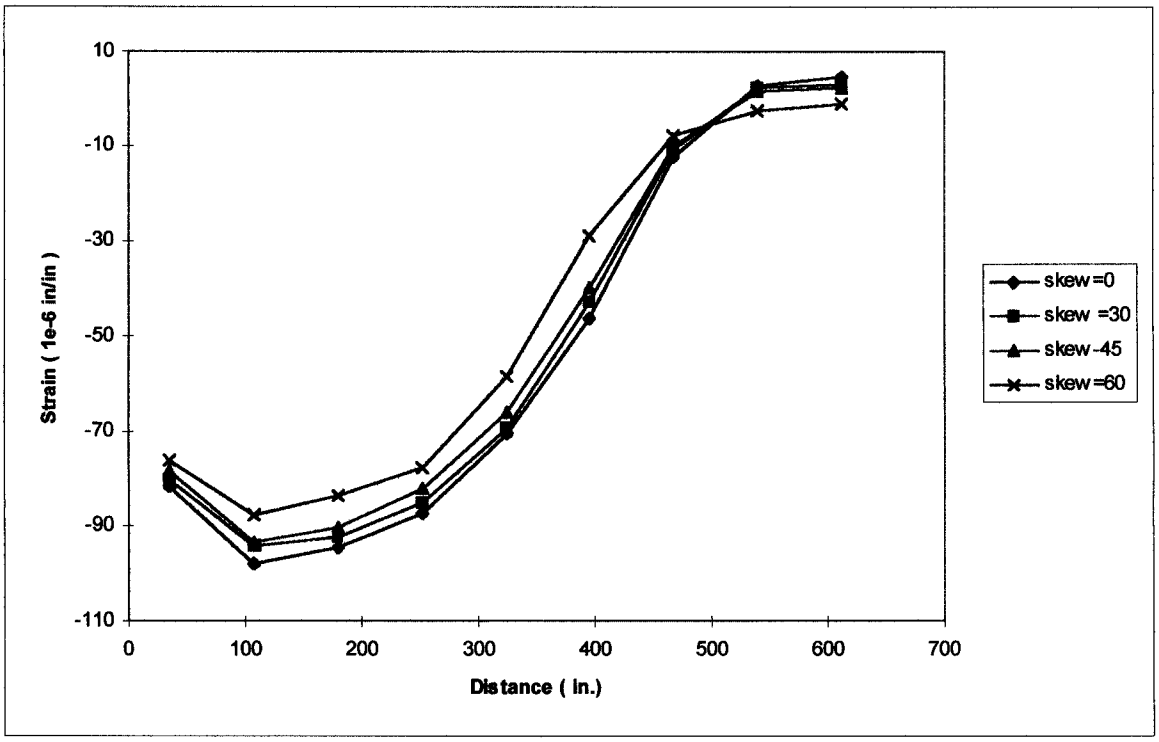

Fig. 6.17 Strain Distribution at the Interior Support for two Span Bridges with Different Skew Angles (Exterior Girder Loading)

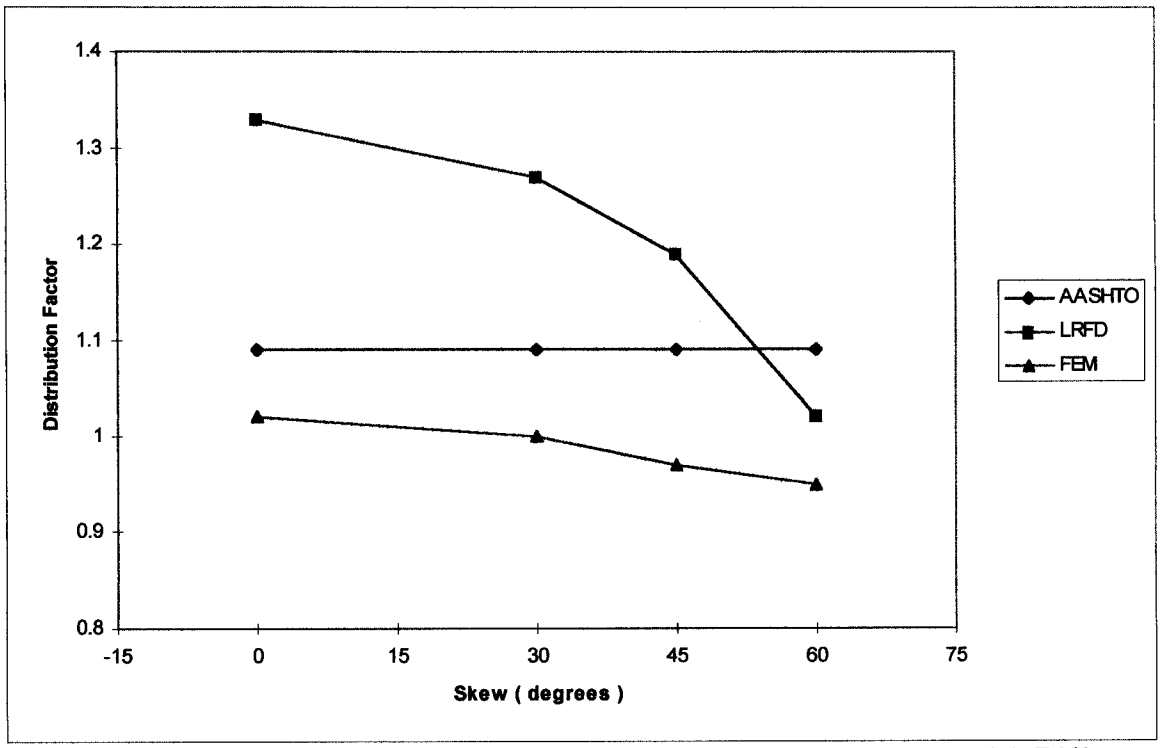

Fig. 6.18 Negative Moment Distribution Factors for two Span Bridges with Different Skew Angles (Exterior Girder)

6.3.3.2 Number of spans

The effect of the number of spans on the distribution factor calculation is evaluated in this section. The study cases are divided into two sets: straight bridges, and skewed bridges with an angle of thirty degrees. Each set has two, three, and four spans for parametric variation. Figures 6.6, 6.7, and 6.8 show the truck load position for positive and negative moments.

Figure 6.20 shows the interior girder distribution factor variation with different number of spans for straight bridges at the midspan. The FEM distribution factors are lower than the LRFD factors and show no variation with an increase in the number of spans. Figure 6.22 shows a small increase (9%) in the exterior girder load distribution factor as the number of spans increase. For a skewed bridge at midspan, the interior girder distribution factor exhibits a small decrease (13%) with an increase in the number of spans (Figure 6.24). The exterior girder load distribution factor has small variations of less than 5% and can be neglected (Figure 6.26). Figures 6.28 and 6.30 show the interior and exterior girder distribution factors for a straight bridge at the interior support. Little variation (3%) is observed with an increase in the number of spans. Similar marginal variations are observed for the thirty degree skew bridge cases shown in Figure 6.32 and 6.34.

In general, the FEM load distribution factors are smaller than those based on LRFD code. Based on the parametric study, the effect of the number of spans on the load distribution factors can be neglected. This conclusion is in agreement with LRFD code.

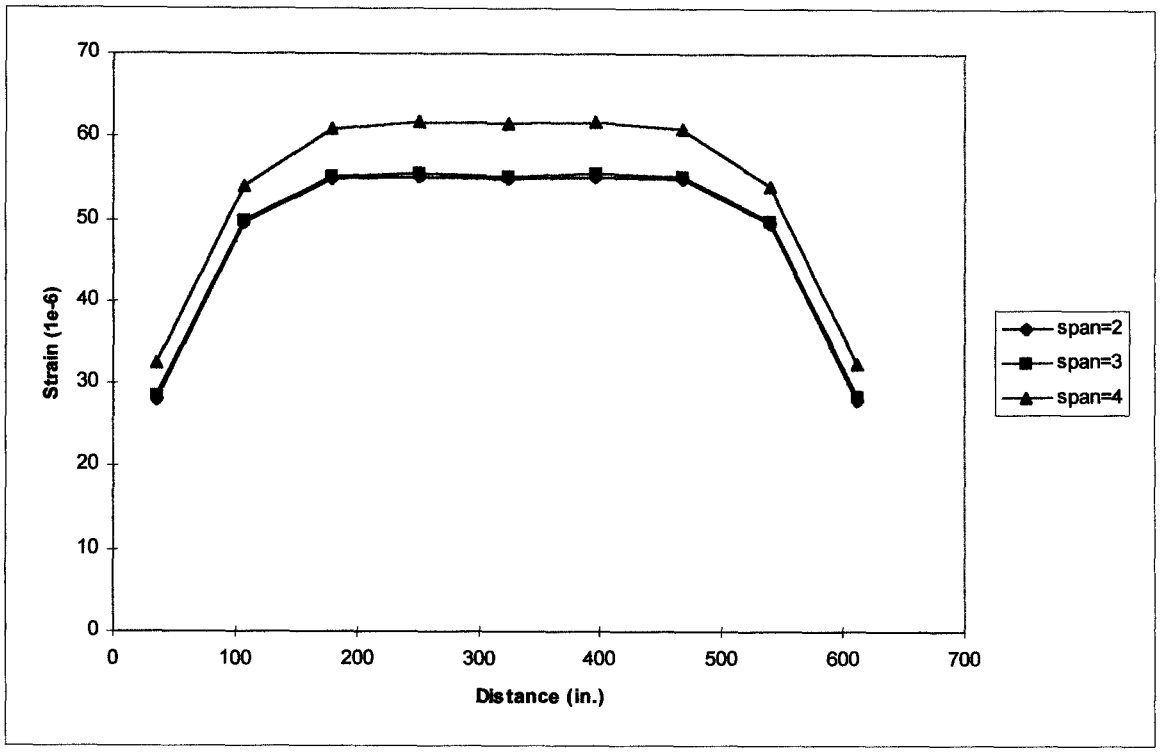

Fig. 6.19 Strain Distribution at Mid-Span for Straight Bridges with Different Number of Spans (Interior Girder Loading)

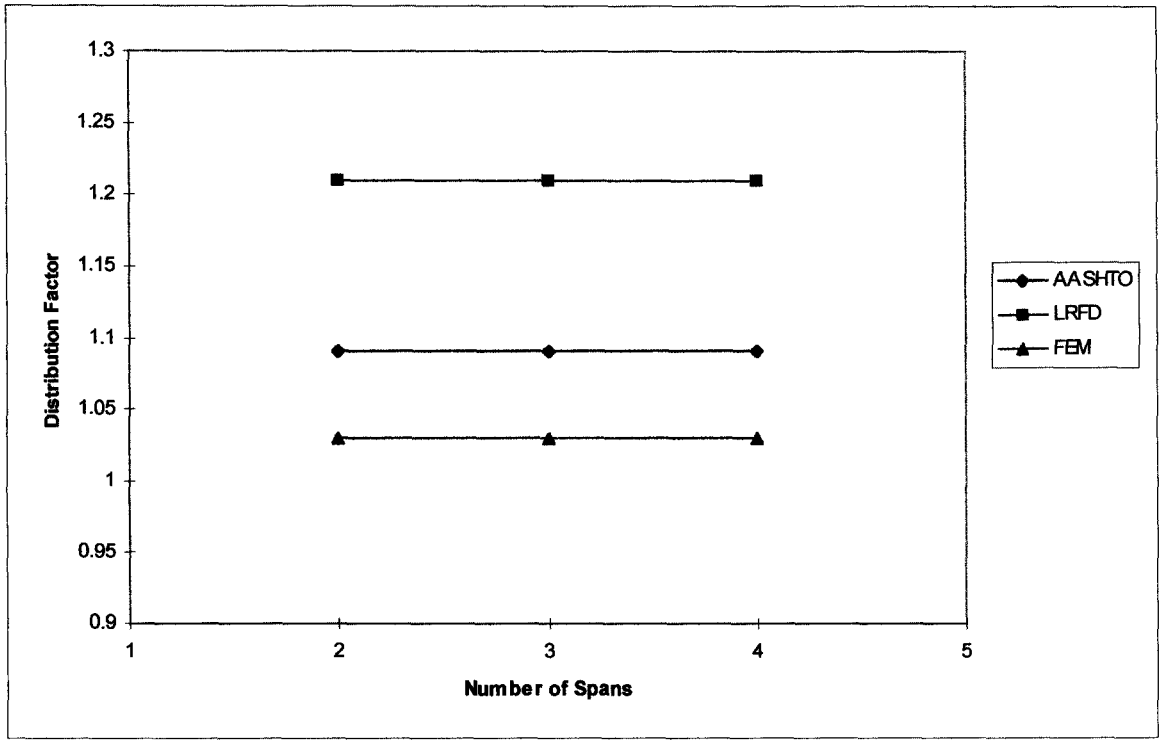

Fig. 6.20 Positive Moment Distribution Factors for Straight Bridges with Different Number of Spans (Interior Girder)

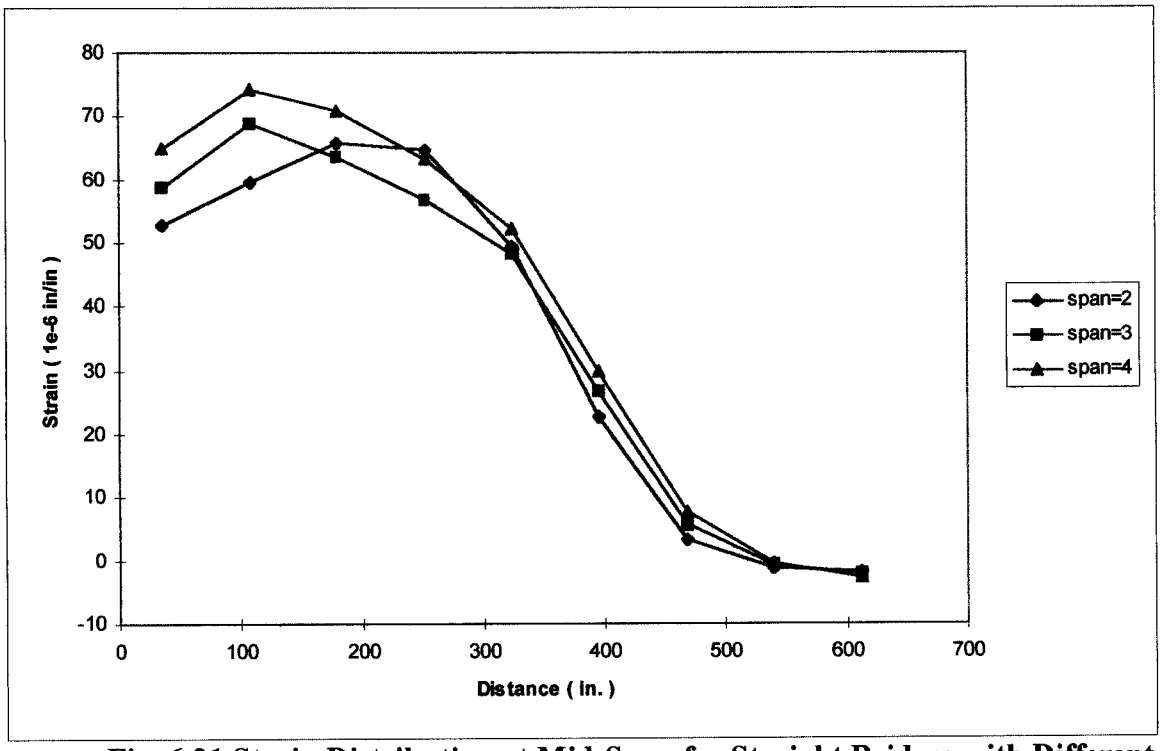

Fig. 6.21 Strain Distribution at Mid-Span for Straight Bridges with Different Number of Spans (Exterior Girder Loading)

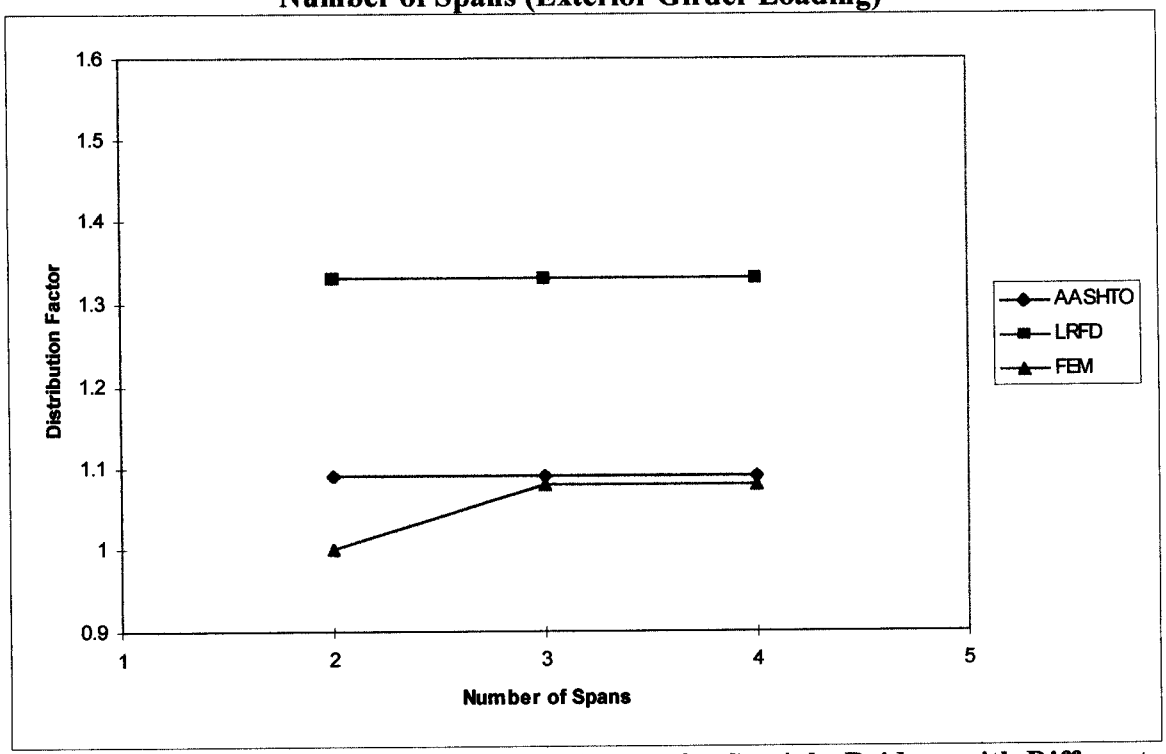

Fig. 6.22 Positive Moment Distribution Factors for Straight Bridges with Different Number of Spans (Exterior Girder)

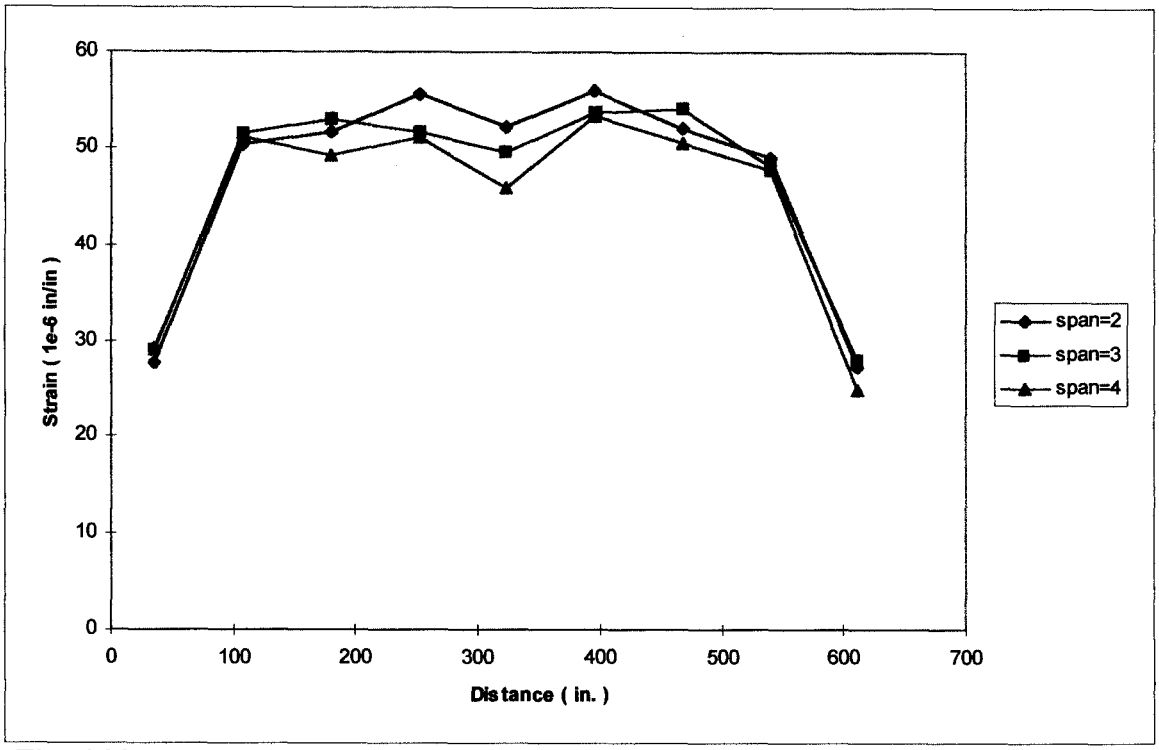

Fig. 6.23 Strain Distribution at Mid-Span for Skew Bridges with Different Number of Spans (Interior Girder Loading)

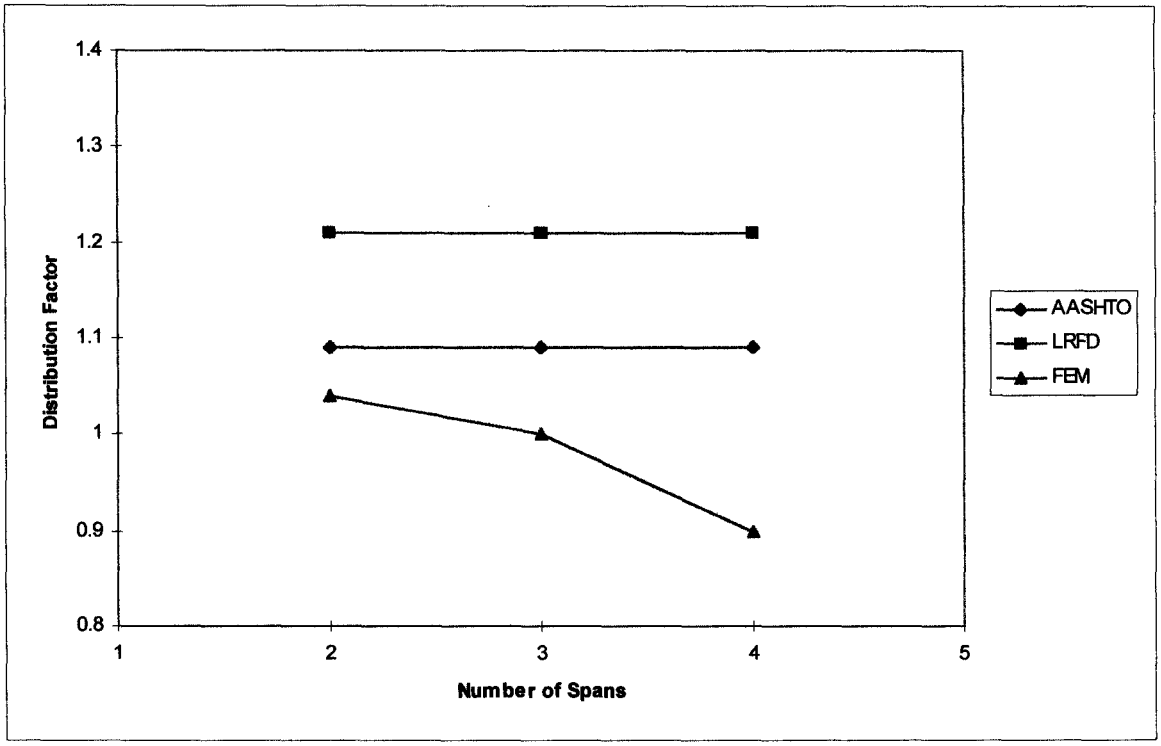

Fig. 6.24 Positive Moment Distribution Factors for Skew Bridges with Different Number of Spans (Interior Girder)

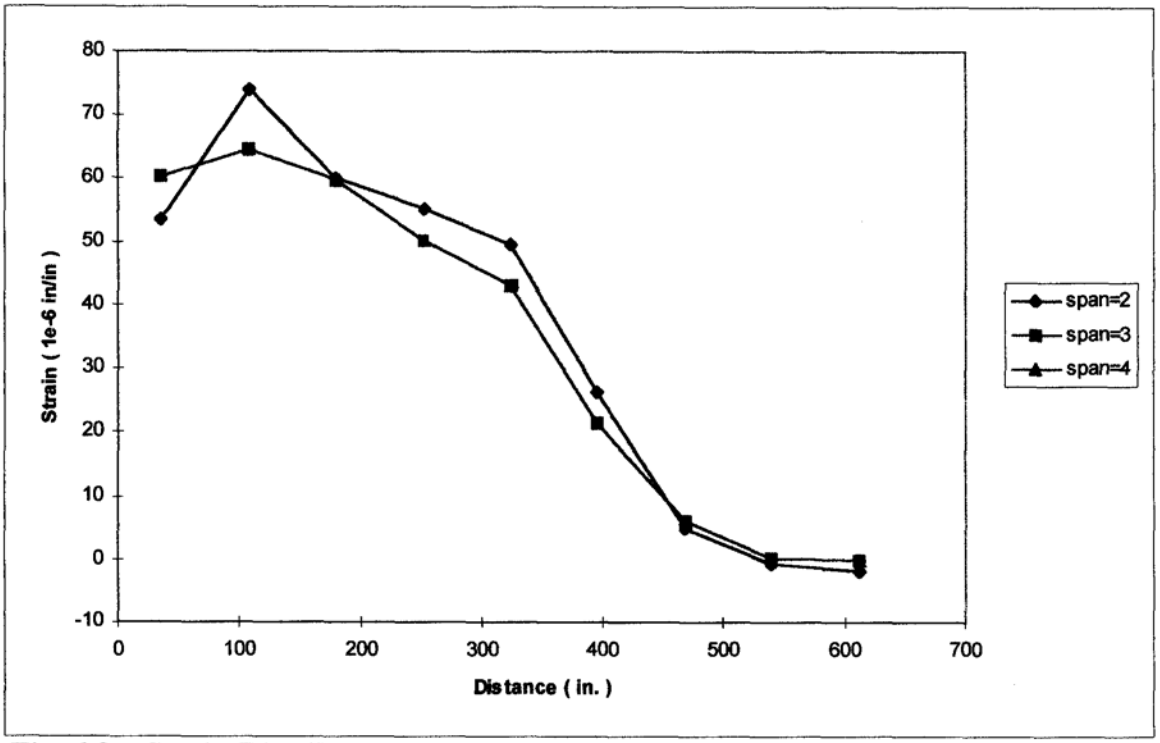

Fig. 6.25 Strain Distribution at Mid-Span for Skew Bridges with Different Number of Spans (Exterior Girder Loading)

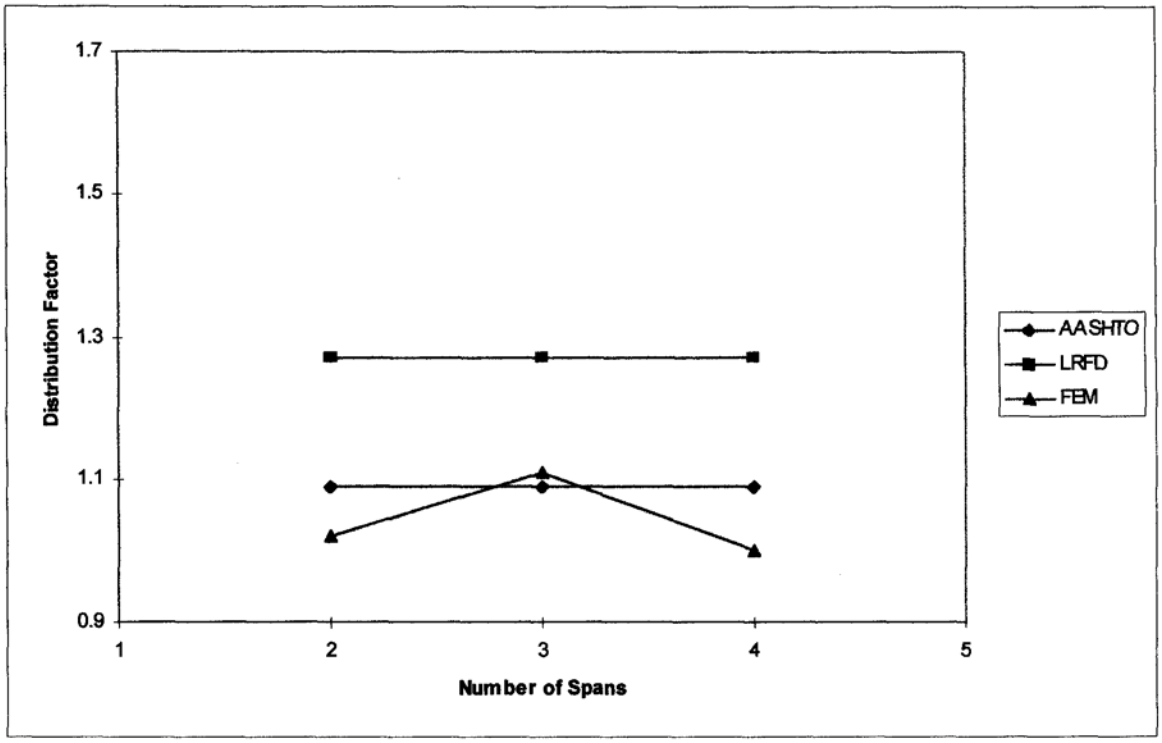

Fig. 6.26 Positive Moment Distribution Factors for Skew Bridges with Different Number of Spans (Exterior Girder)

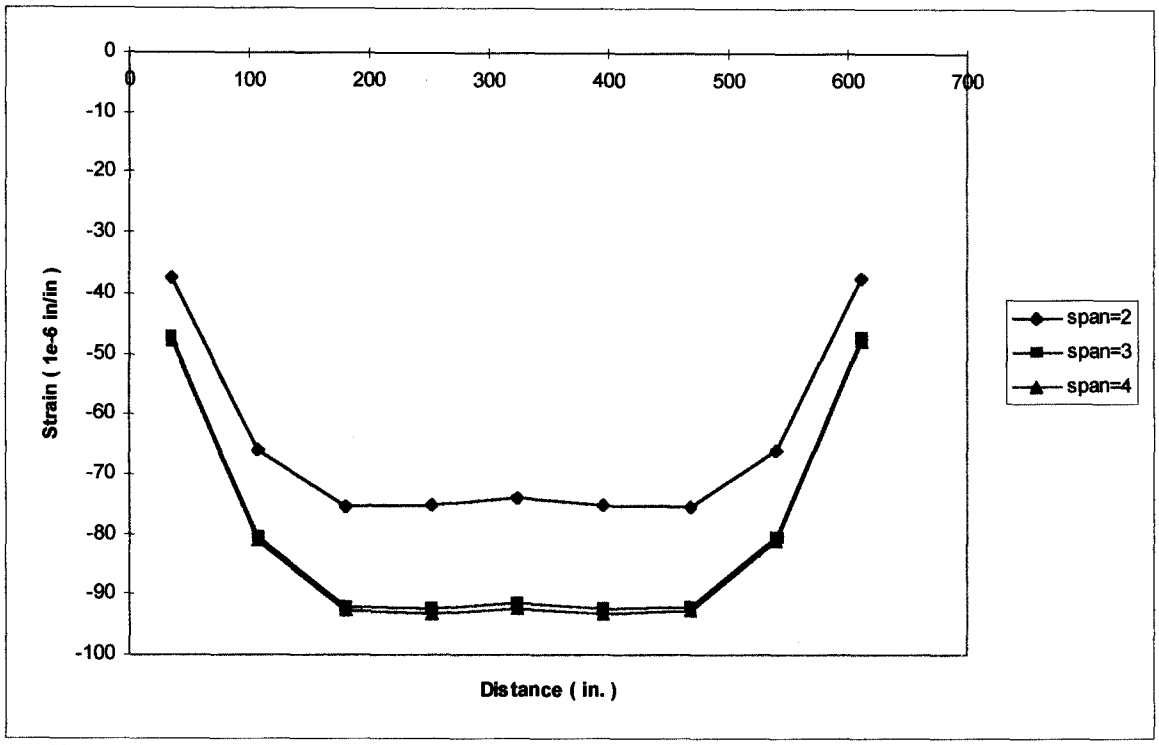

Fig. 6. 27 Strain Distribution at the Interior Support for Straight Bridges with Different Number of Spans (Interior Girder Loading)

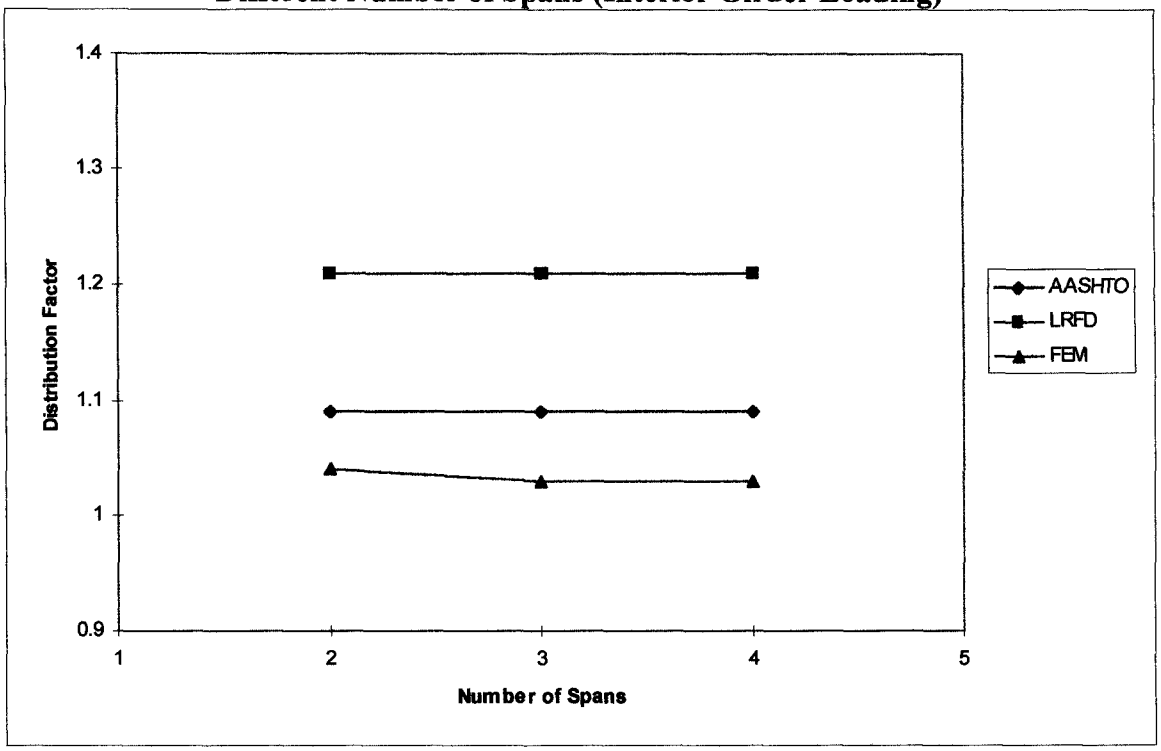

Fig. 6.28 Negative Moment Distribution Factors for Straight Bridges with Different Number of Spans (Interior Girder)

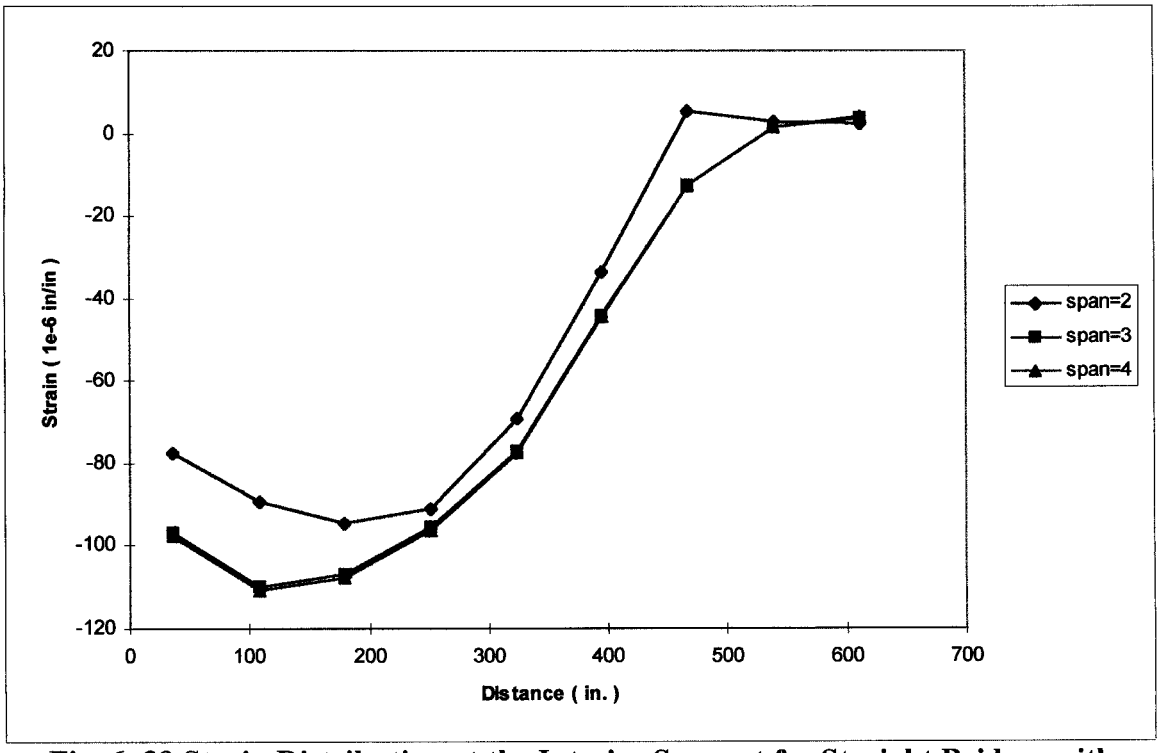

Fig. 6. 29 Strain Distribution at the Interior Support for Straight Bridges with Different Number of Spans (Exterior Girder Loading)

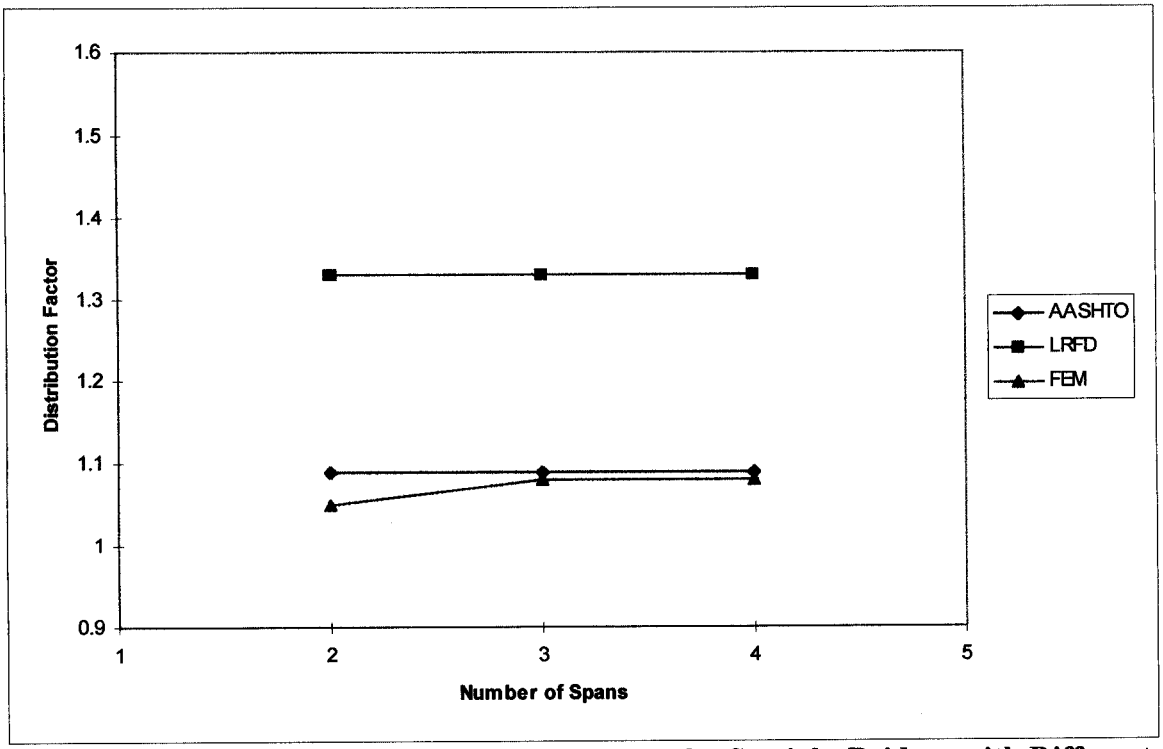

Fig. 6.30 Negative Moment Distribution Factors for Straight Bridges with Different Number of Spans (Exterior Girder)

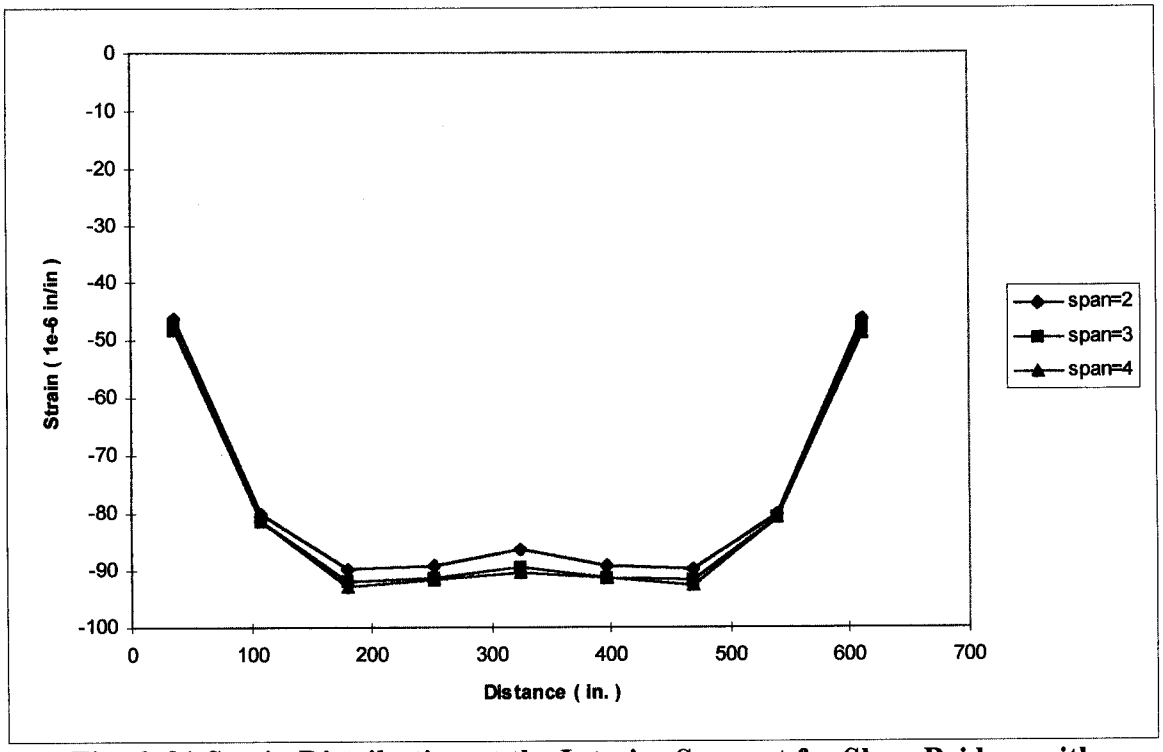

Fig. 6. 31 Strain Distribution at the Interior Support for Skew Bridges with Different Number of Spans (Interior Girder Loading)

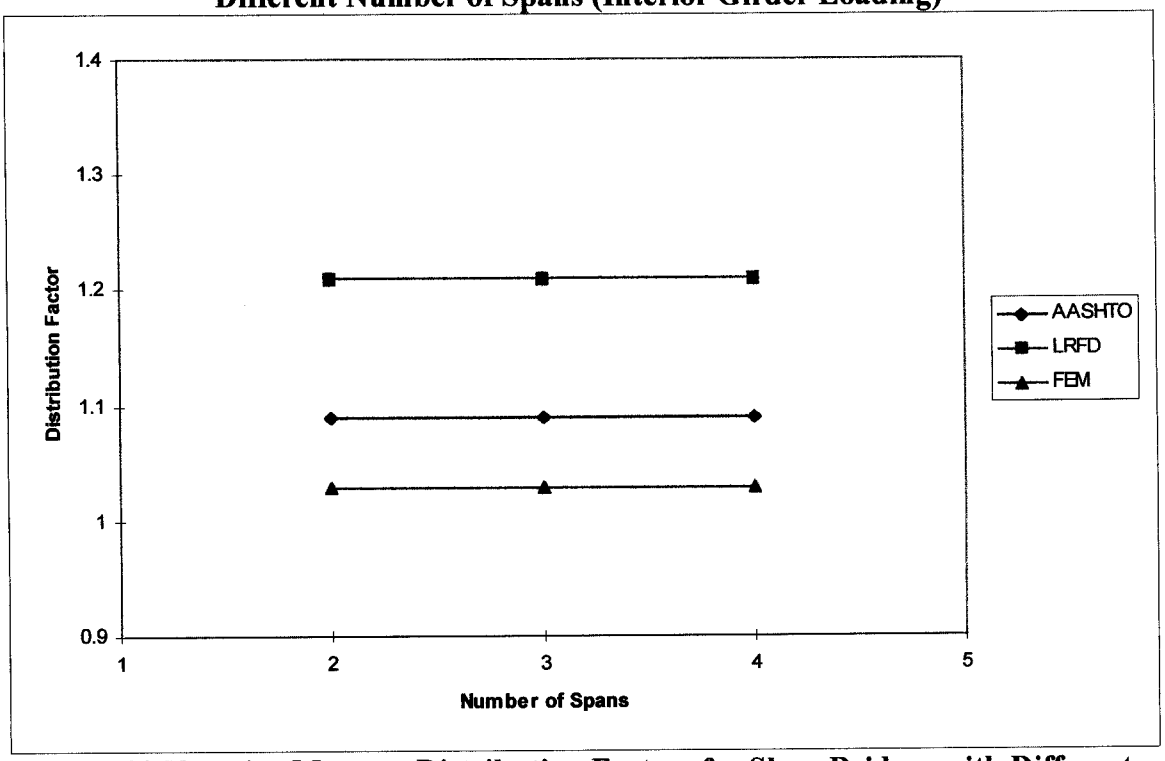

Fig. 6.32 Negative Moment Distribution Factors for Skew Bridges with Different Number of Spans (Interior Girder)

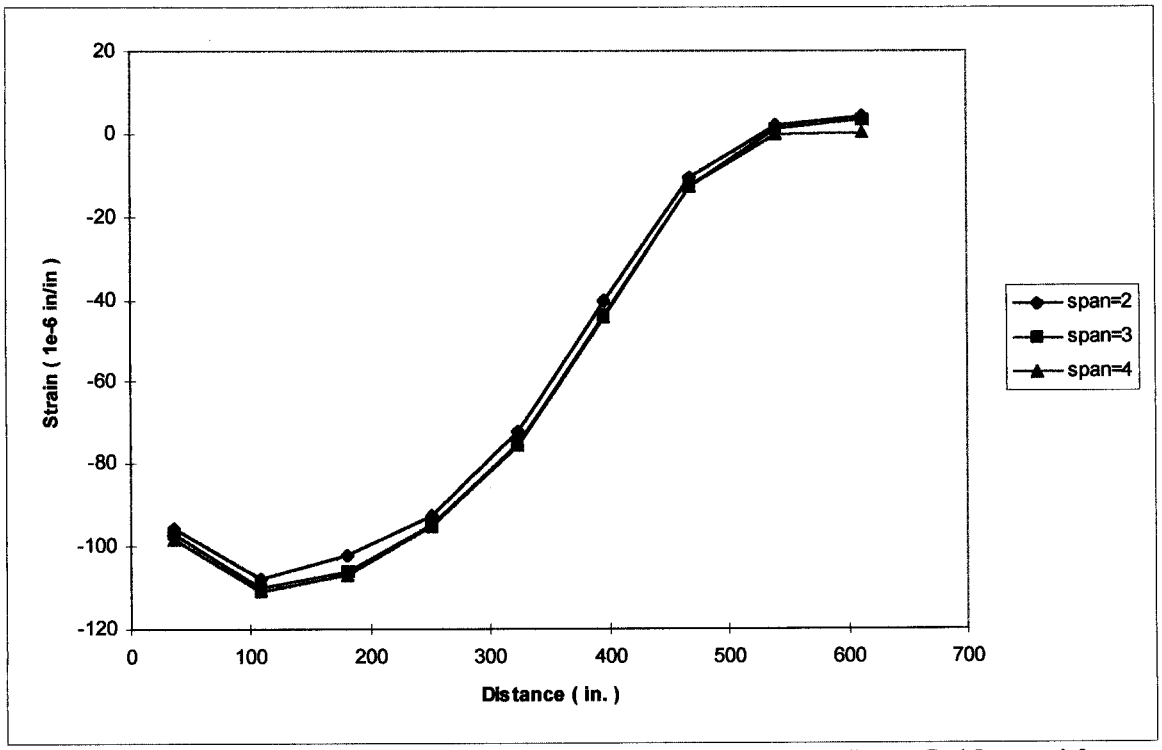

Fig. 6. 33 Strain Distribution at the Interior Support for Skew Bridges with Different Number of Spans (Exterior Girder Loading)

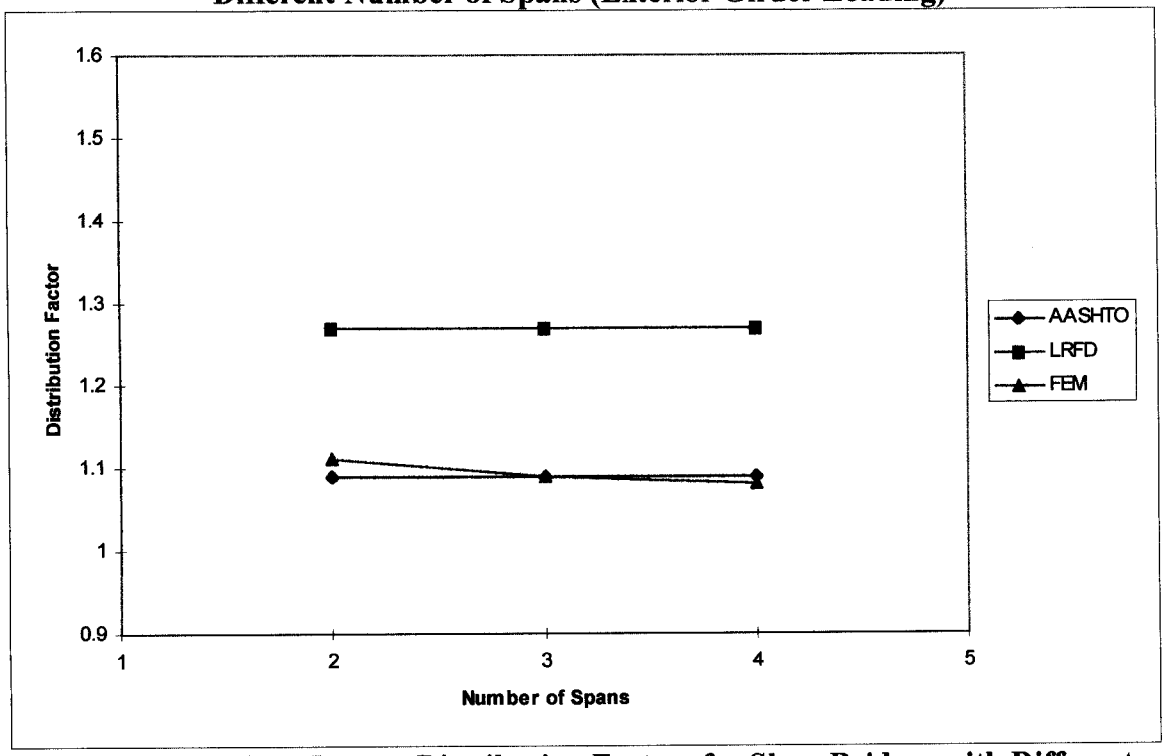

Fig. 6.34 Negative Moment Distribution Factors for Skew Bridges with Different Number of Spans (Exterior Girder)

6.3.3.3 Ratios Between the Spans

The ratios between the spans for two span continuous bridges were varied to study the effects on the load distribution factors. The ratios of the spans used in this study were 1:1, 1:1.5, and 1:2. Bridges with thirty degree skew angle and straight bridges were used in this study. Figures 6.6, 6.9, and 6.10 show the truck load positions for maximum positive and negative moments in the bridges with different ratios between spans. For the cases with the span ratios of 1:1.5 and 1:2, the bridge was loaded for positive moment in each of the two spans.

Figure 6.36 shows the interior girder load distribution factor of a straight bridge at midspan. Little variation in the load distribution factor is observed with increased ratios between the spans. Figure 6.38 shows that the shorter span has a smaller increase (7%) in distribution factor than the larger span (17%). The interior girder load distribution factors of a straight bridge at the interior support are shown in Figure 6.40. Little variation was observed in the negative moment load distribution factors. Similar behavior was observed in the interior girder positive moment distribution factors. Figure 6.42 shows a slight increase (12%) in the exterior girder load distribution factors at the interior support as the ratios increase between the spans.

The bridge with a thirty degree skew angle shows a decrease in the interior girder load distribution factor at midspan with an increase in the ratios between the spans (Figure 6.44). Figure 6.46 shows the exterior girder load distribution factors at the midspan. The distribution factors increase (11%) as the ratios between the spans increase.Figure 6.48 shows a little variation in the interior girder load distribution factor at the support. The exterior girder

distribution factors show a slight increase (11 %) with increases in the ratios between the spans Figure 6.50).

In general, the interior girder load distribution factors show little variation as the ratios between the spans increase for both positive and negative moments. The exterior girder load distribution factors show a general increase (10%-13%) as the ratios between the spans increase.

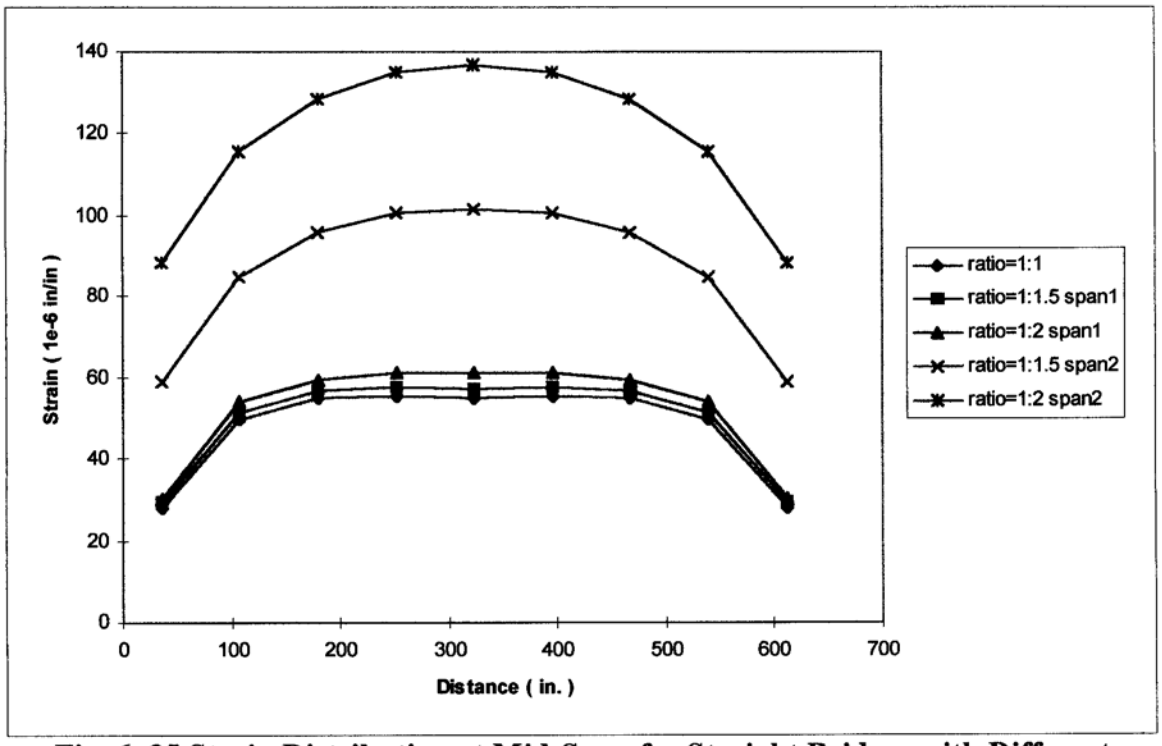

Fig. 6. 35 Strain Distribution at Mid-Span for Straight Bridges with Different Ratios Between Two Spans (Interior Girder Loading)

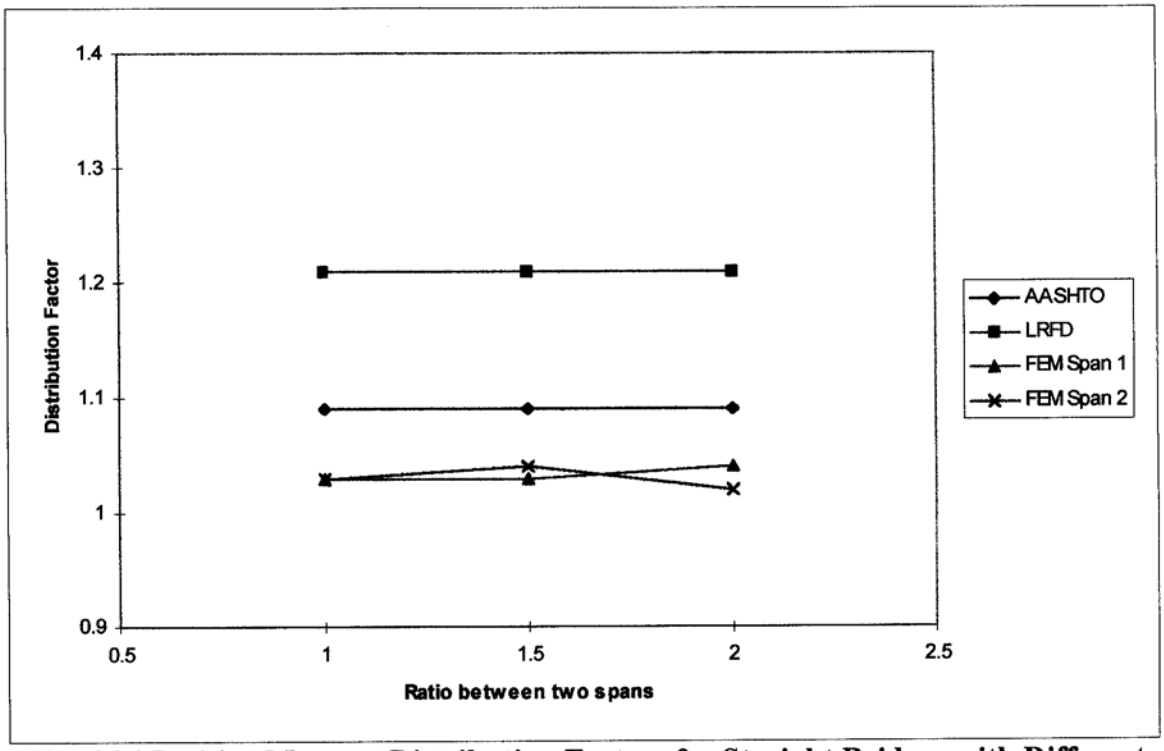

Fig. 6.36 Positive Moment Distribution Factors for Straight Bridges with Different Ratios Between Two Spans (Interior Girder)

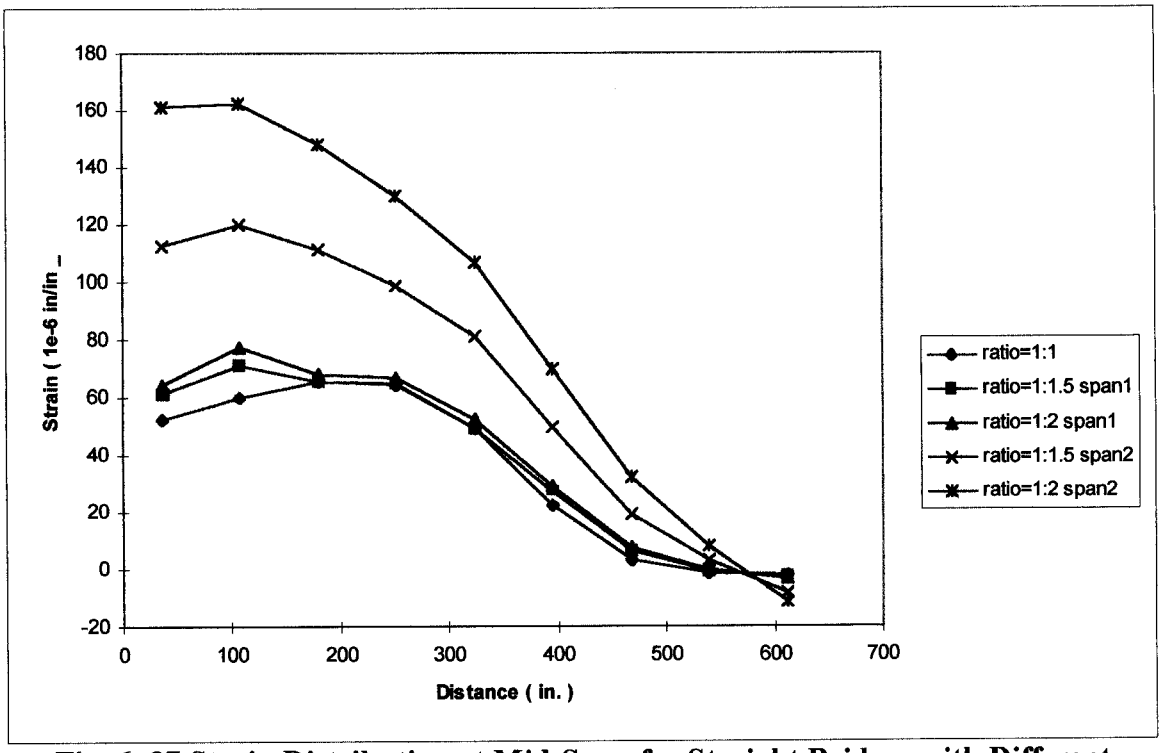

Fig. 6. 37 Strain Distribution at Mid-Span for Straight Bridges with Different Ratios Between Two Spans (Exterior Girder Loading)

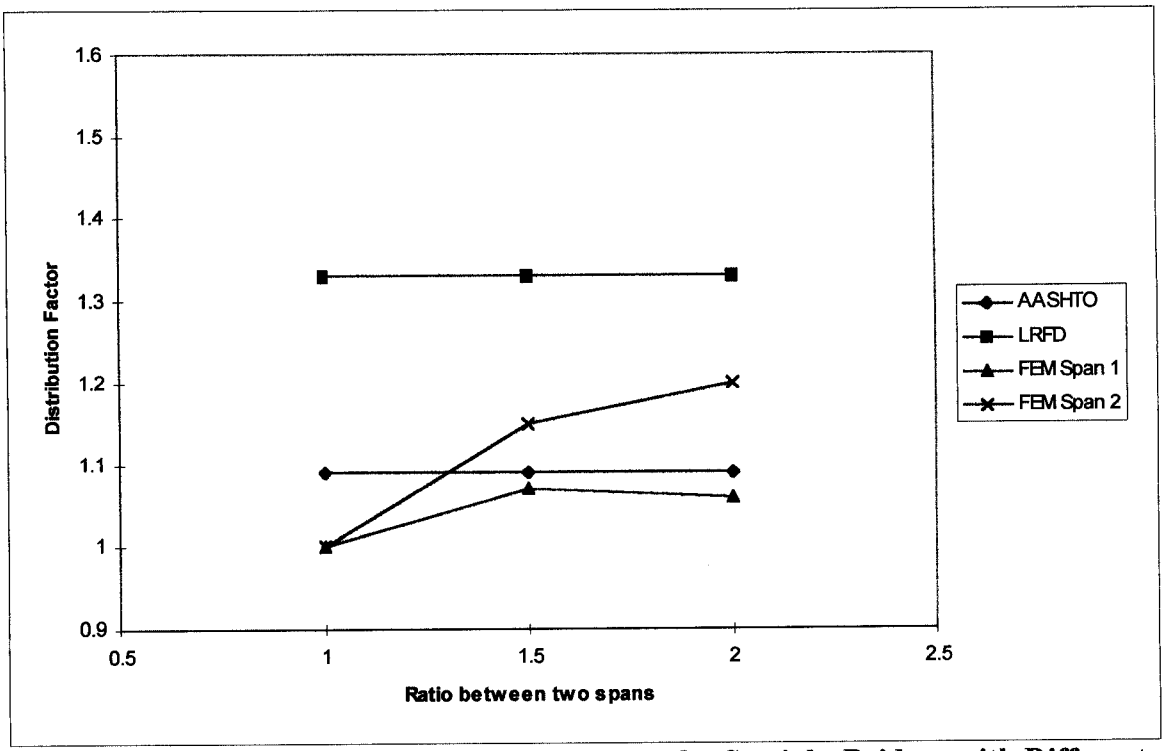

Fig. 6.38 Positive Moment Distribution Factors for Straight Bridges with Different Ratios Between Two Spans (Exterior Girder)

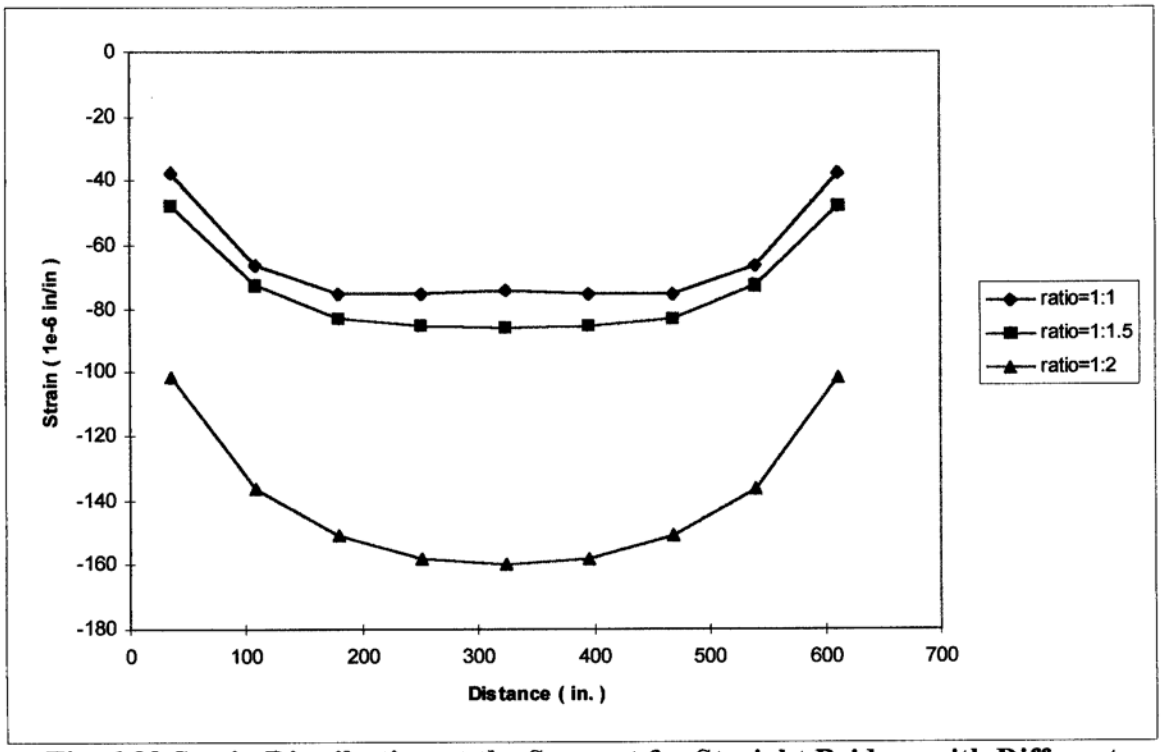

Fig. 6.39 Strain Distribution at the Support for Straight Bridges with Different Ratios Between Two Spans (Interior Girder Loading)

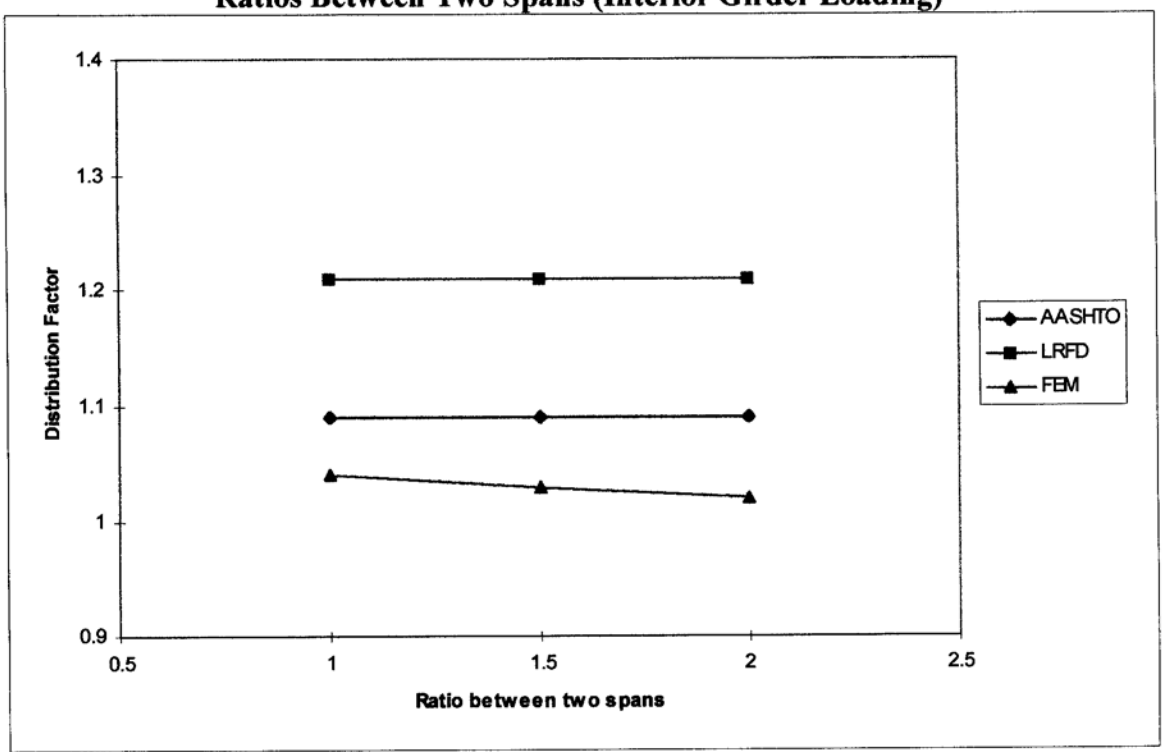

Fig. 6.40 Negative Moment Distribution Factors for Straight Bridges with Different Ratios Between Two Spans (Interior Girder)

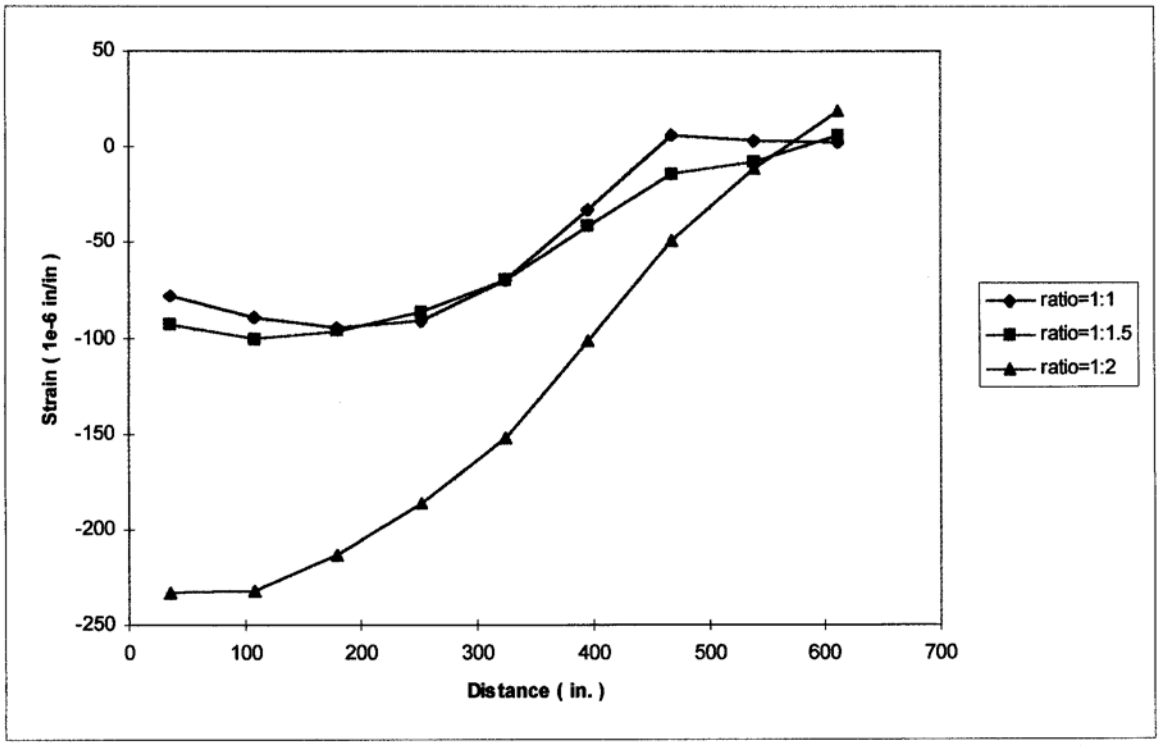

Fig. 6. 41 Strain Distribution at the Interior Support for Straight Bridges with Different Ratios Between Two Spans (Exterior Girder Loading)

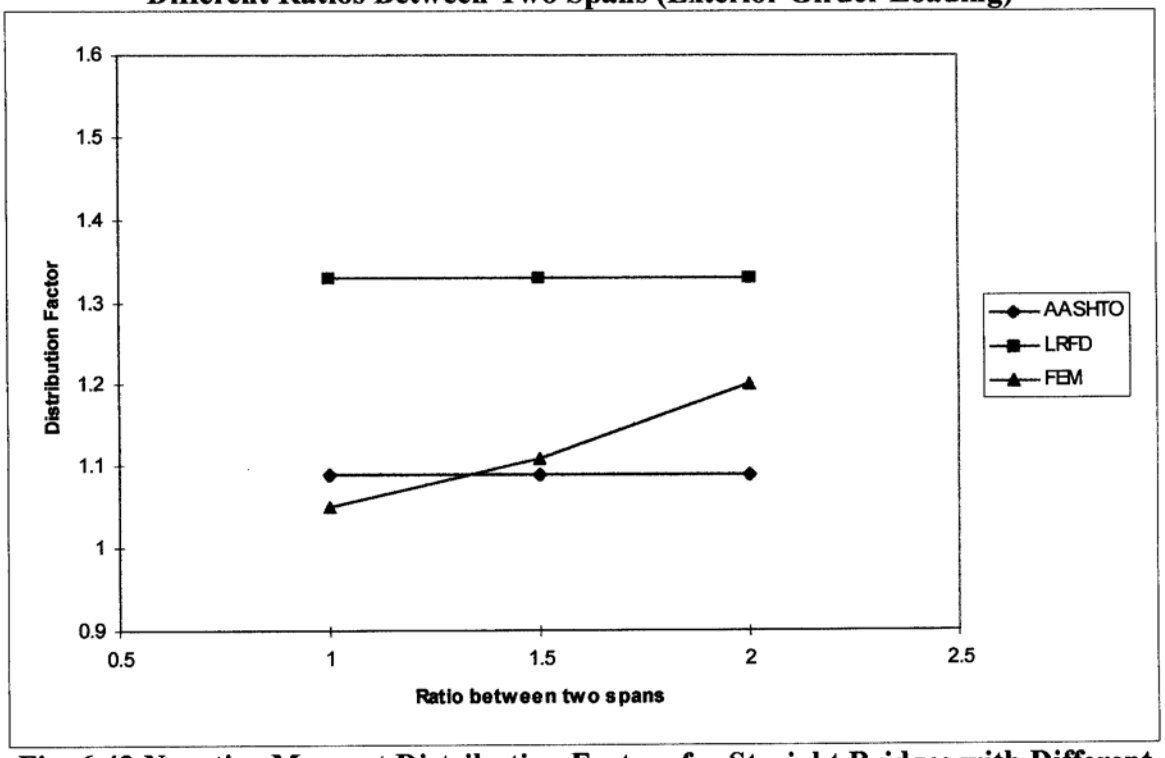

Fig. 6.42 Negative Moment Distribution Factors for Straight Bridges with Different Ratios Between Two Spans (Exterior Girder)

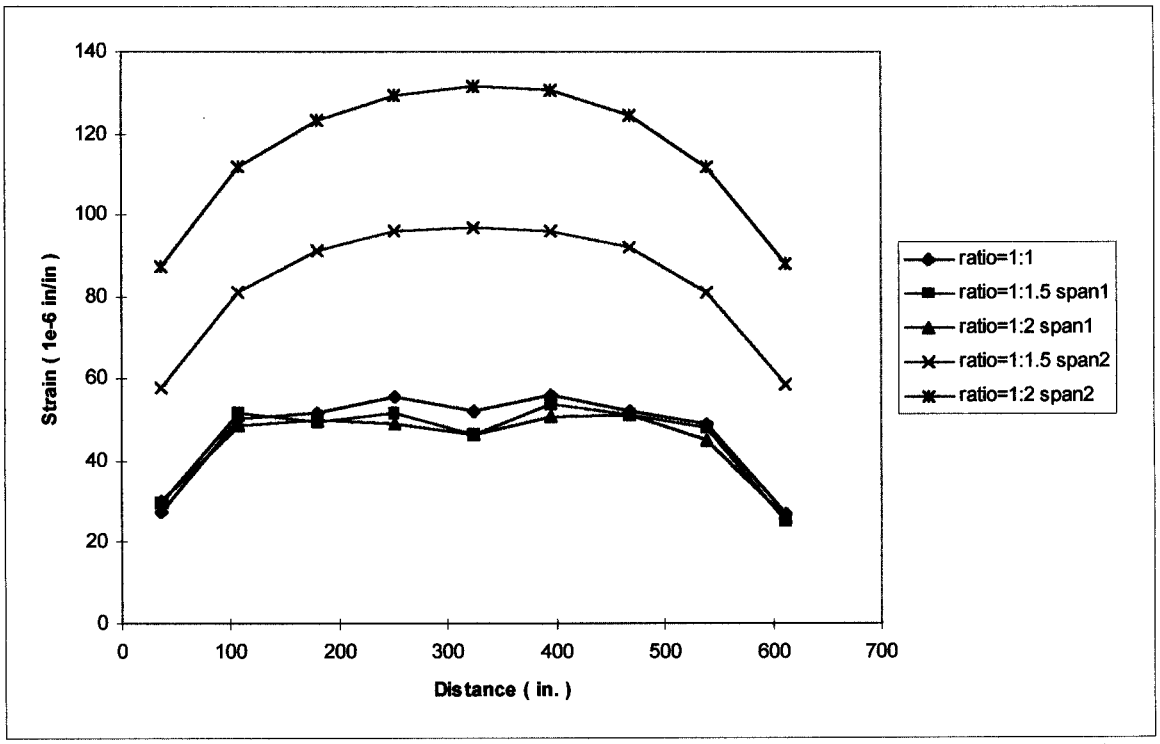

Fig. 6. 43 Strain Distribution at Mid-Span for Skew Bridges with Different Ratios Between Two Spans (Interior Girder Loading)

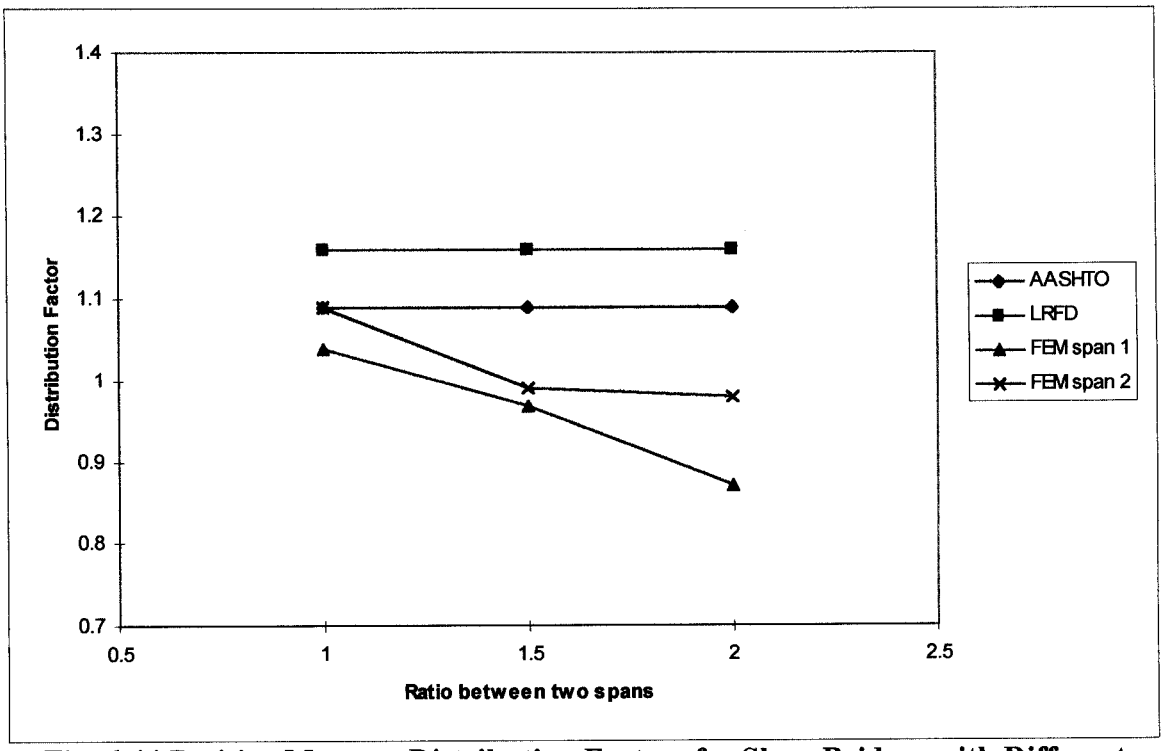

Fig. 6.44 Positive Moment Distribution Factors for Skew Bridges with Different Ratios Between Two Spans (Interior Girder)

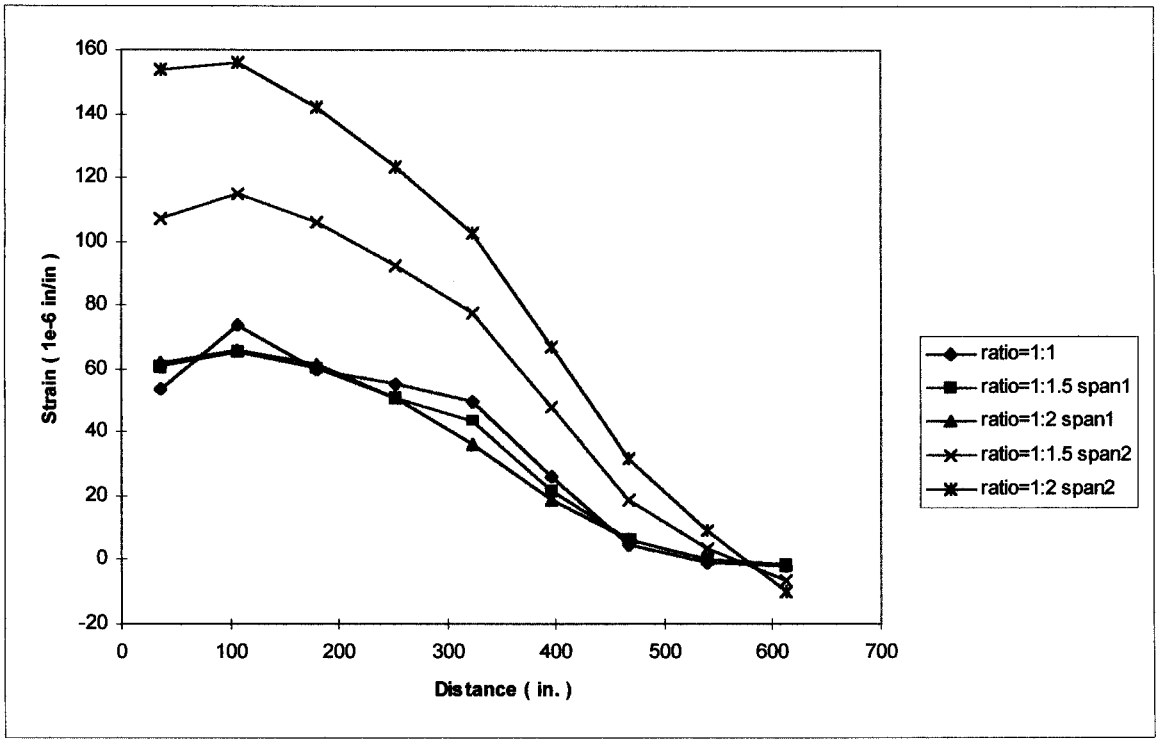

Fig. 6.45 Strain Distribution at Mid-Span for Skew Bridges with Different Ratios Between Two Spans (Exterior Girder Loading)

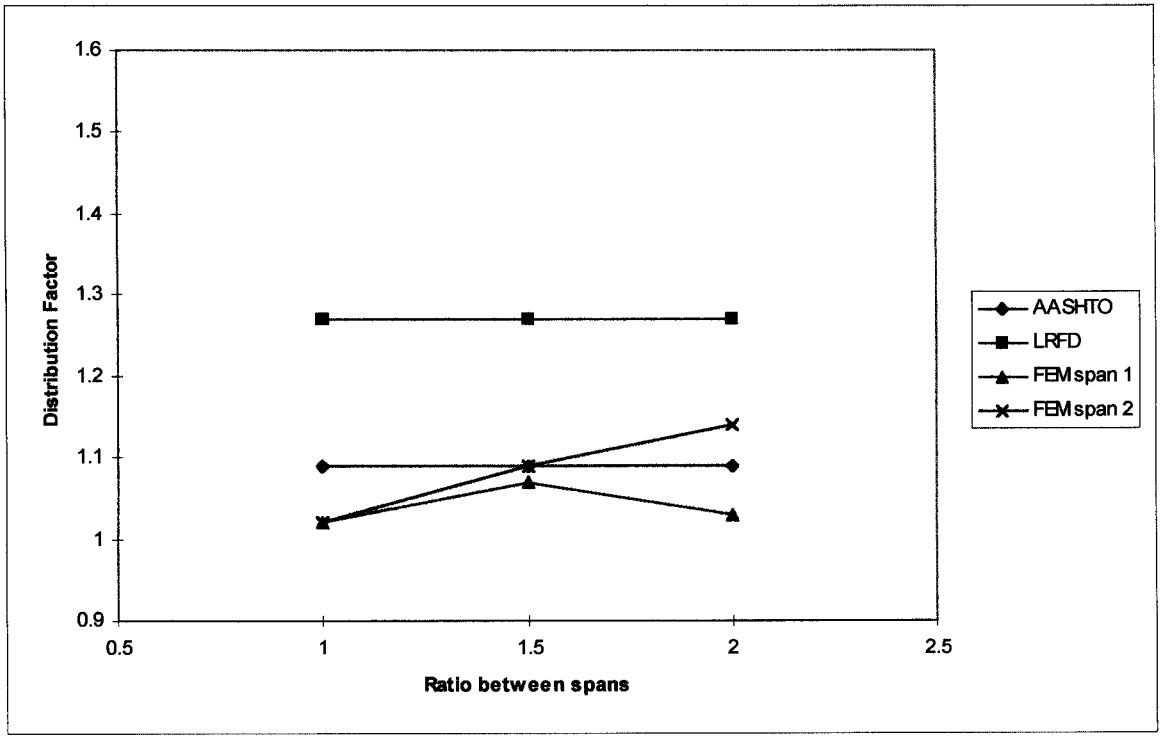

Fig. 6.46 Positive Moment Distribution Factors for Skew Bridges with Different Ratios Between Two Spans (Exterior Girder)

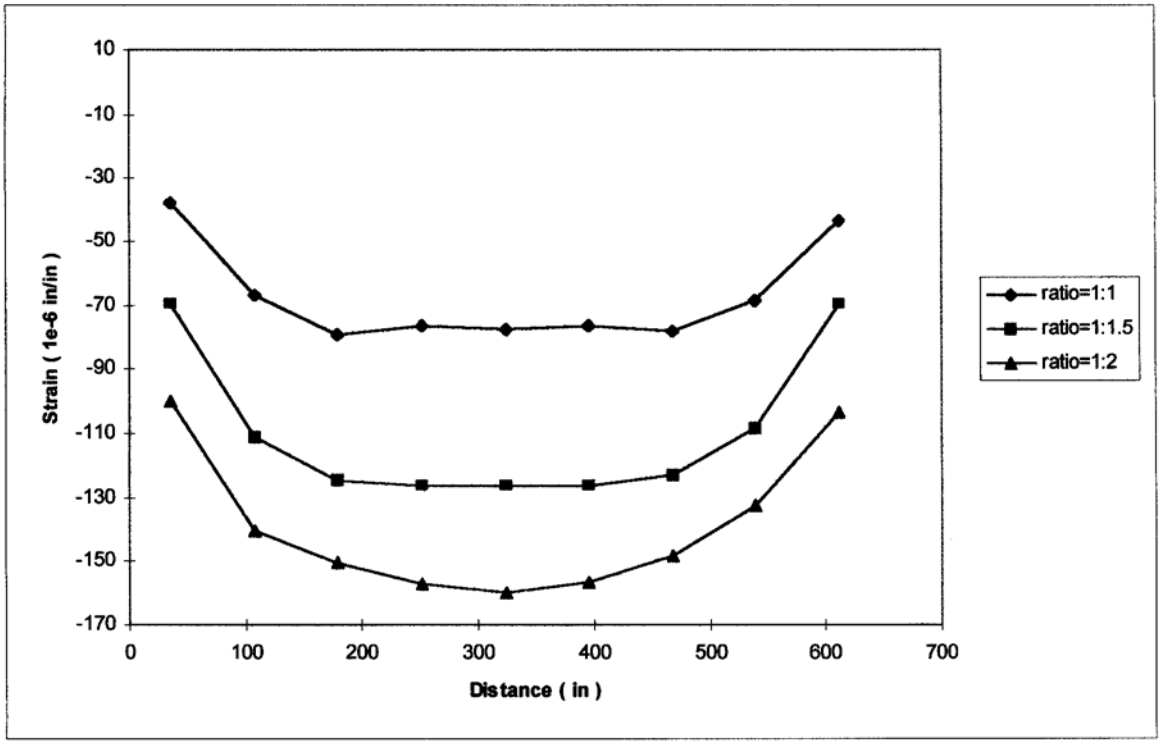

Fig. 6. 47 Strain Distribution at the Support for Skew Bridges with Different Ratios Between Two Spans (Interior Girder Loading)

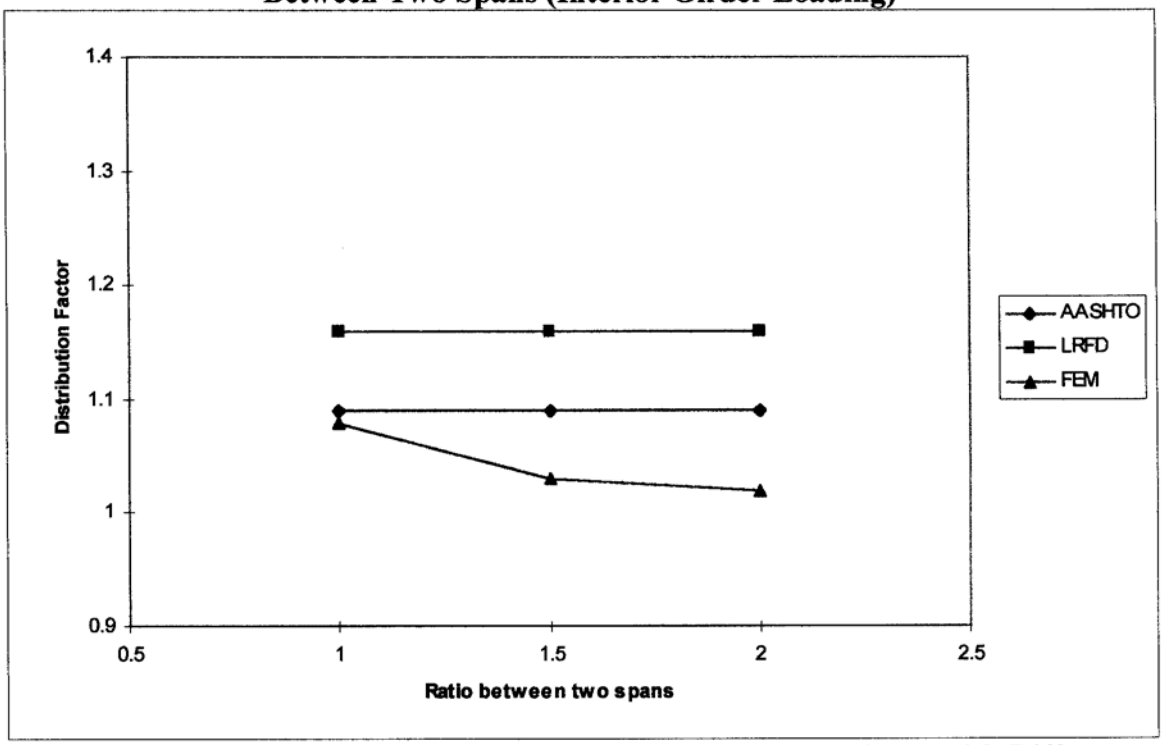

Fig. 6.48 Negative Moment Distribution Factors for Skew Bridges with Different Ratios Between Two Spans (Interior Girder)

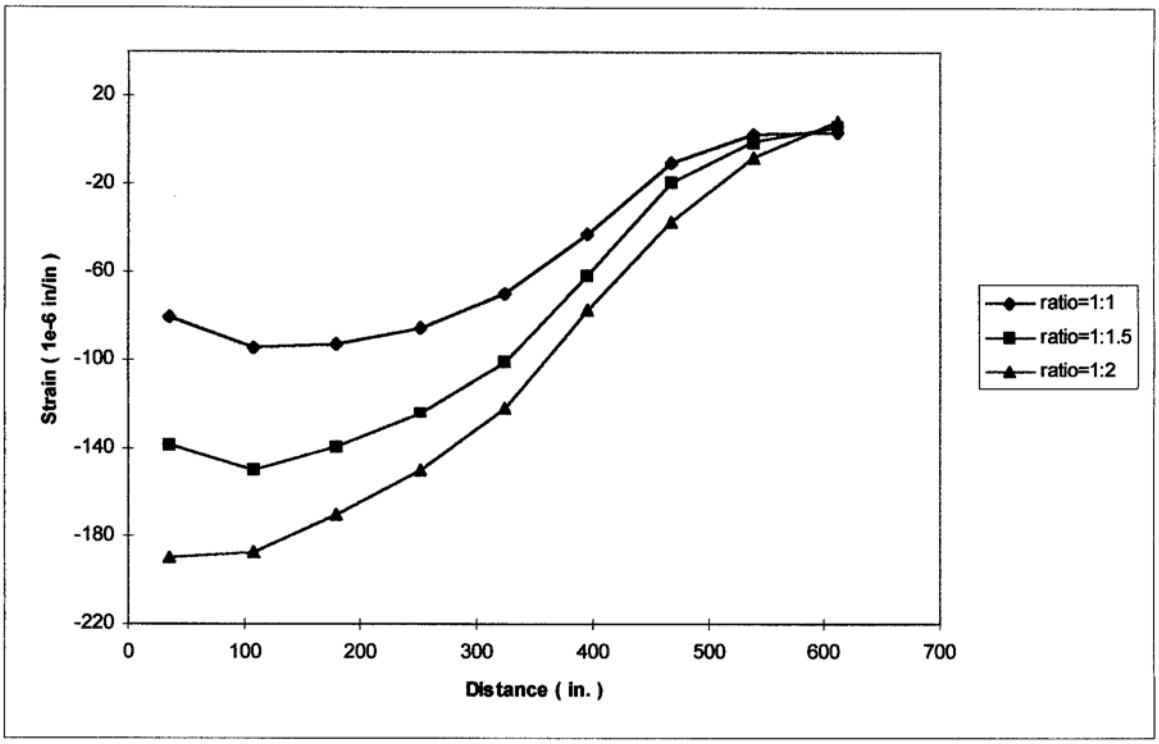

Fig. 6.49 Strain Distribution at the Support for Skew Bridges with Different Ratios Between Two Spans (Exterior Girder Loading)

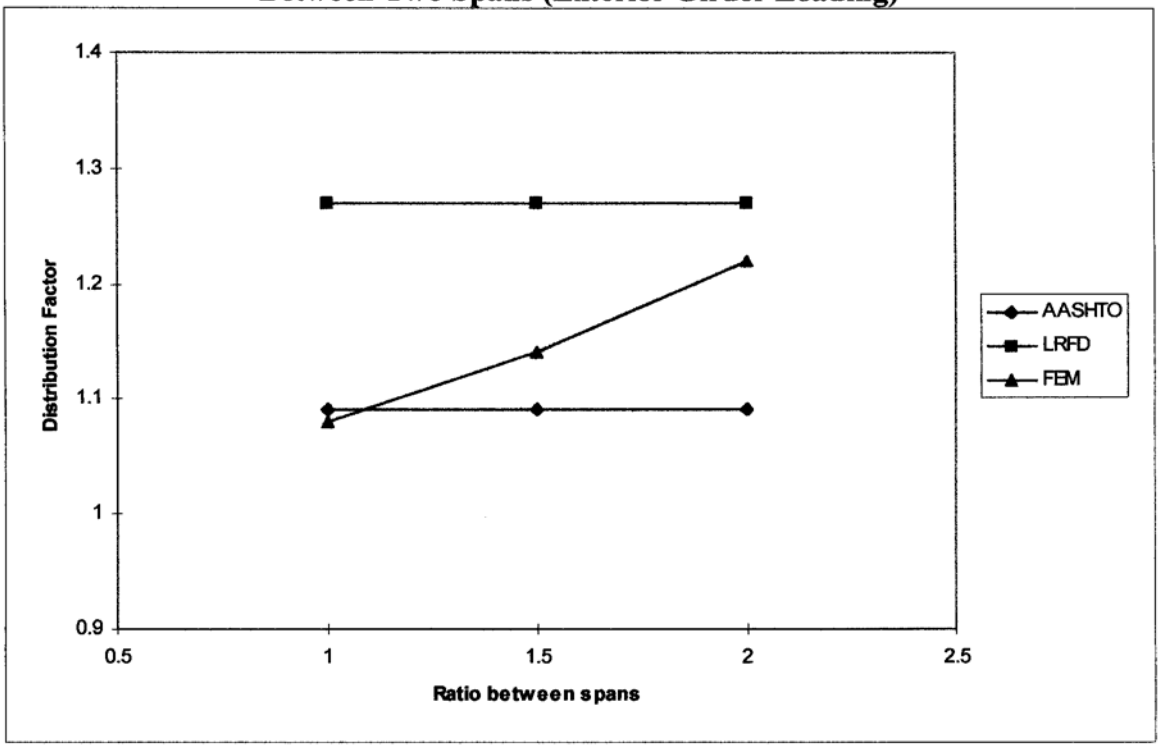

Fig. 6.50 Negative Moment Distribution Factors for Skew Bridges with Different Ratios Between Two Spans (Exterior Girder)

6.4 FIELD TESTS ON CONTINUOUS SLAB-ON-GIRDER BRIDGES

There is an increase in the number of existing highway bridges which need to be evaluated to permit increase in the live loads or for bridge strength determination taking into account deterioration. The evaluation of Florida highway bridges is being conducted by The Florida Department of Transportation Structures Research Center using non-destructive load tests. Load testing provides a realistic evaluation of the bridge and load ratings that are essential for determining safe service loads in the bridges. These ratings are based on the measured strains and deflections due to the applied loads. The wheel load distribution factors are calculated based on the field measurements.

Comparison between strain and deflection measurements of bridges with analytical values gives a perspective of the accuracy of the FEM to analyze the bridge behavior. The accuracy of FEM is dependent on the realistic modeling of the bridge and its boundary conditions.
Three bridges tested by Florida Department of Transportation (FDOT) were analyzed using ANSYS finite element program. Of the three continuous bridges studied, two bridges are continuous through the deck slab and one bridge is continuous through the girder and the deck slab. The FDOT Eau Gallie Bridge was made continuous by post-tensioning the girders at the supports. The negative moment measurement showed that this bridge was truly continuous and is, therefore, used as a typical bridge in the parametric analysis of continuous bridges (Section 6.3).

Field measurements from load tests by MOT and analytical results based on FEM models are used to study wheel load distribution factors for continuous bridges. The FEM models for continuous slab-on-girder bridges are shown in Figs 6.2 and 6.4.

6.4.1 SR-518 Eau Gallie Bridge

The Eau Gallie bridge is located in Melbourne, Florida, and is owned and operated by the FDOT. The structure has spans ranging from 20 to 145 feet. The 7.5 in. thick deck is supported by nine Bulb-T girders placed at 10'-4" center to center. The Bulb-T girders are made continuous by post-tensioning. The deck is 90'-7.5" wide and has six traffic lanes with a 5 ft. pedestrian sidewalk. The live load was applied with two 204 kip testing vehicles. Several load positions were performed to study the effects of shear, maximum bending and twisting moments. The truck load positions are shown in Figures 6.54 to 6.56.

First, the bridge was discretized to be continuous in the deck slab over the interior support with restraint on the translational degrees of freedom at the end supports. In the second idealization, the model was modified by making the girders continuous over the interior support. The analytical results from the second modeling were found to give a reasonable correlation with the field test values. Therefore, this model was chosen as a basis for the parametric study presented in this chapter.

Table 6.4 Material and Sectional Properties for SR-518 Eau Gallie Bridge

Material properties	E_{deck} (ksi)	E_{beam} (ksi)	Poisson's ratio, υ	G (ksi)
	4031	4031	0.2	1679

Section Properties	Slab	Thickness = 7.5 in.				
	Top	A (in^2)	I_y (in^4)	I_z (in^4)	T_{ky} (in)	T_{kz} (in)
	Flange	288	864	55296	48	6
Florida Bulb T Girder	Web	Thickness = 8 in.				
	Bottom	A (in^2)	I_y (in^4)	I_z (in^4)	T_{ky} (in)	T_{kz} (in)
	Flange	532	8689	64017	38	14

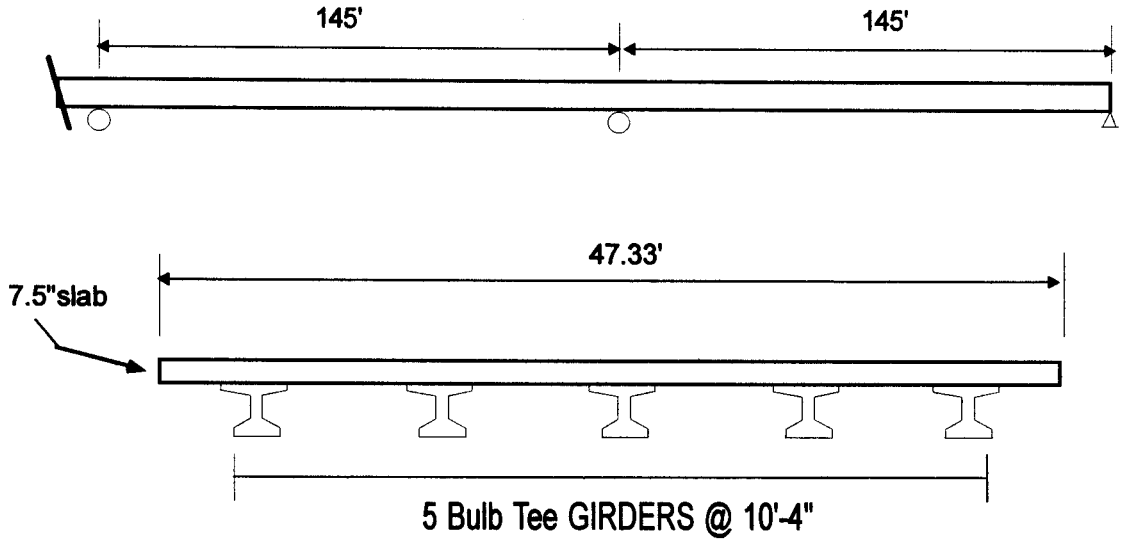

Fig. 6.51 Cross Section of SR-518 Eau Gallie Bridge

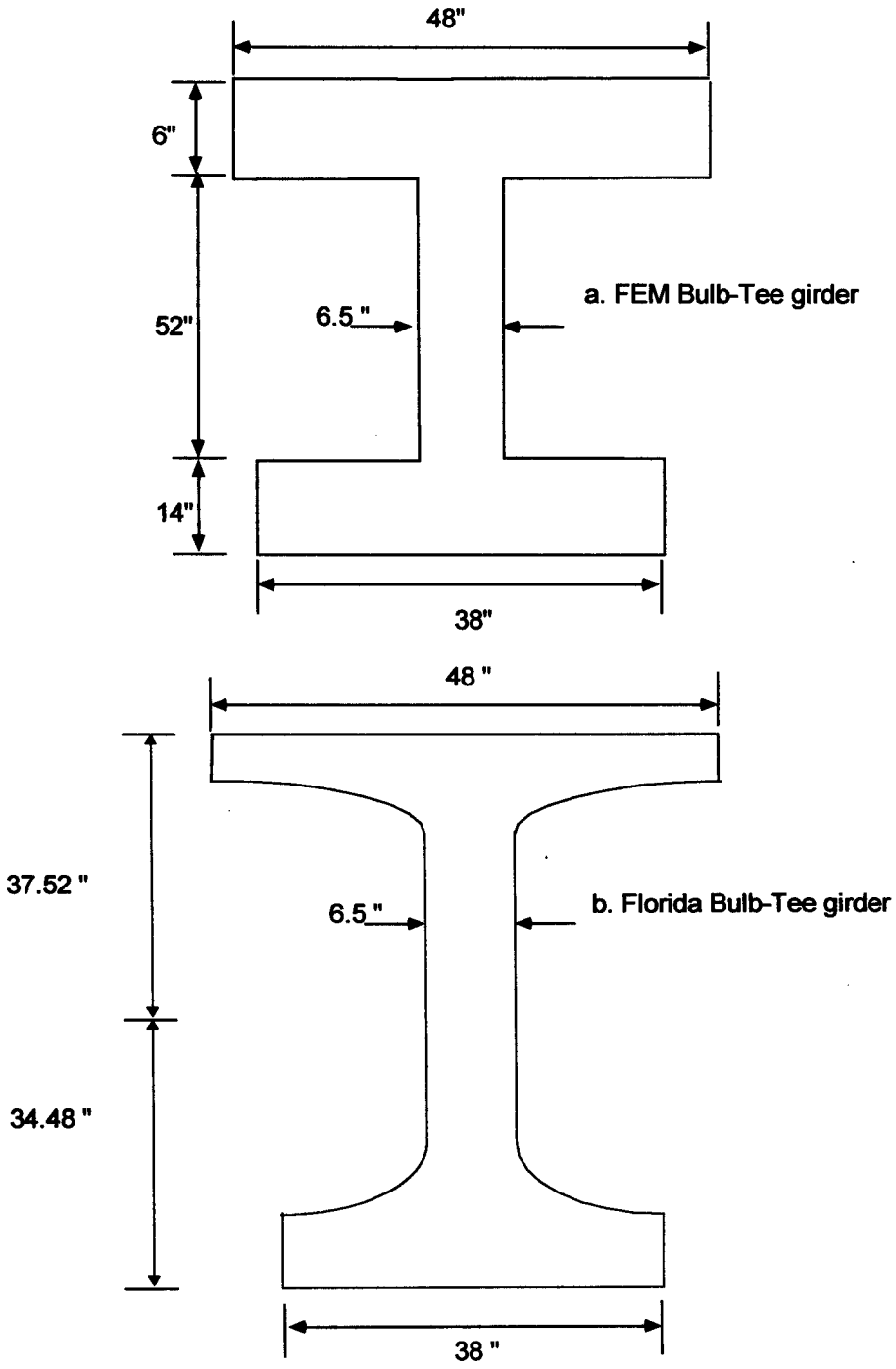

Fig. 6.52 Bulb-Tee Girder Details

Fig 6.53 FEM MODEL of SR-518 Eau Gallie Bridge

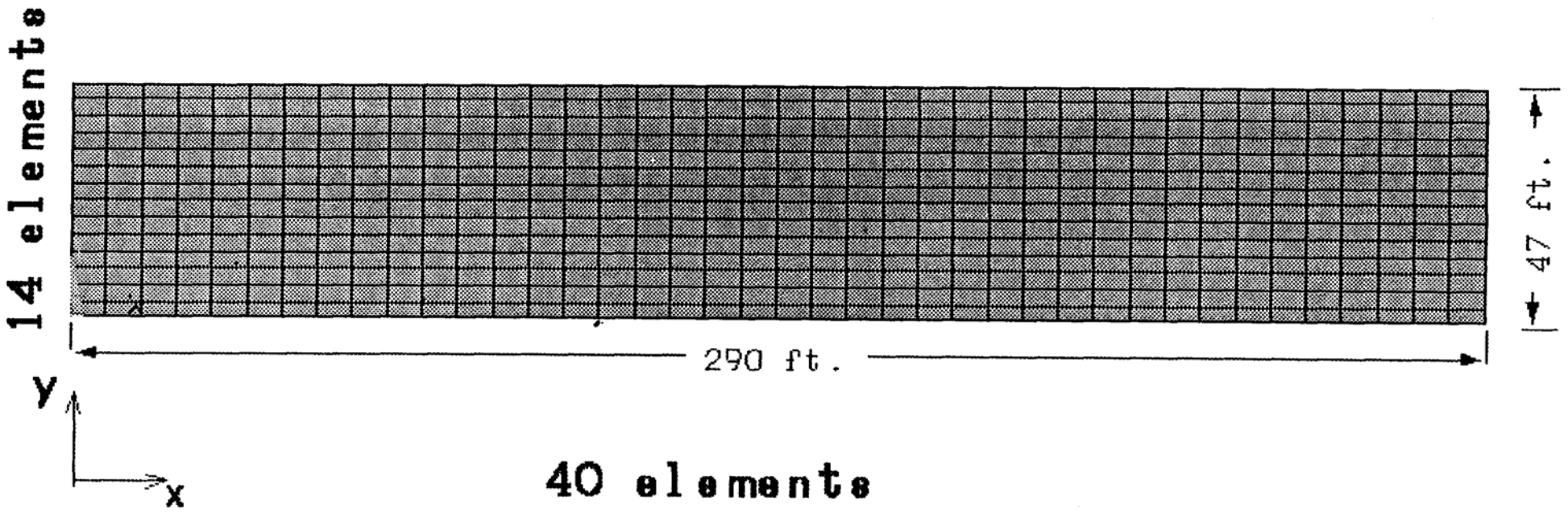

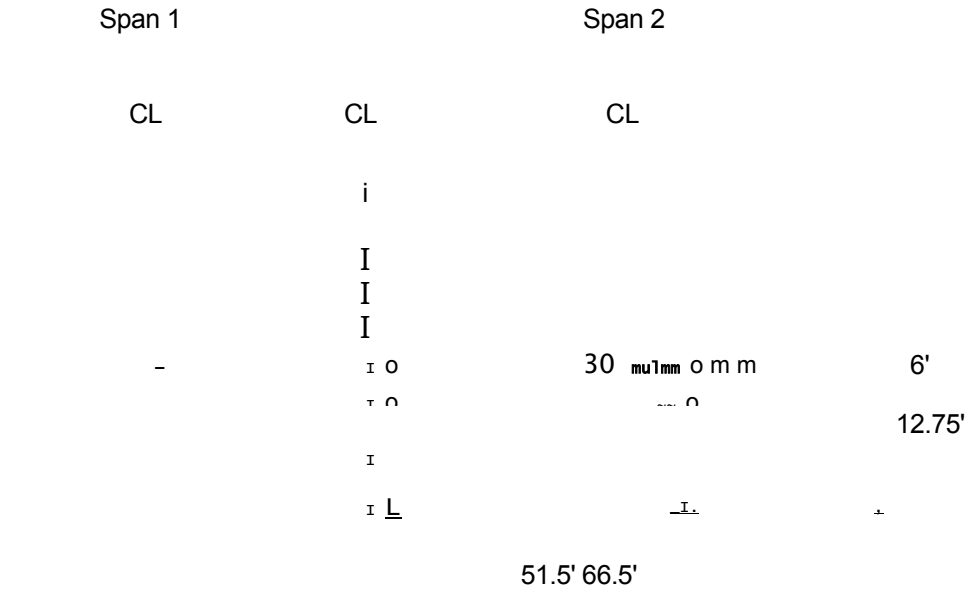

a. Load Position 1

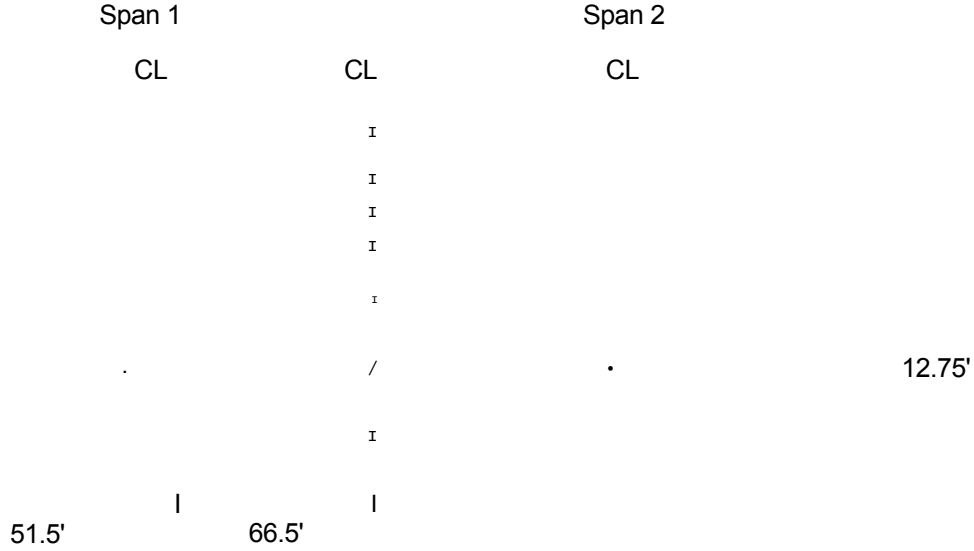

b. Load Position 2

LVDT on Girder 26.16 kips

STRAIN GAUGE on Girder 20.93 kips

7.82 kips

Fig. 6.54 Load Positions 1 and 2/Strain Gauges SR-518 Eau Gallie Bridge

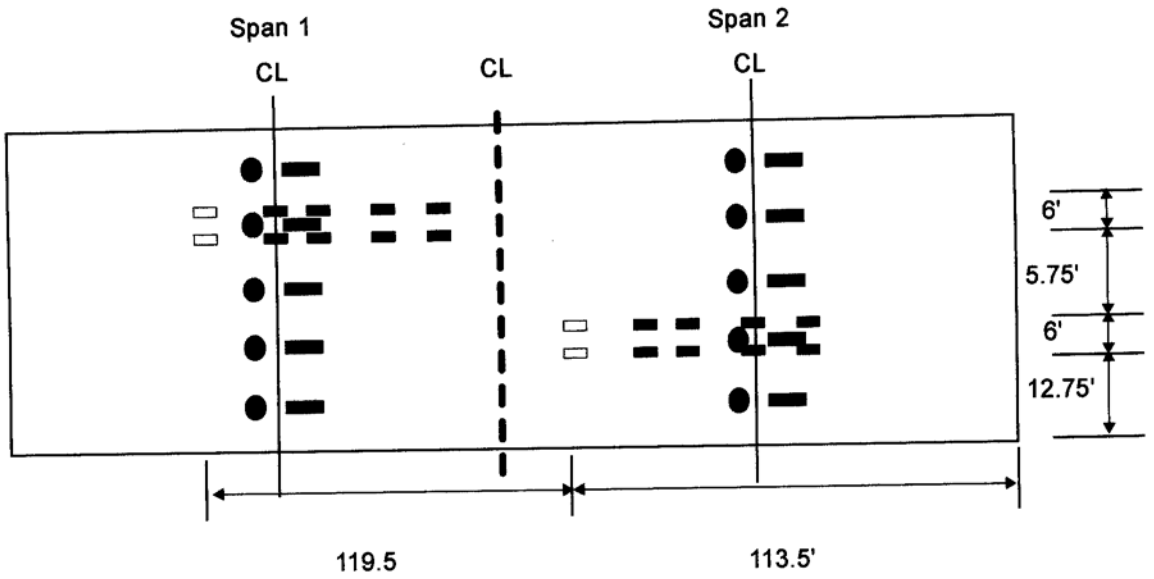

a. Load Position 3

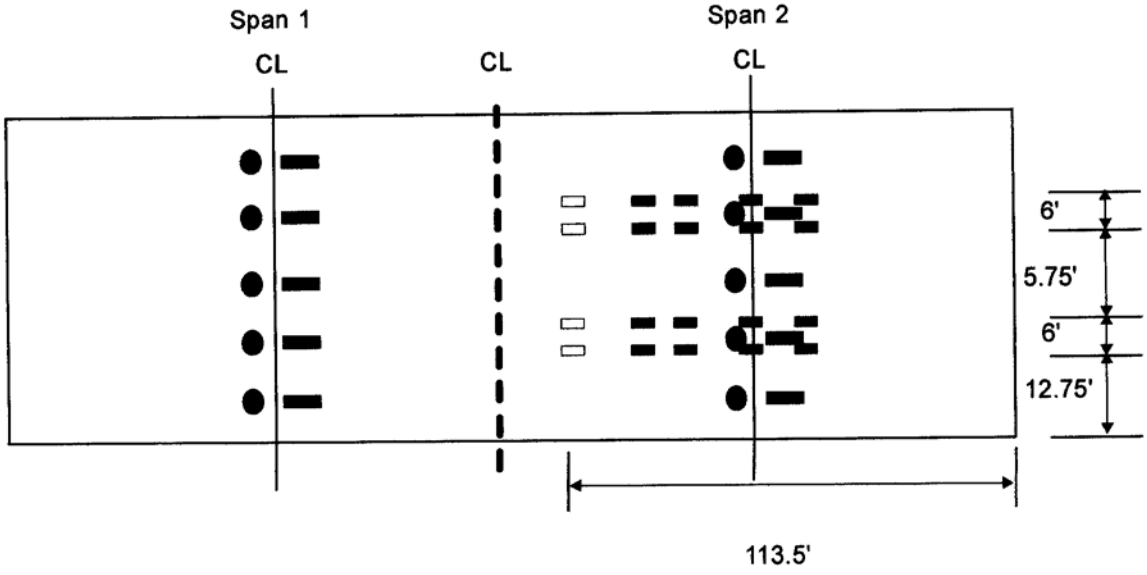

b. Load Position 4

Fig. 6.55 Load Positions 3 and 4/Strain Gauges SR-518 Eau Gallie Bridge

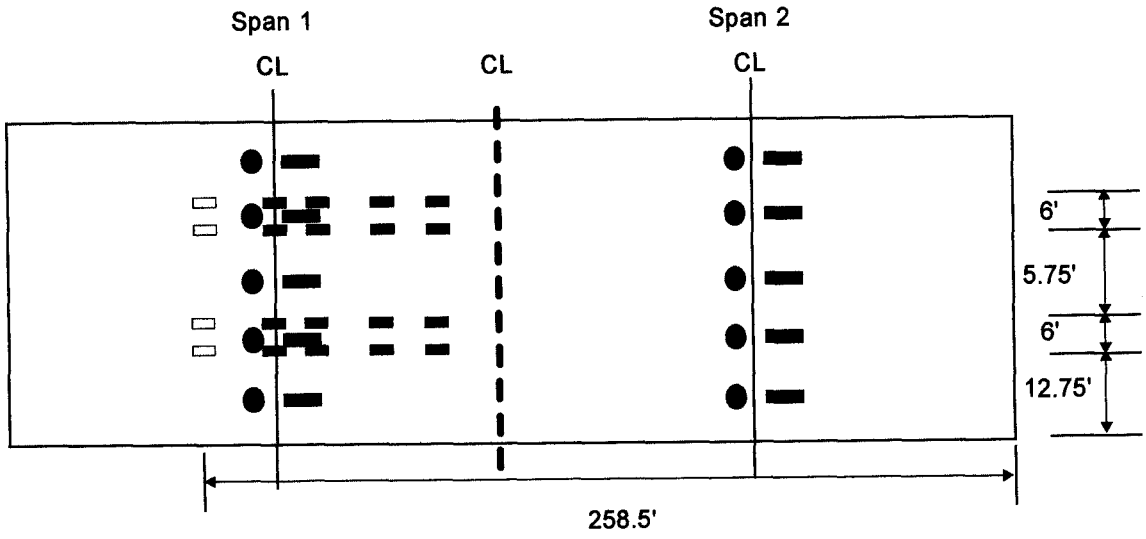

a. Load Position 5

Fig. 6.56 Load Position 5/Strain Gauges SR-518 Eau Gallie Bridge

The truck load positions 1 and 2 induce maximum positive moments in the two spans (Fig 6.54). Load position 2 has the same loading configuration as load position 1 with the trucks advanced forward to span 2. The positioning of the trucks for the third load case was chosen to give maximum twisting moment. Truck load position 4 has two trucks loaded on span 2 to produce maximum deflection. Truck load position 5 is similar to position 4 with the trucks loaded on span l. Figure 6.57 shows the deflection distribution on the loaded span at the midspan for load position 1. The maximum deflection based on FEM is within 10% of the measured maximum deflection. The exterior girders' deflections were less accurately predicted. Figure 6.58 shows the deflection distribution on the unloaded span at the midspan for load position 1. The deflections are predicted accurately using FEM. Figure 6.59 shows the deflection distribution on the unloaded

span at the midspan for load position 2. There is a small difference between the field tests and the FEM prediction. Figure 6.60 shows the deflection distribution on the loaded span at the midspan for load position 2. The measured deflections were supposed to be similar to those for load position 1, however, a significant difference has been observed in the reported data. The FEM deflections were similar for positions 1 and 2.

The deflection variations at midsection of span 1 and 2 for load position 3 are shown in Figures 6.61 and 6.62. Figure 6.63 and 6.64 show the deflection variations at the midsections of the loaded and unloaded spans, respectively, for load position 4. For load position 5, the deflection distributions at midsections for unloaded and loaded spans are shown, respectively, in Figures 6.65 and 6.66. In all of the above cases, it can be observed that the differences between the measured and the analytical values are relatively small.

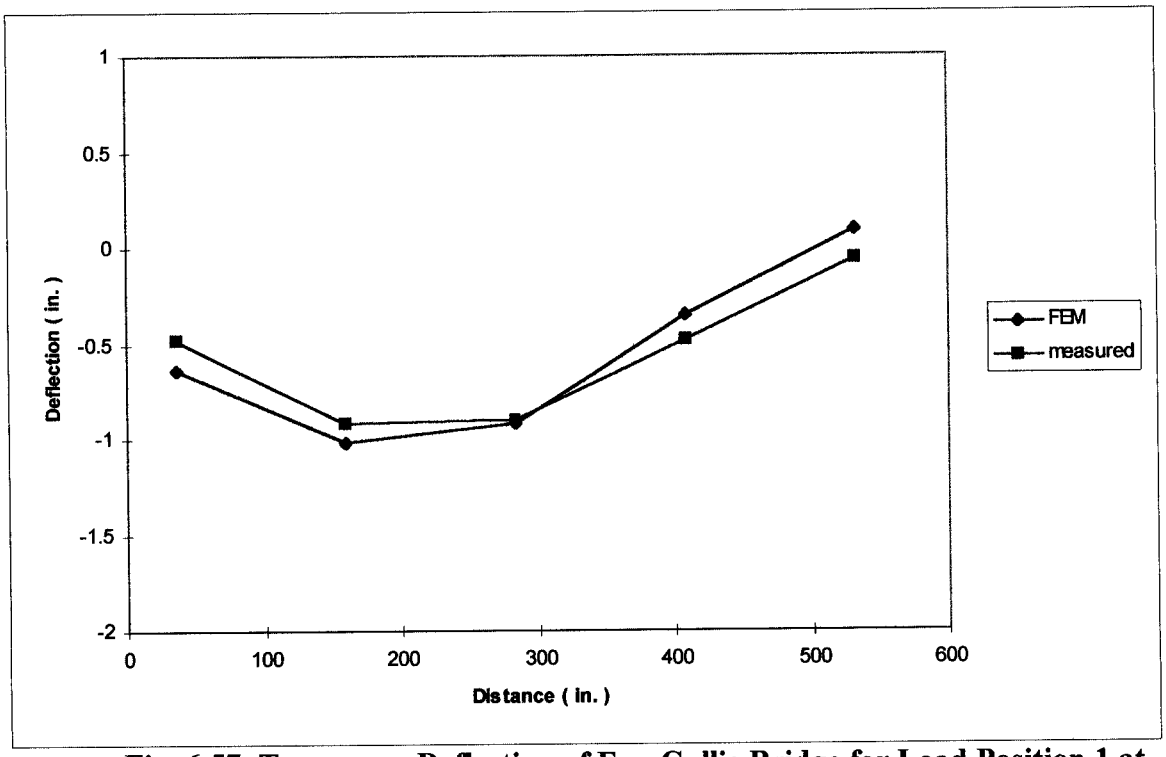

Fig. 6.57 Transverse Deflection of Eau Gallie Bridge for Load Position 1 at Midspan 1

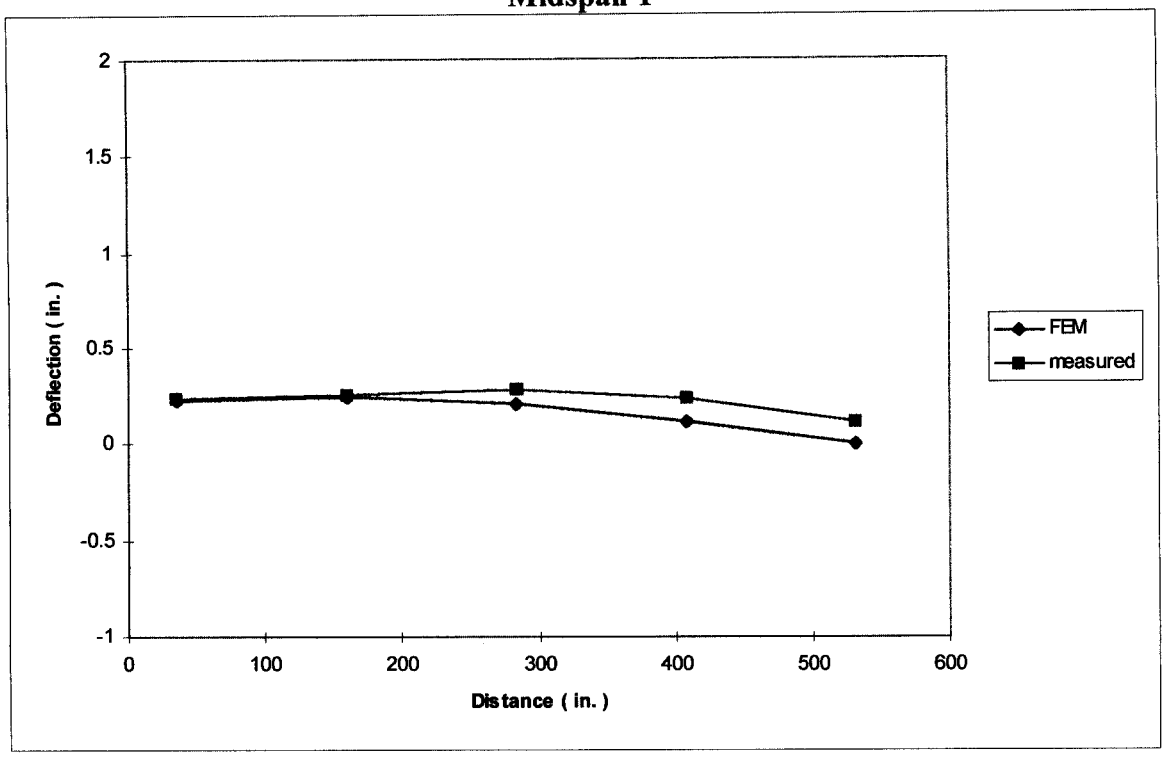

Fig. 6.58 Transverse Deflection of Eau Gallie Bridge for Load Position 1 at Midspan 2

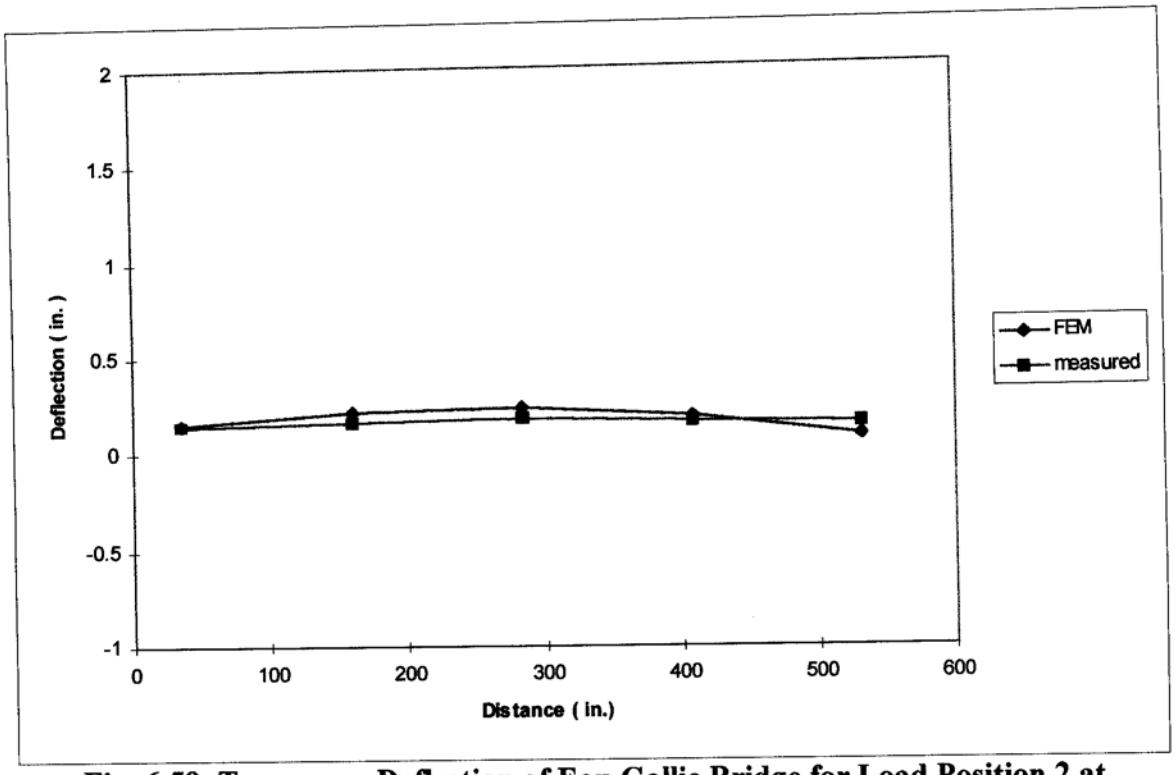

Fig. 6.59 Transverse Deflection of Eau Gallie Bridge for Load Position 2 at Midspan 1

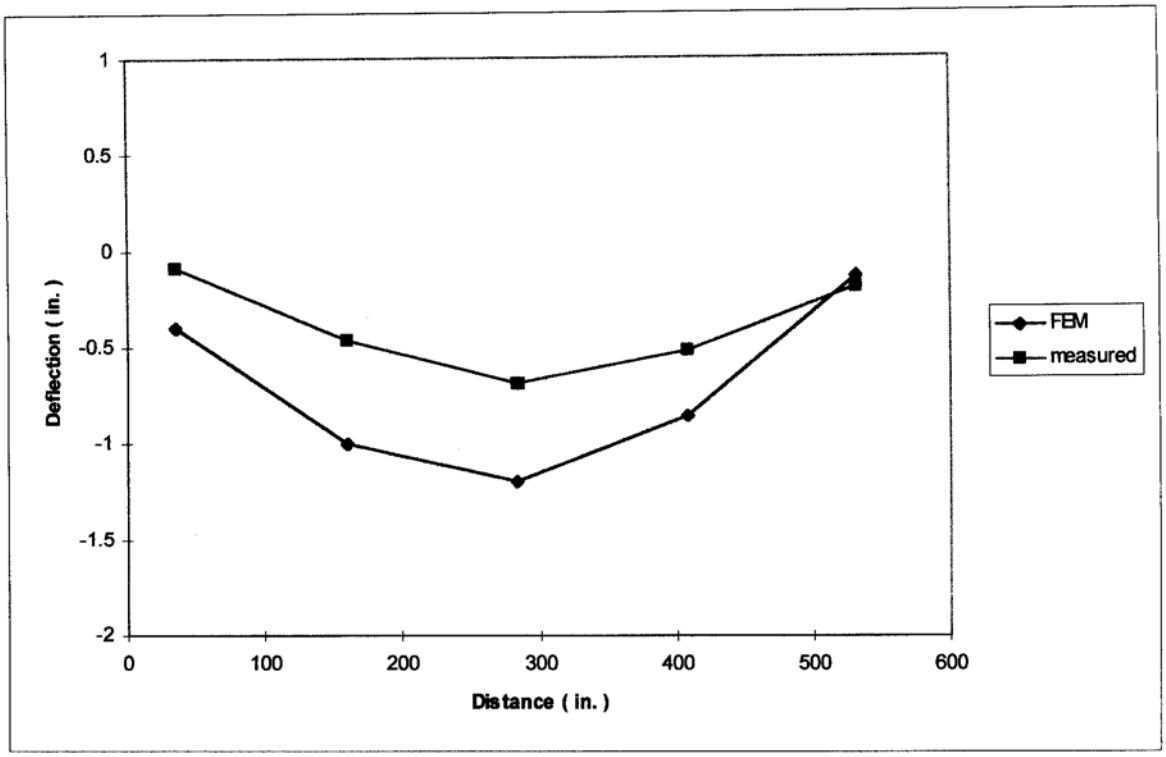

Fig. 6.60 Transverse Deflection of Eau Gallie Bridge for Load Position 2 at Midspan 2

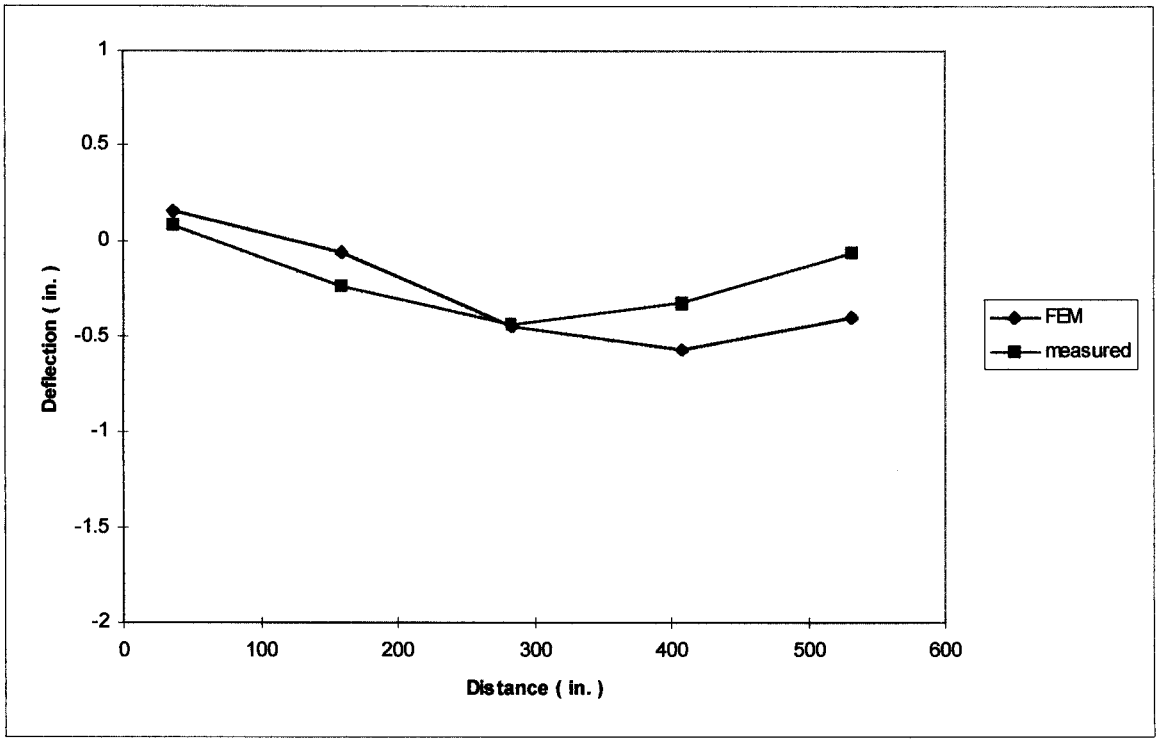

Fig. 6.61 Transverse Deflection of Eau Gallie Bridge for Load Position 3 at Midspan 1

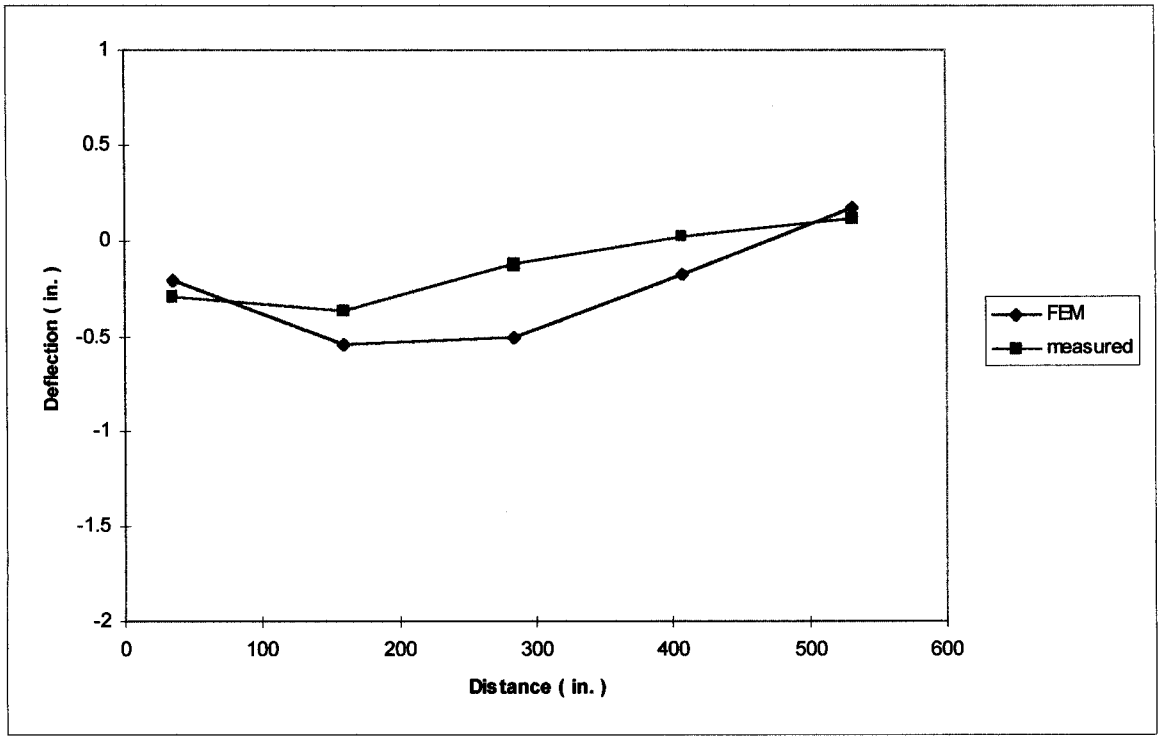

Fig. 6.62 Transverse Deflection of Eau Gallie Bridge for Load Position 3 at Midspan 2

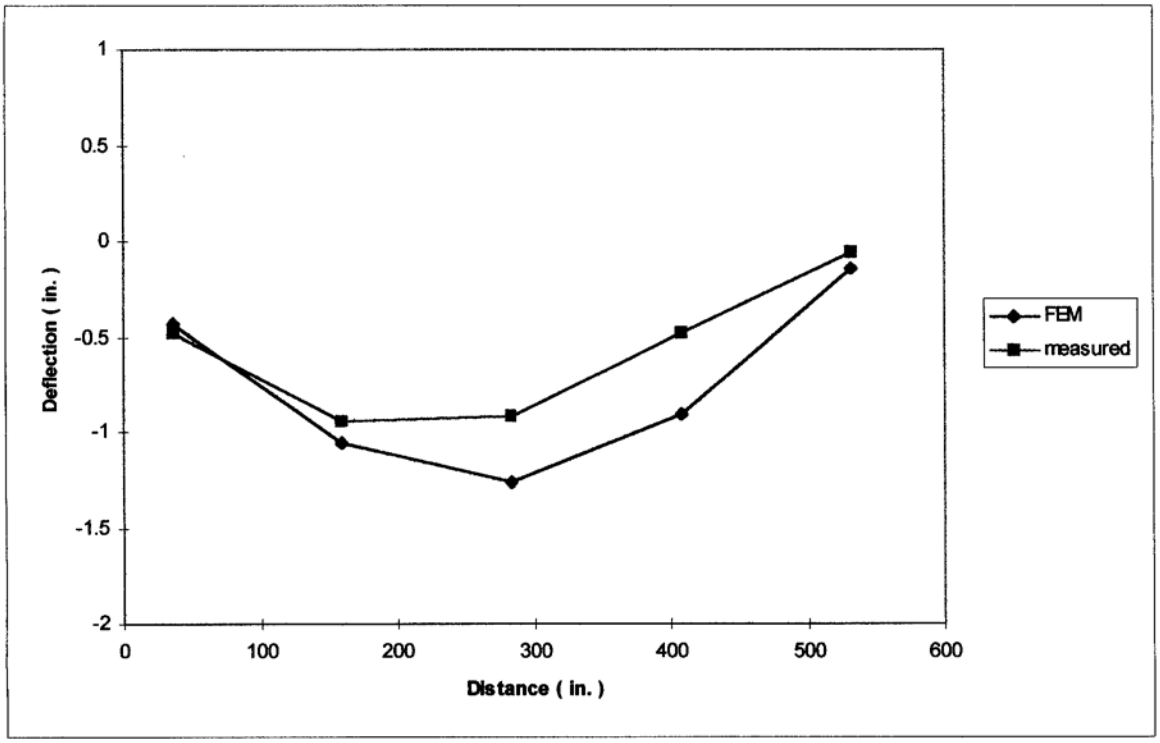

Fig. 6.63 Transverse Deflection of Eau Gallie Bridge for Load Position 4 at Midspan 1

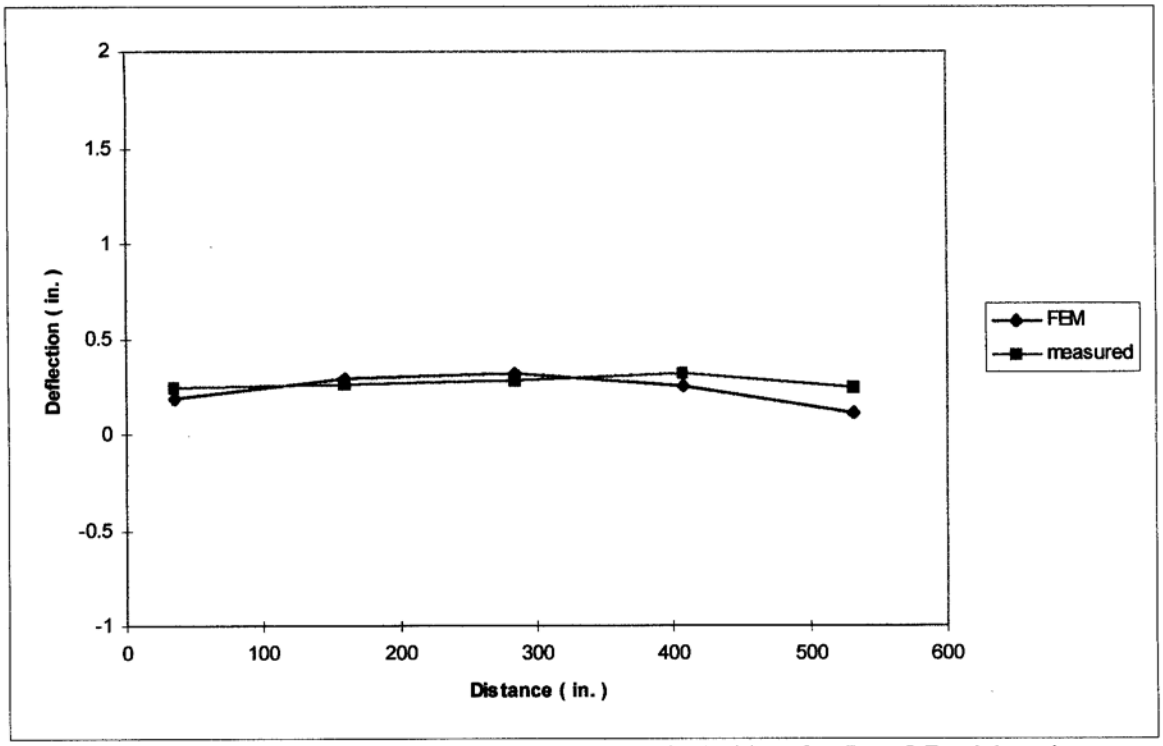

Fig. 6.64 Transverse Deflection of Eau Gallie Bridge for Load Position 4 at Midspan 2

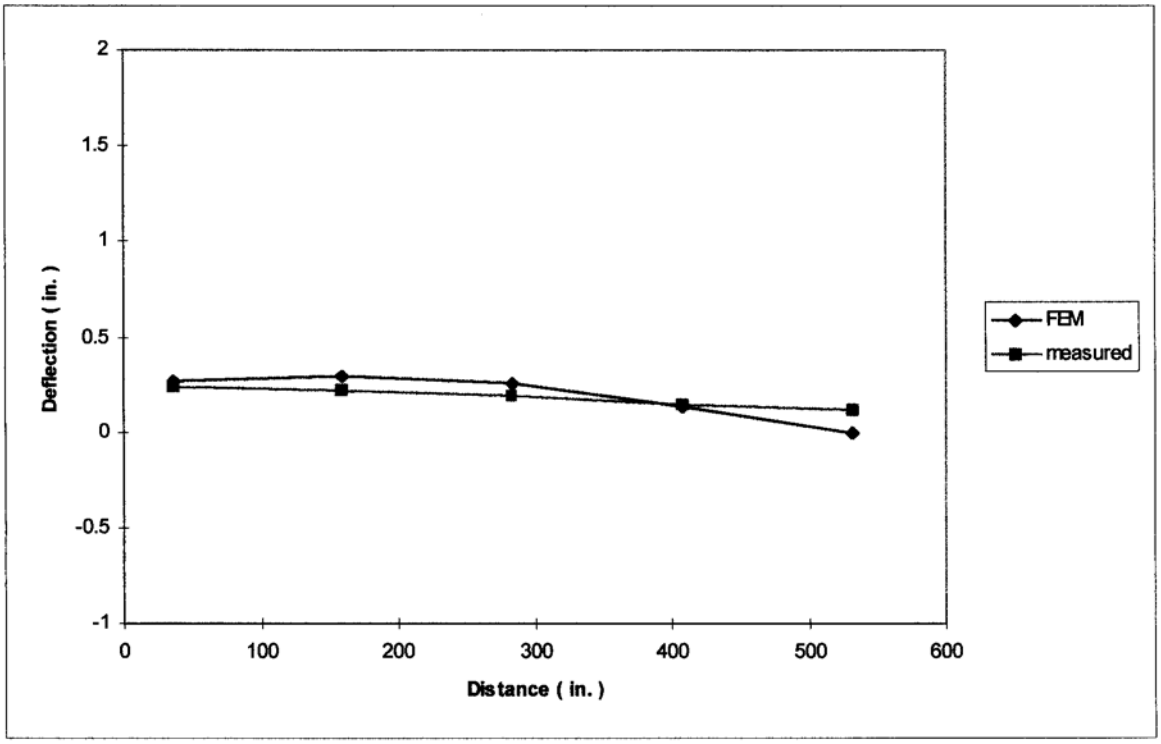

Fig. 6.65 Transverse Deflection of Eau Gallie Bridge for Load Position 5 at Midspan 1

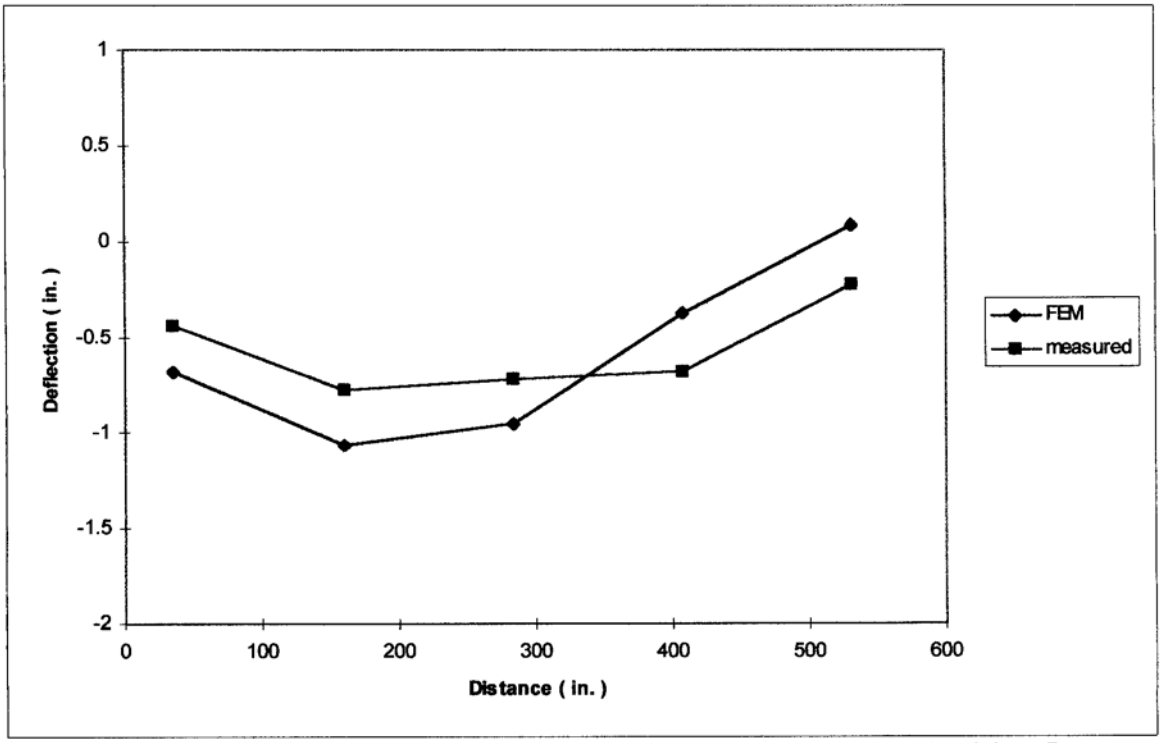

Fig. 6.66 Transverse Deflection of Eau Gallie Bridge for Load Position 5 at Midspan 2

Table 6.5 summarizes the load distribution factors for the Eau Gallie bridge based on AASHTO, LRFD, FEM, and field tests. The distribution factors based on AASHTO and LRFD are larger than those based on the measured deflections and FEM. Load position 4 at span 1 gives the maximum load distribution factor for the field tests and FEM. These factors are lower than the LRFD factor by 16%. The maximum load distribution factor for span 2 corresponds to load position 5. The FEM and measured factors are lower that AASHTO and LRFD distribution factors. The FEM load distribution factors are close to the factors based on the field tests. Therefore, the finite element method should be used for the analysis of existing continuous slab-ongirder bridges.

Table 6.5 Summary of Eau Gallie Load Distribution Factors

	AASHTO	LRFD	FEM Span1	Measured Span 1	FEM Span 2	Measured Span 2
Load Position 1	1.88	1.57	0.72	0.65	0.62	0.49
Load Position 2	1.88	1.57	0.54	0.46	0.66	0.71
Load Position 3	1.88	1.57	0.87	0.89	0.87	1.14
Load Position 4	1.88	1.57	1.32	1.31	1.1	0.96
Load Position 5	1.88	1.57	1.24	1.03	1.43	1.1

6.4.2 SR-55 Bridge Over Suwannee River

The bridge is located on SR-55 over the Suwannee River at Fanning Springs, Florida. The bridge has two 121'-3" spans made continuous through the deck slab and a simple 66' span. The 42'-9" wide 7 in. thick deck slab is supported by eight AASHTO IV girders spaced at 4'-11.5" centers.

The bridge was loaded with two FDOT test vehicles. The bridge was modeled as continuous through the deck slab at the interior support with discontinuous girders at the interior support. The ends of the bridge were restrained against translational degrees of freedom and the bottom of the girders at the interior support of the bridge were constrained in the vertical and transverse directions. Figure 6.69 shows the truck load position and the strain gauge location in span 2 of the SR-55 bridge. The field measurements were taken for three different loads (100, 152 and 204 kips) for this truck load position.

Table 6.6 Material and Sectional Properties for SR-55 Bridge Over Suwannee River

Material properties	E_{deck} (ksi)	E_{beam} (ksi)	Poisson's ratio, υ	G (ksi)
	4031	4031	0.2	1679

Section Properties	Slab	Thickness = 7.0 in.				
	Top	A (in^2)	I_y (in^4)	I_z (in^4)	T_{ky} (in)	T_{kz} (in)
	Flange	220	2218	7333	20	11
AASHTO IV Girder	Web	Thickness = 8 in.				
	Bottom	A (in^2)	I_y (in^4)	I_z (in^4)	T_{ky} (in)	T_{kz} (in)
	Flange	312	3744	17576	26	12

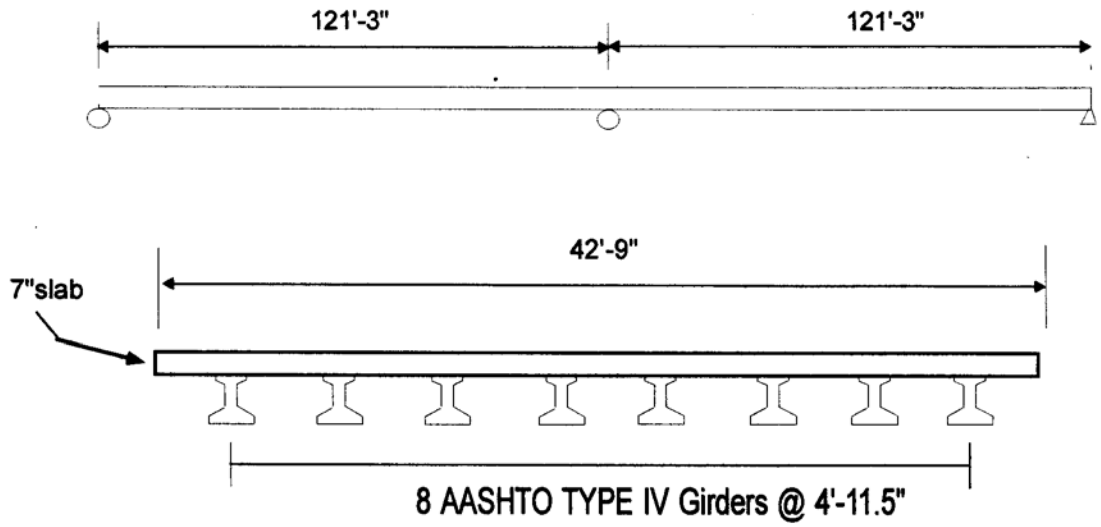

Fig. 6.67 Cross Section of SR-55 Bridge Over Suwannee River

Fig 6.68 FEM MODEL of SR-55 Bridge Over Suwannee River

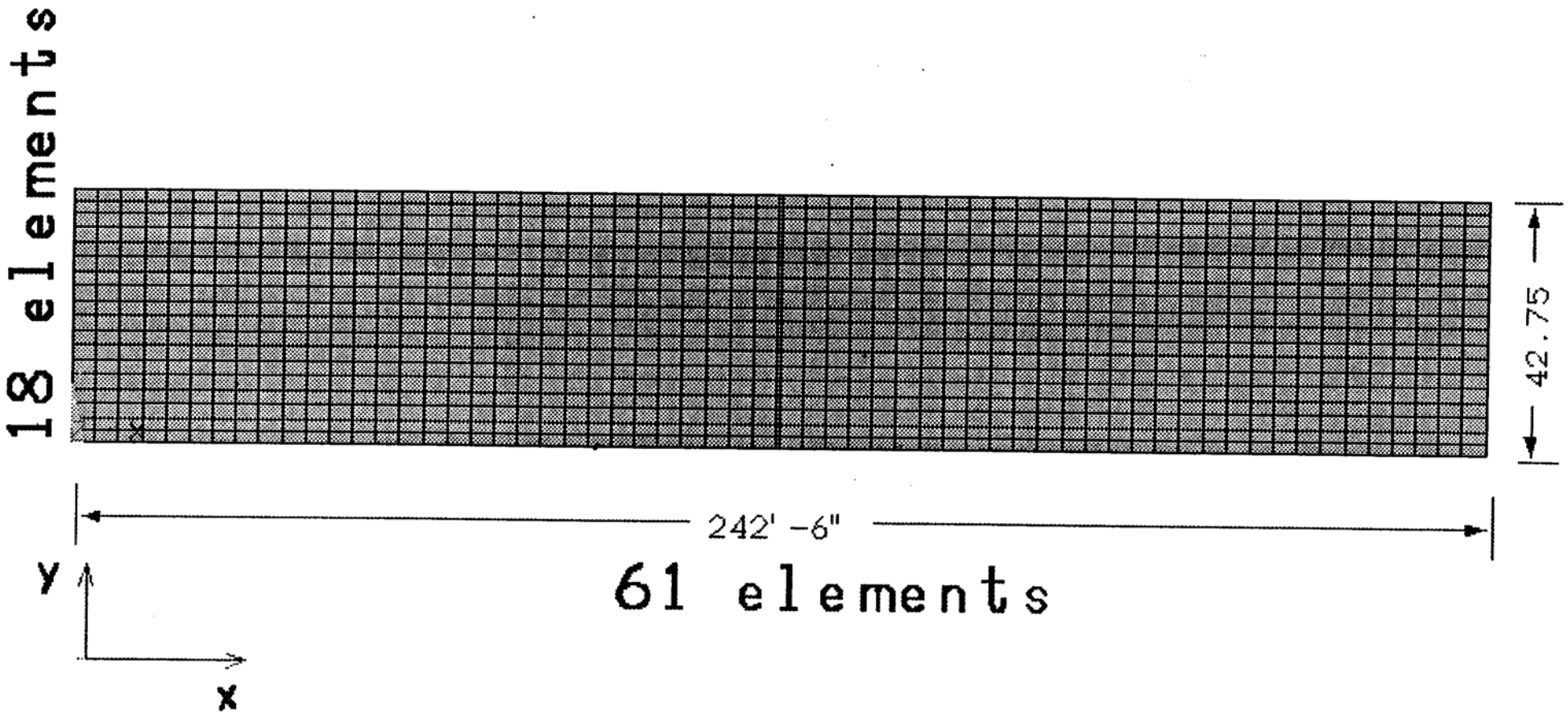

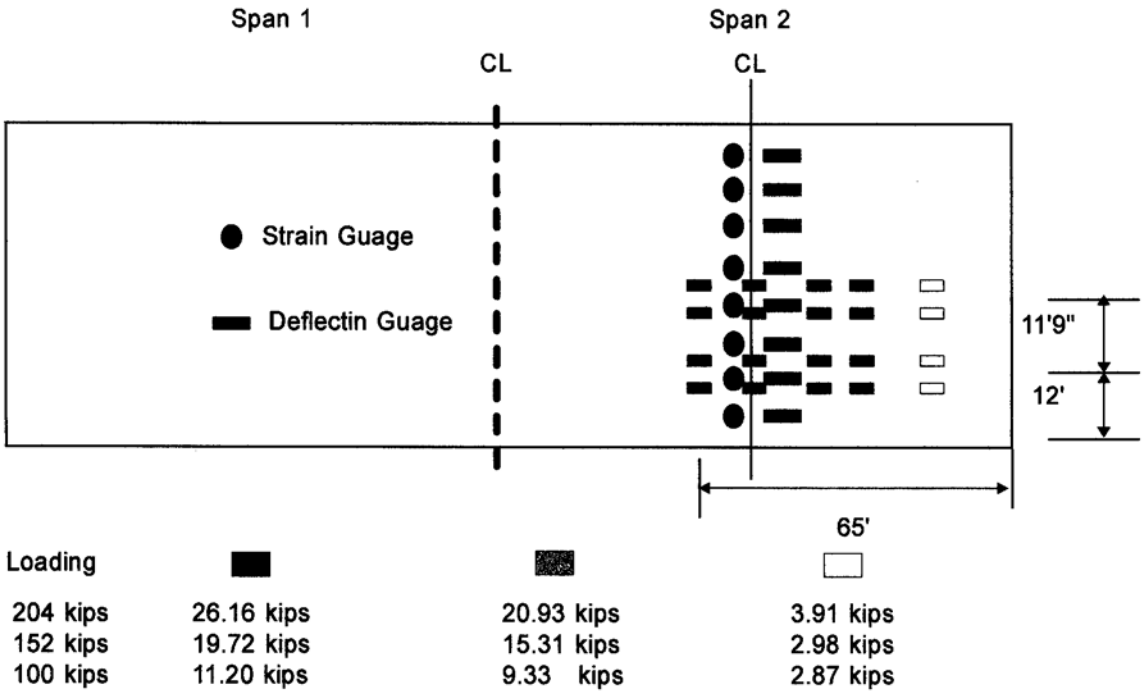

Fig. 6.69 Load Position/Strain Gauges for SR-55 Bridge Over Suwannee River

The measured strains for the different loads on the SR-55 Bridge Over Suwannee River are slightly higher than the analytical values (Fig 6.70). The transverse strain distributions from the measured and analytical values are similar for each of the applied loads. The measured and computed strains compare well in the girders where the trucks are loaded and the girder strains vary only slightly as the girder distance from the trucks increase (Fig 6.70 and Table 6.7).

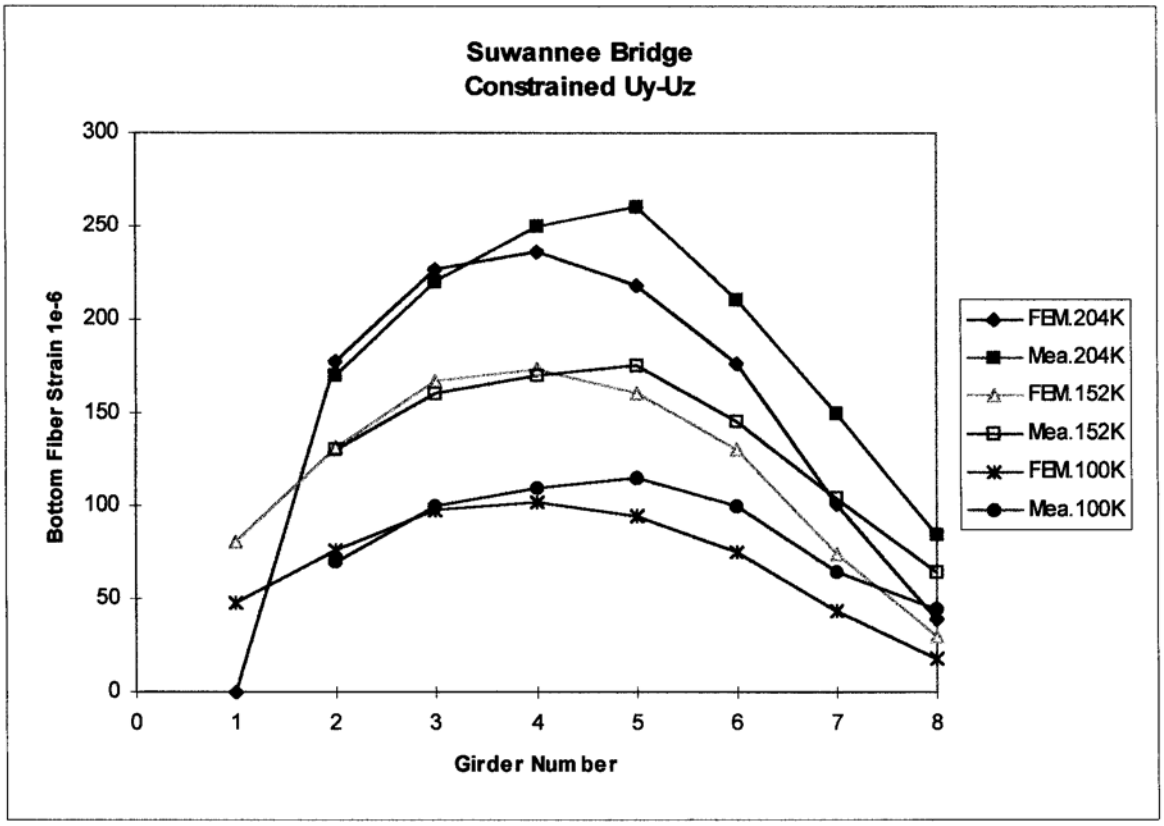

Fig. 6.70 Measured and Calculated Strains for SR-55 Bridge Over Suwannee River

Table 6.7 Measured and Calculated Strains for SR-55 Bridge Over Suwannee River

GIRDER	FEM.204K	Mea.204K	FEM.152K	Mea.152K	FEM.100K	Mea.100K
1	109 μstrain		81		48	
2	177	170	131	130	77	70
3	226	220	167	160	98	100
4	236	250	173	170	102	110
5	218	260	160	175	95	115
6	176	210	130	145	76	100
7	101	150	75	105	44	65
8	40	85	30	65	18	45
	1174	1345	947	950	558	605

Table 6.8 shows small differences in the load distribution factors obtained from the measured and FEM strain values. The AASHTO and LRFD load distribution factors are higher than the FEM and measured distribution factors.

Table 6.8 Summary of SR-55 Load Distribution Factors (Interior Girders)

AASHTO	LRFD	FEM.204K	Mea.204K	FEM.152K	Mea.152K	FEM.100K	Mea.100K
0.9	0.92	0.74	0.77	0.73	0.73	0.73	0.76

6.4.3 Palm Beach County Bridge #930398

The bridge is located in Palm Beach County on Hoods Road over I-95. It has four spans, two of which are continuous. The intermediate continuous spans are 143'-7 3/16" long and 46'-9" wide. The 7 in. **thick deck slab is supported on six AASHTO V girders at T-9.5" centers.**

The bridge is modeled as continuous through the deck slab at the interior support with all end translations restrained. The bridge's six diaphragms were modeled using shell elements (shell 63) in the transverse direction. Two of the diaphragms are located at the interior support and the other four diaphragms are located at third points of each span. The ends of the bridge were restrained against the translational degrees of freedom and the bottom of the girders at the interior support of the bridge were constrained in the vertical and transverse directions. Figure 6.74 shows

the truck load position in span 1 of the Palm Beach County Bridge. The field measurements were taken for a truck load of 140 kips.

Table 6.9 Material and Sectional Properties for Palm Beach County Bridge #930398

Material Properties	E_{deck} (ksi)	E_{beam} (ksi)	Poisson's ratio, υ	G (ksi)
	4031	4031	0.2	1679

Section Properties	Slab	Thickness = 7 in.				
	Top	A (in^2)	I_y (in^4)	I_z (in^4)	T_{ky} (in)	T_{kz} (in)
	Flange	294	1201	43218	42	7
AASHTO V Girder	Web	Thickness = 8 in.				
	Bottom	A (in^2)	I_y (in^4)	I_z (in^4)	T_{ky} (in)	T_{kz} (in)
	Flange	364	5126	23781	28	13

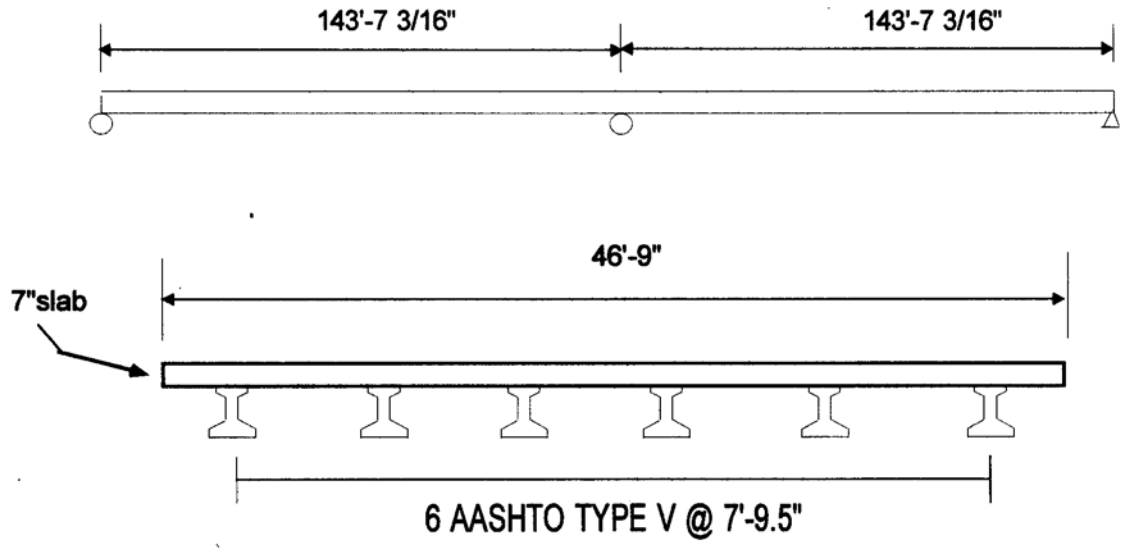

Fig. 6.71 Cross Section of Palm Beach County Bridge #930398

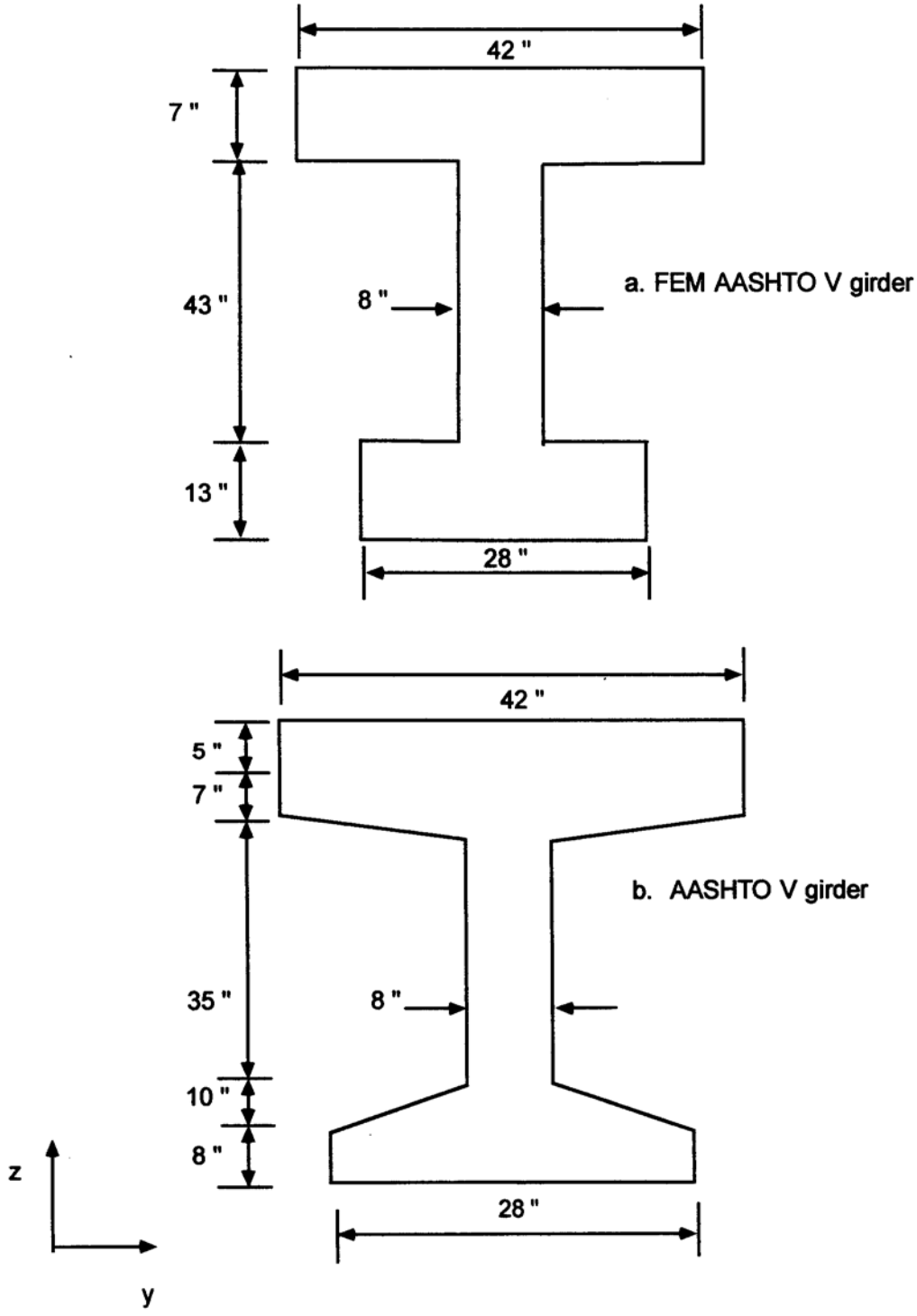

Fig. 6.72 AASHTO V Girder Details

Fig 6.73 FEM Model Of Palm Beach County Bridge #930398

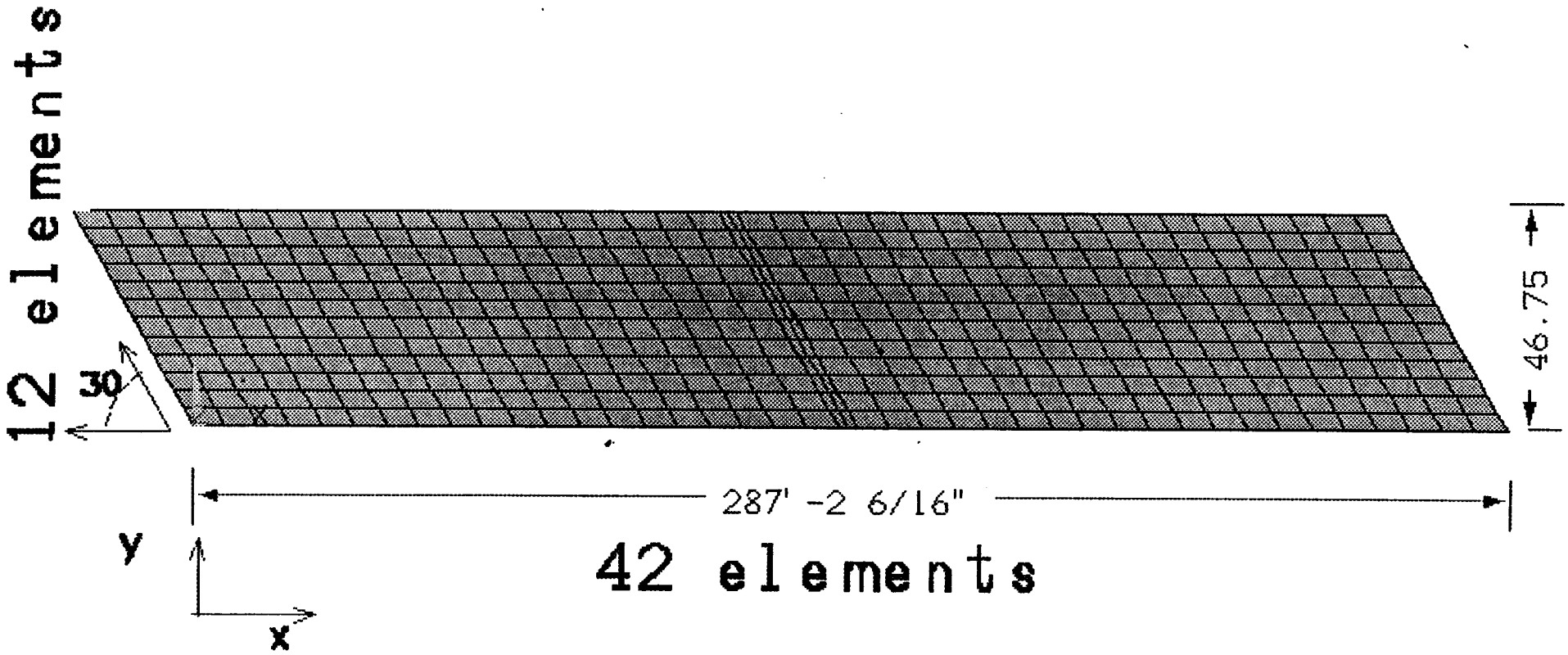

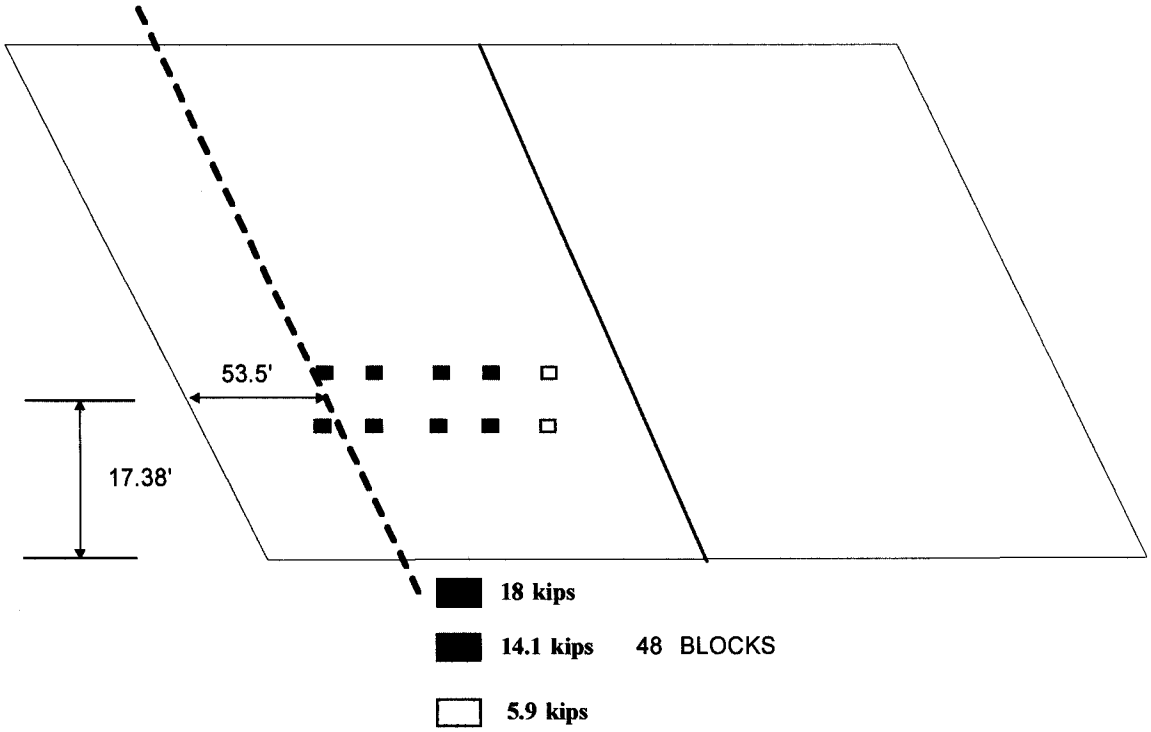

Fig. 6.74 Load Position/Strain Gauges for Palm Beach County Bridge #930398

The measured transverse strains in the bottom of the girders in Bridge #930398 compare closely with FEM values. The strains in the girders, where the trucks are positioned, agree well with the measured values (Fig. 6.75). The AASHTO and LRFD distribution factors are higher than the measured and FEM values. The measured distribution factor is slightly lower than the FEM results (Fig. 6.10).

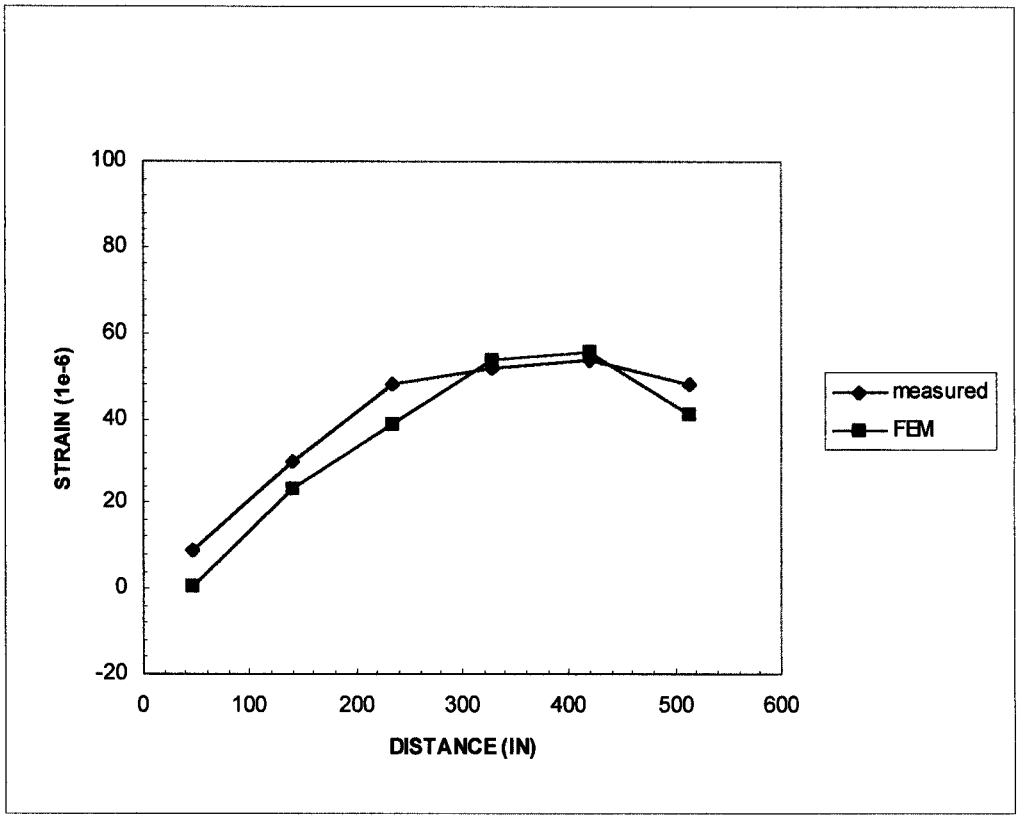

Fig. 6.75 Measured and Calculated Strains for Palm Beach County Bridge #930398

Table 6.10 Palm Beach County Bridge Load Distribution Factors (Interior Girders)

AASHTO	LRFD	FEM	Measured
1.42	1.21	1.04	0.89

CHAPTER 7

SUMMARY AND CONCLUSIONS

7.1 SUMMARY

The present study on wheel load distribution is focused on the skew slab-on-girder and skew solid slab bridges. Chapter 2 reviews the existing different analytical and field load distribution methods for different skew bridge types. Chapter 3 discusses the concepts of the finite element method in bridge modeling and idealization, field test procedures and methodologies.

Both analytical and field studies on the truck load distribution of skew simply supported slab-on-girder bridges are presented in Chapter 4. Finite element method is used to study the various parameters affecting load distribution and suggest which parameters must be considered (70 study cases were performed). In addition to the analytical study, data from field tests performed by Structures Research Center, FDOT, are used to verify the analytical results.

In Chapter 5, both analytical and field studies on the wheel load distribution of skew simply supported solid slab bridges are presented. Finite element method is used as an analytical tool to study the various parameters affecting load distribution and suggest which parameters should be considered. In addition to the analytical study, data from field tests performed by Structures Research Center, FDOT, are compared with those based on the finite element, AASHTO and LRFD codes. Several parameters such as skew angle, span length, bridge width, slab thickness, edge beam and number of lanes are considered in the parametric studies.

In Chapter 6, finite element method is used to analyze continuous skew and striate slab-on-I girder bridges and calculate the corresponding load distribution factors. The analytical results obtained are compared with those based on AASHTO (1989) and the LRFD (1995) codes. Field test data of continuous bridges are analyzed to investigate the load distribution factors.

7.2 CONCLUSIONS **7.2.1**

Skew Solid Slab

Bridges

i) The effective widths calculated using finite element method are larger than those calculated using AASHTO and LRFD codes, which indicate that both AASHTO and LRFD codes give conservative estimate of effective width, E for skew solid slab bridges.

ii) The effective width increases with increase in the skew angle for solid slab bridges. This confirms the LRFD codes in considering the skew angle as a parameter in effective width calculation. The finite element results show smaller skew angle effects than those in LRFD codes except for skew angle higher than 45 degrees where the effects are the same as in the LRFD code.

iii) The span length is an important factor in effective width calculation. The effective width tends to increase as the span length increases. The span length effects on the effective width calculation are the same from finite element analyses, AASHTO, and LRFD codes.

iv) The edge beam moment increases with increase in moment of inertia, i.e. increase in edge beam depth or width. The edge beam depth significantly affects the value of effective width, E. Slab bridges without edge beams or with hidden edge beams have greater maximum moment than similar slab bridges with

edge beams or with hidden edge beams have greater maximum moment than similar slab bridges with edge beam and hence the resulting effective width is smaller. These results suggest that the edge beam size should be taken into account in wheel load distribution. Neither AASHTO specifications nor the LRFD code considers the edge beam effect in the effective width equation.

v) Based on the skew solid slab parametric studies, the skew angle, span length and the edge beam depth are the main parameters, which significantly affect the effective width calculations. Effective width equations are proposed for solid slab skew bridges without edge beams and with edge beams.

vi) Effective widths calculated from finite element method and measured strains are higher than the AASHTO and LRFD values. The effective widths based on the AASHTO and LRFD codes are more conservative.

7.2.2 Skew Slab-on-Girder Bridges

i) Skew angle increase reduces load distribution for the interior girders. Considering the finite element results, it seems that the LRFD code accurately estimates the skew angle effect particularly for skew angles higher than 30 degrees.

ii) Skew angle effect on load distribution for exterior girders is similar to that of the interior girders. The finite element results show decrease in the load distribution factor with the increase in skew angles. These results confirm those based on the LRFD code where the load distribution factors decreases with the increase in the skew angle.

iii) Girder spacing is a very important factor in determining flexural wheel load distributions of skew slabon-girder bridges.

iii) **Girder spacing is a very important factor in determining flexural wheel load distributions of skew slabon-girder bridges.**

iv) **The flexural distribution factors based on LRFD are slightly smaller than those calculated using finite element method particularly for larger girder spacing. It is shown that the distribution factors based on LRFD code are in better agreement with those calculated using finite element method for smaller girder spacings which are more commonly used.**

v) **The interior girder distribution factor calculated using finite element method shows much smaller decrease with increasing span length than those based on LRFD code. However, the load distribution for exterior girders based on finite element analyses and LRFD codes shows conflicting results.**

vi) **For a given skew angle, girder spacing and span length, the LRFD load distribution equation overestimates the effect of slab thickness on wheel load distribution. The finite element results show no or little effect on load distribution for variation of slab thicknesses between 3.85 in to 7 in. which corresponding variation of H between 5 and 30. (H = stiffness ratio = $E_g I_v$, / a D , D = flexural stiffness of slab per unit width)**

vii) **The data from three field tests conducted on skew slab on I-girder bridges in Duval county, State Road 7 and Turnpike were used to validate the finite element model. In addition these field tests were used to calculate the wheel load distribution factors based on measured strains, finite element analyses, AASHTO and LRFD codes.**

viii) **The load distribution factors based on finite element analyses were the most close to those based on the measured strains (less than 30 % difference). This difference may be attributed to the variations in 7-4**

concrete strength and section modulus, which are used in calculating the measured DF. Both DFs based on AASHTO and LRFD were higher than those calculated using the measured strains and finite element method. This confirms that AASHTO code and to a lesser extent, the LRFD code give conservative values for wheel load distribution factor for skew slab-on-girder bridges.

7.2.3 Continuous Slab-on-Girder Bridges

7.2.3.1 Field Tests

From this study of wheel load distribution factors on continuous highway bridges, there exists a need to use computer modeling to accurately predict the behavior of existing bridges. Finite element analysis of continuous bridges has shown that the AASHTO and LRFD codes' wheel load distribution factors are conservative. The conservative approach may be needed in the design of highway bridges. However, rating of existing bridges for load capacity should be based on more accurate methods.

7.2.3.2 Parametric Study

The parametric study of continuous bridges investigated the effects of number of spans, the skew angle, and the ratio between two spans.

i) Changing the skew angle generates strains which are higher at the interior supports than at midspans. The strains at midspan are due to one span loaded with four trucks. The higher strains at the interior support are the result of loading both spans with a total of 8 trucks; four loaded in each span. The strain distributions are similar for both positive and negative moment loading. The FEM analyses show strain distributions become less uniform as skew angle increases.

Based on this parametric study, the effect of the number of spans on the load distribution factors is small and can be neglected. In general, the FEM load distribution factors are smaller than those based on LRFD code.

In general, the interior girder load distribution factors show little variation as the ratios between the spans increase for both positive and negative moments. However, the exterior girder load distribution factors show a general increase (10%-13%) as the ratios between the spans increase.

REFERENCES

1. Arockiasamy, M. and Amer, A., " Load distribution on highway Bridges based on field test data", Final Report, HPR Study No. 0668, Submitted to Florida Department of Transportation, April 1995.

2. Bishara, A.G., Liu, M.C., and El-Ali, N.D.," Wheel load distribution on simply supported skew I-beam composite bridges", J. of Structural Engineering, Vol. 119, No. 2, Feb. 1993.

3. Bishara, A.G.a nd Soegiarso, R.,"Load distribution in multibeam precast pretopped prestressed bridges", J. of Structural Engineering, Vol. 119, No. 3, March 1993.

4. Chen, T.Y., Siess, C.P., and Newmark, N.M.," Studies of slab and beam highway bridges, Part IV: Moments in simply supported skew I-beam bridges", University of Illinois, Engineering Experiment station, Bulletin, no. 439, Apr. 1954.

5. Chen, Y.," Refined and simplified methods of lateral load distribution for bridges with unequally spaced girders: I. theory", Computers and Structures, Vol. 55, No.1, pp 1-15, 1995.

6. Decastro, E.S., et al.,"Live load distribution in skewed prestressed concrete I-beam and spread box-beam bridges" Fritz Engineering Laboratory, Report No. 387.3, Lehigh University, Bethlehem, Pa., Aug., 1979.

7. DeCastro, E.S., Kostem, C.N., Mertz, D.R., and VanHorn, D.A.," Live load distribution in skewed prestressed concrete I-beam and spread box-beam bridges, Report FHWA-PA-RD-&@-$-#, Federal Highway Administration, 1979.

8. El-Ali, N.D.," Evaluation of internal forces in skew multi-stringer simply supported steel bridges", Ph.D. thesis, Ohio State University, Columbus, Ohio, 1986.

9. Gustafson, W.C.," Analysis of eccentrically stiffened skewed plate structures", Ph.D. thesis, 1966.

10. Gustafson, W.C., and Wright, R.N.," Analysis of skewed composite girder bridges", J. Struct. Div., Proc. ASCE, 94(St4),919-941,1968.

11. Hendry, A.W., and Jaeger, L.G.,"The analysis of certain interconnected skew bridges", Proc., Institute of Civil Engineering, Vol. 6, 1957.

12. Kankam, J.A. and Dagher, H.J.," Nonlinear finite element analysis of RC skewed slab bridges", J. of Structural Engineering, Vol. 121, No. 9, Sept. 1995.

13. Khaleel, M.A. and Itani, R.Y.,"Live-load moments for continuous skew bridges", J. of Structural Engineering, Vol. 116, No. 9, Sept. 1990.

14. Kostem, C.N. and DeCasto, E.S.,"Effects of diaphragms on lateral load distribution in beam-slab bridges", Transportation Research Board No. 645, 6-9, 1979.

15. Marx, H.J., Kachaturion, N., and Gamble, W.L.," Development and design criteria for simply supported skew slab-and-girder bridges", Civil Engineering Studies, Structural research Series No. 522, University of Illinois, Jan. 1986.

16. Mehrain, M.," Finite element analysis of skew composite girder bridges", Report No. 67-28, Structures and Materials Research, Department of Civil Engineering, University of California, Berkeley, Nov. 1967.

17. Newmark, N.M., Siess, C.P., and Peckham, R.R.,"Studies of slab and beam highway bridges, Part-I tests of simple-span right I-beam bridges", University of Illinois, Engineering Experiment Station, Bulletin Series no. 375, 1948.

18. Nutt, R.V., Schamber, R.A., and Zokaie, T.,"Distribution of wheel loads in highway bridges" Final Report No. 83, IMBSEN & Associates, Inc., Sacramento, Calif., 1988.

19. Tiedeman, J. L., Albrecht, P. and Cayes, L., " Behavior of two-span continuous bridge under truck axle loading",", J. Structural Engineering, ASCE, Vol. 119, No. 4, April, 1993.

20. Warren, G. and Malvar, L.J., " lateral distribution of loads in one -way continous navy pier decks", J. Structural Engineering, ASCE, Vol. 119, No. 8, August, 1993.

21. Zuraski, P., " Continuous-beam analysis for highway bridges", J. Structural Engineering, ASCE, Vol. 117, No. 1, January, 1991.

22. "AASHTO LRFD bridge design specifications" (1994), 1st Ed., American Association of State Highways and Transportation Officials, (AASHTO), Washington, D.C.

23. "Distribution of wheel loads on highway bridges" National Cooperative Highway Research Program (NCHRP), Transportation Research Board (TRB) No. 187(5), pp 1-31, 1992.

24. "Guide specifications for strength evaluation of existing steel and concrete bridges", 1989, American Association of State Highways and Transportation Officials, (AASHTO), Washington, D.C.

25. "Standard specifications for highway bridges ", 1992, 14th Ed., American Association of State Highways and Transportation Officials, (AASHTO), Washington, D.C.

26. "AASHTO LRFD bridge design specifications", American Association of State Highways and Transportation Officials, Washington, D.C., First Edition, 1994.